THE UNIVERSITY
of LIVERPOOL

Computer Vision Systems For Automated Arc Welding

Thesis submitted in accordance with the requirement of
The University of Liverpool for the degree of
Doctor of Philosophy
by

Jing Zhao

Department of Electrical Engineering and Electronics
October 2000

ABSTRACT

For automated welding, seam tracking and weld penetration control are two fundamental issues, whilst in process control the sensing technique is one of the key technologies. Among the various types of sensors used in welding automation, vision sensors are widely used. In recent years, especially, with the rapid advance of personal computing technology and its associated consumer electronics, microprocessors, video chips and laser diodes have become widely available at a lower cost, resulting in their widespread use.

The work presented in this thesis has been concerned with the development of two vision-based sensors for both seam tracking and weld penetration control. Both these sensors are compact and capable of being mounting on the welding torch. A single PC was used to carry out all image processing work for both sensors and the control functions for the welding system. Consequently, an integrated, compact automated welding sensing and control system was created.

The development of real time image processing software is extensively discussed in this thesis. The image processing algorithms investigated were for weld pool monitoring, to measure and estimate top-side bead width and, for seam tracking, to extract the profile of the joint or seam. Closed loop control trials have shown that the proposed sensors and image processing algorithms can provide reliable feedback information of the bead width and seam position for penetration control and seam tracking.

A third vision-based sensor has been developed for post weld inspection. To extract the parameters of the weld bead profile, i.e. bead width, reinforcement and undercut etc., a novel algorithm for segmenting the laser stripe is given.

ACKNOWLEDGEMENTS

I would like to express my gratitude to my supervisor, Dr J. S. Smith, and to Professor J. Lucas for their guidance and encouragement during the project. Many thanks to Professor W. Lucas for his advice and help in many areas. I also wish to thank the present and previous Heads of the Department, Professor J. D. Parsons and Professor M. Fang, for providing laboratory facilities. Thanks are also due to the Overseas Research Students Awards Scheme and European Community for funding me during my research.

I am sincerely grateful to my family for their continued support and understanding during my years of study abroad.

Finally, many thanks are due to my friends who support and company me to spend much difficult time during my study in UK and make my dream come true.

Contents

ABSTRACT

ACKNOWLEDGEMENTS

CHAPTER 1 INTRODUCTION

1.1 Arc Welding Processes

Arc welding is a joining process using an arc, between an electrode and the metal edges to be welded, to heat the metal to a fusible state. Two types of arc welding processes are in common use, namely TIG (Tungsten inert gas) and MIG (Metal inert gas).

1.1.1 TIG Welding

In the TIG process the arc is formed between a pointed tungsten electrode and the workpiece in an inert atmosphere of argon or helium. The small intense arc provided by the pointed electrode is ideal for high quality and precision welding. It has played a major role in the acceptance of aluminium for high quality welding and structural applications. TIG is applied in all industrial sectors but is especially suitable for high quality welding on thin sheet material because deposition rate can be quite low (using a separate filler rod).

There are two kinds of commonly used TIG processes, DC-TIG and AC-TIG. In DC-TIG, a constant arc current is applied with electrode negative during welding. It is generally used for the TIG welding of stainless steel, mild steel and medium-carbon steel. Pulsed arc current is also applied in this process to obtain a more flexible control of welding current. In AC-TIG, alternating current is used to help to break up the surface oxides on metal and exposes a clean oxide-free metal in the weld area. This is especially necessary for the welding of aluminium. Therefore, AC-TIG welding is mainly used for the welding of aluminium.

1.1.2 MIG Welding

In MIG welding with an electrode having a lower melting point than tungsten, the electrode end melts and molten particles are detached and transported across the arc to the workpiece by the magnetodynamic forces and gaseous streams. Therefore, it offers high deposition rates and high productivity and is suitable for the welding of thick material. Unlike TIG welding, MIG is invariably used with direct current and usually with the electrode positive. MIG is widely used in most industry sectors and an extremely wide range of metals, from mild steel to aluminium.

1.2 Welding Process Control

Over the past decades arc welding process control has been an intensive research topic for a number of researchers world-wide. For automated arc welding, process control is mainly concerned with two aspects: weld penetration control and seam tracking. The techniques concerned with these two issues are reviewed in the following sections.

1.2.1 Penetration Control

Problems are frequently experienced in ensuring consistent weld penetration of a joint, due to minor variations in material composition, component dimensions, joint fit-up or the surface condition of the component. In manual welding, the welder can adjust the welding parameters, or his technique, to compensate for some of the variations. In automated welding, the welding parameters are normally fixed prior to welding. Even if constant welding parameters are used, inconsistent weld penetration still occurs. This, consequently, will influence the performance of the weld in its working condition, especially for critical applications such as nuclear, chemical and aerospace structures. Thus, maintaining consistent penetration during automated arc welding has become a primary objective pursued by researchers.

For penetration control, practical and effective sensors are required. A sensor which observes the back of the weld and modifies the welding parameters to ensure consistent penetration is ideal and direct. However, for many applications, access to the back face of the weld is not possible. The difficulty associated with this problem is to find a precise and reliable way to measure the weld penetration using only top-face sensors that are attached to and move with the torch. To be widely applicable in the fabrication industry, the system should ideally be able to accommodate variety of welding processes, different welding positions and welding joint modes. Of equal importance, the sensor should not make contact with the workpiece, or intrude into the welding area. So far, a wide range of sensor systems applicable to arc welding have been developed, i.e., ultrasonic sensors, weld pool oscillation and visual sensors etc. Among the methods proposed in existing literature, pool oscillation and vision-based sensing methods received more attention, as ultrasonic sensing and acoustic sensing use additional sensing devices which are difficult to attach to the torch and contact with workpiece. A review of these methods is conducted as follows.

1.2.1.1 Weld Pool Oscillation Sensing [1.1][1.2]

When a short current pulse is applied to the arc, the surface of the pool vibrates. The oscillation frequency and amplitude is dependent upon the weld pool size. It can be monitored by measuring the fluctuations in either the arc voltage or the arc light reflected from the weld pool. It appears that the oscillation behaviour of a partially penetrated weld pool is considerably different from that of a fully penetrated weld pool; the frequency of the partially penetrated weld pool being much higher and the amplitude being much lower than those of the fully penetrated weld pool. It was found that the oscillation of the partially penetrated weld pool is dominated by one of two different oscillation modes depending on the welding conditions, whereas the oscillation of the fully penetrated weld pool is characterized by a third oscillation mode. It is possible to maintain partially penetrated weld pool oscillation in a certain mode by choosing appropriate welding conditions. Under these conditions, an abrupt decrease in oscillation frequency occurs when the weld pool transfers from partial penetration to full penetration. Thus, weld penetration can be in-process controlled by monitoring the oscillation frequency during welding.

Weld pool oscillation frequency monitoring is only effective for full penetration. It is unlikely that the oscillation frequency can provide accurate measurements of either the penetration depth or back-side bead width of the weld pool. For example, in practical welding, the desired back-side bead width could be selected from 3 mm to 5 mm. However, the oscillation frequency is not sensitive to the variation in the back-side bead width in this range. So far, the research on this sensor is only limited to the TIG welding without wire feed. Accuracy is reduced as the travel speed increases and by power source ripple, slag islands, the presence of dirt, slag or oxide at the back of the weld pool and the addition of filler wire to the weld pool.

1.2.1.2 Ultrasonic Techniques [1.3][1.4]

The principle behind this method is that the propagation interval for the ultrasound is related to the distance between the ultrasound source and the reflection point and the distance between the reflection point and the receiver. For a single point range measurement, the problem is to measure the transit time for a single ultrasound pulse to travel to and from the reflector, which is a discontinuity in material property. Theoretically, if the dimension of the reflector (for instance, crack, porosity, etc.) is larger than the wavelength of the incident ultrasound pulse, the reflected pulse contains information concerning the size and shape of whatever caused the reflection. Since weld pool constitutes a change in phase and in material properties relative to the unmolten workpiece, its shape and size may be measured through its reflected ultrasound. The depth of penetration of a weld pool can be measured by locating the fusion interface between the weld pool and parent metal using ultrasonic waves generated by an angled piezoelectric transducer in contact with the surface.

Accurate measurements from the top face can only be obtained for plate thickness of greater than 10mm or less than 2mm. To ensure good coupling between the transducer and the workpiece, the workpiece must have a simple, uniform surface geometry with minimum irregularities, and distortion of the workpiece must be avoided. The transducers must track the weld pool. Component vibration or unexpected probe movement must be prevented. Although significant progress has been made, practical applications are still restricted because of the contact sensor. If the problems associated with the noncontact sensor [1.4] are well resolved, its extended applications can be expected.

1.2.1.3 Acoustic Emission Techniques

During welding, the stresses which form in the workpiece because of the thermal gradient about the weld and changes in the volume of fused metal generate acoustic emissions, which travel throughout the workpiece. As penetration changes from partial to full, the frequency spectrum of the acoustic emission can be measured using a stationary acoustic transducer remote from the weld or, in laser welding, a non-contact pressure wave sensor. However, the relationship between the acoustic emissions and the weld penetration depth is not fully understood. Further, a number of microstructural features may also influence the performance of these techniques.

1.2.1.4 Vision-based Sensing [1.5]-[1.19]

For a skilled human welder, penetration information can be obtained by viewing the weld pool. This means that sufficient information about weld penetration exists in the geometrical appearance of the weld pool. Thus, this technique assumes that if the weld pool size on the top-face remains constant, then the penetration is constant. The weld pool may be viewed using a camera, which can be incorporated into the welding torch.

Direct weld pool viewing functions independently of welding position, process and joint type, and has received more attention than the other methods. However, the development of this technique has been affected by the high expense of the components of the system, such as the video camera, frame grabber etc. In recent years the rapid advance of personal computing technology and its associated consumer electronics has brought about a new, silent revolution worldwide. Microprocessors and video chips have become commercially available at a lower cost and compact size, resulting in their widespread use. Consequently vision based sensors have become the most prospective methods for robotic welding sensing and have shown their significant advantages over the other sensing techniques.

Intensive research on this technique has been done in recent years. Stone and Smith [1.5] developed a vision-based sensor for measuring, in real time, the size of the weld bead at the top face during automated welding. The technique involves the periodic interruption of the arc for a short time duration, during which the image of the weld pool is captured by a CCD camera. The size of the bead is measured by hardware techniques. Bicknell and Smith [1.6] described a passive vision-based sensor using an infrared camera combined with selective optical filtering instead of arc interruption and external illumination techniques to reduce excessive arc glare and improve contrast between an weld pool and heat affected zone. The sensor head was compact and suitable for practical applications. In this technique, image processing software was applied to measure the size of bead. More work has been done by Zhang and Kovacevic [1.7][1.9][1.11][1.13] to investigate the correlation between weld pool geometry and weld penetration in TIG welding. In their research, a high shutter speed camera assisted with pulsed laser illumination was used to capture the clear image of the weld pool. The shutter of the camera was synchronised with the laser pulse. From developed image processing algorithms in their study, the edge of weld pool could be extracted successfully.

The principle behind this technique is quite similar for all this kind of system developed with little differences in acquiring vision information of weld pool. In the development of vision-based sensing techniques, both hardware and software play important roles. As hardware is concerned, all efforts have been made to get the clear images of weld area, especially the weld pool, using components as compact and as simple as possible to make the system suitable for practical applications. As software is concerned, great potential exists in developing novel image processing algorithms to effectively and robustly extract the features of weld area. So despite the achievements in vision-based sensing techniques, no one sensor is commercially available because of the limitations of individual methods. Therefore, there is still need to develop a vision based top face sensor, which should be flexible, robust and portable in hardware, reliable in software, and suitable for a wide range of applications.

In this thesis, a vision-based top face sensor is described for weld pool monitoring in real time. A high shutter speed CCD camera combined with band pass filters mounted on the welding torch is positioned in front of the weld. A standard frame grabber, plugged into the computer, is used to capture images from the camera. Image processing, on a PC, is then performed on the images. The resultant data extracted from weld pool, mainly its width, is output to the control interface board for manipulating the welding parameters, i.e. welding current, voltage (via. power supply) and welding speed (via. stepper motor drive unit) to ensure the required weld bead and penetration. Novel image processing algorithms have been developed for the pool edge extraction in the welding processes of TIG and MIG on aluminium, stainless steel and mild steel.

1.2.2 Seam Tracking

Seam tracking plays a fundamental and critical role in generating good arc welds and continues to make great improvements. Most systems use one or more of the four established sensing systems: touch, through-the-arc, ultrasonic and visual sensor.

The touch sensor uses the welding wire to find the beginning and end of the seam before welding begins. This is the earliest method with poor accuracy and limited to seams with grooves only.

1.2.2.1 Ultrasonic Sensor [1.20]-[1.23]

Mahajan [1.20] developed an ultrasonic seam tracking system for robotic welding which tracks a seam that curves freely on a two-dimensional surface. The seam is detected by scanning the area ahead of the torch and monitoring the amplitude of the waves received after reflection from the work piece surface. Scanning is accomplished by using two ultrasonic sensors (a transmitter and a receiver) mounted on a stepper motor such that the transmitter angle is the same as the receiver angle. The motor is mounted on the end-effector just ahead of the welding torch and covers a ninety-degree arc in front of the torch. If there is no seam then the receiver receives most of the transmitted waves after reflection, but if there is a seam then most of the transmitted waves are dispersed in directions other than that of the receiver. The system has been tested and is robust in the harsh environments generated by the arc welding process. The robustness of the system stems from using various schemes such as time windowing, a waveguide, air and metal shields, and an intelligent sensor manager. It can be used to weld very shiny surfaces, and is a very economical method in terms of cost as well as computational intensity. The system can be used to detect seams less than 0.5mm wide and 0.5mm deep.

Zhang [1.21] improved this approach using noncontact ultrasonic sensing. The noncontact ultrasonic sensor was first introduced to seam tracking in the early 1980's by Estochen [1.22]. Umeagukwu [1.23] used a 100 kHz airborne ultrasonic transducer to measure the joint orientation and lateral deviation caused by curvature or discontinuities in the part. A data acquisition system was developed for V-groove joints and lap joints.

1.2.2.2 Arc Sensor

Through-the-arc sensing is based on the correlation between the arc length and arc voltage. With through-the-arc seam tracking, the head moves in a weave pattern over the area where the seam is supposed to be. Variations in current and voltage as the torch brushes over the seam give signals that can be converted to control commands. Because of its robustness against smoke, spatter, and arc radiation, it is the most prevalent method for seam tracking today. However, in order to apply this technique, the joint sidewalls must be well defined or have a groove. Also, the mandatory weave of the torch causes an undesired coupling between the sensing and the welding process. In addition, it is only effective in gas metal arc welding. The arc light intensity and welding resistance can also be utilised as a seam tracking sensor [1.24].

1.2.2.3 Visual Sensor [1.25]-[1.32]

The basic principle of the laser-stripe sensor remained unchanged over the years. State of the art charge-coupled devices (CCDs), laser diodes, and a microprocessor, which controls and monitors the major functions, form the basis of a new, compact, lightweight sensor head. The advantages of this design are its small size and the absence of moving parts, resulting in an extremely reliable system.

Optically, the structured light principle is employed. A fan of laser light emanating from one or more laser collimators strikes the surface of the workpiece. The resulting contour line is viewed by the CCD camera at a given angle, termed the "triangulation angle". This captured profile carries all the information necessary for determining the height and location of a given feature representing a joint or seam in order to track the seam (automated seam tracking) and to adapt the welding parameters to the actual groove geometry (adaptive welding).

As moving parts are omitted high mechanical ruggedness is guaranteed. By modification of the optical layout the measurement range and resolution of the sensor can be adapted to the actual problem. Active lighting results in a minor dependency of surface properties. Filtering the scattered laser light with an optical narrow band pass filter, chosen according to the laser diode's wavelength, reduces impact of surrounding day-light or an open welding arc.

Although laser stripe sensors for seam tracking have been available since the mid 80's wide scale industrial acceptance has not taken place yet. Reasons for this are unaffordable high prices and poor reliability and accuracy in harsh industrial environments. However, in recent years, the cost for computer related consumer electronics, such as video chips and laser diodes, has decreased dramatically. Therefore the price for this kind of system has drastically reduced, while the problems concerned with reliability and accuracy still remain unsolved. Lots of efforts have been made to improve the reliability and accuracy of these systems from both hardware and software. However most work has been conducted on V preparation and lap joint because the seam features in these two instances are comparatively easy to be extracted. Limited work has been done on the butt joint [1.33].

A large variety of sensors have been developed for seam tracking but up to now only non-contact laser-optical sensors have proven their general ability to cope with the most common seam types without major restrictions.

Research work relating to vision-based seam tracking systems has been in progress at the University of Liverpool for some time. The early systems used specialised hardware to provide the required image analysis [1.33][1.34]. More recently, real time systems have been developed around standard, low cost PC hardware that use software based image analysis algorithms. The results obtained from the use of this type of software based seam image analysis system are presented in this thesis. The system is applicable to a number of applications using differing plate thickness and welding processes.

1.3 Bead Profile Inspection

All industrial welds are very carefully designed and scrutinised. In industry only welds produced using an approved welding procedure can be performed. Since welding is a non-deterministic process the final weld may still not conform to the original specification. Thus a final level of inspection is required.

The process of inspection is generally carried out by a qualified inspection body. Inspection is an 'expert' task, the results of some inspections being not definitive but open to interpretation, the most widely used method of inspection being that of visual inspection.

Visual inspection is generally quick to apply, relatively inexpensive and gives very important information about the conformity of the weld as specified in the initial specifications. The British Standard for visual inspection of fusion welded joints makes specific suggestions concerning the measurement of the dimensions of a weld preparation, a weld, or an imperfection. The inspector usually checks the following items:

- *Penetration and root examination*. The penetration and root concavity, burn through or shrinkage grooves need to be within limits specified by the code of practice.
- *Contour*. The weld face and height of any excess weld metal must be within the code of practice.

- *Weld width.* The width of the weld needs to be consistent over the entire joint. It must also be within the dimensional limits as specified by the welding code of practice.

- *Undercut.* Undercut must be measured and checked against the acceptance criteria.

To date, measurement of weld profile dimensions has been made manually, off-line, using variety of gauges and weld replicas. These methods are time consuming, limited in accuracy and require significant operator skill. The inaccessibility of certain welds (e.g. in pressure vessels) also makes the method problematic.

This thesis describes a vision-based system capable of providing fast, accurate and repeatable post weld inspection. The weld gauge uses the same principle as the one used in seam tracking. Triangulation-based laser-stripe sensor has been used to get the profile of the weld, and novel, software based, image analysis algorithms have been developed to measure the parameters of the weld bead and evaluate its quality.

In general, this thesis covers all the important issues of the process control in automated welding: seam tracking, penetration control and bead profile inspection. Attention has been placed to software development for the visual sensors in three instances. The results obtained in this research have demonstrated the prospects of a vision based integrated system capable of multi process control before (seam tracking), during (pool monitoring) and after welding (weld inspection).

1.4 Thesis Overview

This thesis has been structured into eight chapters. A brief description of the remaining chapters is given below.

Chapter 2 describes the hardware structures used in this research, its components and their functions. Block diagrams are given to illustrate the principles of the sensing and control systems.

Chapter 3 discusses the image processing algorithms concerned with weld pool monitoring. The principle and methodology of edge detection are described and the edge detectors commonly used in machine vision are presented and compared. The algorithms of weld pool edge extraction for the images of different welding processes on different materials are discussed.

Chapter 4 discusses the image processing techniques needed to analyse the images provided by both laser stripe sensor and the direct viewing method used for seam tracking, while attention has been placed on the first one. The principle and methodology of corner detection in machine vision is presented. The techniques for seam recognition from laser line and direct viewing images for the most common seam types are described.

Chapter 5 then discusses the problem with respect to the bead profile measurement. The definitions of the measurements, which are universally considered to be important for evaluating the quality of a weld, are given. Hough transform techniques, which are used for line segmentation in bead profile measurement, are discussed. The algorithms for profile segmentation and feature point extraction are presented.

Chapter 6 describes the software design using Visual C++ for three cases described in chapters 3, 4 and 5. Their software structure, interface design and the procedures implementing the variety of tasks are discussed.

Chapter 7 gives the results of preliminary control trials conducted for pool monitoring and seam tracking.

Finally, the Conclusions of this thesis are made in chapter 8. Future work for this project is suggested.

CHAPTER 2 VISION SYSTEM STRUCTURE

This chapter describes the hardware structure of the vision systems used for weld pool monitoring, seam tracking and bead profile measurement for both automated TIG welding and MIG welding.

2.1 Vision System Components

All vision systems used for welding automation in this thesis are composed of four basic components: camera (with lens), filter, frame grabber and a personal computer for image processing.

2.1.1 Cameras

Video camera are used to convert light signals into electrical voltages that can be transmitted, via electrical cabling, and used to reproduce the scene, viewed by the camera, elsewhere.

Charge Coupled Device (CCD) cameras were chosen for the research work because of their advantages over the traditional Vidicon tube cameras. First of all, they are physically more compact which makes them highly suited for mounting on robotic system. They are also much more robust as they are entirely solid state apart from the lens system. Another advantage of CCD cameras is their wide spectral response, they respond well in the infrared region.

Most CCD cameras produce a standard composite video signal output, which is the most common output from video cameras. Images are displayed on a line by line basis scanning down the screen. The composite video signal contains timing information to indicate when new images and new lines within that image are being displayed. The brightness of a particular point on the screen is controlled by the intensity of the voltage of the video signal corresponding to that particular point.

The timing of the video signal is closely coupled to the frequency of mains electricity (50 Hz). In order to prevent strobing of the image, if it were to be displayed on a monitor, a new image is displayed at exactly the same rate as the mains frequency. Thus a new image is displayed every 20 ms. As the image is made up of a series of lines, the vertical resolution of the image is dependant on the number of lines displayed. However, increasing the number of lines displayed in the 20 ms, decreases the time to display each line. The horizontal resolution of the image is a function of the bandwidth of the signal and the time in which it is displayed. A compromise has to be made between the vertical and horizontal resolution of the image. For the composite video signal a line period of 64 μs was chosen. This gives 312.5 line periods per 20 ms.

However, if greater resolution is required the images are interlaced. The first image is displayed and then the second image, however, rather than overwriting the first image, the second image is displayed in between the lines of the first image. Thus the vertical resolution is increased by two. Each separate image is called a field, with the two fields being used to make up a frame. Therefore a new frame is displayed every 40 ms. The two fields which make up a frame in an interlaced image are called the odd and the even field, with each field contributing 312.5 lines to the frame. The frequency of displaying a frame is 25 Hz, half of the mains frequency.

Newly developed Complementary Metal Oxide Semiconductor (CMOS) cameras use arrays of photodiodes as the imaging sensor instead of charge accumulation used in Vidicon and CCD cameras. These sensors can be accessed to give an output voltage proportional to the instantaneous illumination. Normally the electronics are configured to give a logarithmic response to the illumination; this allows a wider dynamic range to be viewed than can be observed with CCD cameras. As the output voltage is proportional to the instantaneous illumination there is no requirement for charge accumulation and consequently these devices are not prone to blooming. There is also no need to repeatedly read the image as there is in Vidicon and CCD cameras. Normally, the photodiodes of the array are individually addressable by providing the row and column addresses. The instantaneous current from the addressed photodiode can then be measured. This allows the image to be randomly accessed under external computer control.

CMOS cameras would appear ideal for arc monitoring systems. However, the technology is relatively new and does have some shortcomings, the main one being the non-uniformity of the response of the individual pixels. Subjecting the camera to a calibration procedure and then using a computer program to modify the read intensities, based on the calibration values, normally overcomes this.

2.1.2 Filters

Optical filters are used to allow transmission of light from the light source into the image processing system, but to block the transmission of any corrupting light from, for example, the welding arc.

The welding arc is an extremely powerful light source covering the range of the optical spectrum from ultra violet to infrared. It is impossible to view the weld pool by a camera without getting rid of the arc light using filters, especially for weld pool monitoring. Firstly, a normal welding glass is applied to attenuate the arc light thoroughly. Then, a band pass filter is used to block the unrelated light from the weld area to make the weld pool edge clearly visible. However, for different welding processes, such as TIG and MIG, and different welding materials, e.g. aluminium and stainless steel, the radiation from the welding area differs. So filters with different central wavelengths and bandwidths are used.

In the system used for seam tracking and bead profile measurement, as a laser light source was used, it becomes possible to use band pass filters to prevent unwanted light entering the camera system.

2.1.3 Frame Grabbers

The frame grabber is the link between the video signal and the computer. In order for a computer to be able to analyse an image, the image has to be stored so that the processor can access the data. It is the function of the frame grabber to capture and store the image from the camera, so the computer can access it. Most frame grabbers also have the ability to provide a real time display of its contents to a monitor.

In order to pursue the integration of the welding control system only one computer was used for the both visual sensors, one for pool monitoring and another for seam tracking. So two frame grabbers are required in one machine. Since the device driver for the frame grabber does not support two identical cards in one machine, two different kinds of frame grabbers, WIN/TV and PICOLO, were used for the pool monitoring and seam tracking respectively.

2.1.3.1 WIN/TV Frame Grabber

Hauppauge's WinTV-pci is a low cost single slot PCI card with 125-channel TV-tuners. The TV-source can be from aerial or cable TV. With the external audio/video inputs, it can also be connected to a video camera, VCR or camcorder. It is capable of capturing high resolution video images from a TV broadcast or any external video source.

Live video is digitized from either the built-in 125-channel cable TV tuner or an external video-input source using high quality 4:2:2 video sampling at 60 fields per second (50 fps in PAL). Maximum digitized image size is 640x480 for NTSC video sources, which is the video standard used in North America, 758x576 for PAL, which is the standard used in the most parts of Europe including UK. The digitized video is sent over the PCI bus in a PC into the memory of the VGA display adapter. This allows the digitized video to move efficiently, and takes a fraction of the available bandwidth of the PCI bus. Figure 2. 1 shows the layout of the WinTV-pci board.

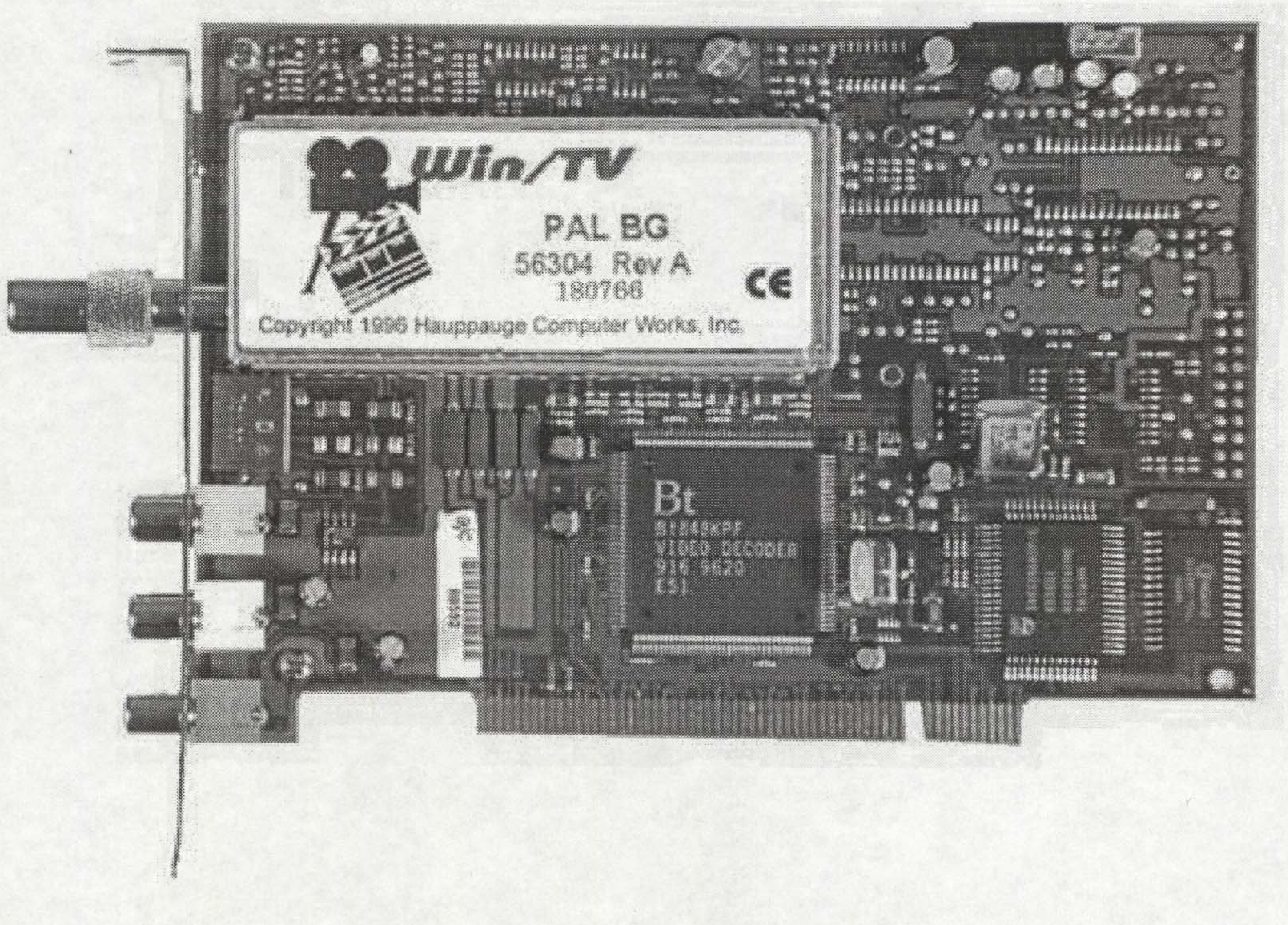

Figure 2. 1 WIN/TV Board

2.1.3.2 PICOLO Frame Grabber

The PICOLO board from Euresys is used as frame grabber for the seam tracking system. It acquires PAL, CCIR, NTSC, EIA, SECAM or S-Video (625 or 525 standard) colour or monochrome signals directly to PC memory. It is compatible with Windows 95, Windows 98, Windows NT and DOS 32-bit environments and supports the real-time image transfer of full resolution (up to 768×576 pixels) colour images and sequences of images to the PC memory (video capture). Its PCI management hardware and drivers have been optimised to allow high-speed image transfer under 32-bit environments. Figure 2. 2 shows the board layout whilst Figure 2. 3 shows the function units.

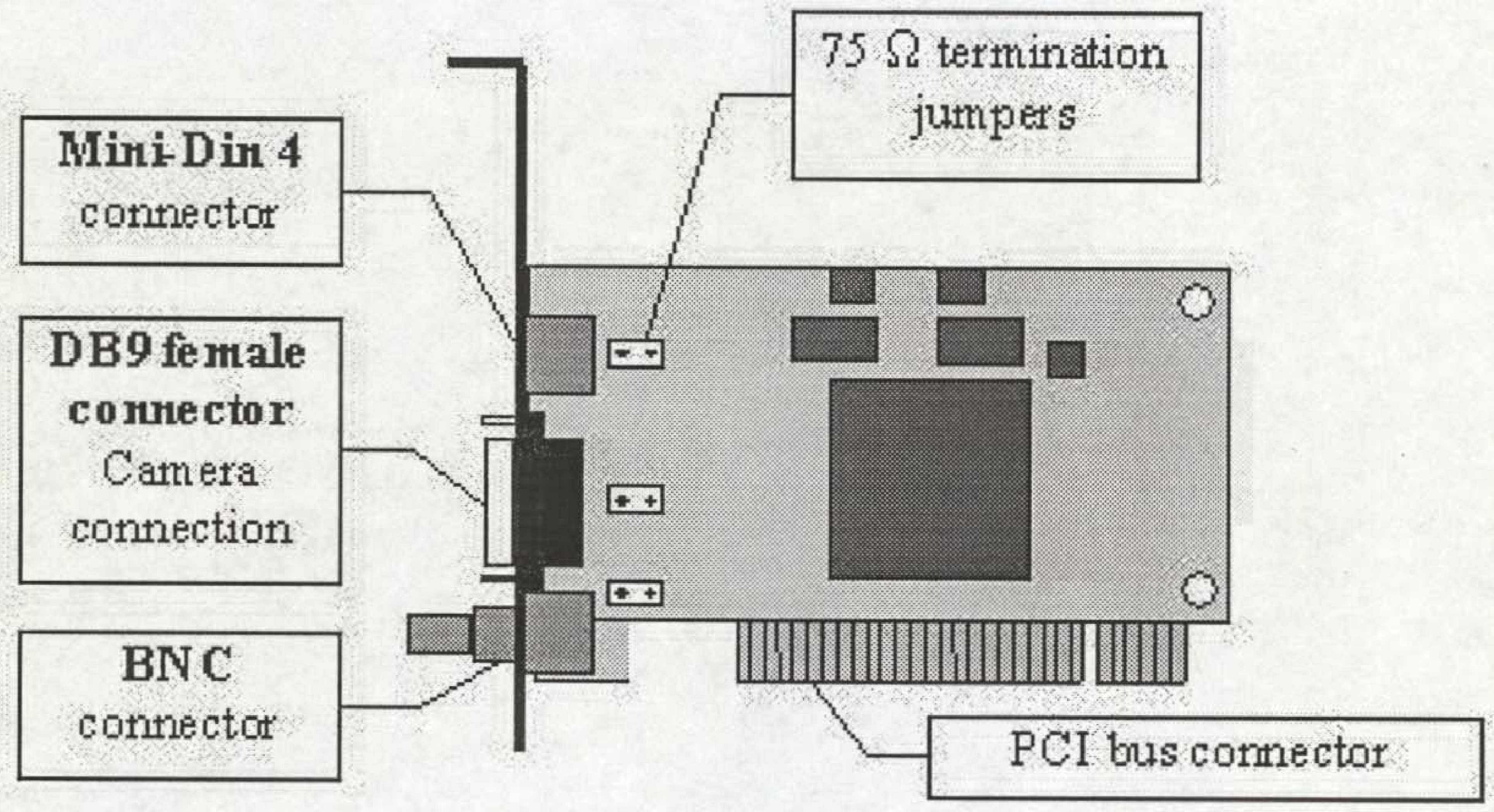

Figure 2. 2 Picolo Board Description

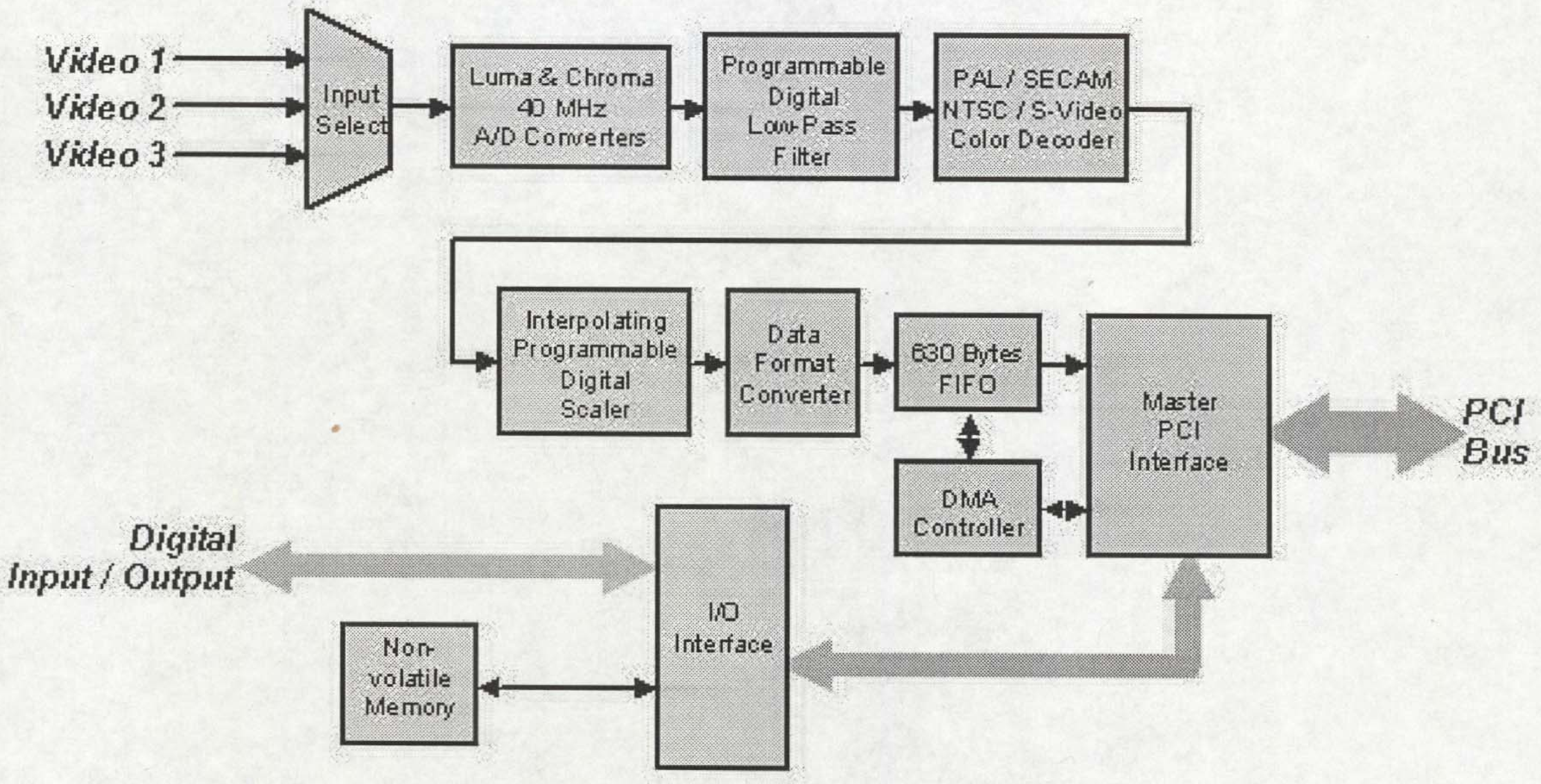

Figure 2. 3 PICOLO Block Diagram

2.1.4 PC

A personal computer is an essential part used for both image data analysis and control implementation in welding process control system. It uses Microsoft Windows NT as its operating system because of its numerous advantages. Microsoft Windows NT is a powerful 32-bit operating system, which have specially been optimised for network operations as well as embedded applications. It is built to run on several different families of computer processors: x86, MIPS, the DEC Alpha, and Power PC. Also, it can run on computers running more than one processor. Moreover, its multitasking operation and multi-threaded process have made it ideal for welding control applications.

2.2 Vision System Structure

Principally, the vision systems used for pool monitoring, seam tracking and bead profile measurement are similar, but slightly different in their structures.

2.2.1 Pool Monitoring System

The principle layout of the pool monitoring system is shown in Figure 2. 4. The weld torch is held fixed while the workpiece is moved by a stepper motor. Direct and pulsed currents are used in TIG and MIG welding. The CCD camera mounted on the welding torch was positioned in front of the weld. A standard frame grabber, plugged into the computer, is used to capture images from the camera. Image processing, on a PC, is then performed on the image.

The resultant data extracted from the weld pool, mainly its width, is output to the control interface board for manipulating the welding parameters, i.e. welding current, voltage (via. power supply) and welding speed (via. stepper motor drive unit) to ensure the required weld bead and penetration. Novel image processing algorithms have been developed and are described in this thesis for the pool edge extraction in the welding processes of TIG and MIG. These are introduced in detail in Chapter 3.

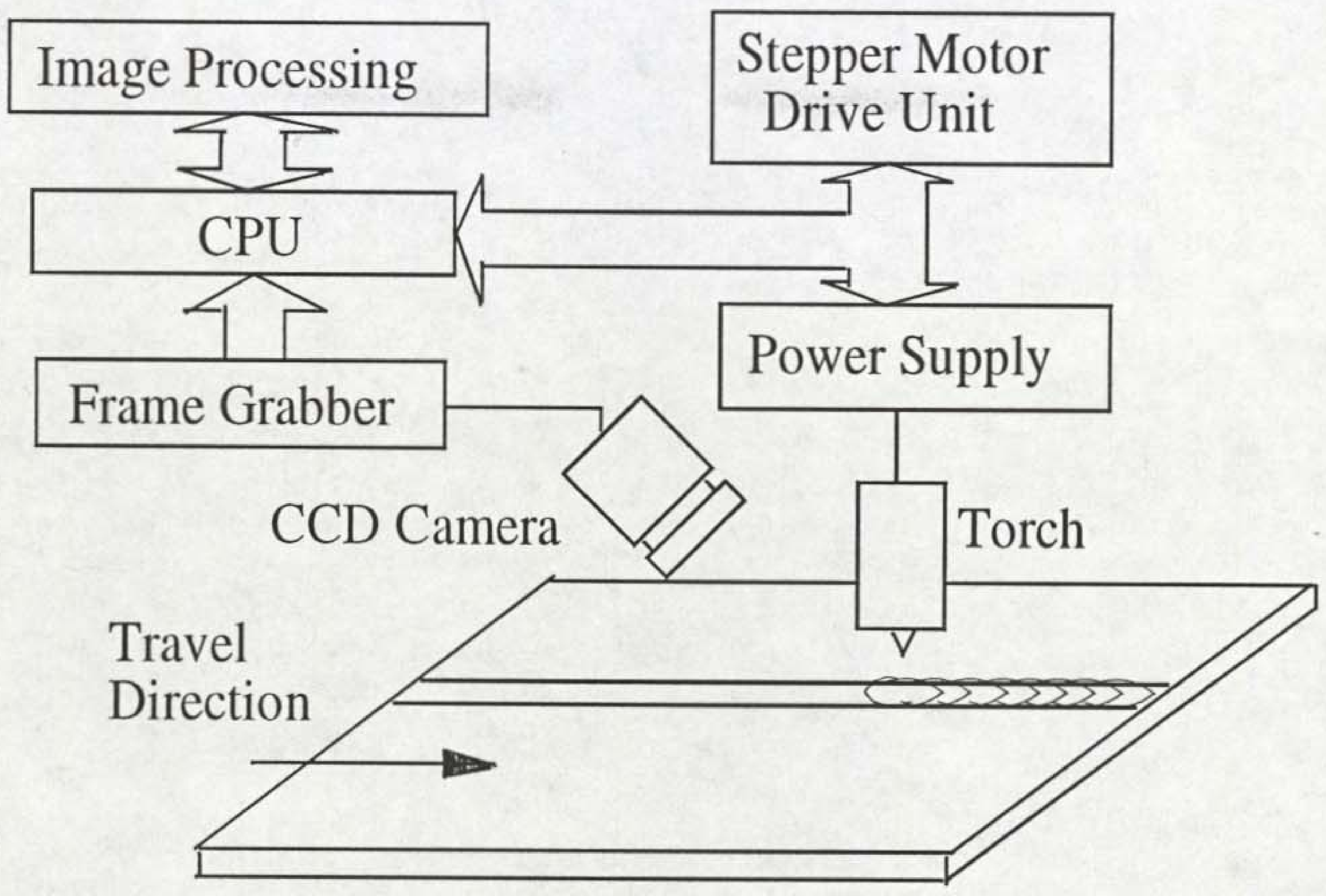

Figure 2. 4 Experimental Set up

2.2.2 Seam Tracking System

A typical optical seam sensor system consists of a CCD camera, a laser diode, a computer based frame processing system. The seam is illuminated by a laser line at a given angle and viewed by a CCD camera usually placed vertically. The image of the laser line images contains all the information necessary for determining the features representing a joint or seam. The CCD images are captured and analysed by a computer based image analysis system. A number of image processing activities are undertaken on these images, in real time, to derive the geometrical information of the seam such as the centre position, gap and misalignment between two plates.

The resultant parameters of image processing are transmitted to the control system to adjust the manipulator path to ensure that the torch is at the correct position with respect to the seam and furthermore to generate the welding parameters for compensating the gap and misalignment.

Figure 2. 5 shows a block diagram of the seam monitoring system. This sensor comprises a sensing head and the image processing system. The sensing head, including CCD camera, filters and laser (680nm) was mounted onto the welding torch and acquires visual information with regard to the seam position. In order to suppress the disturbances due to the arc light and the radiation from the hot metal, a narrow-band filter has been employed operating at the same wavelength range as the diode laser. The composite video signal output from the CCD camera is transmitted to an

image capture board or frame grabber fitted to the computer system. The frame capture board is capable of storing images from the camera at resolutions up to 768×567 pixels at a frame rate of 25Hz.

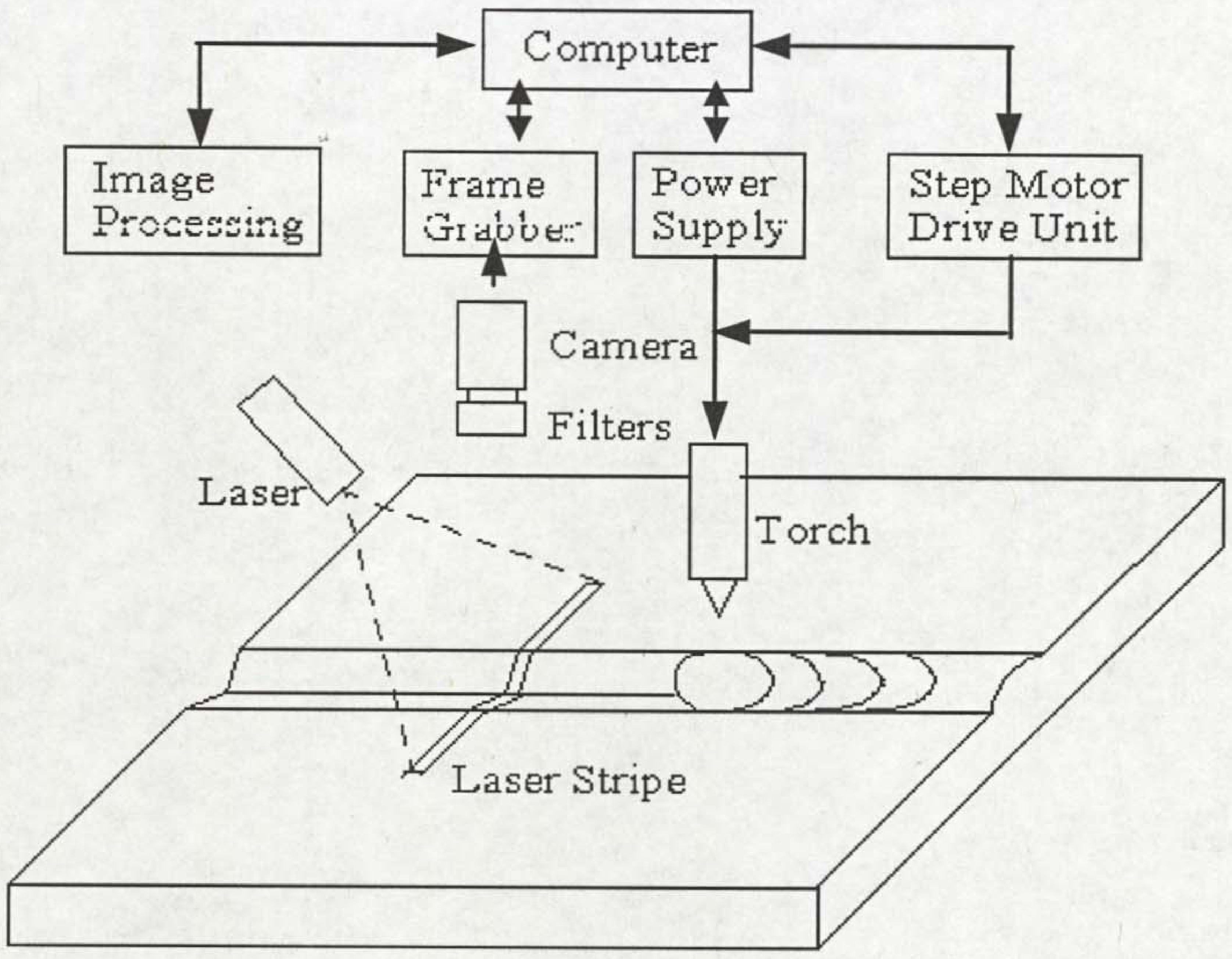

Figure 2. 5 Seam Monitoring System

The corresponding real time image processing algorithms developed to derive the geometrical information of the seam such as the centre position, gap and misalignment between two plates are presented in Chapter 4.

The pool monitoring and seam tracking system can be integrated into one unit, in which two cameras are mounted onto the welding torch, one for viewing the pool and another for the seam. Consequently, two frame grabbers are required in one computer, associating with two cameras. Figure 2. 6 is a photo of the sensing head of this system. Figure 2. 7 is the central computer used for image processing and the control function in this system.

2.2.3 Bead Profile Measurement

The system used for bead profile measurement is quite similar to the one used for seam tracking, as shown in Figure 2. 5. It also uses a laser line projecting onto the bead behind the torch instead of in front of it. A CCD camera mounted on the welding torch is positioned behind the weld pool for viewing the image of laser line, which carries the bead profile information. Chapter 5 describes the image processing algorithms developed to perform bead profile measurement such as bead width, reinforcement and surface imperfections wherever they occur.

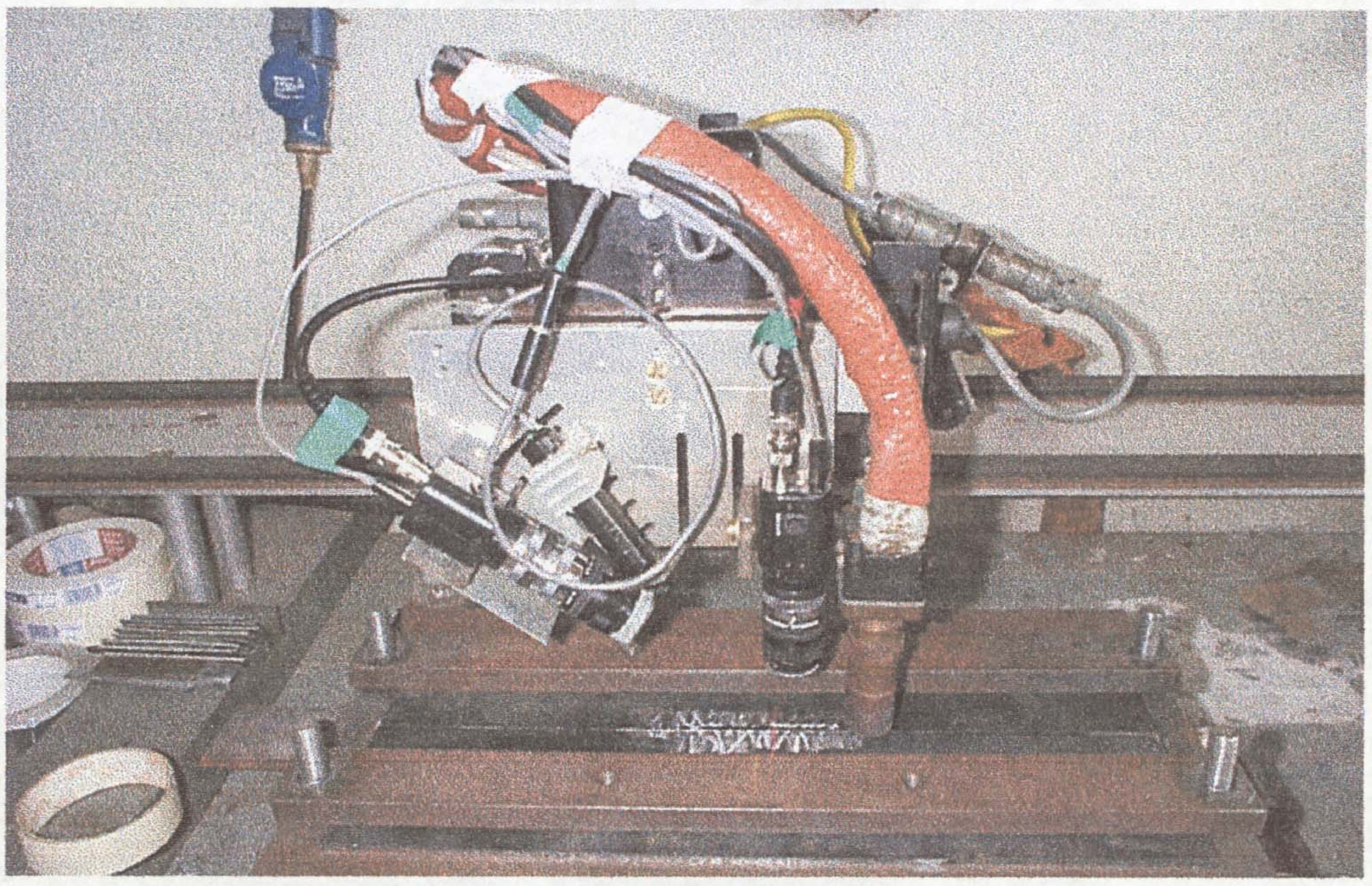

Figure 2. 6 Sensing Head of the Pool and Seam Monitoring System

Figure 2. 7 Central Computer of the Pool and Seam Monitoring System

CHAPTER 3 IMAGE PROCESSING FOR WELD POOL MONITORING

In this chapter, the background knowledge of edge detection and the commonly used edge detectors are firstly reviewed. Then the application of the edge detectors on weld pool monitoring is investigated based on the analysis of the image data from different weld pool images.

3.1 Theory of Edge Detection

The category of edges in digital images as well as their natures is discussed, several typical edge detectors are introduced and compared in this section.

3.1.1 The Nature of Edges

An edge in an image is a significant local change in the image intensity, usually associated with a discontinuity in either the image intensity or the first derivative of the image intensity. Discontinuities in the image intensity can be either (1) *step* discontinuities, where the image intensity abruptly changes from one value to a different value, or (2) *line* discontinuities, where the image intensity abruptly change value but then returns to the starting value within some short distance. However, step and line edges are rare in real images. Because of low-frequency components or the smoothing introduced by most sensing devices sharp discontinuities rarely exist in real signals. Step edges become *ramp* edges and line edges become *roof* edges, where intensity changes are not instantaneous but occur over a finite distance. Illustrations of these edge profiles are shown in Figure 3. 1.

Step-Edge Ramp-Edge Line-Edge Roof-Edge

Figure 3. 1 Examples of edge profiles

Among the above edges, step edge or ramp edge detection in real image is the most significant in computer vision and many effective step edge detectors have been developed in the last two decades.

3.1.2 Edge Detector

To estimate the performance of an edge detector, three performance criteria are defined as follows:

- *Good detection.* There should be a low probability of failing to mark real edge points, and a low probability of falsely marking nonedge points. This criterion corresponds to maximising the signal-to-noise ratio.
- *Good localisation.* The points marked as edge points by the operator should be as close as possible to the centre of the true edge.
- *Only one response to a single edge.* This is implicitly captured in the first criterion since when there are two responses to the same edge, one of them must be considered false.

According to the definition, an edge refers to places in the image where there appears to be a jump in image intensity or a local extremum in the first derivative of the image intensity. The aim of all edge detectors is to find either where the intensity gradient magnitude is sufficiently large to be taken as a reliable indicator of the edge or where a local extremum of the first derivative exists, as shown in Figure 3. 2. This means that at the edge points, there will be a peak in the first derivative and, equivalently, there will be a zero crossing in the second derivative.

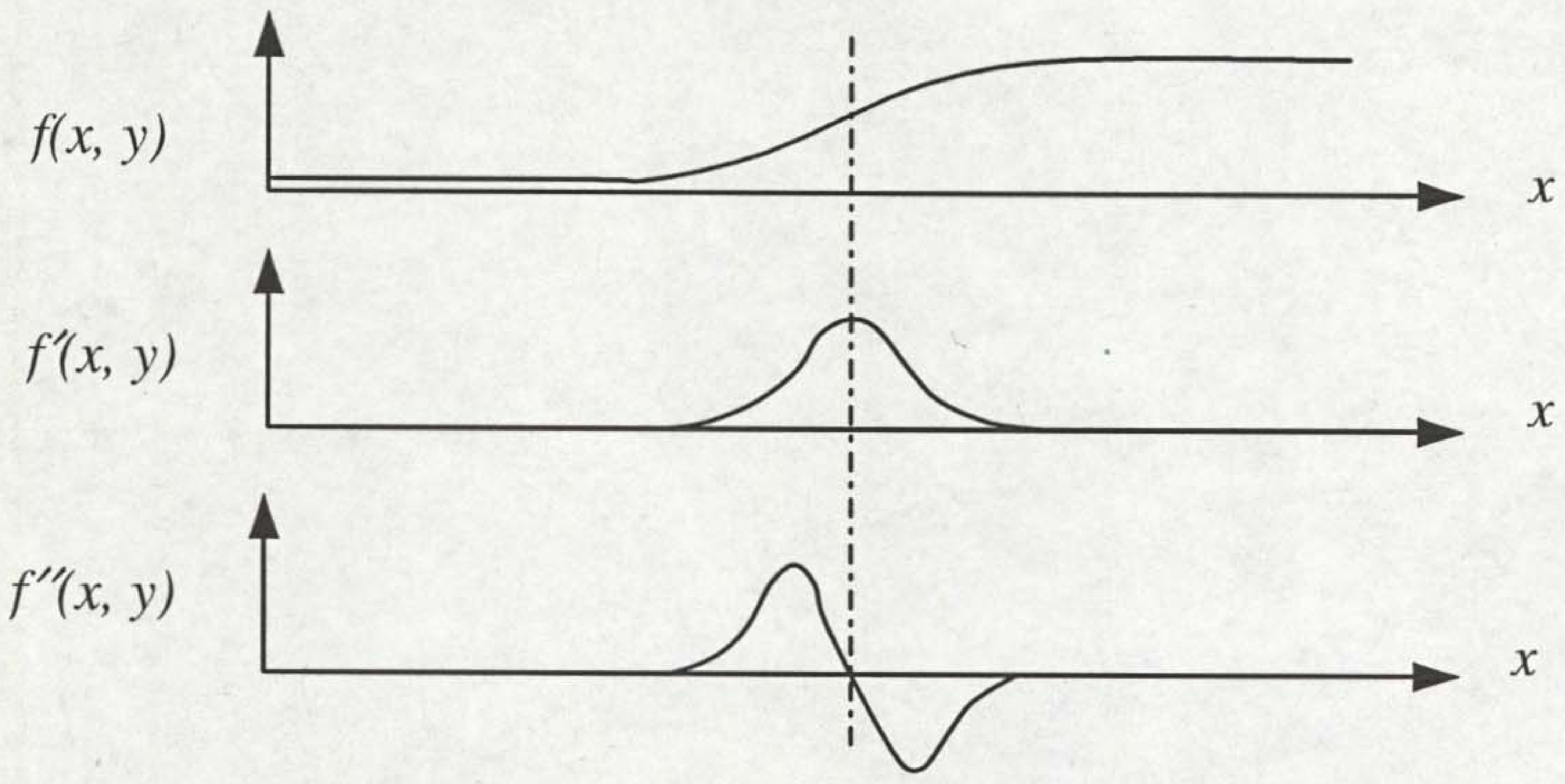

Figure 3. 2 Step Edge and its First and Second Derivatives

The commonly used edge detectors i.e. Roberts, Sobel and Prewitt operators (Table 3.1), look for the high gradient magnitude using a threshold. They use separate component masks in different directions. Using these edge detectors, only edge areas can be extracted rather than the exact edge centre, also they are very sensitive to noise. The more complex, second generation edge detectors, which combine properties in a single operation or mask, attempt to detect edges in the presence of noise. They are methods developed by Marr & Hildreth [3.1] and Canny [3.2]. In their methods, Gaussian smoothing is employed to reduce noise. As a result, another problem is raised -- scale, which is to use different operators to function in different scales.

Many image processing work locally, theoretically at the level of individual pixels, edge detection methods are an example. The essential problem in such computation is scale. Edges correspond to the gradient of the image function, which is computed as a difference between pixels in some neighbourhood. There is seldom a sound reason for choosing a particular size of neighbourhood, since the 'right' size depends on the size of the objects under investigation. The idea of scale is fundamental to Marr's and Canny's edge detection techniques, where different scales are provided by different sizes or different standard deviations σ of the Gaussian filter masks. The aim is not only to eliminate fine scale noise but also to separate events at different scales arising from distinct physical processes.

Table 3.1 Edge Detection Operators

Roberts Operator	$G_x = \begin{matrix} 1 & 0 \\ 0 & -1 \end{matrix} \qquad G_y = \begin{matrix} 0 & -1 \\ 1 & 0 \end{matrix}$
Sobel Operator	$S_x = \begin{matrix} -1 & 0 & 1 \\ -2 & 0 & 2 \\ -1 & 0 & 1 \end{matrix} \qquad S_y = \begin{matrix} 1 & 2 & 1 \\ 0 & 0 & 0 \\ -1 & -2 & -1 \end{matrix}$
Prewitt Operator	$S_x = \begin{matrix} -1 & 0 & 1 \\ -1 & 0 & 1 \\ -1 & 0 & 1 \end{matrix} \qquad S_y = \begin{matrix} 1 & 1 & 1 \\ 0 & 0 & 0 \\ -1 & -1 & -1 \end{matrix}$

A Marr-Hildreth mask is a combination of a Gaussian smoothing function and a Laplacian difference operator. It has the following format,

$$\begin{aligned} M(x, y) &= \nabla^2 G \\ &= \partial^2 G/\partial x^2 + \partial^2 G/\partial y^2 \end{aligned}$$

$$\text{where } G = exp((x^2 + y^2)/2\sigma^2)$$

The Gaussian part of the operation is a more considered smoothing operation than the smoothing component of the Sobel operator and overall the method works better than simple gradient edge detection, particularly when edges are more blurred and the noise level is high. The scale σ is the standard deviation of the Gaussian and controls its width. The higher the value of σ the greater the smoothing and at the same time the more the image is blurred. The Laplacian is used to detect edges by finding zero crossings, the key idea being that edges as zero crossings are easier to detect than edges as extrema, which is the case with derivative images.

The Canny edge detector, reported in 1986, also uses Gaussian smoothing. This operator detects edges at zero crossings of the second directional derivative of the Gaussian smoothed image in the direction of the gradient (where the magnitude of the gradient must be above a threshold). That is:

$$C(x, y) = \partial^2 G/\partial n^2$$

where n is the direction of the gradient of the smoothed image.

3.2 Gaussian Filters

Gaussian filters are a class of linear smoothing filters with the weights chosen according to the shape of a Gaussian function. The Gaussian smoothing filter is a very good filter for removing noise drawn from a normal distribution. The zero-mean Gaussian function in one dimension is:

$$G(x) = exp(-x^2/2\sigma^2)$$

To apply a Gaussian filter to digital image processing, a one-dimensional discrete approximation to a Gaussian is provided by the coefficients of the binomial expansion:

$$(1+x)^n = (n\ 0) + (n\ 1)x + (n\ 2)x^2 + \ldots + (n\ n)x^n$$

where n refers to the point number in a filter. For example, the five-point approximation is {1, 4, 6, 4, 1}. This technique works well for filter sizes up to around n = 10. For larger filters, the coefficients in the binomial expansion are too large for most computers. However, arbitrarily large Gaussian filters can be implemented by repeatedly applying a smaller Gaussian filter.

Another approach in designing Gaussian filters is to compute the mask weights directly from the discrete Gaussian distribution to obtain a kernel or mask, for which the value at [0, 0] equals 1.

For a specific application, to obtain the best filtering result using a Gaussian filter, scale space analysis is needed to find the optimum filter. That is to select different filters with different scale σ or different point number n.

3.3 Pool Edge Detection

A weld pool is the molten part of a weld during welding. It moves with the torch and forms a special object in the scene. Because of the different existent states, an edge can be seen between the pool and the surrounding solid metal in the illumination of the arc. The weld pool is also different from an object in the real world due to the following reasons: (1) It is a flexible object with continual changes in shape and size under different welding conditions. (2) The images of the weld pool viewed from the camera change drastically for different welding processes and different welding materials because of the arc property and surface reflection change. Therefore, the edges of weld pool represent different features in different cases. As a result of this, the detection of weld pool edges has been categorised into three cases: AC-TIG on aluminium (TA), DC-TIG on stainless steel (TS) and MIG welding on mild steel. Figure 3. 3 shows the images of these three cases and the corresponding intensity changes in the direction perpendicular to the pool edge. The weld is being viewed ahead of the electrode as the workpiece travels away from the camera.

As can be seen from Figure 3. 3, a roof edge is presented for TA welding and step edges or ramp edges for TS welding and MIG welding. Pool edge detection is conducted in one dimension along the black horizontal line (Figure 3. 4) from pool centre to two sides as two dimensional edge detection is time consuming and not necessary for pool monitoring. Pool edge detection results are given in Figure 3. 4. The white crosses on the black detection line are the detected pool edges. The pool width is obtained by calculating the distance between these two white crosses.

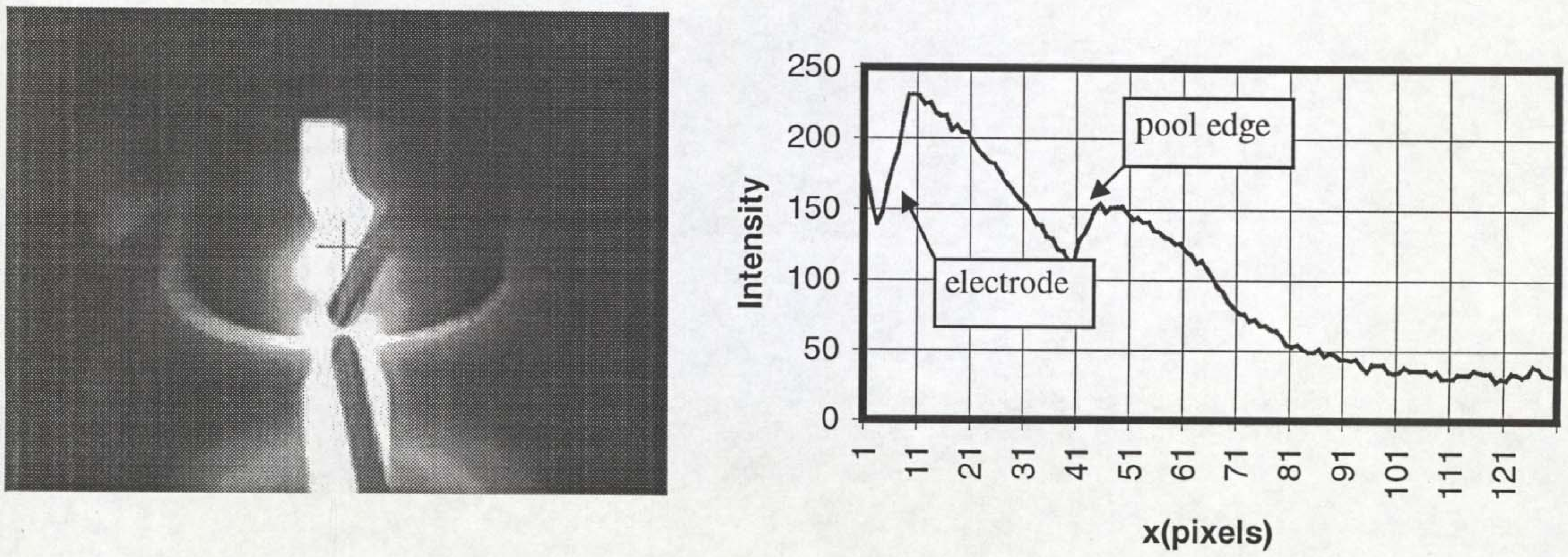

(a) TA weld pool

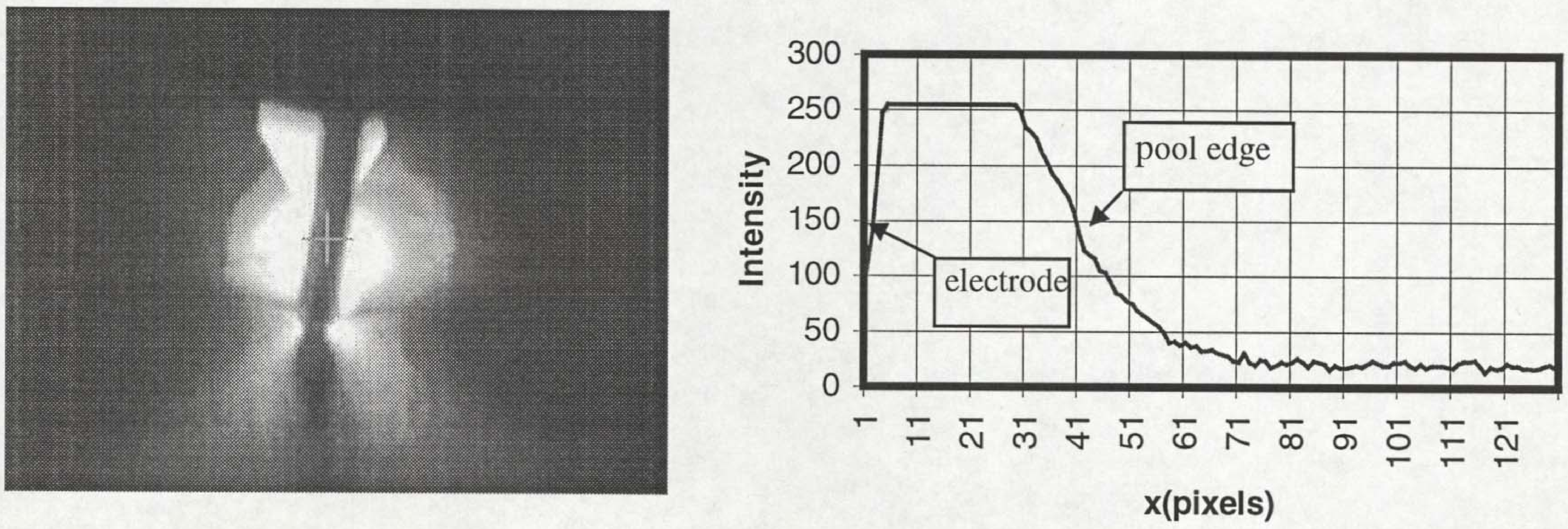

(b) TS weld pool

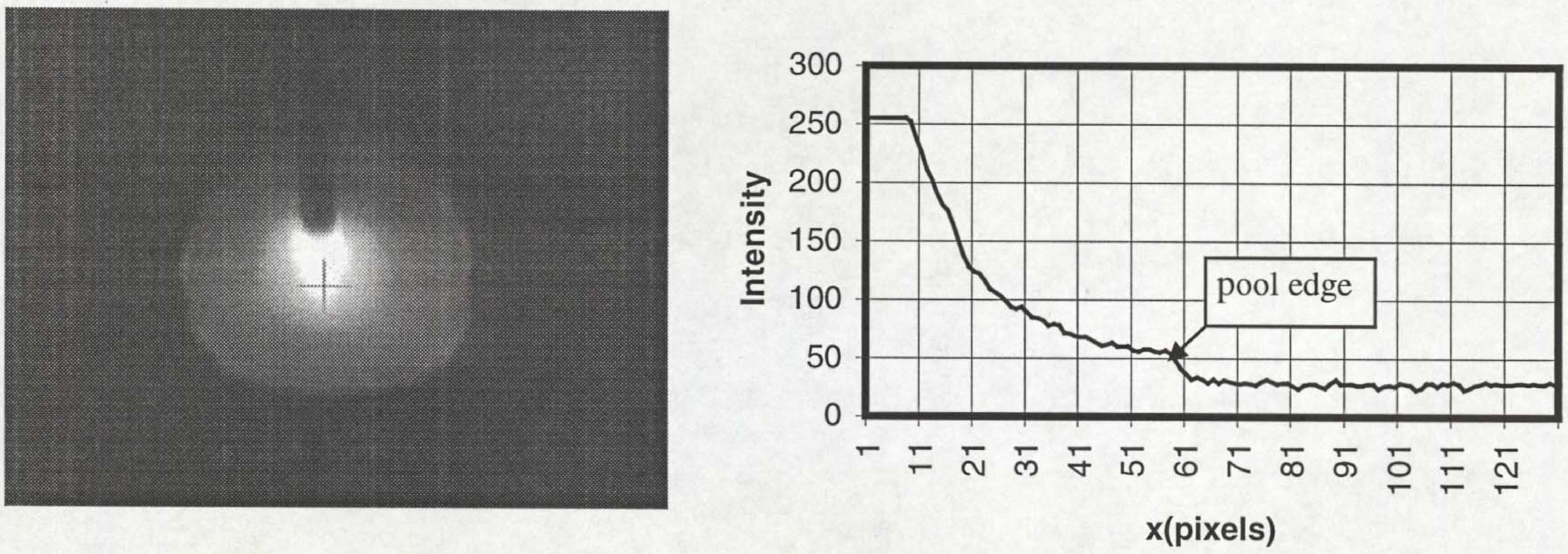

(c) MIG weld pool

Figure 3. 3 Weld Pool Images and Intensity Distributions

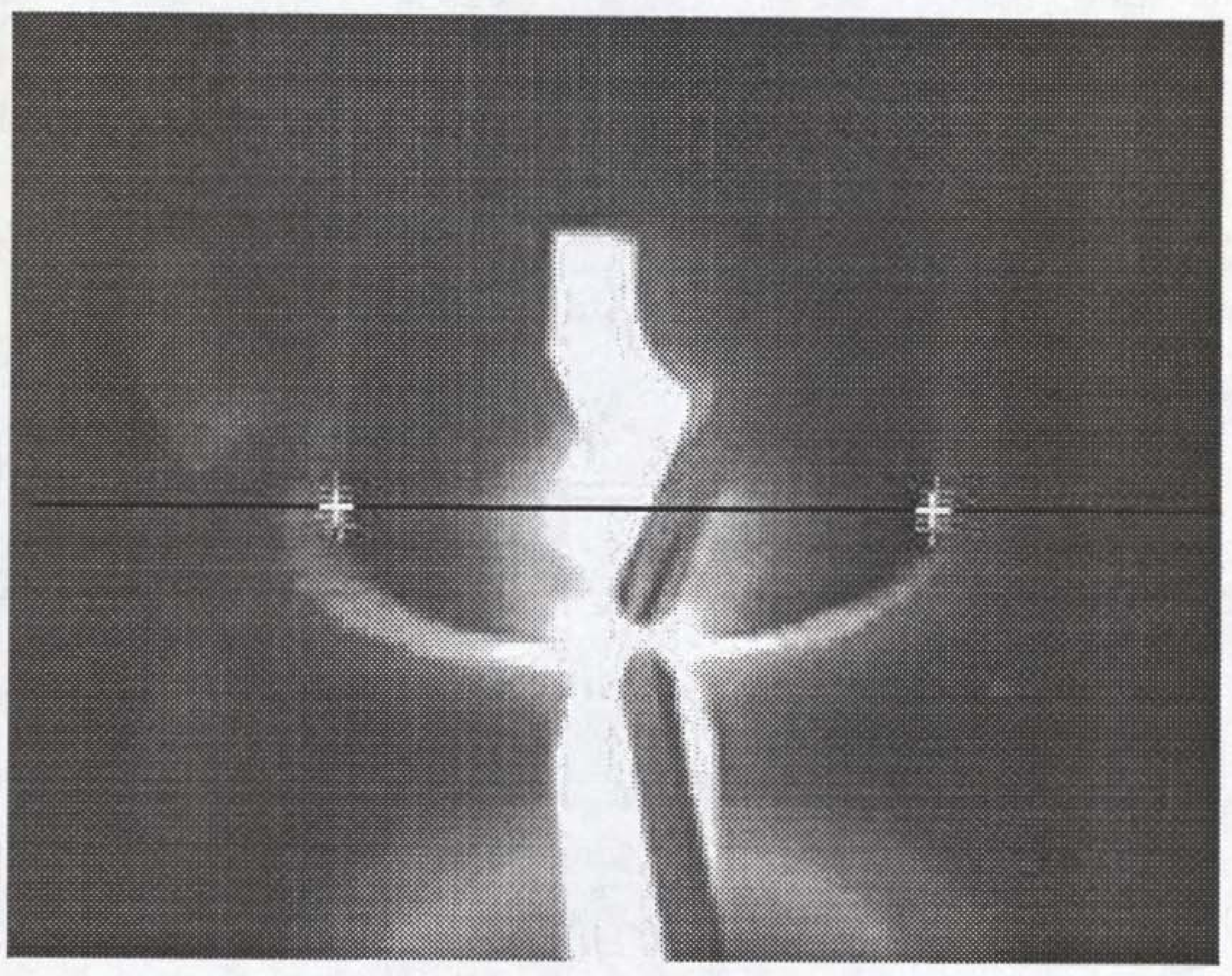

(a) TIG on Aluminium

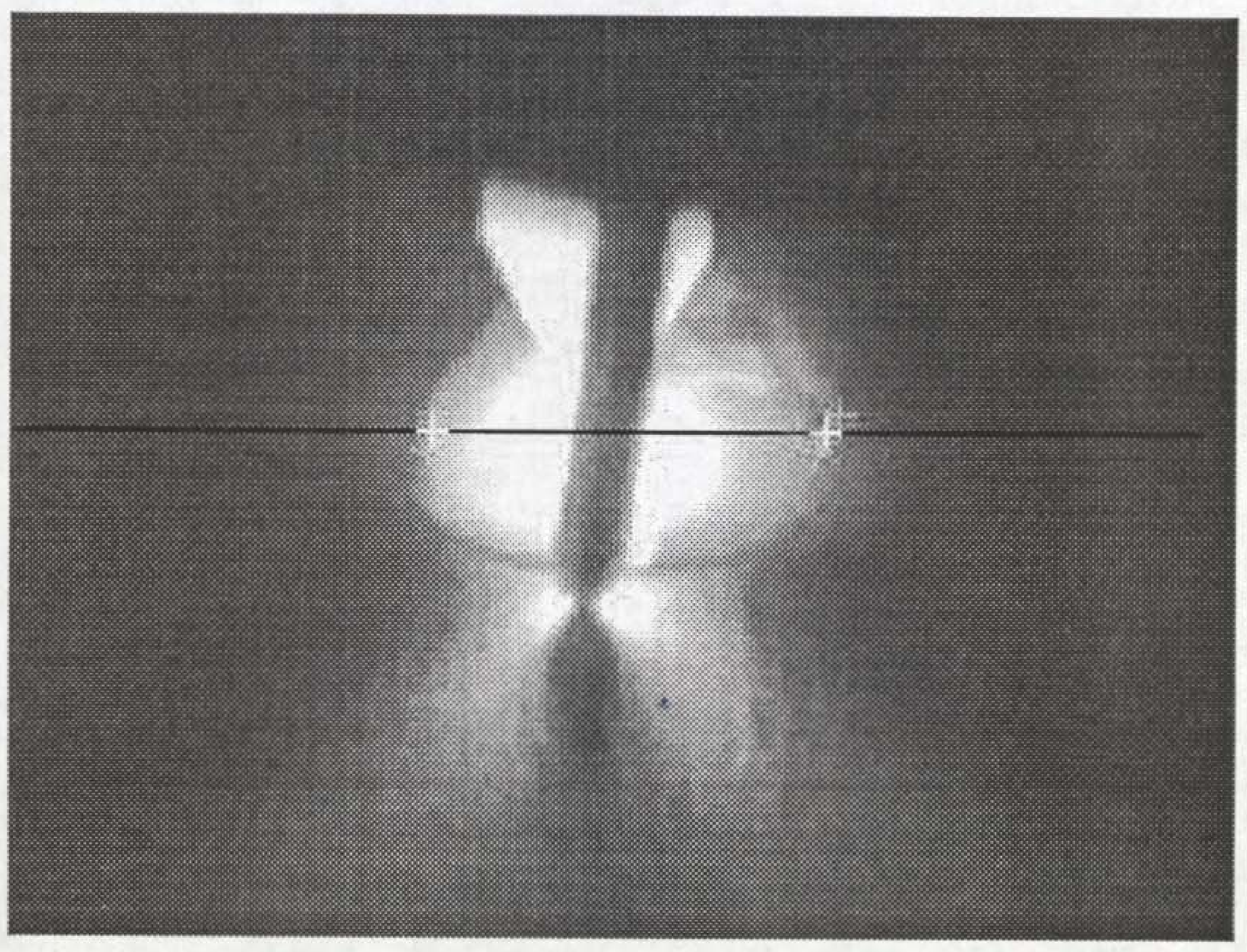

(b) TIG on Stainless Steel

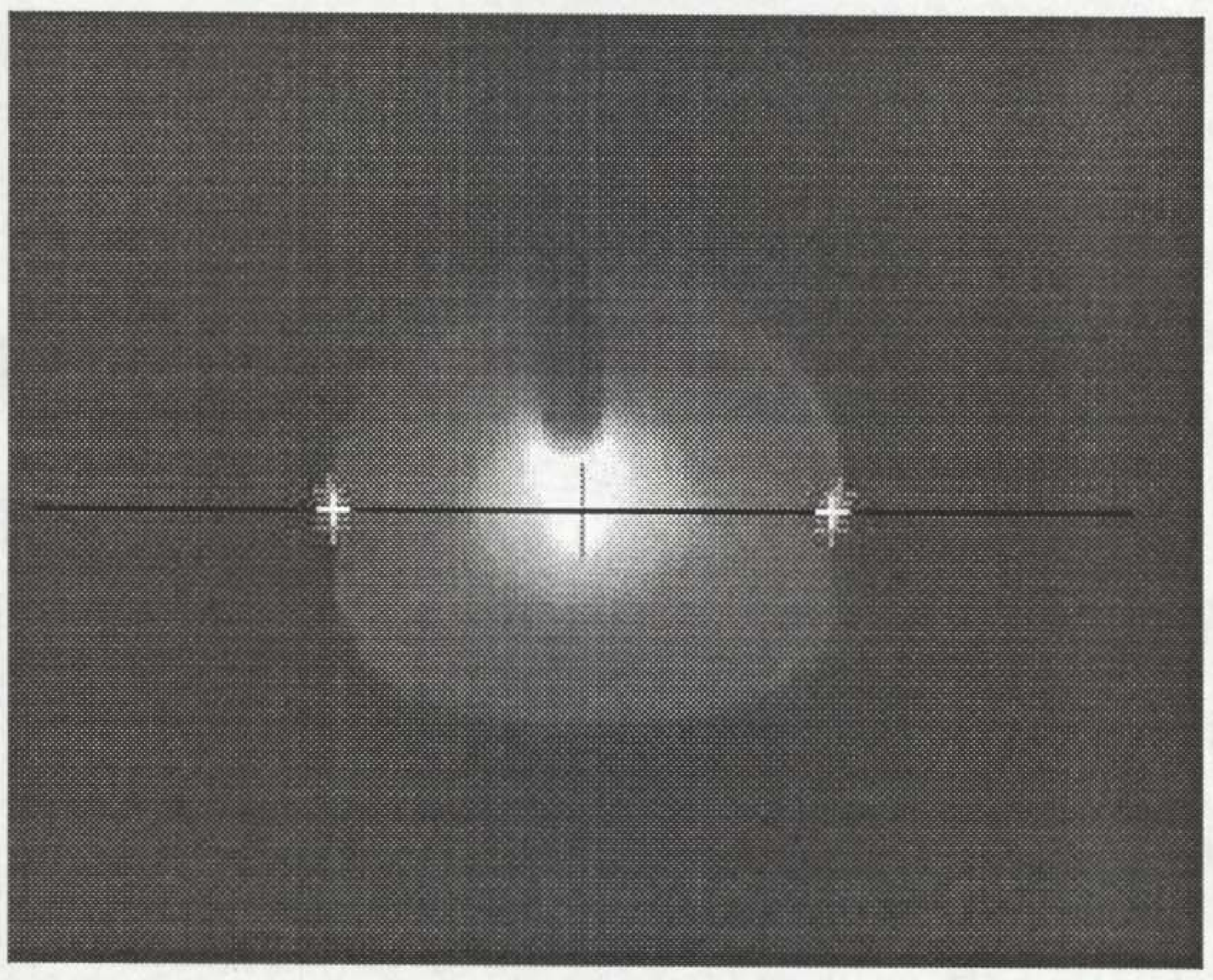

(c) MIG on Mild Steel

Figure 3. 4 Pool Edge Detection

The procedure for the detection of the pool edge is described as follows:

1. Determination of the pool centre

Although it's very easy for a human to locate the centre of the weld pool, it is difficult to code as an algorithm. It has been experimentally observed that the centre of the weld pool is in line with the position of the highest brightness when the arc is initiated. Consequently, this is the basis of the software algorithm. Good results have been obtained when "Lift TIG" is used to initiate the arc. However, it does not work well in other situations. Thus, manual selection for the centre point is made using the mouse and cursor. However, due to the camera setup, the centre position of the weld pool can be stored for use in subsequent welds.

2. Gaussian filtering

Since derivative computations based on intensity values of only two points are susceptible to noise and other vagaries in discrete computations, filtering is commonly used to improve the performance of an edge detector with respect to noise. However, there is a trade-off between edge strength and noise reduction. More filtering to reduce noise results in a loss of edge strength. Three Gaussian filters, with different scale σ, $G_1(1,2,1)$, $G_2(1,4,6,4,1)$ and $G_3(1,3,7,9,7,3,1)$, are investigated on the weld pool images. Figures 3.5-3.7 shows the results of these three filters and the corresponding gradients for TA, TS and MIG images respectively. It can be seen that with the increase of σ, fine degrees of fluctuations in both intensity and its gradient are removed, confirming some improvement in the signal to noise ratio as a result. The best smoothing is obtained using filter G_3 and meanwhile edge strength becomes weak. Therefore, to keep the balance between edge strength and smoothing, filter G_2 was used as the edge detector. It reduces the background noise outside the weld pool significantly and keeps the edge strength detectable, conforming the highest signal to noise ratio among the three filters. Furthermore, good localization is also obtained.

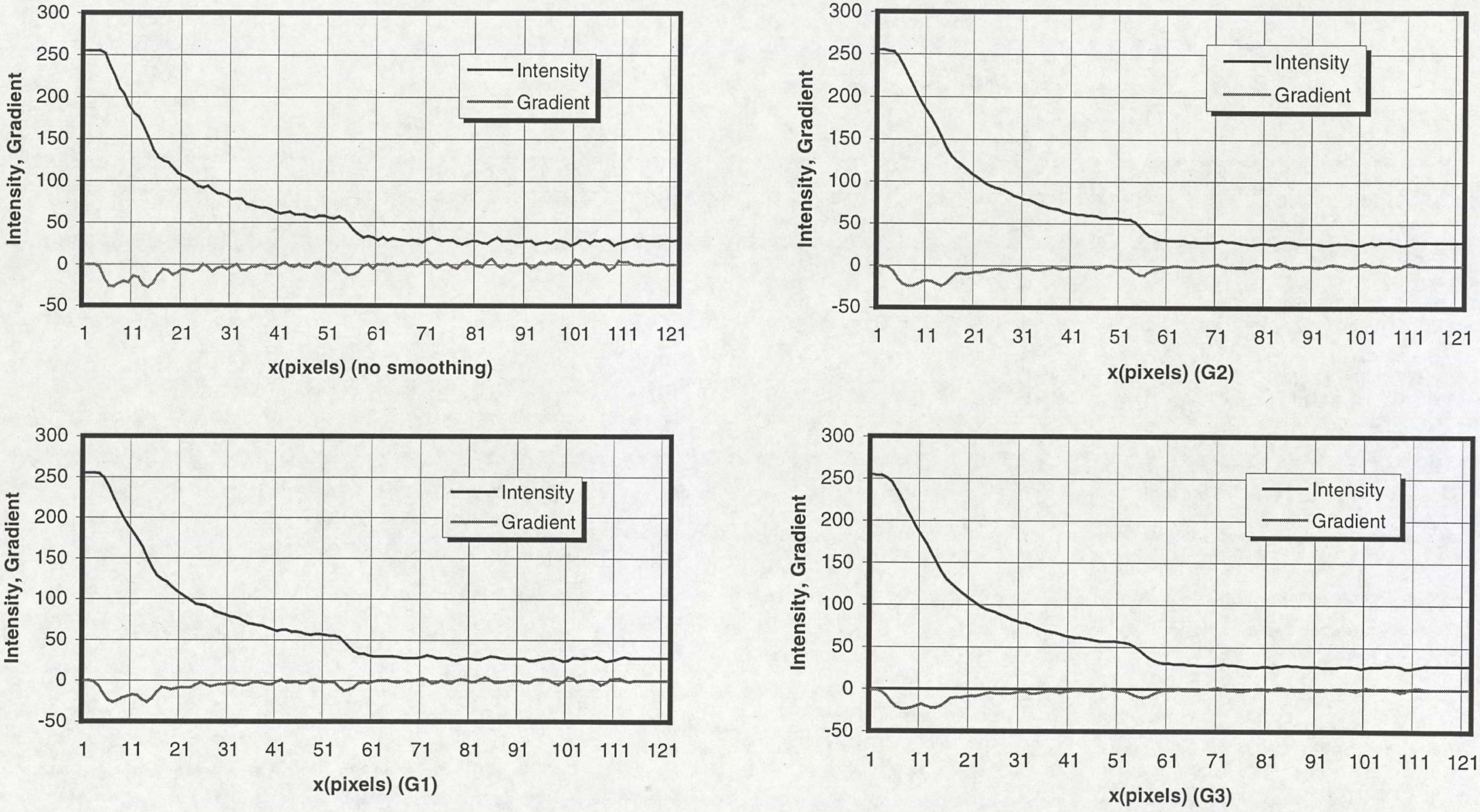

Figure 3. 5 Gaussian Filters on MIG Image

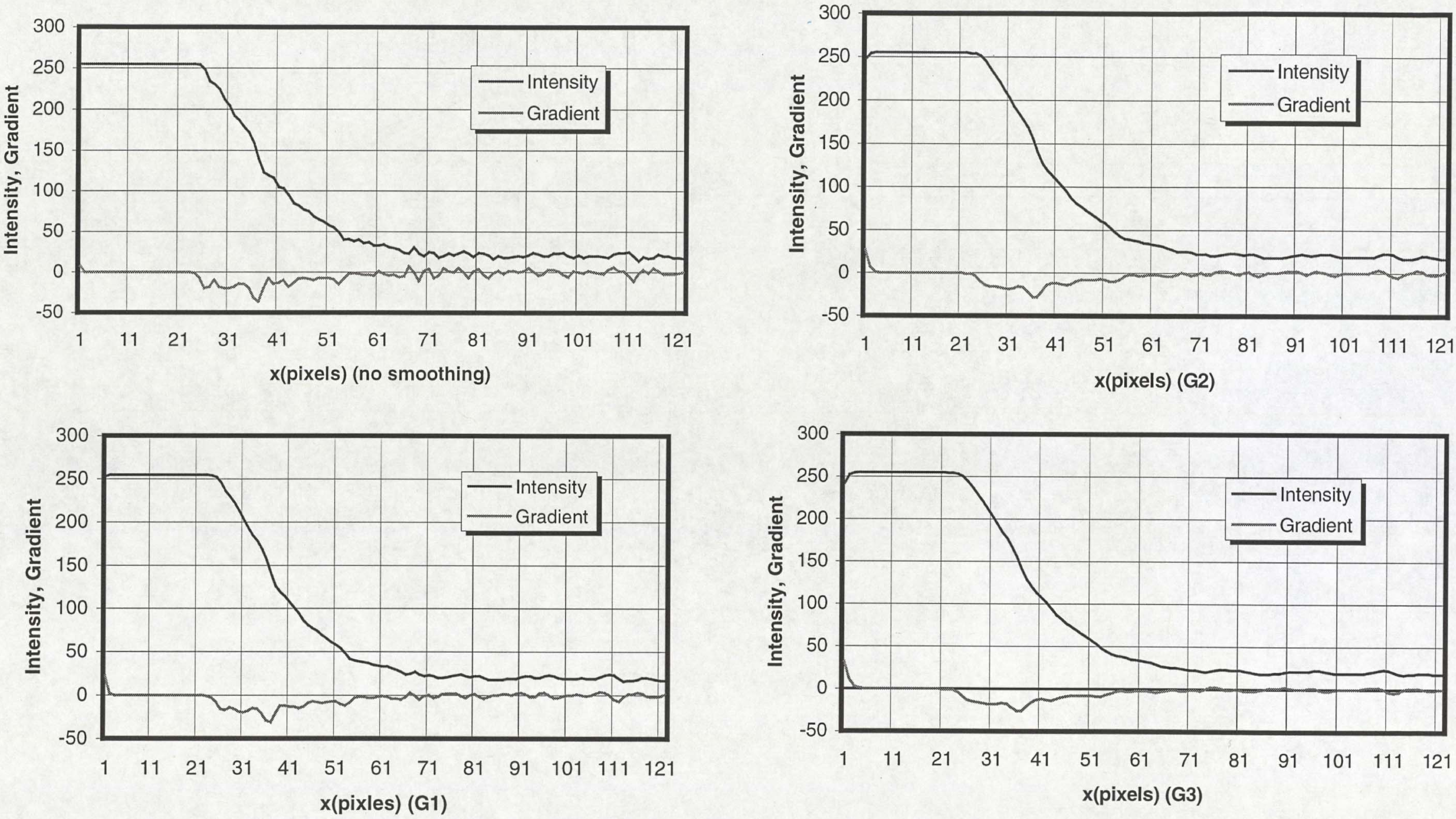

Figure 3. 6 Gaussian Filters on TIG-Stainless Steel Image

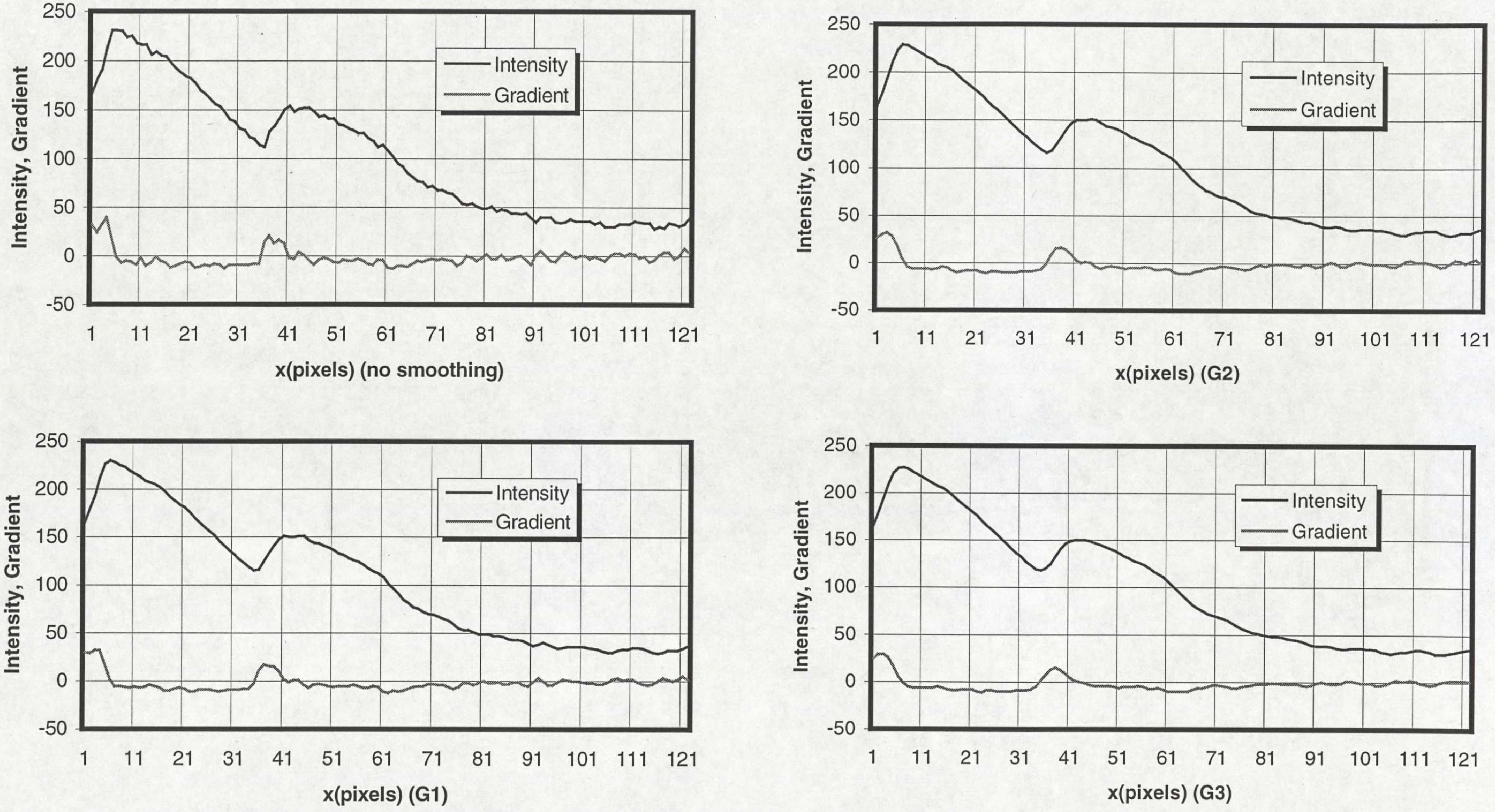

Figure 3. 7 Gaussian Filters on TIG-Aluminium Image

3. Pool edge detection

As discussed in section 3.2, the methods developed by Marr & Hildreth, and Canny detect edges at zero crossings of the Laplacian and the second directional derivative of the Gaussian smoothed image respectively. But in one dimension, these two operators are the same. Local extrema in the first derivative are associated with the edges. For a digital image, the derivatives are approximated by differences. These can be implemented with a simple convolution mask (-1, 1) or (-1, 0, 1). Using the first mask, it is actually the approximation to the gradient at the interpolated point (i+1/2). This fact may lead to some confusion. Therefore, an alternative approach is to use the second mask and calculate the gradient about the centre pixel.

As can be seen in Figures 3.5-3.7, there are many local extrema in the first derivative. However, not all of these points are edges for a particular application. Therefore, some method should be used to determine which points are edge points. The windowing method was used in the research to avoid the influence of the arc and the filler wire in the centre part. The windowing region has been limited to an area of interest whose size has been determined experimentally.

For TA welding, edges are represented by local maxima of the first derivative within the window of interest, while for TS and MIG welding, local minima are presented at the edges. In addition, these extrema at the edges are thresholded to decide if it is the real edge of the pool, the most significant edge along the detection line. In general, two criterions are applied to extract the pool edge:

- $\Delta g_k = \max|\Delta g_i|$, where Δg is the first derivative of image intensity. k is the edge point.
- $\Delta g_k > T_{\Delta g}$, where $T_{\Delta g}$ is the threshold.

4. Temporal filtering

With the previous algorithm, there is still a possibility of mis-detection. According to the continuity of the edge, a temporal filter is applied by monitoring the degree of a change Δp in edge positions between the value of the current frame and the average from the previous n frames:

$$\Delta p = p_i - \frac{1}{n} \sum_{j=i-(n-1)}^{i-1} p_i$$

If *Δp* exceeds the allowance set beforehand, a judgement is made that the result is caused by noise and has to be thrown away. Then the average from the previous frames is used to replace the current value.

5. Spatial filtering

In order to further improve the robustness of the detection, five edge points are detected at either side of the pool instead of only one. This means that four other lines, two above the centre detection line and two below it, are searched. After these five edge points are extracted about the centre detection line, a selected average is conducted on them. First of all, the average of these five points is calculated and the point with the biggest distance from the average is thrown away. Then the average of the four remaining points is calculated and similarly the worst one is thrown away. After this the final result is obtained by averaging the three remaining points. The final edge points are displayed by the white crosses in Figure 3. 4.

6. Averaging smoothing

After the temporal and spatial filters are applied, there are still jumps in pool width, which are assumed to be impulse noises. These can be seen on the red curve displayed in Figure 3. 8, where the x direction represents the time or frame sequence. To remove these noises and, furthermore, to avoid deterioration of control performance, averaging smoothing is conducted by taking the average of several successive frames. The number of frames n to be averaged is determined experimentally based on the consideration of both smoothing and the performance of control. When n is chosen to be small, not enough smoothing is obtained, while n is large, over smoothing may occur and control procedure might become insensitive to the real fluctuation of pool width, thus the dynamic property of the control system will be worsen. $n = 8$ was chosen as the default value in this application, but it can be adjusted, on line, according to the performance of control system. The blue curve in Figure 3. 8 shows the result of averaging smoothing with $n = 8$ for MIG welding.

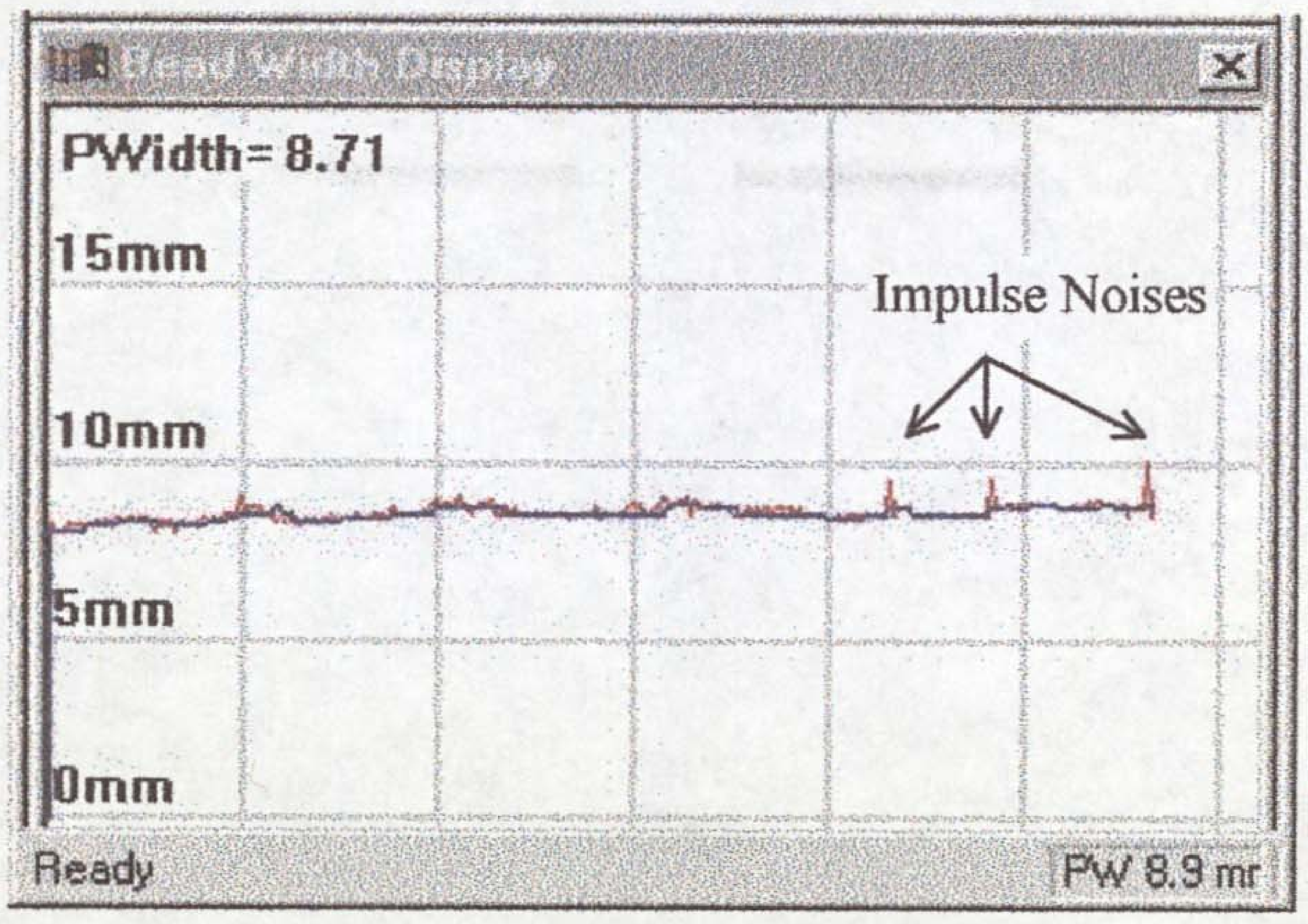

Figure 3. 8 Averaging Smoothing

3.4 Pool Contour Approximation

Currently pool monitoring is implemented by the pool width measurement and control. In this way, only the pool width is extracted and related to the welding parameters. Pool shape and area are also very important with respect to welding parameters. Therefore the extraction of pool contour is required for further analysis of the relationship between pool shape or area and welding parameters.

The algorithm for detecting the pool edge was explained in the previous section. Using the same algorithm, several typical points on the pool edge are extracted instead of detecting the complete edge of weld pool, as shown in Figures 3.9-3.10, along the spider-like black lines originated from the pool centre. Then, the edge contour could be approximated using curve approximation. There are several ways to approximate curves, depending on the reliability with which edge points can be grouped into contours. If it is certain that all of the edge points linked into a contour actually belong to the contour, then total least-squares regression can be used to fit a curve to the edge points. If some grouping errors are present, then robust regression methods [3.3] can be used for computing the curve approximation. Finally, if the grouping of edges into contours is very unreliable, or if the edges are so scattered that grouping cannot be easily done using the edge linking or following methods discussed previously, then cluster analysis techniques must be used to perform grouping and curve fitting simultaneously. An excellent example of an algorithm for grouping and fitting scattered edge points is the Hough transform. The principle of the Hough transform is explained in Chapter 5.

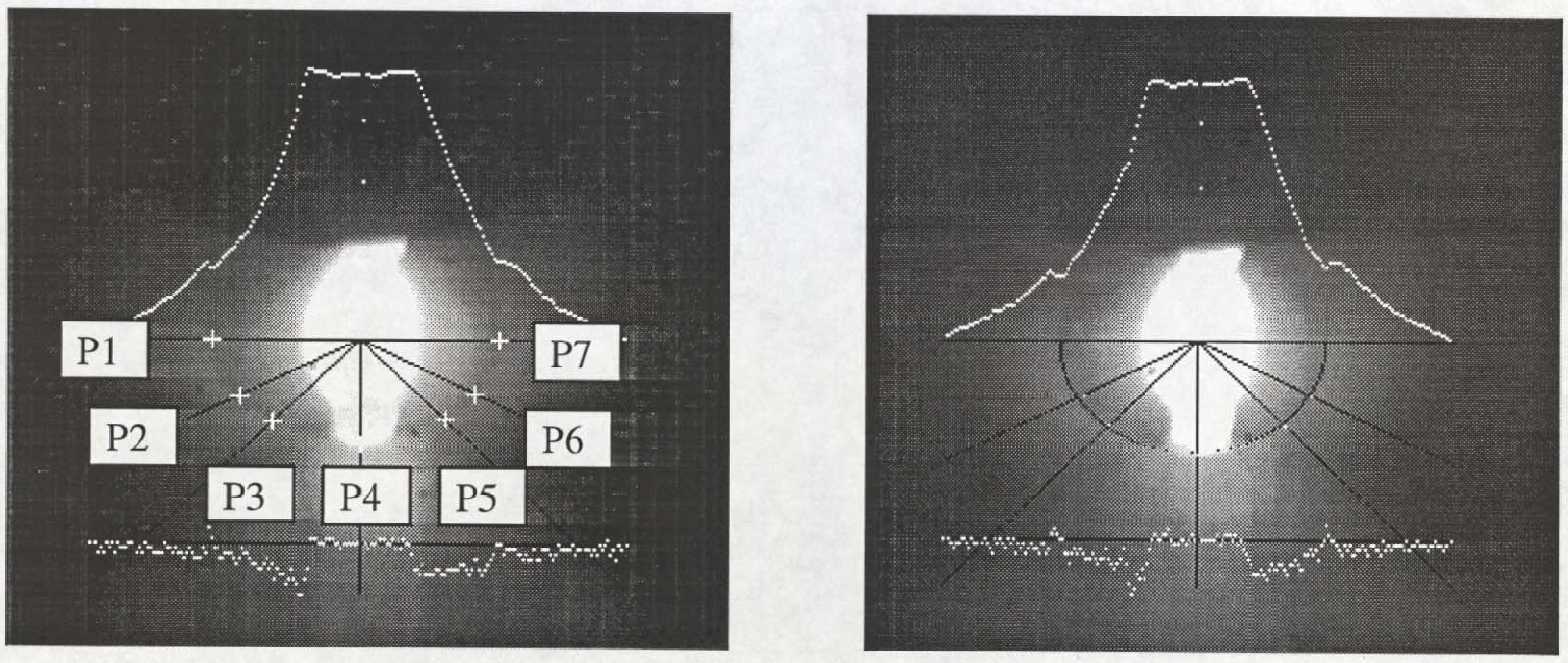

(a) (b)

Figure 3. 9 Multi-line Detection on TS Image

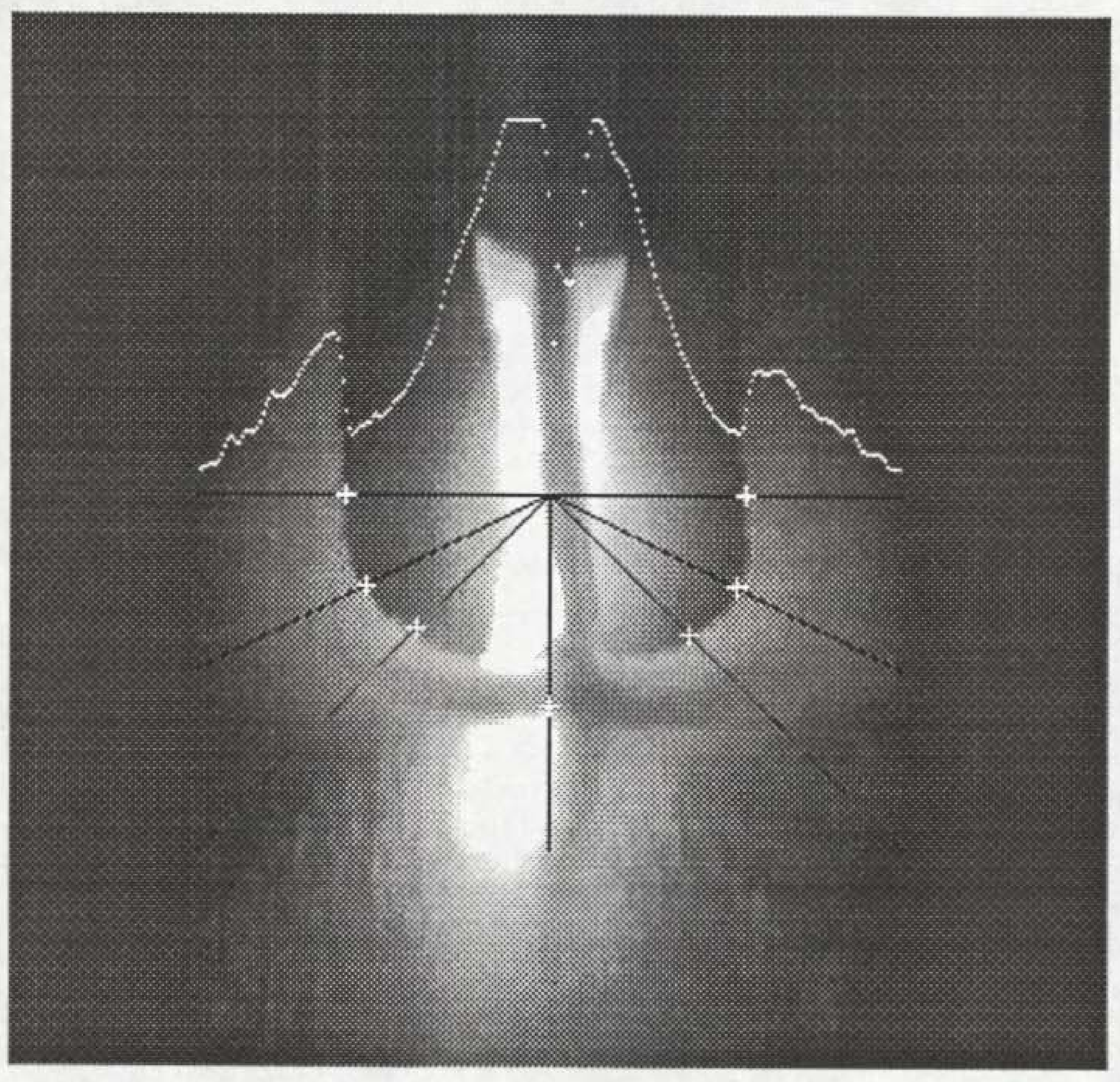

Figure 3. 10 Multi-line Detection on TA Image

Classical linear regression minimizes the difference between a data point and the model in only one dimension, the dimension of the dependent variable. In machine vision, lines and other curve models are fitted to edges using total regression, which minimizes the sum of the squares of the perpendicular distances of the data points from the regression model.

Analysing the images of weld pool, it has been found that the front half of the weld pool is geometrically similar to a half-ellipse. Therefore ellipse model is used to describe the weld pool:

$$\frac{(x+\zeta)^2}{\alpha^2}+\frac{(y+\eta)^2}{\beta^2}=1$$

where (ζ, η) denotes the centre of the ellipse, and α and β are the half-lengths of the major and minor axes, respectively. Using least square regression for this model is more complicated than for a linear model. To make it simple, four edge points were used to formulate four equations for the four unknown ellipse parameters, ζ, η, α, β, provided these edge points belong to the contour. They are calculated by $\zeta = x_1+(x_7-x_1)/2$, $\eta = y1$ and $\alpha= (x_7-x_1)/2$, while the estimation of β is not straightforward since the edge just below the arc is not easy to obtain because of the arc light, therefore edge points P_3 and P_5 are used to calculate β. Figure 3. 11 shows the ellipse model, which almost totally matches the surface shape of the weld pool in MIG welding. Once this model is established, the crucial features of weld pool geometry such as bead width, half-length as well as the ratio of width and length, which closely correlate to penetration, can be evaluated. Similarly, the back half of weld pool, when images are captured from behind the arc, can also be described as a half ellipse, as shown in Figure 3.12, but the parameters in the equation are quite different from those of the front half.

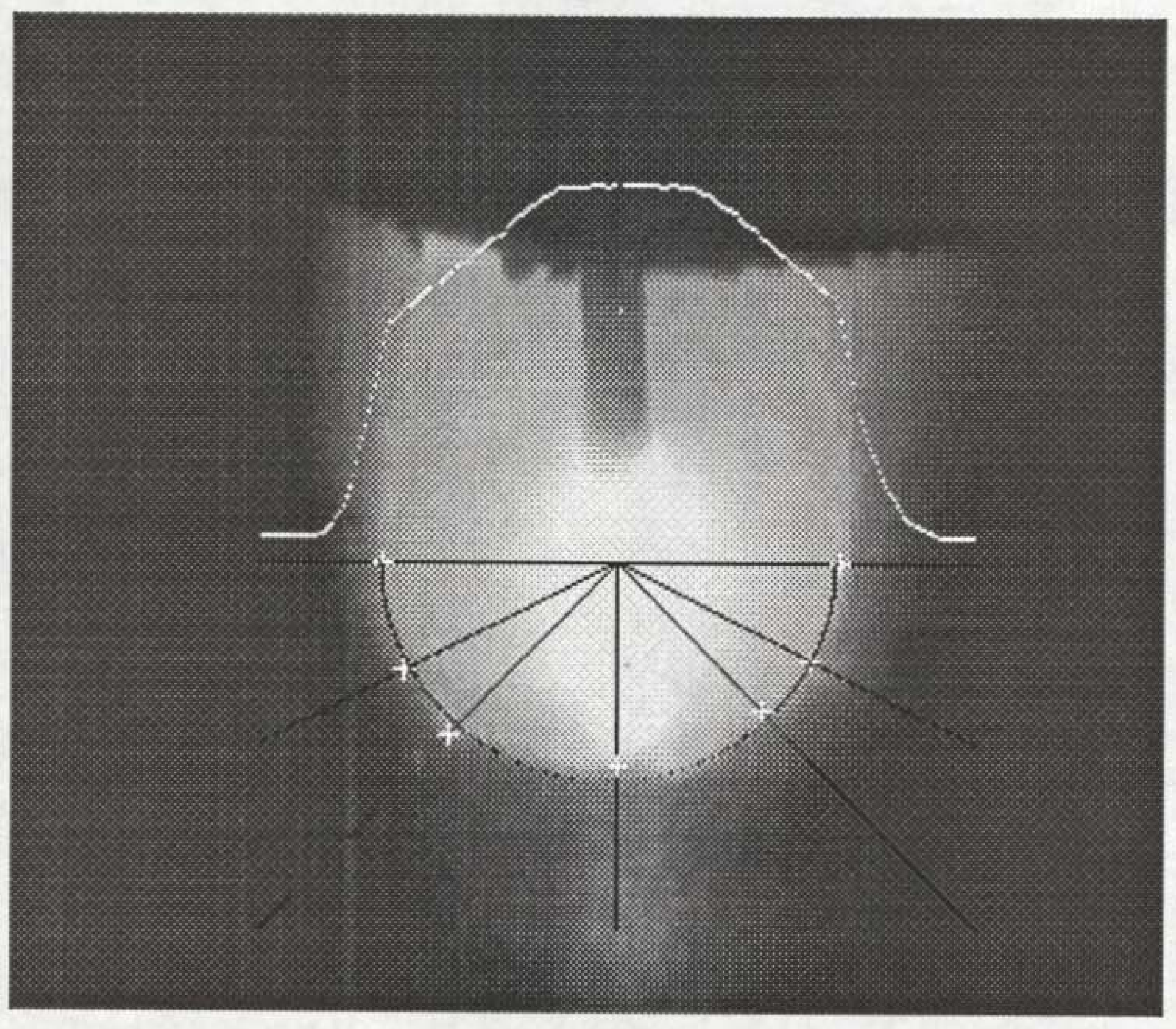

Figure 3. 11 Ellipse Model of MIG Weld Pool

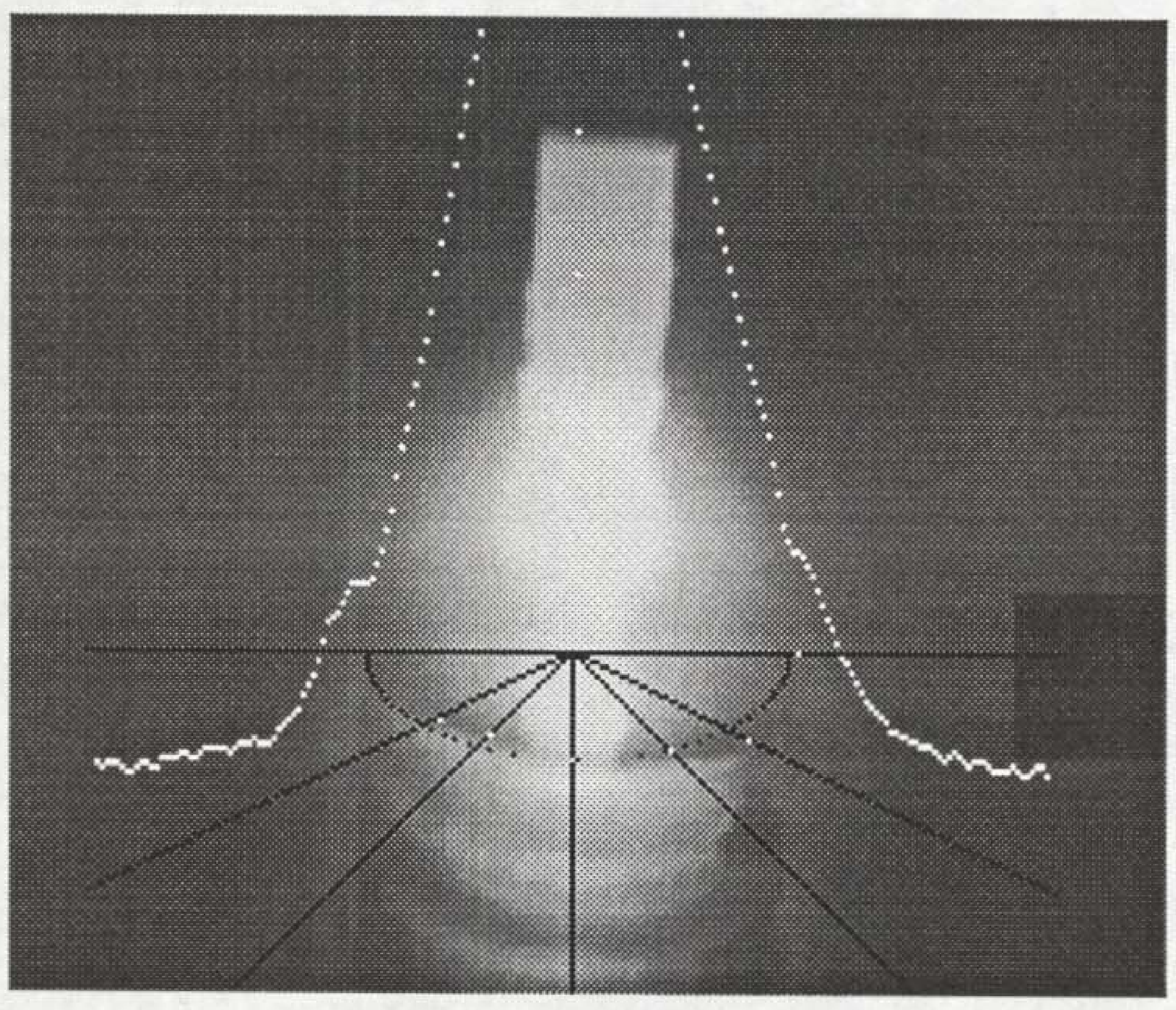

Figure 3. 12 Behind View of TIG Weld Pool

CHAPTER 4 IMAGE PROCESSING FOR SEAM TRACKING

Two seam tracking methods have been investigated in this research, both of them are vision based. One of them uses a laser line to reflect the profile of the seam and extract seam parameters based on the analysis of the laser line image. The principle of this method was introduced in Chapter 2. The other one recognises the seam by directly viewing the dark line in front of a butt weld pool, in which no laser line is used. This chapter discusses these two methods, with more attention being placed on the first one.

4.1 Seam Tracking Using a Laser Line

This section will introduce image processing algorithms developed for laser line images on three typical joint modes: butt joint, V preparation and lap joint.

4.1.1 The Basis of the Seam and their Laser Line Images

Based on the thickness of plates to be welded, there are three kinds of commonly used joint modes in arc welding. They are the butt joint, the lap joint and the V prep, as shown in Figure 4. 1, along with the corresponding laser stripe images captured by this sensing system. V prep grooves are used in the welding of thick plate sections (3-20 mm) where the thickness is so great that full penetration of the weld cannot be achieved in a single pass. The groove is prepared so that full penetration can be achieved on the root run and the rest of the weld is then performed with the addition of filler material to build up the bulk of the weld. The butt joint is used on thin plate, usually less than 3 mm, where the parts can be fused, with full penetration, in a single pass. The lap joint is used mostly on thin plate in some special constructions.

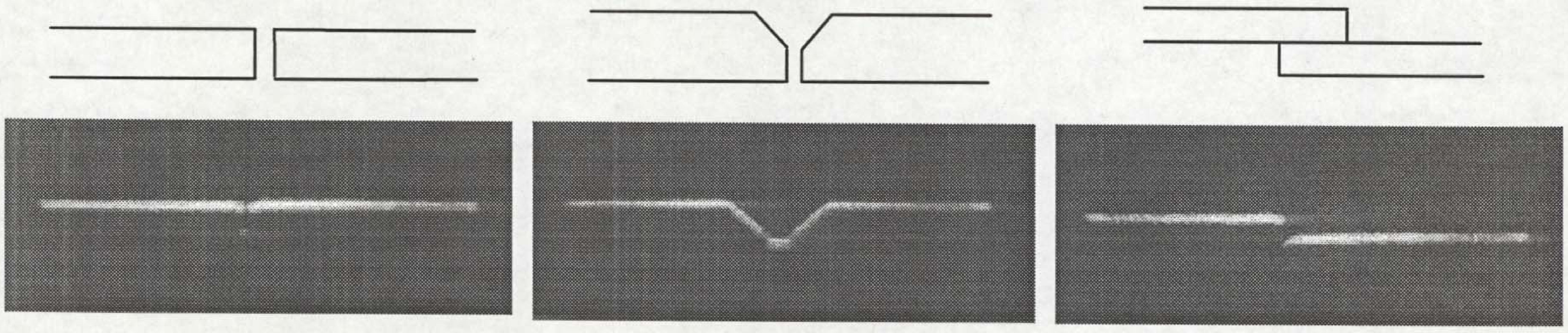

Butt Joint V Preparation Lap Joint

Figure 4. 1 Weld Joint Modes

It can be seen from Figure 4. 1 that the image patterns vary for the three joint modes. For V prep and lap joints, obvious features are presented around joints while for butt joints no significant changes occur, which brings about the difficulty for recognition. Consequently different image processing algorithms are required.

4.1.2 Corner Detection

The laser line is actually a planar curve in an image. The features of the seam are presented by the corners on this planar curve. Therefore, the seam detection from the laser line image is actually the problem of corner detection. In this section, some elements of corner detection are reviewed. The review includes the Freeman chain code, the measurement of discrete curvature and the region of support, as well as adaptive smoothing.

4.1.2.1 Freeman Chain Code

A digital curve C can be denoted by a sequence of n integer-coordinate points,

$$C = \{p_i = (x_i, y_i),\ i = 1, \ldots, n\},$$

where p_{i+1} is a neighbour of p_i.

The Freeman chain code of C consists of n vectors, written as $\{c_i, i = 1, 2, \ldots, n\}$, where

$$c_i = \overline{p_{i-1}\, p_i}$$

and c_i takes on an integer f

$$f = \{0, 1, \ldots, 7\},$$

as shown in Figure 4. 2, where $(1/4\pi)f$ is the angle between the x axis and the vector. The chain of C is defined by $\{c_i, i = 1, \ldots, n\}$. All integers are of modulus n.

3	2	1
4	$P_{i\text{-}1}$	0
5	6	7

Figure 4. 2 Freeman Code

4.1.2.2 The Discrete Curvature

A corner is an isolated curvature change, for which the tangent orientation to the contour is discontinuous. Corner detection is usually implemented by detecting local maxima of curvature. There are two major problems with corner detection. One is the precise definition of discrete curvature, the other is the determination of the region of support for the computation of the curvature. We are working in a quantized plane in which the continuous curvature concept, based on derivatives, cannot be applied. In the Euclidean plane, the curvature κ of a plane curve at a point p is defined as the rate of change of the angle ψ of the slope of the tangent at p versus the traversed arc length l, $\kappa=d\psi/dl$. Nevertheless, for a digital curve, this consideration cannot be directly applied, since slope changes are not arbitrarily small. In the case of the Freeman chain code of order 8, the adjacent slopes can only differ in multiples of 45°. This is overcome using significance measurements described as follows.

Smoothing methods are used by a number of authors [4.3][4.4][4.5] to compute a smoothed version of the discrete curvature. For example, the slope at p_i can be computed as $(y_{i+k} - y_k)/(x_{i+k} - x_k)$ for $k>1$, rather than simply using the first difference ($k=1$). For each point p_i, of the contour, a support region will be found as the set of points in its vicinity that will be used to evaluate the different discrete curvature measurements considered. k is defined as the radius (number of points from the central point p_i, in which the discrete curvature is computed, to the extremes) of the support region $S(p_i)$. It is selected based on the level of detail represented by the digital curve. If the support region is set to be very large, the algorithm will miss fine details, and if it is very small, it will detect a lot of redundant points with fine details. This is a fundamental problem of scale because the features describing the shape of a curve vary enormously in size and extent, and there is seldom a well-defined basis for choosing an appropriate scale (or smoothing) parameter correspond to a particular feature size. Different algorithms have been proposed [4.3] for dynamic determination of $S(p_i)$.

The following discrete curvature measurements have been used [4.3][4.5][4.6] when looking for high curvature points:

(1) *k-curvature*: if c_i represents the direction arriving at the points p_i, then the k-curvature is defined as the difference between the average directions of k before and after p_i within the support region:

$$\kappa_k(p_i)=\frac{1}{k}\sum_{j=-k}^{-1}c_{i-j}-\frac{1}{k}\sum_{j=0}^{k-1}c_{i-j}$$

(2) *1-curvature*: This is a particular case of the k-curvature with k = 1: $\kappa_1(p_i)=c_{i+1}-c_i$

(3) *k-angular bending*: Another way to consider k-smoothed slope change, that is robust to quantization noise, is the following: two points are defined p_a and p_b, preceding and following the considered point p_i, with coordinates equal to the centroid of the k points before and after p_i. The coordinates of p_a are:

$$x_a=\frac{\sum_{j=i-k}^{i}x_j}{k+1},\qquad y_a=\frac{\sum_{j=i-k}^{i}y_j}{k+1}.$$

Those of p_b are:

$$x_b=\frac{\sum_{j=i}^{i+k}x_j}{k+1},\qquad y_b=\frac{\sum_{j=i}^{i+k}y_j}{k+1}.$$

With these values, the k-vectors are calculated:

$$\begin{aligned}\alpha_{ki}&=(x_a-x_i,y_a-y_i)\\ \beta_{ki}&=(x_i-x_b,y_i-y_b),\end{aligned}$$

The k-angular bending at p_i is defined as the angle $\Delta_k\phi(p_i)=\alpha_{ki}\beta_{ki}$.

(4) *k-cosine*: Let two k-vectors defined at p_i be:

$$\begin{aligned}a_{ki}&=(x_i-x_{i-k},y_i-y_{i-k}),\\ b_{ki}&=(x_i-x_{i+k},y_i-y_{i+k}).\end{aligned}$$

Then, the k-cosine is defined at p_i in the following way:

$$\cos_k(p_i)=\frac{a_{ki}\cdot b_{ki}}{|a_{ki}||b_{ki}|}.$$

The method (4) is similar to the one for *k*-angular bending, but here the curvature is assessed as a trigonometric function of the angle. Moreover, the angle considered here only depends on the relative positions of the extreme points of the support region, while in the previous three methods all the *k* points preceding and following p_i are involved.

4.1.2.3. Adaptive Smoothing

A planar curve in an image can be defined using the parameterisation $(x(i), y(i))$, where $x(i)$ and $y(i)$ are two functions of the index variable i. Usually, these two functions are not smooth because of discretization and other sources of noise. Therefore, smoothing is generally necessary when significant local features, such as corners, need to be extracted from this contour.

The concept of adaptive soothing is firstly proposed by Saint-Marc and Chen [4.1], based upon some iterative weighted averaging methods, in 1991. The general idea behind adaptive smoothing is to apply a versatile operator, which adapts itself to the local topography of the signal to smooth. Adaptive smoothing of a signal is achieved by repeatedly convoluting the signal with a very small averaging mask weighted by a measure of the signal continuity at each point. As the method preserves discontinuities while smoothing any original signal, it is extremely attractive for the detection of corners in a curve with noise.

Let $S^{(0)}(x)$ be a one dimensional signal before smoothing. The smoothed signal $S^{(t+1)}(x)$ at the $(t+1)$th iteration can be formulated as

$$S^{(t+1)}(x) = \frac{1}{W} \sum_{i=-N}^{N} S^{(t)}(x+i) \cdot \omega^{(t)}(x+i)$$

with

$$W = \sum_{i=-N}^{N} \omega^{(t)}(x+i)$$

where $\omega^{(t)}(x+i) \geq 0$, $-N \leq i \leq N$, are weights of convolution. For adaptive smoothing, $N=1$, $\omega^{(t)}(x)$ is a decreasing function of the degree of discontinuity at point x. A possible choice for $\omega^{(t)}(x)$ is

$$\omega^{(t)}(x) = e^{-|s'^{(t)}(x)|^2 / 2k^2}$$

where $S'^{(t)}(x)$ is the derivative of the signal $S^{(t)}(x)$, and k is a positive parameter.

The parameter k determines the magnitude of the segments to be preserved during the smoothing process. If k is chosen to be large, all discontinuities disappear, and the result is the same as if Gaussian smoothing were used. If k is chosen to be small, then all the discontinuities are preserved, and no smoothing is performed. The appropriate value depends on the complexity and noisy level of the curve to be segmented and is generally resolved through experiments.

Since corners are discontinuities of tangent orientation, they can be extracted by applying adaptive smoothing to the tangent orientation, i.e., taking the tangent orientation along the curve as the original signal of adaptive smoothing,

$$\theta^{(0)}(i) = \tan^{-1}\frac{dy(i)}{dx(i)} \approx \tan^{-1}\frac{y(i+l)-y(i-l)}{x(i+l)-x(i-l)}$$

where i is the pixel index along the curve and l is the support length:

$$\theta^{(t+1)}(i) = \frac{1}{W}\sum_{j=-1}^{1}\theta^{(t)}(i+j)\cdot\omega^{(t)}(i+j)$$

with

$$\omega^{(t)}(h) = e^{-|\theta'^{(t)}(h)|^2/2k^2}$$

and

$$W = \sum_{j=-1}^{1}\omega^{(t)}(i+j)$$

$$\theta'^{(t)}(h) = \frac{d[\theta^{(t)}(x)]}{d\rho}\bigg|_{x=h},$$

where ρ is the length of the curve from the beginning point.

Two effects can be observed during adaptive smoothing. One is the sharpening of discontinuities, which would eventually become the break points of segmentation, and the other is the smoothing within regions defined by the adjacent discontinuities.

Therefore, the corners are detected by first applying adaptive smoothing to the tangent orientation along the curve, then taking the derivative of the smoothed tangent orientation, and finally locating the high spikes on the derivative [4.2].

4.1.3 Recognition of the Seam

In order to extract the features of a seam, i.e., seam position, gap and the mismatch between the two plates, from laser line images, pre-processing or laser stripe thinning is required.

4.1.3.1. Laser Stripe Thinning

The purpose of thinning is to reduce the image components to their essential information to ease the task of image analysis and recognition. In order to vertically locate the laser line, the laser stripe is thinned from about five pixels to only one pixel in width to generate a media axis $p_1 \dots p_i$, $i = 1, \dots, N$, denoted collectively by P (Figure 4. 3). The actual laser line thinning is performed by using a localised image intensity averaging technique. For every column of the laser line image, the average intensities of several neighbouring pixels are calculated. The highest average intensity value in a column is picked up and compared with a threshold T_i. If this value is greater than $T_i K_T$, where K_T is a coefficient with the value of (0, 1), then the location with the highest average intensity is marked as the centre of the laser line p_i. Otherwise, the algorithm puts a value of (-1) in the media axis array P to mark it as a hole for the further processing. For lap joint and V prep, these holes will be filled with relevant values while for butt joint, these will be analysed to determine whether it is the gap between two plates or just a hole on the medial axis. Extensive experiments have shown that $K_T = 0.8$ is ideal in this application.

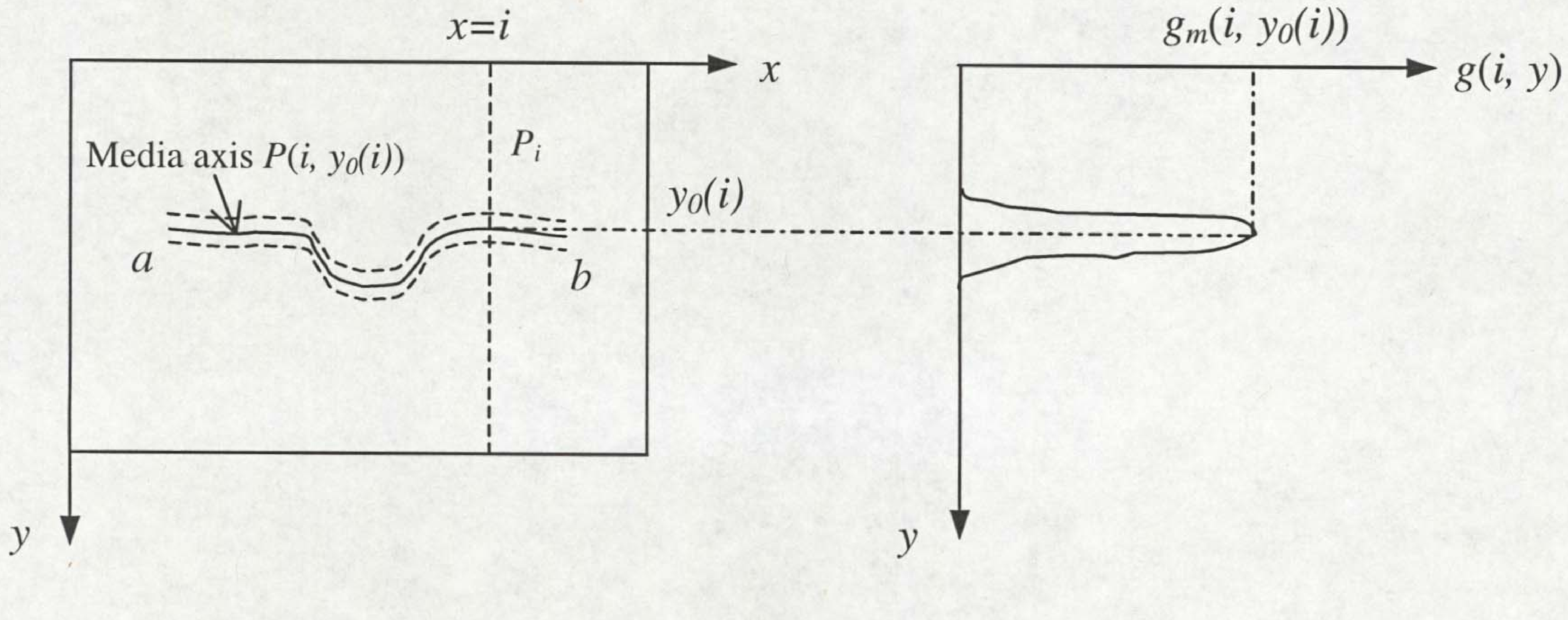

(a) (b)

Figure 4. 3 Media Axis Definition of a Laser Stripe

Due to the uneven intensity distribution of the laser stripe along the *x* direction, a method named adaptive threshold is applied instead of using a fixed threshold. The idea behind this is to select a threshold for a specific column with respect to the average greyness of its neighbouring columns. In this study, the following recursive equation has been used to calculate the adaptive threshold T_i:

$$\begin{aligned} &5T_i = 5T_{i-1} - g((i-6), y_0(i-6)) + g((i-1), y_0(i-1)) && (i = a+6,\ldots,b) \\ &T_i = T_0 && (a \le i < a+6) \end{aligned}$$

where $g(j, y_0(j))$ is the greyness at point p_j, T_0 is a constant relating to the intensity of laser line. It can be seen that the threshold T_i varies with the greyness of the laser stripe and has been calculated as an average greyness of the laser stripe in the interval $(x = i - 5, x = i - 1)$.

A windowing technique has been used to cut down wasteful averaging calculations from the full height of the window to a small range. The search range is determined dynamically according to the position of the previous extracted centre, for example, the window for p_i is given as $(p_{i-1}-1/2h, p_{i-1}+1/2h)$, where *h* is the height of the search window. For the first column or when the positions of any of the holes are encountered, the full frame is processed, as no previous positions exist. This dynamic windowing technique has the potential to significantly reduce the per frame computational time. The search range should not be too restrictive, as large positional changes may sometimes occur along the laser line, especially for the lap joint. For correct operation the algorithm assumes that the laser line is always within the search window.

4.1.3.2 Algorithms for V Prep

After the above mentioned stripe thinning, a media axis of laser profile *P* is obtained. However, because the intensity of the laser stripe is not uniform along the *x* direction due to variable reflections on the surface of the workpiece, some holes exist on the media axis. Analysing the holes filled with (-1) in the media axis array *P*, it has been found that the size of the holes varies from one pixel to more than five pixels. For the bigger holes, bridging them by simply using the value next to the hole will cause errors in the subsequent derivative analysis. Therefore, linear interpolation was used to bridge the holes. For any element i in a hole with size n, its value p_i can be calculated as:

$$p_i = p_{a-1} + i \times \frac{p_{b+1} - p_{a-1}}{(b+1)-(a-1)}$$

where a and b are the array indices for the hole beginning and the hole end, $i = 1, \ldots, n$.

Two methods were applied to the V prep laser line for corner detection. The principle of the first one is to detect the discontinuities of tangent orientation. Adaptive smoothing was performed on the tangent orientation to sharpen the discontinuities. The other method was to detect local maxima of curvature, which was calculated using smoothing measurements of discrete curvature as explained in section 4.1.2.2. Finally, the comparison of these two methods was made.

1. The adaptive smoothing method

According to the definition of tangent orientation, it can be observed that the tangent orientation of a curve is just proportional to its first derivative. Therefore, it is reasonable to use the first derivative to replace the tedious calculation of tangent orientation. The first derivative P' of media axis array P can be calculated as,

$$p_i' = \frac{y(i+l) - y(i-l)}{x(i+l) - x(i-l)}$$

Since $x_{i+l} - x_{i-l}$ is the same for every p_i, the calculation can be simplified to,

$$p_i' = y(i+l) - y(i-l)$$

where l is the support length. It was determined experimentally based on the level of detail represented by the digital curve. Figure 4. 4 shows the influence of l on the distribution of P', where Figure 4. 4(a) is the original laser line centre of seam profile (it is upside down with respect to the laser line in the image, as the origin of the image window is on top left corner rather than bottom left corner), Figure 4. 4(b) is its first differentials calculated using support lengths of 1, 3, and 5 respectively.

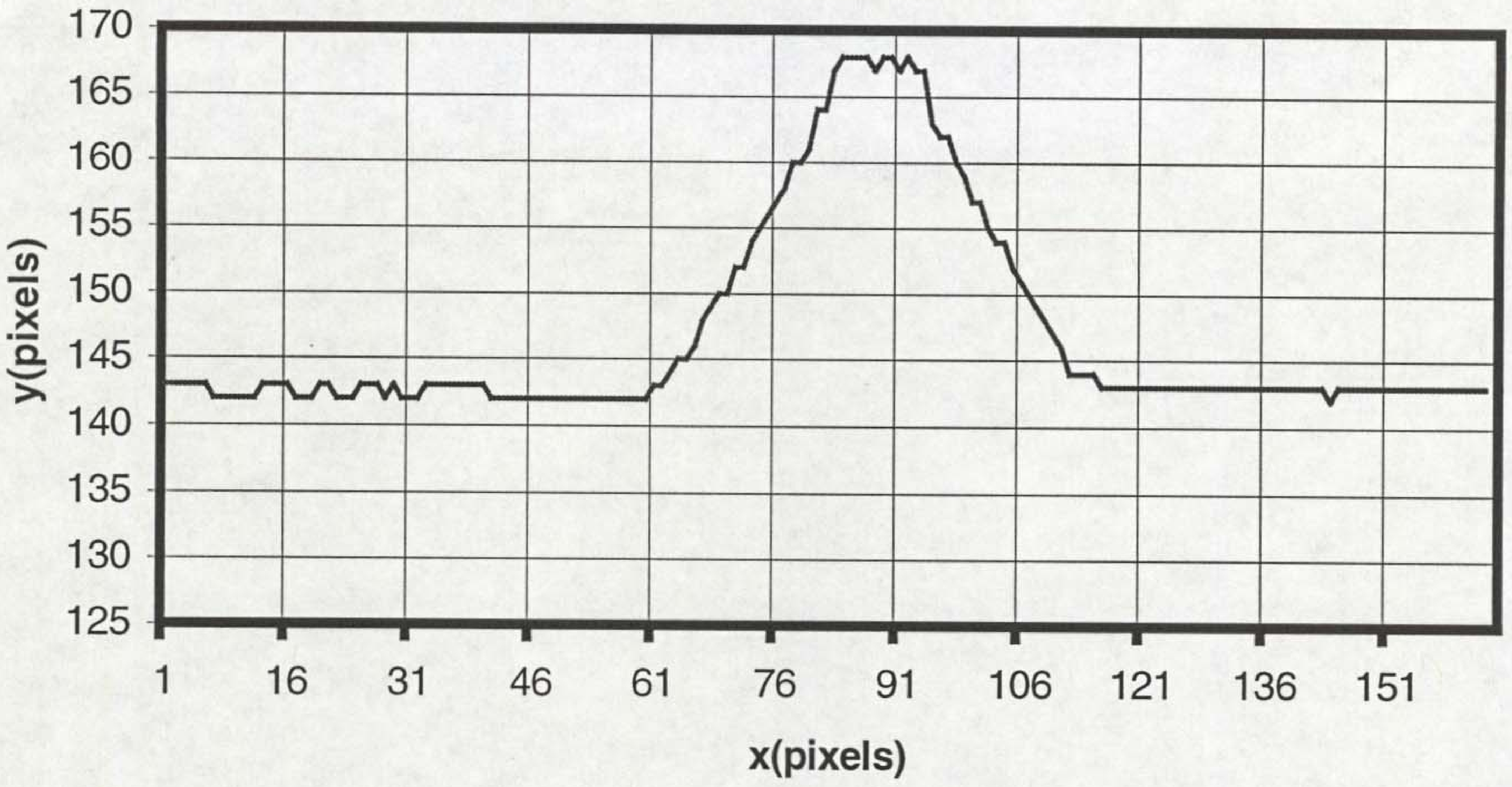

(a) Laser profile on a V prep seam

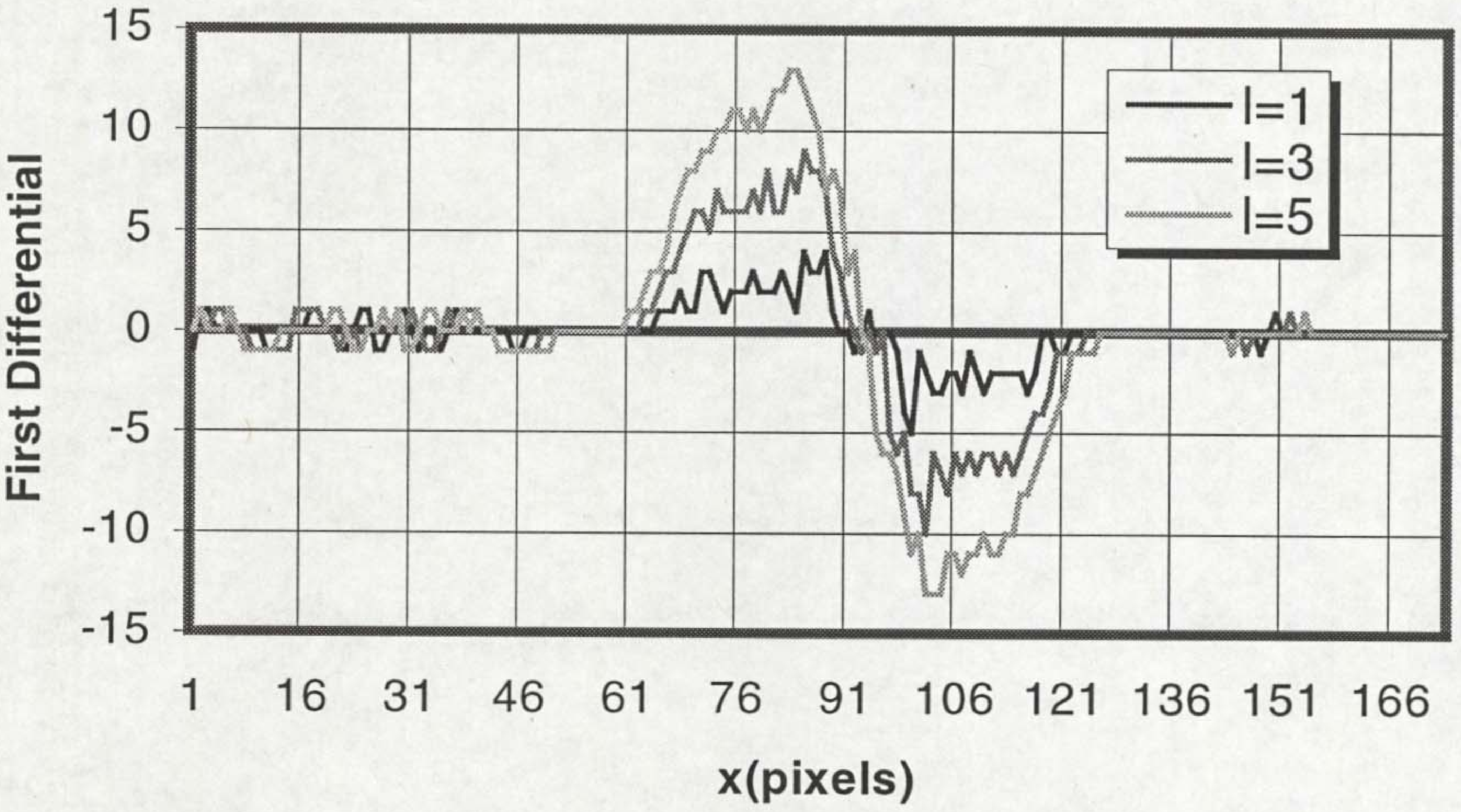

(b) First differentials

Figure 4. 4 First Differentials Calculated Using Different Support Length

It was observed that when the support length is set to be large, the magnitude of differential is also large, while some fine details are missed. For the seam profile in Figure 4. 4(a), the plateau at the top represents the gap between two plates and is important detail which need to be extracted. This is well preserved when $l = 1$ and $l = 3$ and totally disappear when $l = 5$. Therefore, $l = 5$ is too big in this application. When $l = 1$, all the details are preserved and many of them are redundant. Thus $l = 3$ is the best choice.

The previously mentioned adaptive smoothing is applied to P' to sharpen the discontinuities and smooth the other regions. Figures 4.5-4.7 show the sharpened and smoothed effect using parameter $k = 0.5$, 1, and 5 respectively after different iterations with $n = 1, 5, 10$, where the Original is P', Smoothed is the curve after adaptive smoothing and Derivative is the derivative of the smoothed curve or the second differential of the seam profile. Several characteristics of adaptive smoothing can be seen:

1) Iterative Behaviour: It is important to notice that there are two different operations affecting the image as the iteration proceeds: One is the sharpening of the discontinuities that will survive, the other is the smoothing of regions. The sharpening effect is obtained after just a few iterations, but the smoothing part is slow. It is therefore reasonable, for the purpose of corner detection, to perform only a few iterations, since discontinuities do not change a lot afterwards.

2) The parameter k: The parameter k is actually the sensitivity or the threshold of the gradient magnitude. Gaussian smooth is a special case when k is set to infinity. When k is set to be large, only smoothing is achieved, no sharpening happened as the iteration progresses. This can be seen in Figure 4. 7 when k equals 5. It is known that the behaviour of adaptive smoothing includes interregion gradient sharpening as well as intraregion gradient smoothing. The locations of the interregion discontinuities will basically remain unchanged as the iteration progresses, while the locations of the intraregion discontinuities will deviate along the iteration until they finally disappear [4.1]. In addition, when the gradient is large enough, it will increase its magnitude as the iterations progress, achieving the sharpening effect. On the other hand, if the gradient is small, it will be smoothed eventually. The parameter k approximately sets the threshold to the gradient magnitude where discontinuities are preserved.

Figure 4. 8 has the same parameters as in Figure 4. 5, but with the support length l = 1 instead of l = 2 for the derivative calculation. Better sharpening and smoothing effect are observed. Accordingly, this was chosen to be used in the corner detection for seam tracking. As can be seen, very good sharpening is obtained after only five iterations. Local maxima of the second derivative are presented clearly at corners.

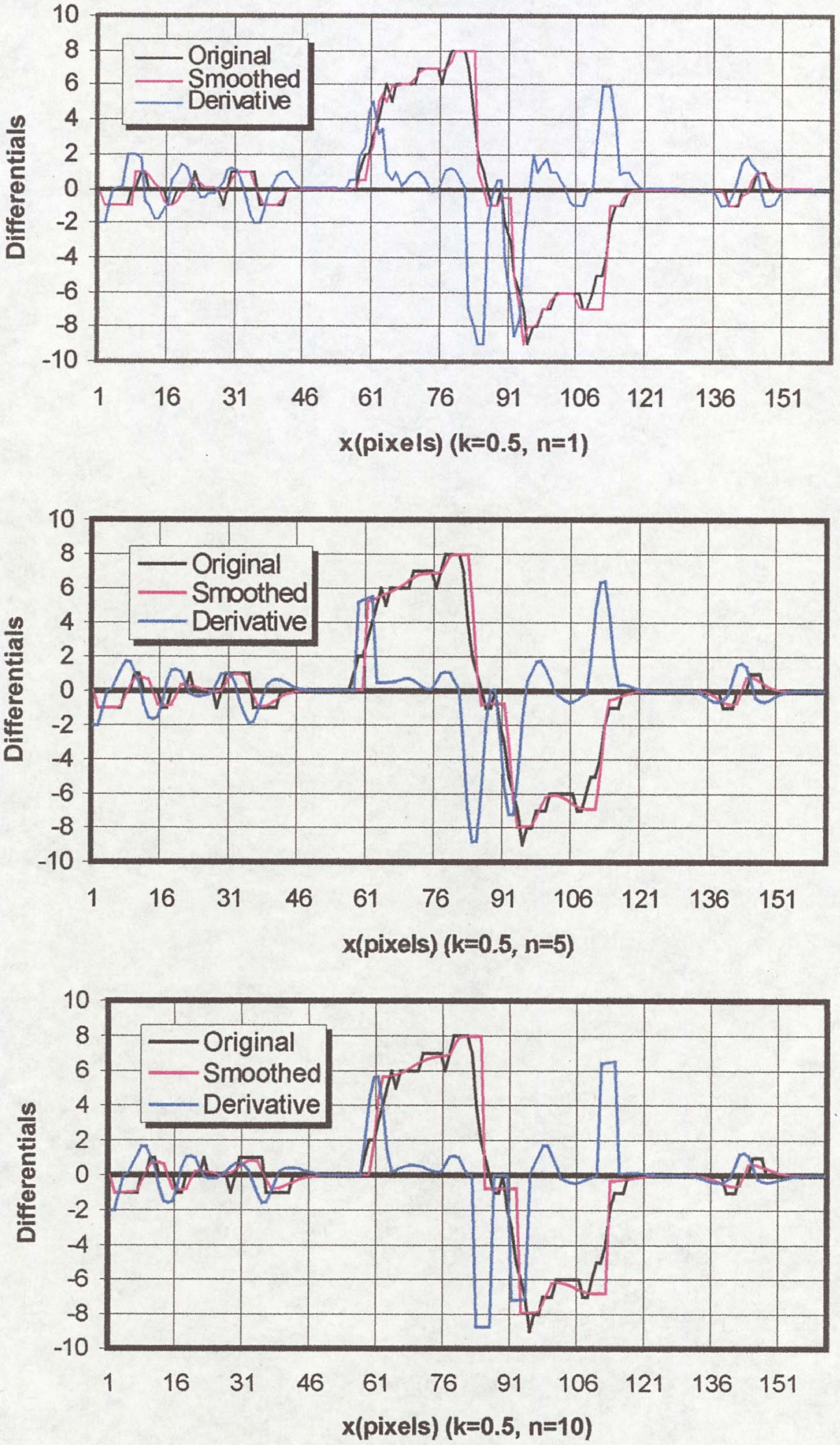

Figure 4. 5 Adaptive Smoothing k=0.5

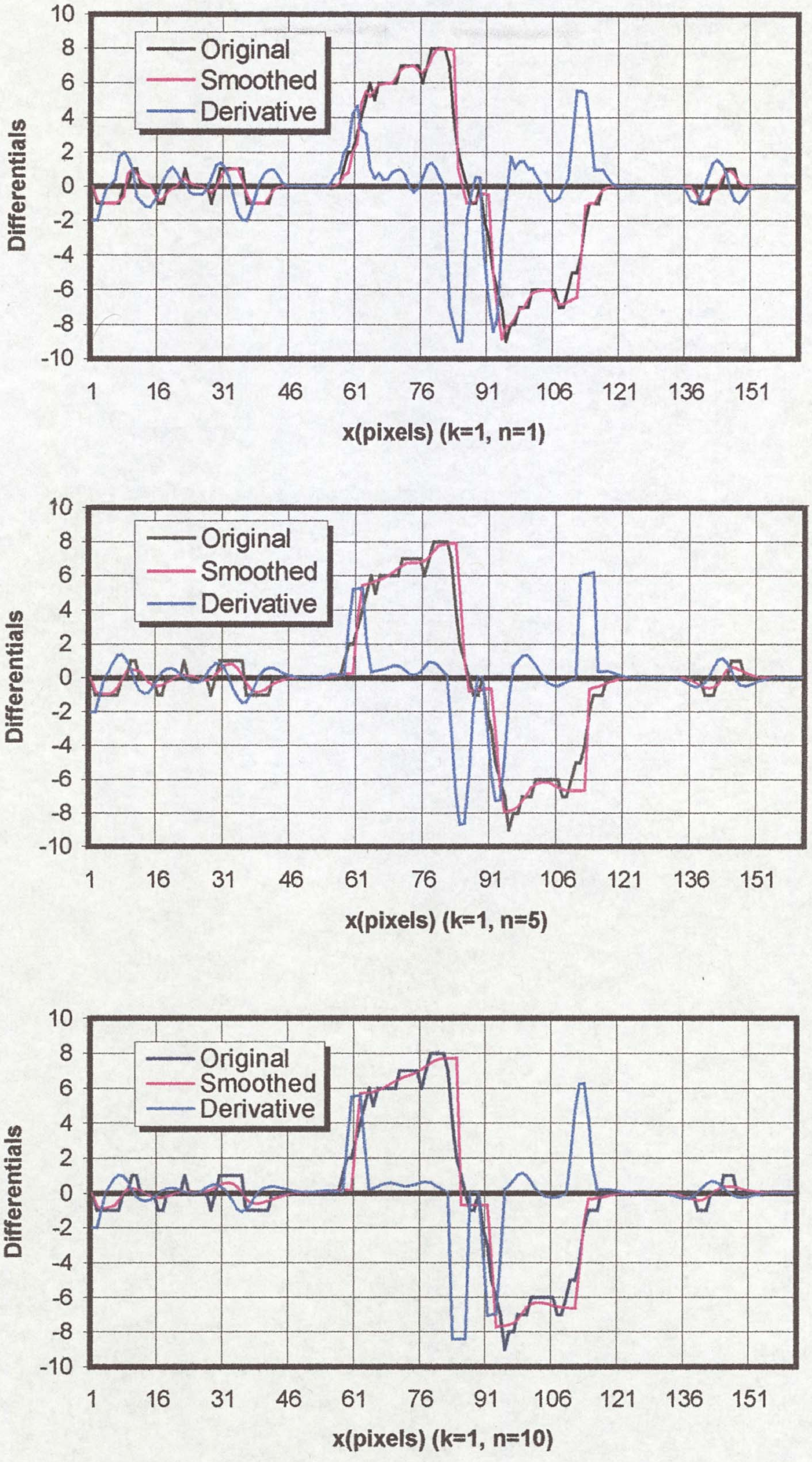

Figure 4. 6 Adaptive Smoothing k=1

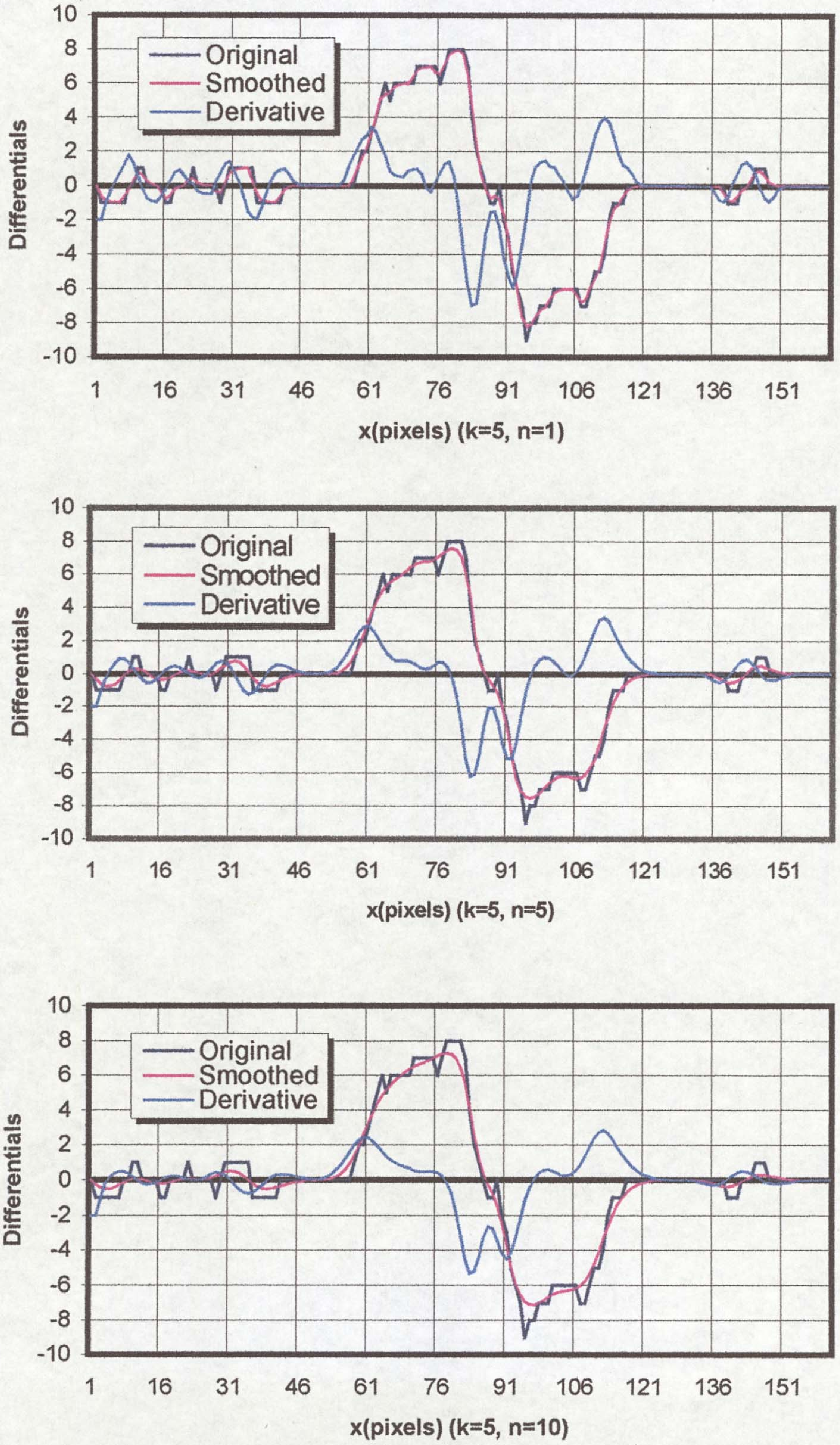

Figure 4. 7 Adaptive Smoothing k=5

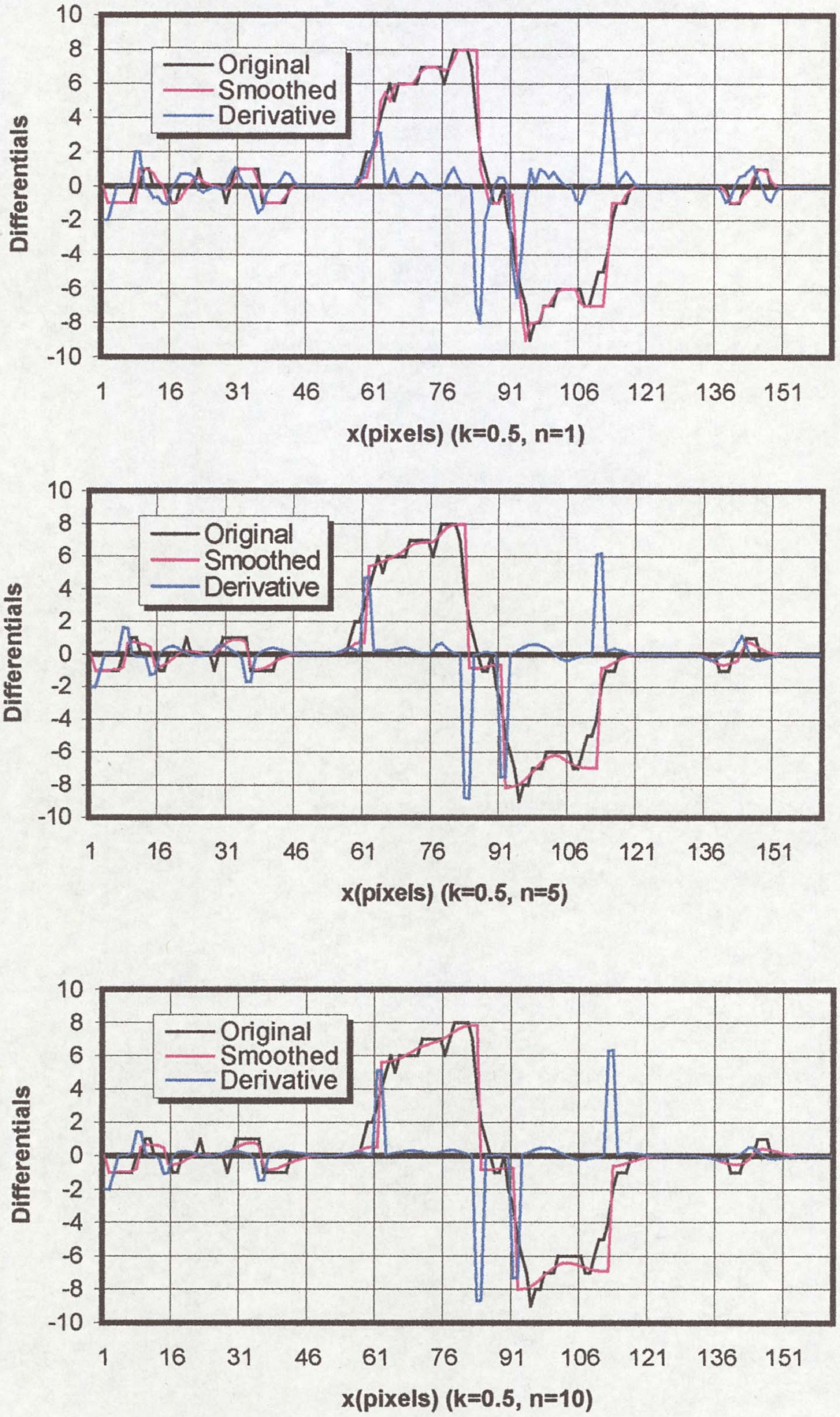

Figure 4. 8 Adaptive Smoothing k=0.5, Derivative Calculated with Support Length l=1

2. Curvature measurement

Four digital curvature measurement methods have been explained before. After they were tested on different curves, Inesta [4.6] concluded that none of the curvature measurements showed significantly better behaviour than the others in terms of efficient representation and the choice of one of them should be made taking into account criteria of computation velocity or easy implementation. Therefore, the digital curvatures that are evaluated in a simple way (1-*curvature* and *k-curvature*) could be the most suitable ones according to these rules. Only *k-curvature* method will be examined, as 1-*curvature* will not work on a noisy curve. The comparison of *k-curvature* with the second derivative calculated in the adaptive smoothing method is shown in Figure 4. 9, where k equals to 3 in *k-curvature*. The calculation for the latter only depends on the relative positions of the extreme points of the support region, while for the former all the k points preceding and following p_i are involved, in this way smoothing is performed. It is not difficult to see that *k-curvature* doesn't perform better than the other one at corner positions. The conclusion from Inesta is further verified. After the above comparison, it has been found that the adaptive smoothing method is much more effective than the other smoothed curvature measurement approaches.

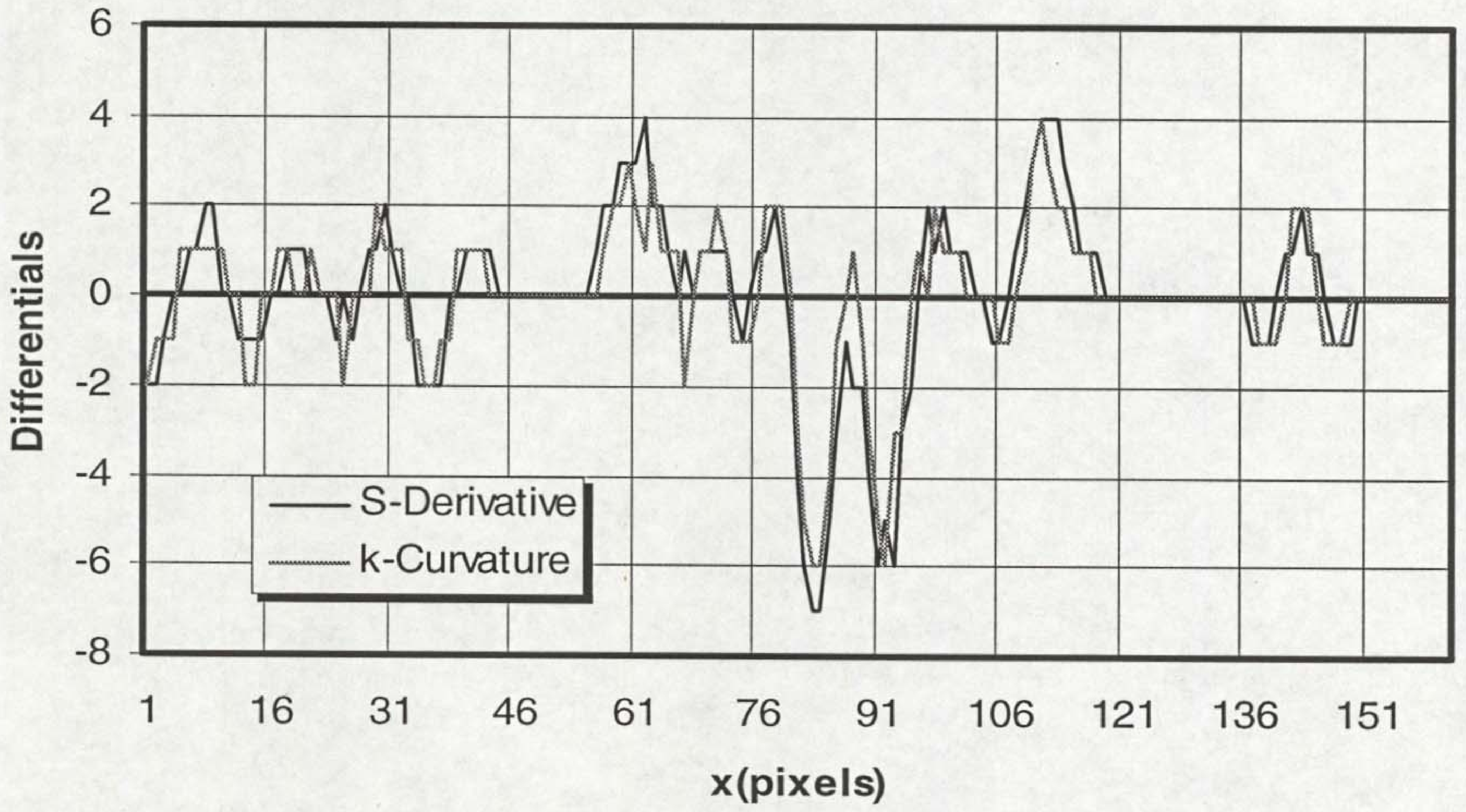

Figure 4. 9 Comparison of the k-curvature with Second Derivative

When applying adaptive smoothing to the first derivative or tangent orientation, significant spikes can be obtained at corner positions with very good localization on the second derivative, provided proper k and iterations are selected. This can be seen in Figure 4. 10. The next step is to extract these spikes and locate the significant corners, A, B, C and D. At the bottom of the seam, if there is no gap, only one local negative minimum exists, otherwise, there will be two local negative minima there. The search for the bottom points is started from the two sides respectively and stops when the first local minimum is found, and then the positions are saved with the local minima. If the two positions from two sides are the same that means that there is no gap between the plates. Otherwise, if these two positions are different then they are assumed to be points C and D. Based on the bottom points, the search for two top points is started from the bottom position to the two sides. The positions with local positive maxima are the top feature points A and B. Using this algorithm, the feature points can be extracted successfully in most situations. However failures still occur occasionally. So a temporal filter was used to provide the continuity of the seam position. This has been discussed in the previous chapter.

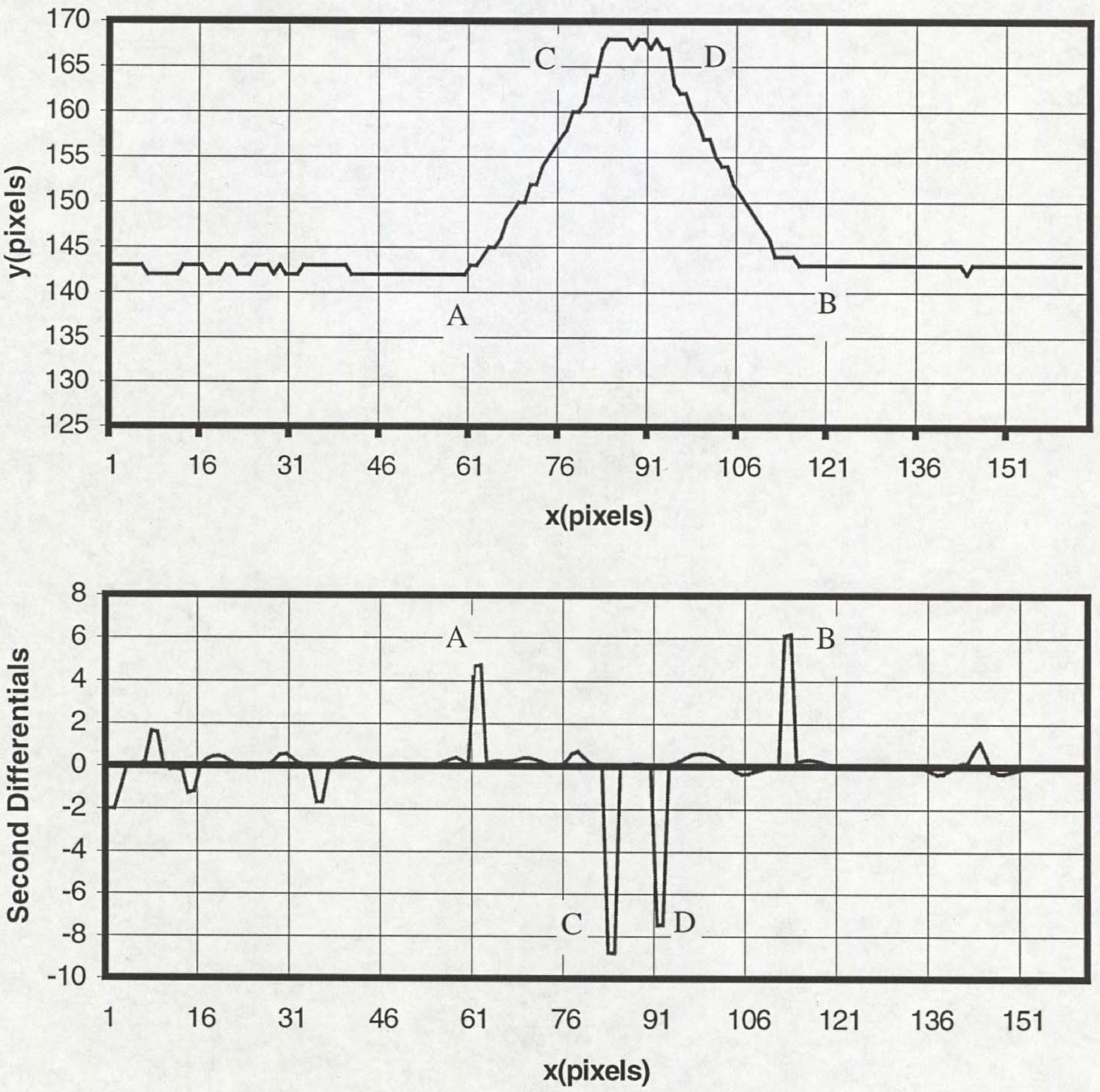

Figure 4. 10 Derivative of the Adaptive Smoothed Tangent Orientation

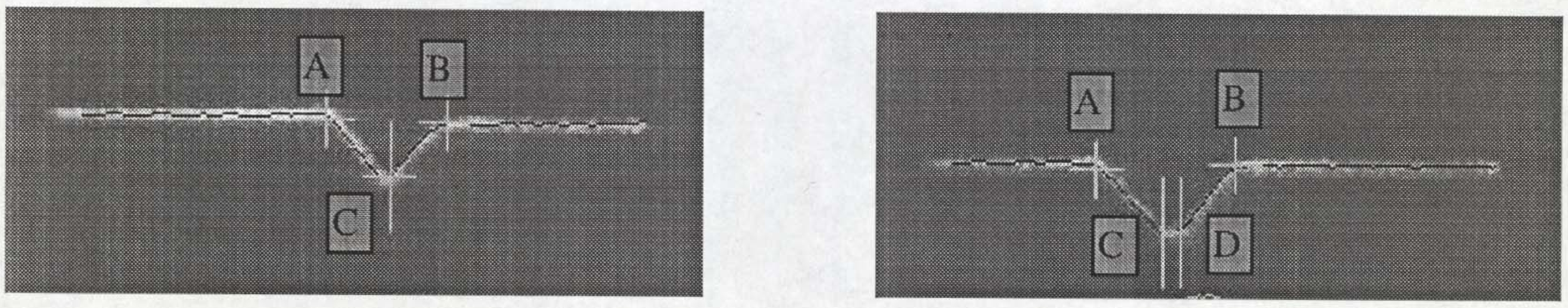

(a) without gap **(b) with gap**

Figure 4. 11 V Preparation Images (a) without Gap and (b) with Gap

The result of image processing are shown in Figure 4. 11, where the feature points are marked by white crosses. After the feature points are derived from the V prep image, three seam parameters are calculated and transmitted to the control system. They are the seam position (the horizontal centre of C and D), the gap (the horizontal difference of C and D) and the 'high-low' (the vertical difference of A and B).

4.1.3.3 Algorithms for Butt Joints

The seam recognition for butt joint is more difficult than that for V prep because of the following reasons: (1) The laser stripe is not always continuous due to the existence of the black gap at seam, which is just the characteristic of the seam and must not be bridged by the interpolation method mentioned in section 4.1.3.2. Therefore, the derivative method for the continuous line analysis could not be used. (2) The patterns of the laser profile vary a lot during welding. Usually butt joints are used on thin plate, so the plate distortion is quite severe. This can be seen in Figure 4. 12, where four typical image patterns are shown. The most common pattern is shown in Figure 4. 12(a). In this case, a clear gap can be seen at the seam. In the second situation, a reflection of the backing plate is displayed in the gap (Figure 4. 12(b)) while in the third case, only high-low difference exists with a very small gap (Figure 4. 12(c)). In the last situation (Figure 4. 12(d)), no obvious gap and high-low are presented around the seam, so other characteristics are needed to locate the seam.

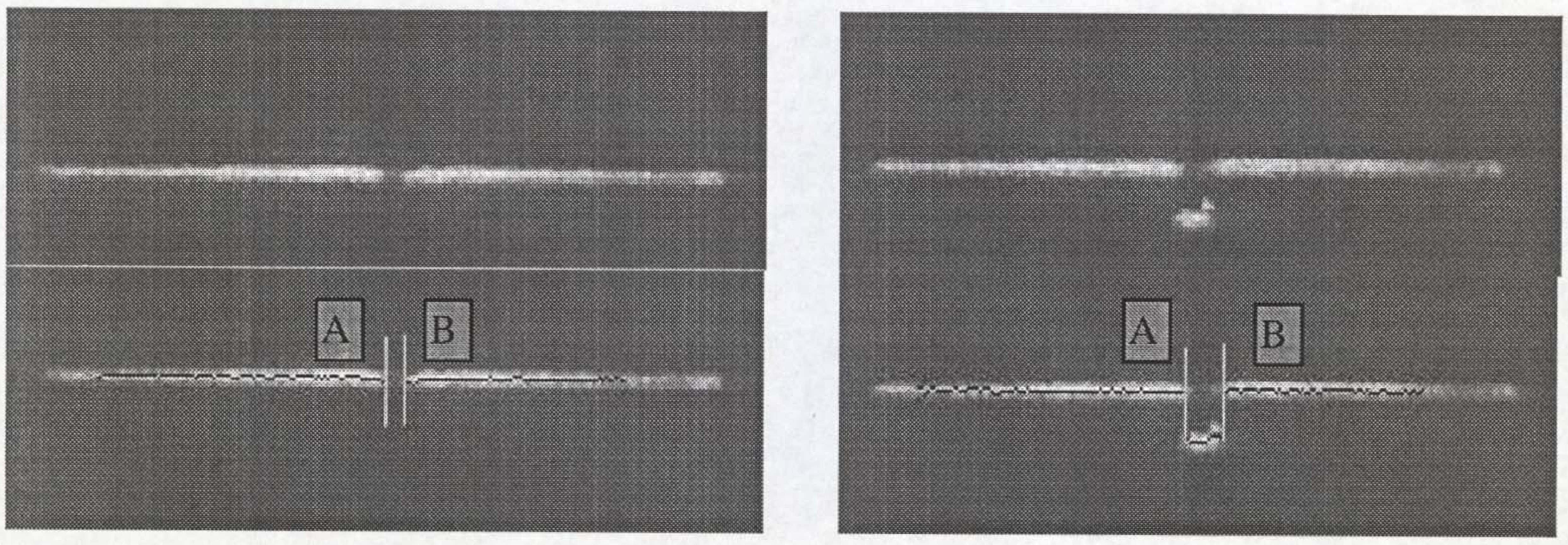

(a) without backing plate (b) with backing plate

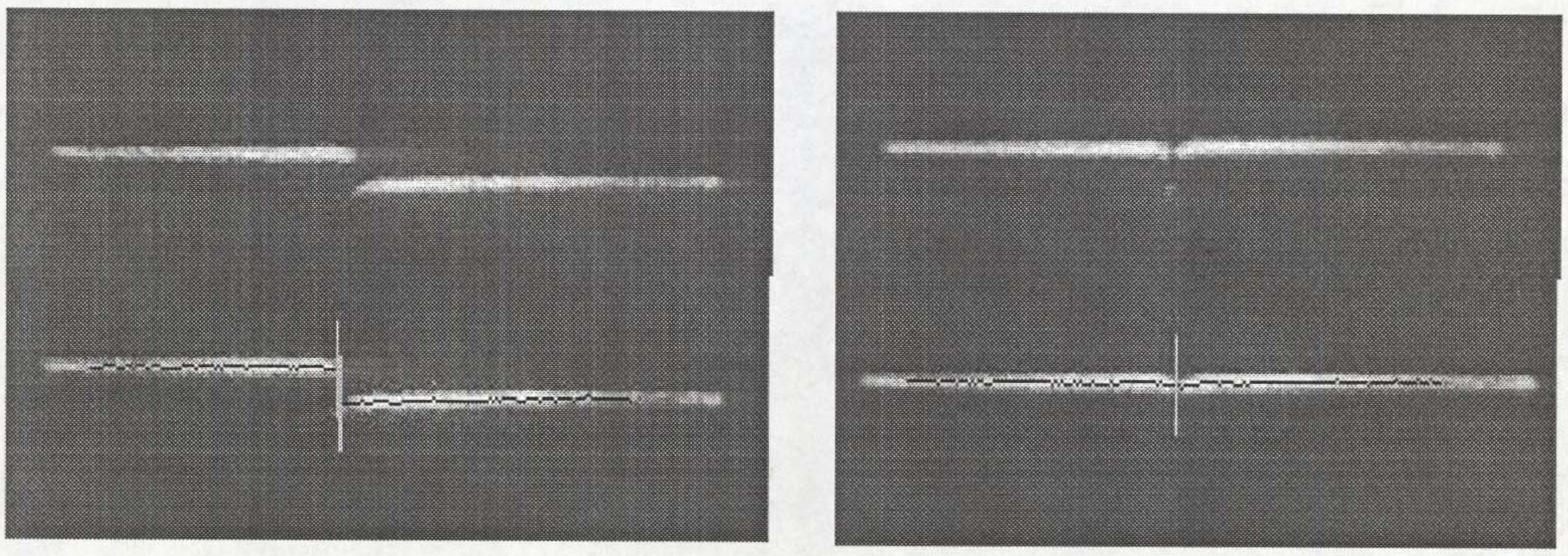

(c) high-low only (d) touching seam

Figure 4. 12 Butt Joint Images

The first step for seam extraction is to determine which pattern the image belongs to. Here two flags are used. They are ValidLeftDrop and ValidRightDrop representing the existence of the laser line position drops at the left and the right sides of the seam. The searches for maximum position drops max(Δp_i) are taken from left to right and from right to left along the media axis respectively. If max(Δp_i) is greater than a threshold the flag is set to be true, otherwise false. Then the image is categorised according to the states of these two flags. If only one flag is true the image goes to pattern (c) where only high-low exists. If both flags are true it goes to pattern (b), while if both are false there will be two possible situations, pattern (a) or (d). So the further categorisation is done based on the degree of the gap between two plates. This process of judgement is expressed in Table 4.1. In this way, images can be categorised into four patterns successfully.

Table 4.1 Pattern Judgement Table

ValidLeftDrop	ValidRightDrop	Patterns
True	True	(b)
False	True	(c)
True	False	(c)
False	False	(a) or (d)

For pattern (b) and (c), the two feature points A and B are obtained during the process of looking for the maximum position drops max(Δp_i). Then seam parameters, such as central position, gap and high-low are derived. For the other two patterns, since no drops are found, a further search is taken to look for the position with the maximum hole. This could be found without difficulty for pattern (a), but with difficulty for pattern (d) as the gap is tiny there and easily confused with the holes on the stripe elsewhere. By analysing the images belonging to pattern (d), it was found that there always would be a bright dot under the seam, which is the useful information to indicate the seam position. Accordingly, a window is set just below the laser line and, then, the position with the bright reflection is searched within the window. The algorithm used for pattern (c) can also be used on the image of the lap joint, which exhibits the same image characteristics.

The temporal filter, mentioned in the previous chapter, was also used here to improve the robustness of seam detection. Figure 4.13 shows a typical real time measurement of a varying gap and high-low for a butt weld. It can be seen that the fluctuation of gap and high-low over a 200 mm length is up to 1mm. This is quite severe for a quality weld. Therefore a neural network has been developed which encapsulates all the seam geometry data and relates it to the preferred welding parameter values. This neural network can be used to predict the required changes in welding parameters when changes occur in the seam geometry of gap and high-low.

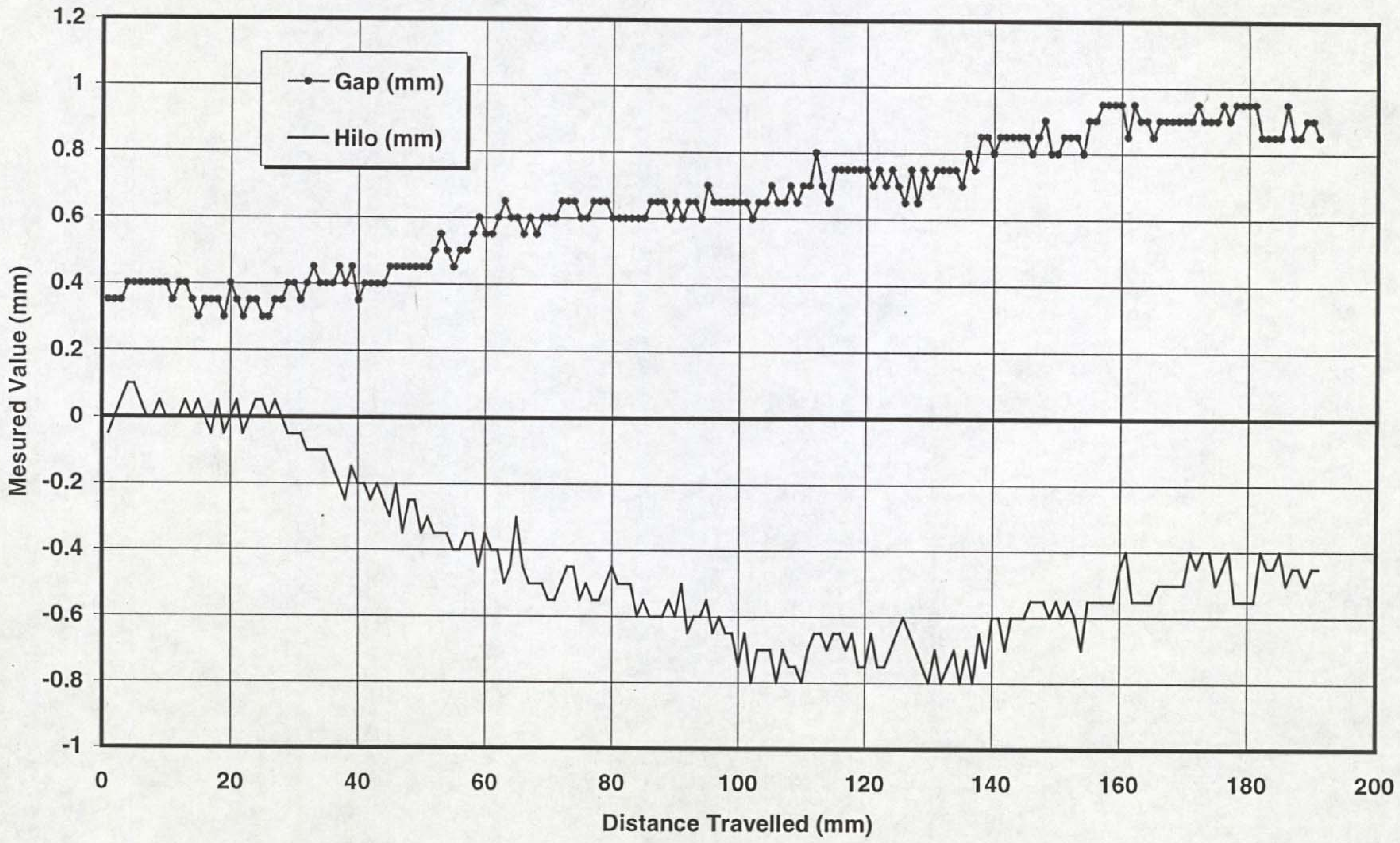

Figure 4. 13 Measured Gap and Hilo

4.2 Seam Tracking without a Laser Line

The approach of using arc light to illuminate the seam instead of a laser line, is described in this section. By the illumination of the arc, the butt seam in front of the weld pool becomes visible to the camera. Then the seam position can be detected by developing proper image processing algorithms. In this method, only one visual sensor is required for both pool monitoring and seam tracking. All the information concerned with weld pool and the seam is in a single image. The algorithm used for pool edge detection can still be used here, while a new algorithm is required for seam detection.

Figure 4. 14 shows the intensity distribution on the surface of the parent metal along the black horizontal line across seam with length of 100 pixels shown in Figure 4.15(a). Figure 4. 14(a) is the original intensity curve, Figure 4. 14(b) being the curve after smoothing using a Gaussian filter. The parent metal used was aluminium plate whose surface is polished with emery paper to remove the oxide film. It can be seen that the position of the weld line can be detected as the point with the lowest brightness in spite of the arc light.

However, using this algorithm, there is a high possibility of a recognition fault if, in the vicinity of the weld, there are optical noise sources such as a scratches, corrosion, dirt etc. which adversely affect recognition of the weld line. What is thought to be effective in this sort of case is processing taking account of the continuity of the weld line, that is, by monitoring the direction of the weld line constantly on the software, if the degree of a change in its direction exceeds the allowance set beforehand, a judgement is made that the signal is caused by noise.

When tracking is actually by generating the arc, a part of the seam line with low brightness disappears owing to reduced resolution induced by the arc light. Therefore, multiple line processing is proposed. In contrast to the conventional methods in which one scanning line is used to probe the weld line, more than one horizontal line is detected in this method and the final seam position (the vertical line shown in Figure 4.15(b)) was obtained by the selected average of seam data from multiple lines. This means that several horizontal lines are processed for the seam positions and the resultant seam data are analysed. The data the farthest from the average position are discarded and the new average position is calculated using the remaining seam data. This process is repeated several times until the remaining data are all within a limit of the average position.

Ideally, the seam position should be in line with the centre of the weld pool. Hence, the shift of seam position from the weld pool centre is taken as the parameter to manipulate the torch movement. A real time measurement of this shift during welding, without closed loop control, is shown in the display window in Figure 4. 15(b). Three curves from top to bottom in the figure represent the fluctuations of pool width, cleaning width and seam error respectively, and the current detected values are also displayed in the window in real time. As can be seen in Figure 4.15(b), very robust results are obtained with high accuracy.

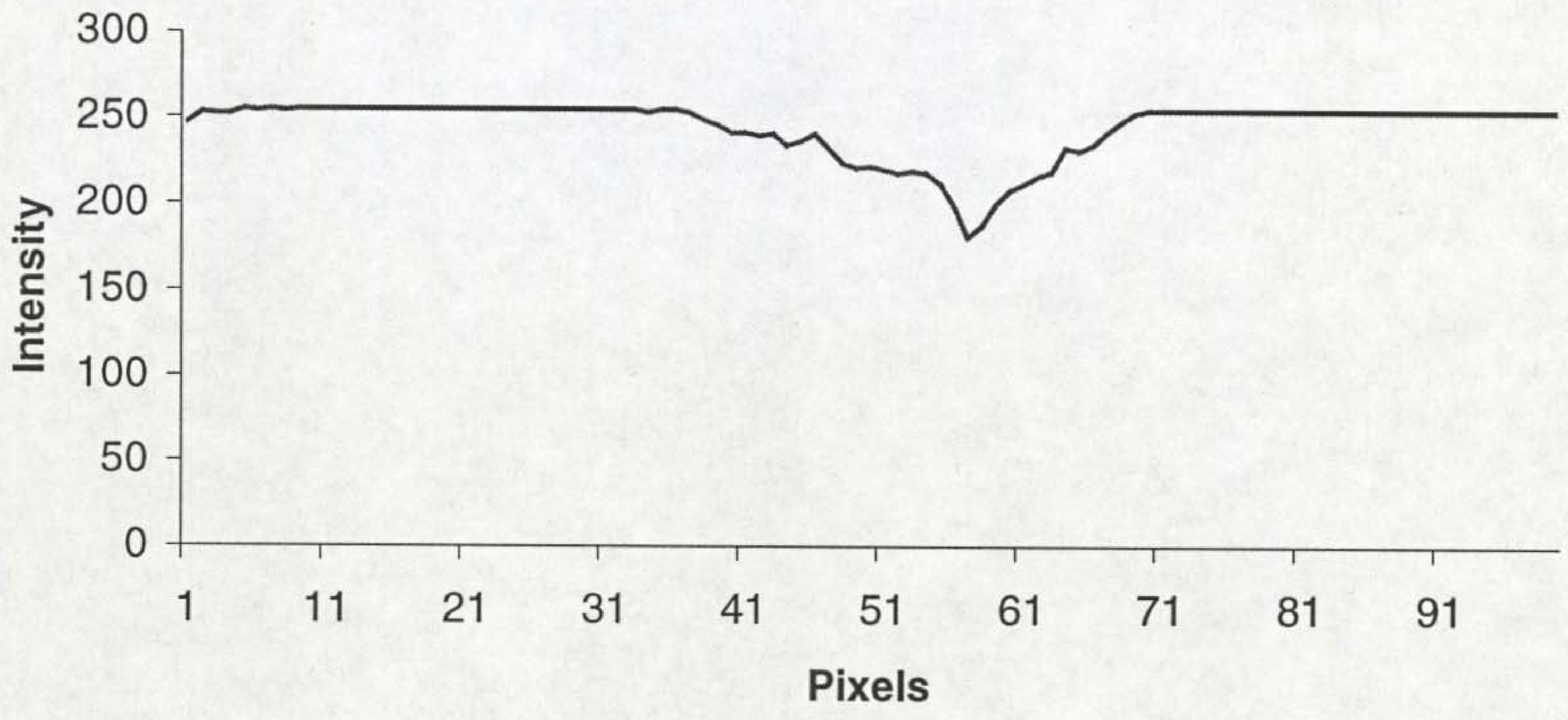

(a) Original intensity distribution

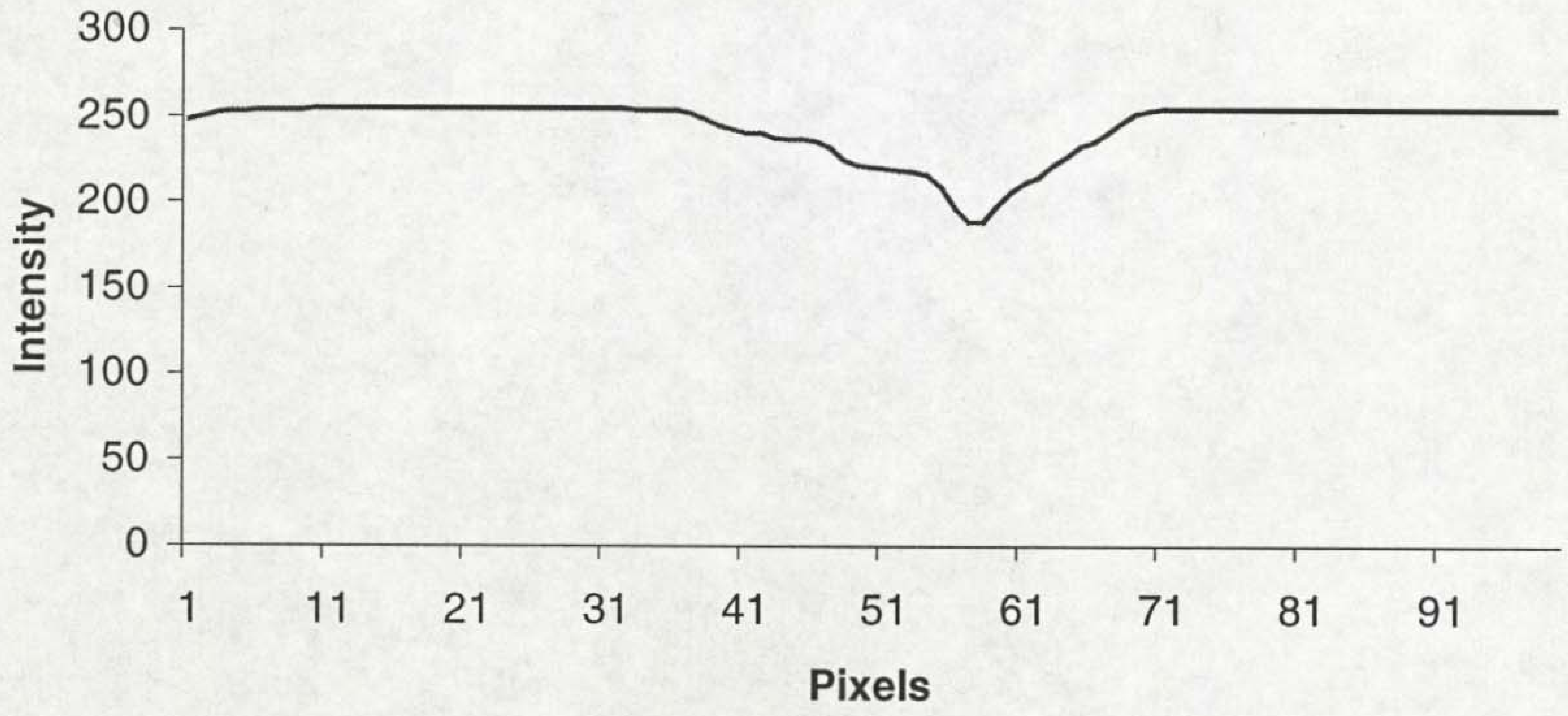

(b) Smoothed intensity distribution

Figure 4. 14 Intensity Distribution Across Seam

The method to detect the seam position without using a laser line is currently only possible for TIG welding on butt joints and fillet joints without grooves. Since in MIG welding, very dense optical filters are usually applied to eliminate the strong arc light, this results in darkness of the surrounding welding area except the weld pool. As a result, the seam is difficult to see in MIG images. Therefore, the laser-stripe method has proven its general ability to cope with the most common seam types in different welding processes without major restrictions.

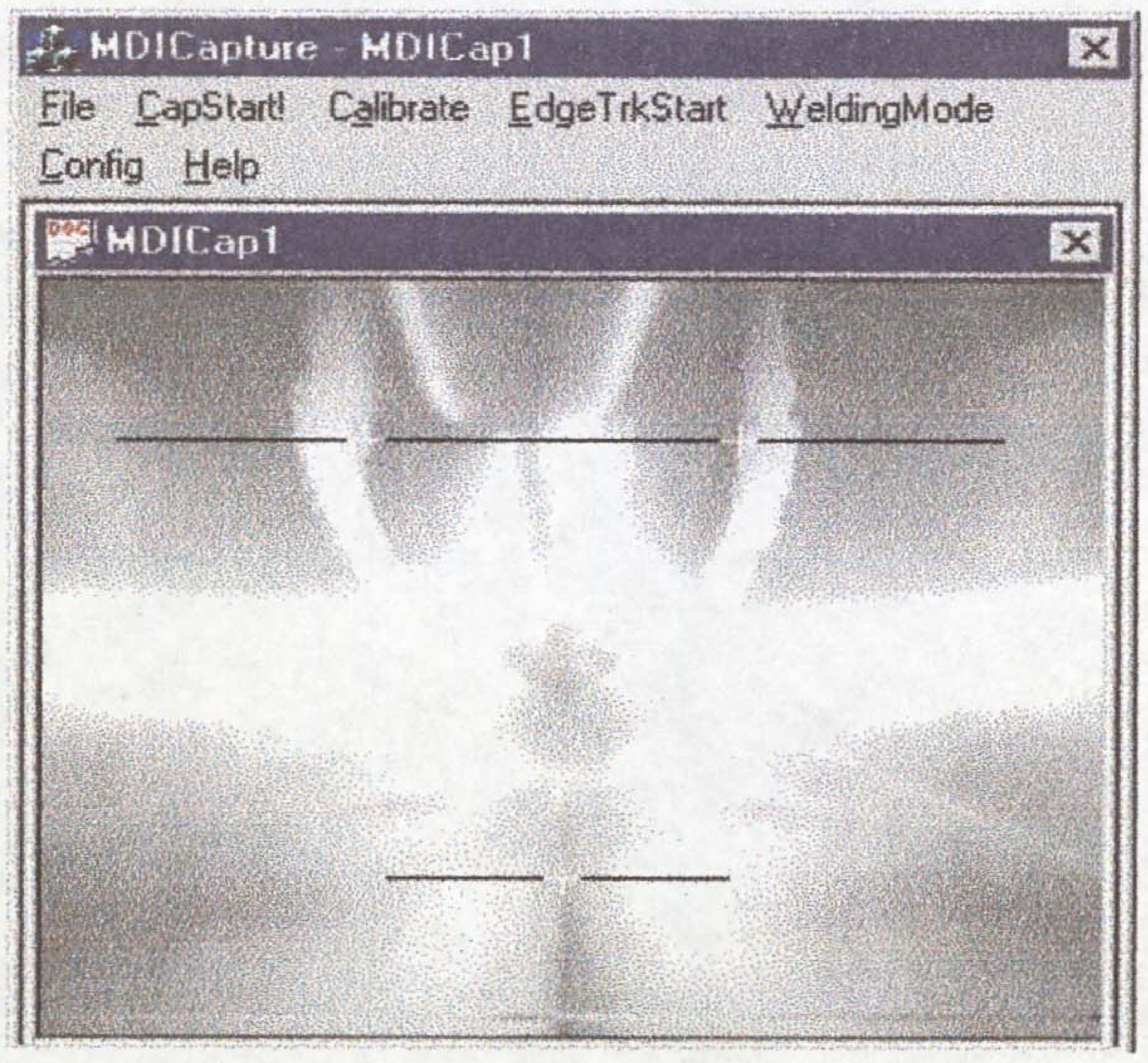

(a)

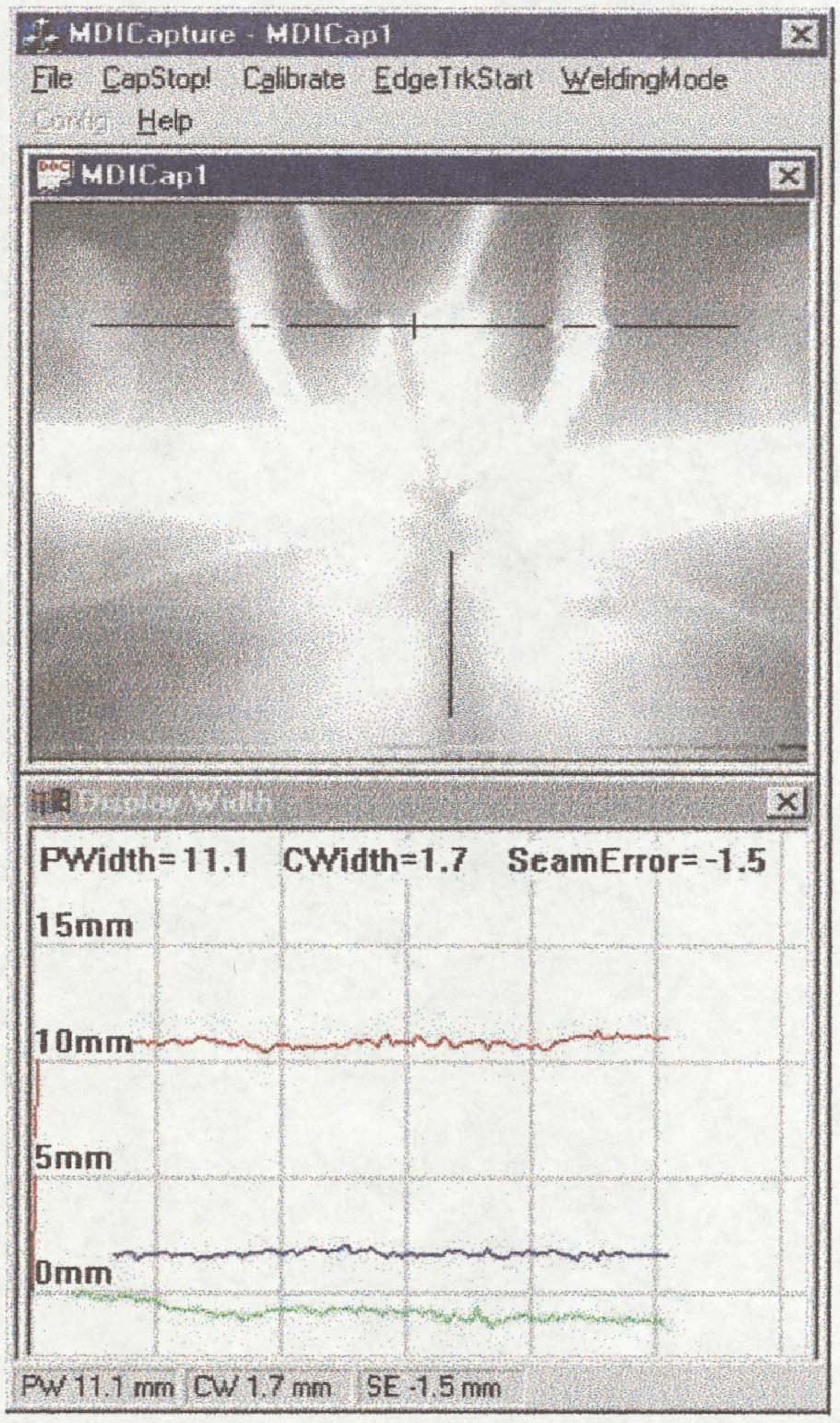

```
PWidth=11.1   CWidth=1.7   SeamError=-1.5
PW 11.1 mm  CW 1.7 mm  SE -1.5 mm
```

(b)

Figure 4. 15 Seam Tracking without a Laser Line

CHAPTER 5 BEAD PROFILE MEASUREMENT

The principle of bead profile measurement using a laser line was introduced in chapter 2. In this chapter, the image processing algorithms for bead surface parameter measurement will be examined.

5.1 Bead Profile and Surface Imperfections

Bead profile or the surface shape of a weld is one of the key aspects to evaluate the quality of a weld. Irregular bead profile or imperfections on the bead surface, i.e., too much reinforcement or the occurrence of undercut etc., will result in a poor quality weld. The welding procedure and welder technique have a direct effect on fabrication imperfections. An incorrect procedure or a poor technique may produce imperfections leading to premature failure in service.

For a weld bead the measurements which are universally considered to be important are: reinforcement, width, undercut, toe angle, plate angle.

- *Reinforcement:* This is defined as the maximum height to which the weld material has formed above the parent metal.
- *Width:* The width of a weld is defined as the distance between points where the weld metal meets the parent metal on either side of the weld.
- *Undercut:* Undercut may occur at either side of the weld, at a point close to where the weld metal meets the parent metal. It is defined as a recess in the parent metal adjacent to the weld. Undercut is measured with respect to the adjacent parent plate as a dip below its level.
- *Toe angle:* The toe angles of weld profiles are the angles at either side of the weld between the parent plate and the weld at the corners.
- *Plate angle:* The angle between the two plates of the parent metal is taken as the plate angle where 180° indicates a butt weld and 90° a tee joint fillet weld. It gives a measure of angular distortion.

Figure 5. 1 shows the typical geometry of a butt weld and the parameters to be measured, where W and R are top bead width and reinforcement, w and r are bottom

bead width and reinforcement, α is toe angle, which is very important for evaluating the risk of stress. Too small an α means excessive weld deposit, due to incorrect current settings, travel speeds or electrode manipulation, and may result in high degree of stress at the corner of the angle. δ and ρ (Figure 5. 1(b)) represent the depth and width of undercut respectively. The formation of undercut is particularly undesirable, as it reduces the plate section at a part where metallurgical changes may already have increased the brittleness of the parent material. Undercuts are usually due to excessive welding current, which melts a relatively large amount of parent material and causes it to sag under its own gravity, the crater is not being filled because of too high a rate of travel of the electrode. If the electrode is not held at the correct angle in relation to the parent plates, one-sided undercut may be caused through the heat being too concentrated on one side of the joint.

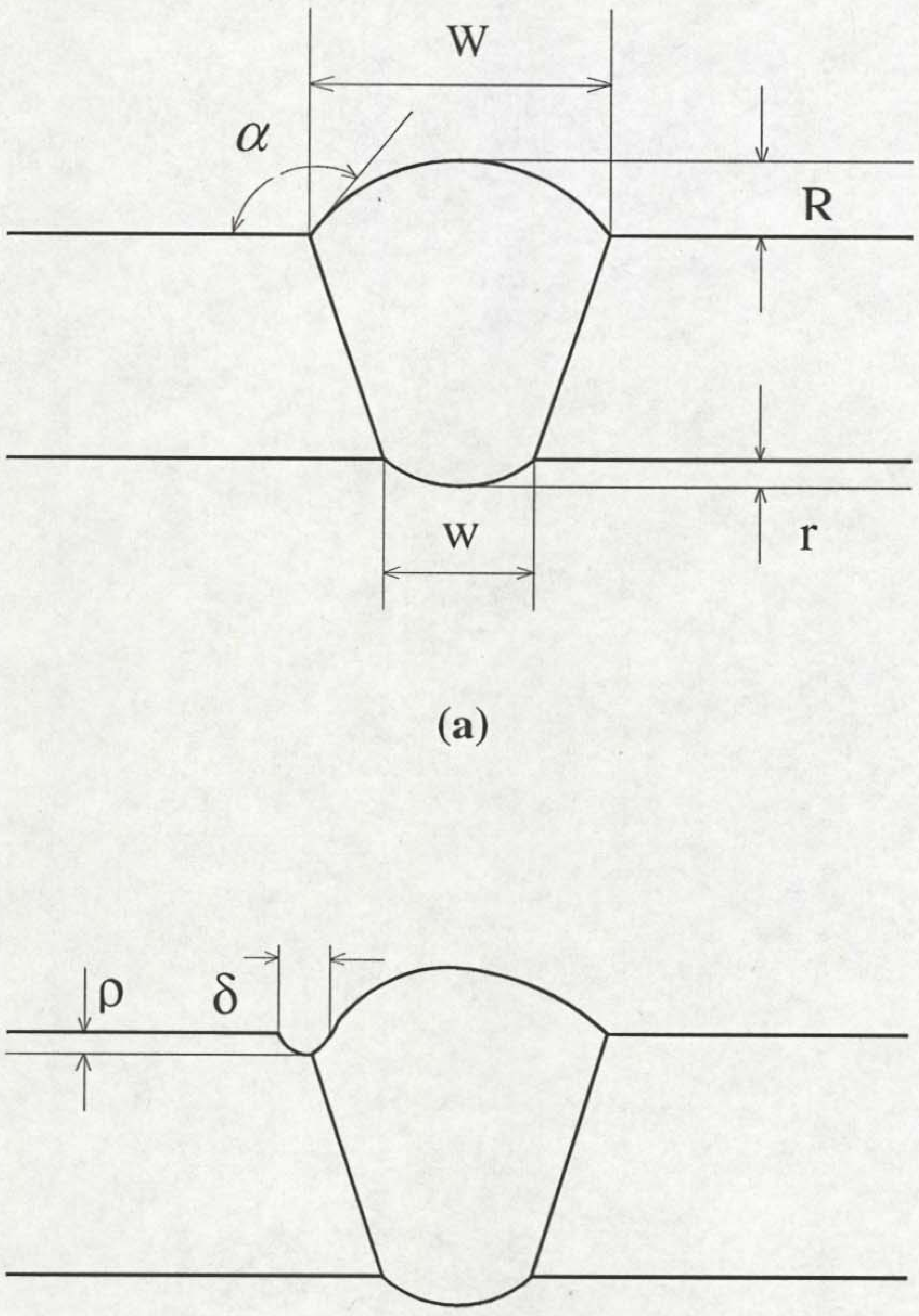

(a)

(b)

Figure 5. 1 Bead Geometry

To measure the surface geometry of bead manually is not only time consuming, but gives low accuracy, especially when surface imperfection occurs. Currently, some weld inspection replicas for different kinds of weld are used to inspect the degree of imperfections, such as undercut and toe angle. The results using this method will be greatly affected by different individuals. So it is rather human dependent. This could be overcome by using the weld profile sensing system developed in this research.

There are two applications for this system: online profile sensing and offline profile measurement. The first one is implemented during welding for welding parameter adjustment based on the measured geometry of a weld. If a bead with high reinforcement or small toe angle is detected, it is required either to decrease wire feed speed or to increase welding traverse speed to make the reinforcement lower or the toe angle bigger. In this way, the weld quality will be further improved by not only ensuring consistent bead width through sensing pool width, as mentioned in chapter 4, but also guaranteeing reasonable weld geometry. The second application for offline profile measurement uses this system as a gauge to evaluate the quality of a weld by measuring its geometry and surface imperfections. Both applications could use the same image processing algorithms developed in the thesis, which will be introduced in detail in the following sections.

5.2 The Images of Bead Profile

The normal bead profile images of TIG and MIG welds are displayed in Figure 5. 2, where (a) shows the images of TIG weld, (b) shows the images of MIG weld. The bottom two images in Figure 5. 2 are those with band-pass filters chosen according to the laser diode's wavelength, which remove all the light except those from laser. In this way, image processing can be carried out without disturbance from other light source. Figure 5. 3 shows the bead profile with two-sided undercuts.

It can be seen that the laser lines of normal bead profile for both TIG and MIG welds have regular shapes, an obvious hump in the middle, which just represents the bead. Therefore, the task of image processing is to extract the width and height of the hump as well as the angle between hump and straight line, which relates to the toe angle. It is necessary to have a point of reference from which the heights or depths of the weld are measured. As with the traditional weld gauge, the point of reference is chosen to be the surface of parent metal on one side of the weld. This highlights one of the constraints of the measurement system, namely that surfaces on either side of the weld must be visible in the digitised image. Later it will be shown that these two surfaces should occupy >40% of the total line length in the image, since all bead profile measurements are made with respect to the surface of the parent weld metal.

The approach of corner detection presented in last chapter can be used here to extract two corners of hump roots, and then the width of the bead could be obtained. The difference of the tangent slope at the detected corner gives the toe angle. The height of the hump can be extracted by locating the point on the hump where the tangent slope is the same as the slope of the line connecting the two detected corners.

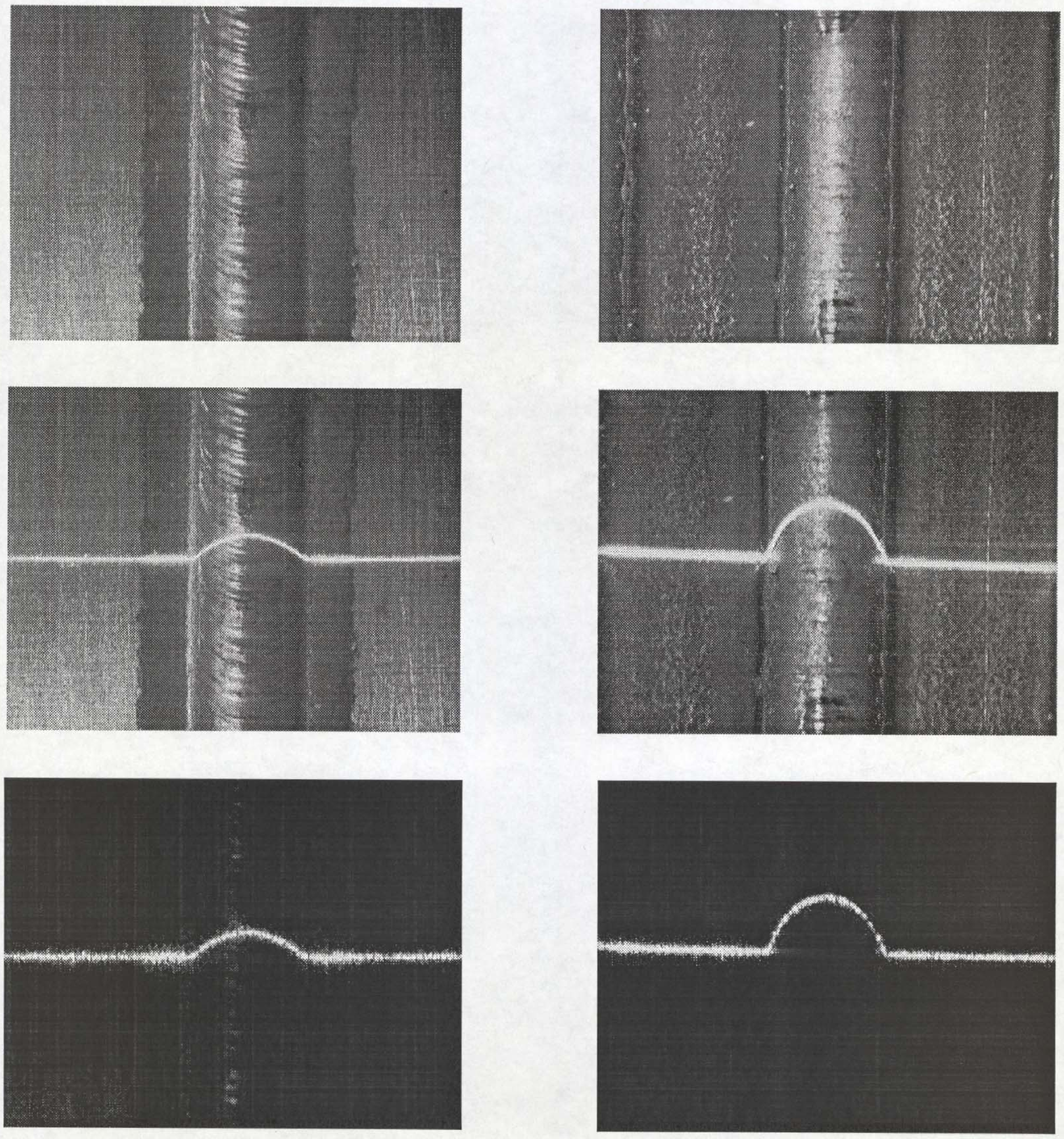

(a) TIG weld **(b) MIG weld**

Figure 5. 2 Normal Bead Profile Images of TIG and MIG Welds

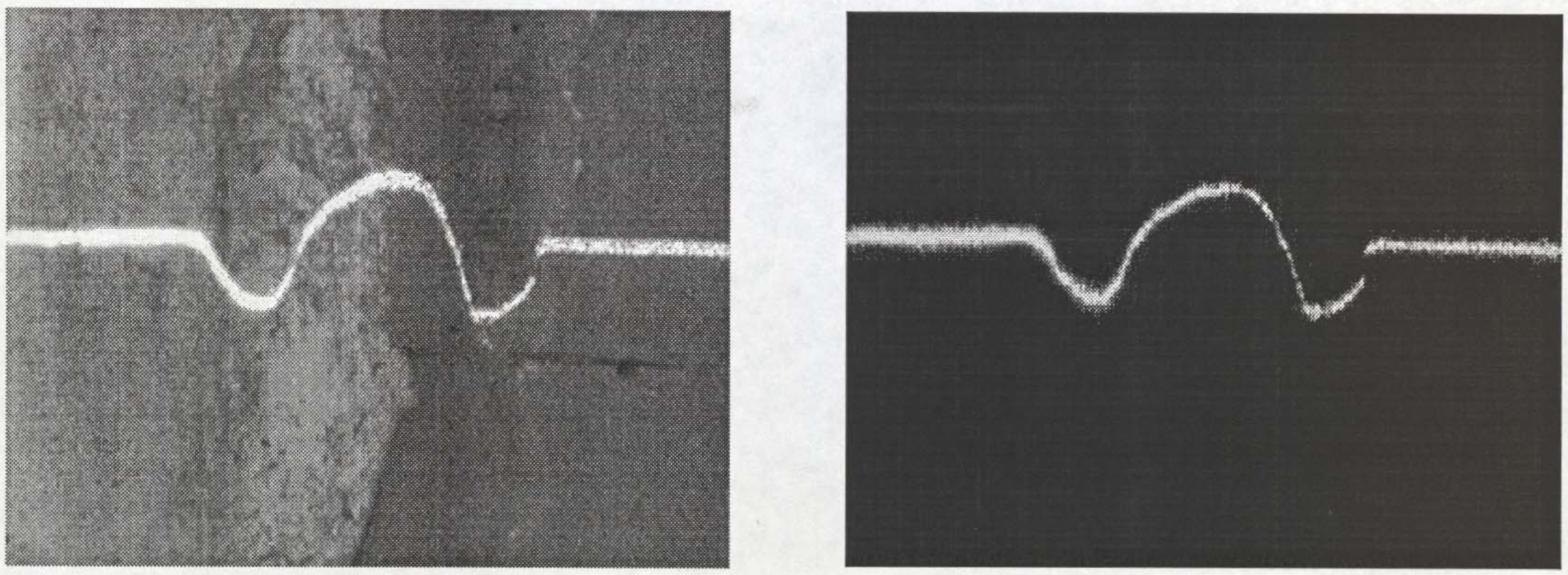
(a) (b)

Figure 5. 3 Bead Profile with Undercut

However, the laser line image of bead profile, where undercuts present, is more complicated than those of a normal bead. In order to evaluate the degree of undercut, their width and height should be measured. To measure the width of undercuts, further segmentation of the laser line is required. Specifically identification of the intersection between the surfaces of the parent metal and the weld bead (the inner points of undercuts *a*' and *b*', as shown in Figure 5. 4) is needed. Using the previously mentioned corner detection, only two corners *a* and *b* could be detected. The other feature points on the curve, such as *a'*, *b'*, *c*, *d*, and *e*, will be missed, since they are actually smooth joins, which have continuous tangent and discontinuous curvature, rather than corners, for which both tangent and curvature are discontinuous. The detection for smooth joins is more difficult than corners and not robust enough to be used in industry.

Analysing the contour in Figure 5. 4, it can be seen that the detection of four feature points *a*, *a'*, *b*, *b'* are crucial for the whole process. As long as these four points are extracted, the other three *c*, *d* and *e* could be obtained by finding the points, which have the same tangent slope as those of the line *a'b'*, *Aa* and *bB* respectively. A very effective method that can solve this problem is the Hough transform, which is used to detect lines, either straight lines or curves. The application of the Hough transform in this research is to locate four crucial feature points by detecting two straight lines on two sides, to which these four points belong. This will be discussed in detail in the following sections.

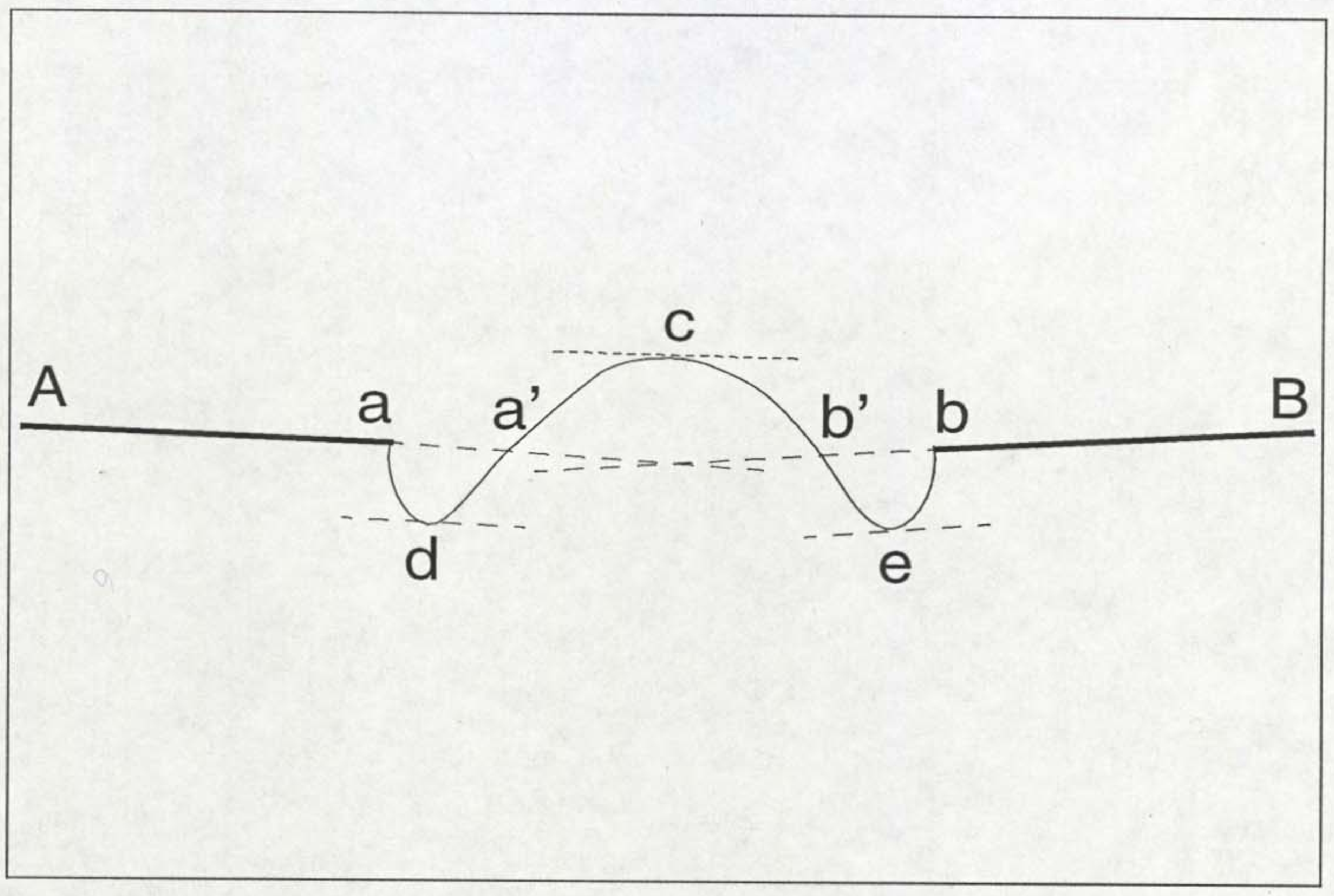

Figure 5. 4 Measurement of Bead Profile with Undercuts

5.3 Hough Transform

Finding line segments in an intensity image has been one of the most fundamental issues in the area of computer vision. The Hough transform is used to link points by determining whether they lie on a curve of specified shape.

Suppose that, for n points in an image, we want to find subsets of these points that lie on a straight line. One possible solution is first to find all lines determined by every pair of points and then find all subsets of points that are close to particular lines. The problem with this procedure is that it involves finding $n(n-1)/2 \sim n^2$ lines and then performing $(n)(n(n-1))/2 \sim n^3$ comparisons of every point to all lines. This approach is computationally prohibitive in all but the most trivial applications.

5.3.1 Standard Hough Transform

Hough proposed an alternative approach, commonly referred to as the Hough transform. Consider a point (x_i, y_i) and the general equation of a straight line in slope-intercept form, $y_i=ax_i+b$. Infinitely many lines pass through (x_i, y_i), but they all satisfy the equation $y_i=ax_i+b$ for varying values of a and b. However, writing this equation as $b=-x_ia+y_i$ and considering the ab plane (also called parameter space) yields the equation of a single line for a fixed pair (x_i, y_i). Furthermore, a second point (x_j, y_j) also has a line in parameter space associated with it, and this line intersects the line associated with (x_i, y_i) at (a', b'), where a' is the slope and b' the intercept of the line containing both (x_i, y_i) and (x_j, y_j) in the xy plane. In fact, all points contained on this line have lines in parameter space that intersect at (a', b'). Figure 5. 5 illustrates these concepts.

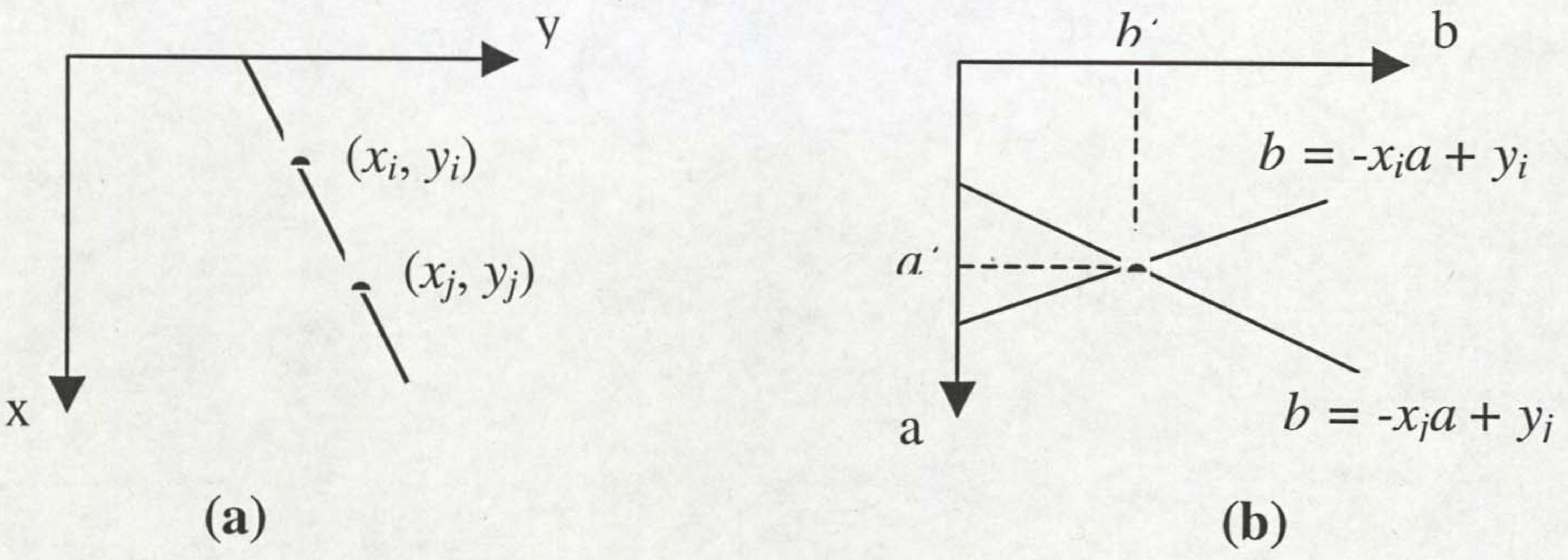

Figure 5. 5 (a) xy plane; (b) parameter space

The computational attractiveness of the Hough transform arises from subdivision of the parameter space into so-called accumulator cells. The cell at coordinates (i, j), with accumulator value $A(i, j)$, corresponds to the square associated with parameter space coordinates (a_i, b_i). Initially, these cells are set to zero. Then, for every point (x_k, y_k) in the image plane, we let the parameter a equal each of the allowed subdivision values on the a axis and solve for the corresponding b using the equation $b=-x_k a+y_k$. The resulting b's are then rounded off to the nearest allowed value in the b axis. If a choice of a_p results in solution b_q, we let $A(p, q)=A(p, q)+1$. At the end of this procedure, a value of M in the xy plane lie on the line $y=a_i x+b_j$. The accuracy of the collinearity of these points is determined by the number of subdivisions in the ab plane.

A problem with using the equation $y=ax+b$ to represent a line is that both the slope and intercept approach infinity as the line approaches the vertical. One way around this difficulty is to use the normal representation of a line instead:

$$x\cos\theta + y\sin\theta = \rho$$

Figure 5. 6 shows the meaning of the parameters used in this equation. The use of this representation in constructing a table of accumulators is identical to the method discussed for the slope-intercept representation. Instead of straight lines, however, the loci are sinusoidal curves in the $\rho\theta$ plane. As before, M collinear points lying on a line $x\cos\theta_j+y\sin\theta_j=\rho_i$ yields M sinusoidal curves that intersect at (ρ_i, θ_j) in the parameter space. Incrementing θ and solving for the corresponding ρ gives M entries in accumulator $A(i, j)$ associated with the cell determined by (ρ_i, θ_j).

The range of angle θ is ±90°, measured with respect to the x axis. Thus a horizontal line has $\theta = 0°$, with ρ being equal to the positive x intercept. Similarly, a vertical line has $\theta = 90°$, with ρ being equal to the positive y intercept, or $\theta = -90°$, with ρ equal to the negative y intercept.

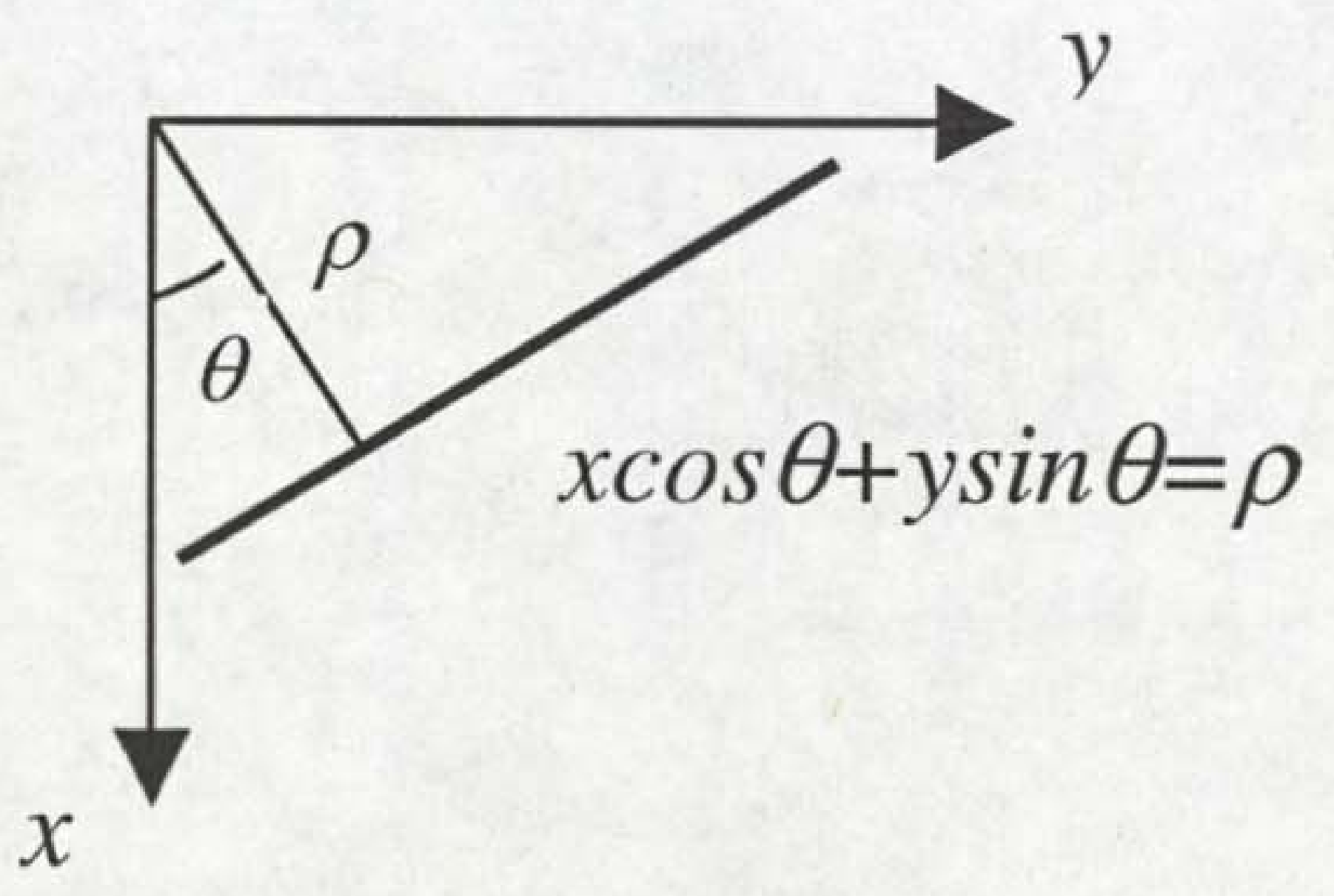

Figure 5. 6 Normal representation of a line

An approach based on the Hough transform consists of the following steps:

- Specifying subdivisions in the $\rho\theta$ plane.
- Examining the counts of the accumulator cells for high pixel concentrations.
- Examining the relation (principally for continuity) between pixels in a chosen cell. The concept of continuity in this case usually is based on computing the distance between disconnected pixels identified during traversal of the set of pixels corresponding to a given accumulator cell. A gap at any point is significant if the distance between that point and its closest neighbours exceeds a certain threshold.

5.3.2. Modified Hough Transform (MHT)

The heavy burden of computational complexity and massive storage requirement is the drawback of the standard Hough transform because for each point in the image space, all the points on the corresponding curve in the parameter space are calculated and stored. Figure 5. 7 shows the typical votes in parameter space for the curve shown in Figure 5. 4. The x axis represents discrete θ with an interval $\Delta\theta = 5°$, y axis is discrete ρ with interval $\Delta\rho = 10$. This means that the size of the accumulator cell in the parameter space is 5°×10. The total number of cells is 36×50 with the θ range from -90° to 90°, ρ from –250 to 250. Here we have to point it out that the discretization of parameter space is very important for the performance of the Hough transform. This will be discussed in the later sections.

From Figure 5. 7, it is noticed that most of cells are only incremented to 1 or 2. This means that most of computation is unnecessary. Given a line with N pixels, then the computation time will be proportional to N×K. Here K is the quantity of the sampling parameter θ. To overcome these weaknesses of the Hough transform, many modified approaches have been presented [5.1].

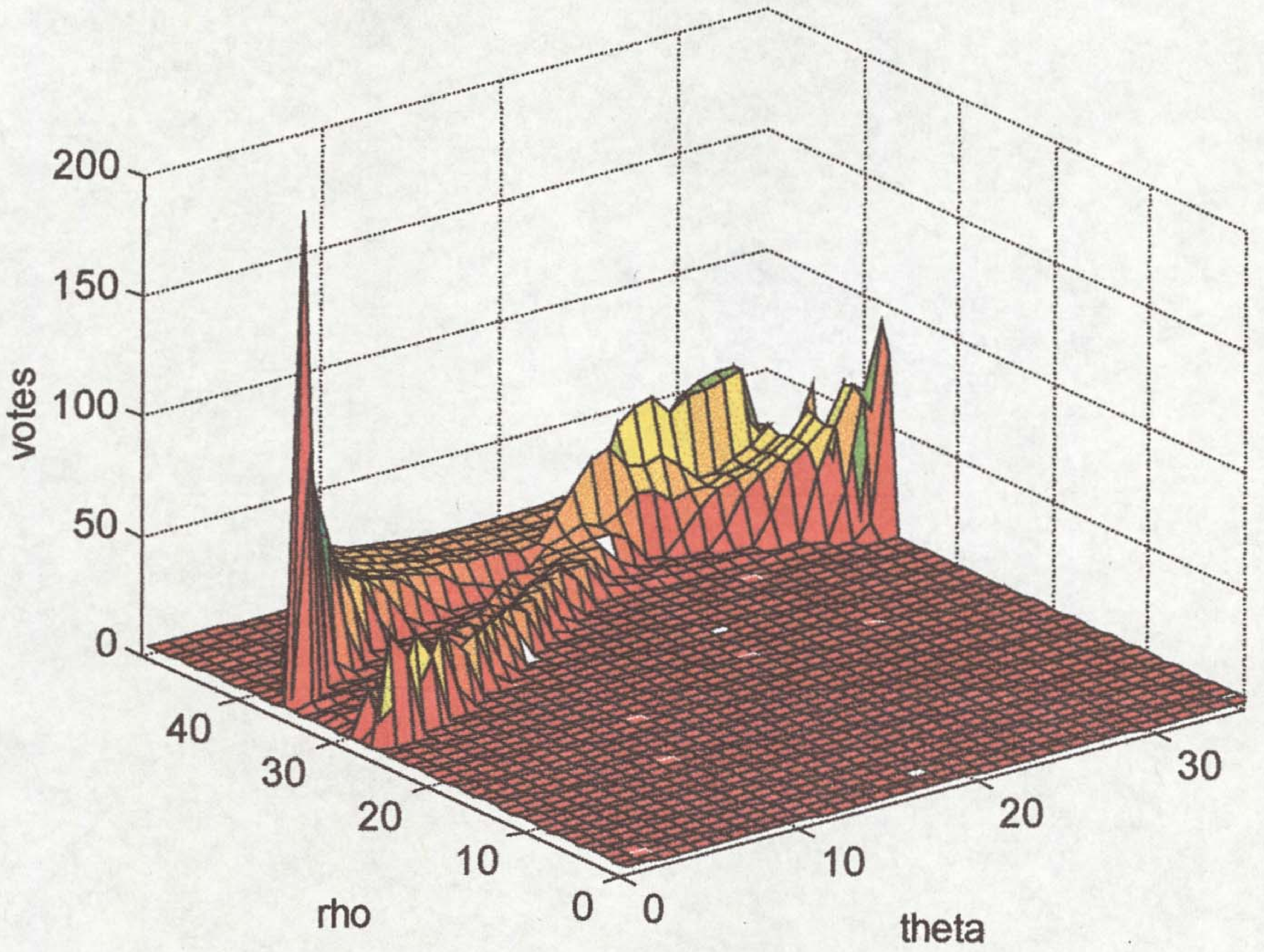

Figure 5. 7 Standard Hough Transform of Bead Profile with Undercut

A new technique of the Hough transform the "probabilistic Hough transform (PHT)", has appeared in recent years [5.2]-[5.6]. All the PHT approaches, although differing in many respects, share a common feature: each set of *n* feature points in the image, where *n* equals the number of parameters in Hough space, is mapped into just one cell in the parameter space. That is to map manifold into one. Therefore, the computational time and storage requirement are reduced greatly.

One classical PHT algorithm is the Randomised Hough Transform (RHT), which is based on the fact that every pixel pair $d(x_i, y_i)$ and $d(x_j, y_j)$ on the detected line can be mapped into a single parameter point (θ, ρ) using following equations:

$$\theta = \tan^{-1} \frac{x_i - x_j}{y_j - y_i}$$

$$\rho = x_i \cos\theta + y_i \sin\theta$$

The pixel pair (d_i, d_j) is selected randomly and removed after mapping. For a line with N pixel length, the computation time is N/2. If considering that two parameters are calculated, the computation time will be N, which is still K times less than the standard Hough transform.

5.4 Measurement of Bead Profile

The laser stripe projected on the bead carries sufficient information for measuring the bead profile. The first step of image processing is to perform stripe thinning on the laser line to extract its media axis. This has been discussed in chapter 4. Then further analysis of this one pixel width curve is conducted.

First of all, examination is made along the curve to determine the existence of undercuts, which is presented by two flags: leftundercut and rightundercut. It starts from two sides to the centre to look for the position drops that are bigger than a predefined threshold. If these position drops can be found, the corresponding flags are set to be true. This procedure can be illustrated as follows:

```
Procedure ExamineUndercut ()
begin
    Bool      leftundercut = false,
    Bool      rightundercut = false;
    Point     start, end;
    Integer   differential, threshold;
    Integer   $x$, $y$, $l$;
    for $x$ = (start.$x$+$l$) to (end.$x$-start.$x$)/2 do
        differential = $y(x+l)$ - $y(x-l)$;
        if differential < -threshold then
            leftundercut = true;
            left_undercut_loc = $x$;
            break;
    endfor
```

```
    for $x$ = (end.$x$-$l$) to (end.$x$-start.$x$)/2 do
        differential = $y(x+l) - y(x-l)$;
        if differential > threshold then
            rightundercut = true;
            right_undercut_loc= $x$;
            break;
    endfor
end
```

5.4.1 Line Detection using MHT

In this application, the objective is to extract two straight lines, the locations of which are already known. Thus, it is not necessary to randomly select all the point pairs for calculation in parameter space. Instead, one seed point is assigned for each straight line and the remaining point is selected in turn. The selected point and the seed point would jointly comprise a pair of points, which define one straight line in the image. Since seed points for two lines have been assigned as the left and right ends on the curve, it is guaranteed that they are the points located on two straight lines. Thus only one calculation of θ in parameter space is needed. As a result, a one-dimensional accumulator array is created instead of two-dimensional array. The calculation time and storage requirement is, therefore, reduced greatly.

In order to detect two straight lines located on two sides, the MHT was carried out from two sides to the centre separately. The process of the MHT is explained as follows:

1) *Select seed point* $S(x_s, y_s)$.

Seed points are chosen on two sides, one for each line separately. In this case the leftmost and the rightmost points A and B, as shown in Figure 5. 4, were selected.

2) *Select each remaining point on the line* $P(x_i, y_i)$ $(i = 1, 2,\ldots N, i \neq s)$, *where* N *is the total number of the points on the line.*

After the seed points have been selected, each remaining point on the line will be selected in turn according to the sequence of the elements. For the left half of the curve, it is from left to right, but the reverse for the right half of it. The selected feature point and the seed point would jointly comprise a pair of points, which would definitely decide one straight line in the image.

3) Calculate θ in parameter space for each point pair $S(x_s, y_s)$, $P(x_i, y_i)$.

From the standard HT, we have:

$$\rho_{s,i} = x_s \cos\theta_{s,i} + y_s \sin\theta_{s,i},$$
$$\rho_{s,i} = x_i \cos\theta_{s,i} + y_i \sin\theta_{s,i}.$$

Then

$$\theta_{s,i} = \tan^{-1}(\frac{x_i - x_s}{y_s - y_i})$$

and

$$\left|\rho_{s,i}\right| = \frac{\left|x_s \cdot y_i - x_i \cdot y_s\right|}{\sqrt{(x_s - x_i)^2 + (y_s - y_i)^2}}.$$

As only parameter θ is needed in this method, ρ need not be calculated in this step.

4) Accumulate parameter space.

An accumulator array $A(\theta)$ is created to store the votes for the accumulator cells. Each θ calculated from the last step is round off to the nearest cell. Then the corresponding cell is incremented by 1:

$$A(\theta) = A(\theta) + 1.$$

Meanwhile, a two dimensional array $X(A, \theta)$ (where $A = 1, 2, \ldots, A(\theta)$) is created for storing the coordinates of the image pixels corresponding to every vote in the accumulator cells. Here, only the x coordinate is needed because for each x only one corresponding y exists.

5) Detect peaks in the parameter space.

The largest vote in the accumulator array $A(\theta)$ is detected and regarded as the straight line on the parent metal.

6) Save results in another space for further calculation of the bead parameters.

The θ value for the detected line and the corresponding coordinate for every point on the line are stored for further calculation.

The above process of MHT on straight line detection can be formulated as the following procedure:

```
Procedure ModifiedHoughTransform()
begin
    Point   seed;
    Double $\theta$, $\Delta\theta$;
    Integer $x$, $y$, $n_\theta$;
    Integer A[$n_\theta$];                    /* accumulator array */
    Integer X[$n_\theta$][window_width/2]; /* coordinate array */
    A=NIL;
    X=NIL;
    $n_\theta$ = int($\pi/\Delta\theta$);
    for $x$ = seed.x to x = window_width/2 do
        if $y \neq seed.y$ then
            $\theta$ = atan(($x$-seed.x)/(seed.y-$y$));
        else
            $\theta = \pi/2$;
        endif
        $q$ = int(($\theta + \pi/2$) / $\Delta\theta$);      /* round off $\theta$ to $q$ */
        A[$q$] = A[$q$] + 1;
        X[$q$][A[$q$]] = $x$;
    endfor
end
```

5.4.2 Discretization of Parameter Space

Ideally, $A(\theta_i)$ is the number of image pixels that any curve in cell θ_i passes through. However, this is not always correct for two reasons. Firstly, this assumes that there is no localisation error in the image pixels. When a localisation error presents, the cell corresponding to the position of the curve may not receive a vote for various pixels that belong to the curve. Secondly, a single cell may receive votes from multiple image pixels that cannot lie on the same line, even when the localisation error is considered. It is implicitly assumed that the cells are large enough to catch the votes for the curves of interest, yet small enough not to catch a large number of votes from false positive curves. Therefore, the determination of the cell size is the key for the discretization of the parameter space.

In the MHT, the parameter space has been simplified to one dimension, only parameter θ is considered. The range of θ is $(-\pi/2, \pi/2)$. Given the quantization interval $\Delta\theta$, then the size of accumulator array would be $\pi/\Delta\theta$, while the size of coordinate array $X(A, \theta)$ would be $(\pi/\Delta\theta)\times N$ (where N is defined as before). The size of Hough space would then be:

$$S = \frac{\pi}{\Delta\theta} + \frac{\pi}{\Delta\theta}\cdot N = \frac{\pi}{\Delta\theta}\cdot(N+1).$$

In several proposed quantization schemes of Hough space, $\Delta\theta$ is determined in different ways. The three typical quantization schemes of the Hough transform are Diagonal quantization [5.9], Hifi quantization [5.10], and Yuan's quantization method [5.11]. The quantization interval $\Delta\rho$ and $\Delta\theta$ of each method is:

1) *Diagonal quantization*

$$\Delta\rho = \frac{1}{2\sqrt{2}}, \qquad \Delta\theta = \frac{1}{2N}.$$

2) *Yuan's quantization*

$$\Delta\rho = 1, \qquad \Delta\theta = \frac{2}{N}.$$

3) *Hifi quantization*

$$\Delta\rho = \frac{1}{N(N-1)^2}, \qquad \Delta\theta = \frac{1}{2(N-1)^2}.$$

In this application, since $N = 192$ (half the window width), even though Yuen's method is applied, $\Delta\theta \cong 0.01$ (about 0.57°), which is still far too small as peak spread occurs. This means that the cell is not large enough to catch the votes for the lines of interest. This is illustrated in Figure 5. 9(a), in which the detected line is broken severely. When $\Delta\theta = 0.08$ (about 4.6°) (Figure 5. 11(a)), it seems that the detected line is extended too much. So $\Delta\theta$ was determined by experiment and the best result is obtained when $\Delta\theta = 0.04$ (about 2.3°) (Figure 5. 10) for this application. The images in Figure 5. 9(a), 5.10(a) and 5.11(a) are the original laser contour with the detected two straight lines (white dot lines above the contour) using the modified Hough transform, where the white crosses mark the ends of the detected lines and their intercepts with the contour. The bar graphs (b) and (c) under these images represent the vote distributions in the accumulator array for the left half curve and the right half curve in the image window respectively. The x axis is the number of quantized θ corresponding to a range of $-\pi/2$ to $\pi/2$. This number is decreased with the increase of quantization interval $\Delta\theta$. It can be seen that the maximum votes always occur around $\pm\pi/2$, as the detected lines are close to horizontal.

An accumulator cell (θ_l, θ_r) of width $\Delta\theta$ corresponds to a fan shaped area originated from a seed point with an angle of $\Delta\theta$ in image space, as shown in Figure 5. 8. All the feature points on the profile line, within this fan shaped area, will contribute to this cell in the parameter space. Using the fan shaped mapping, fan top area is very sensitive to the distortion of the detected line. Therefore the selection of the seed point is crucial to ensure the correct detection of the straight line.

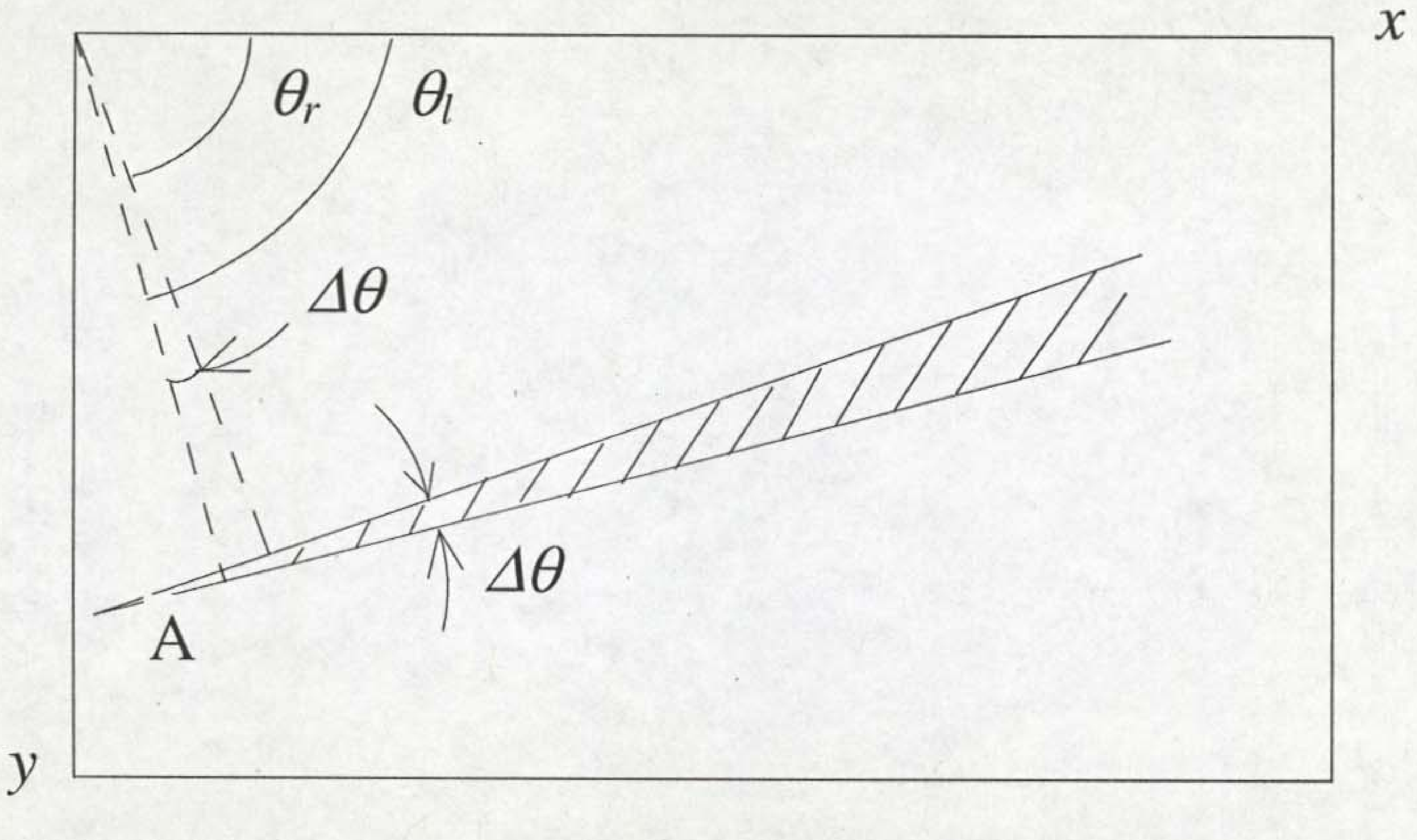

Figure 5. 8 Mapping of an Accumulator Cell to Image Space

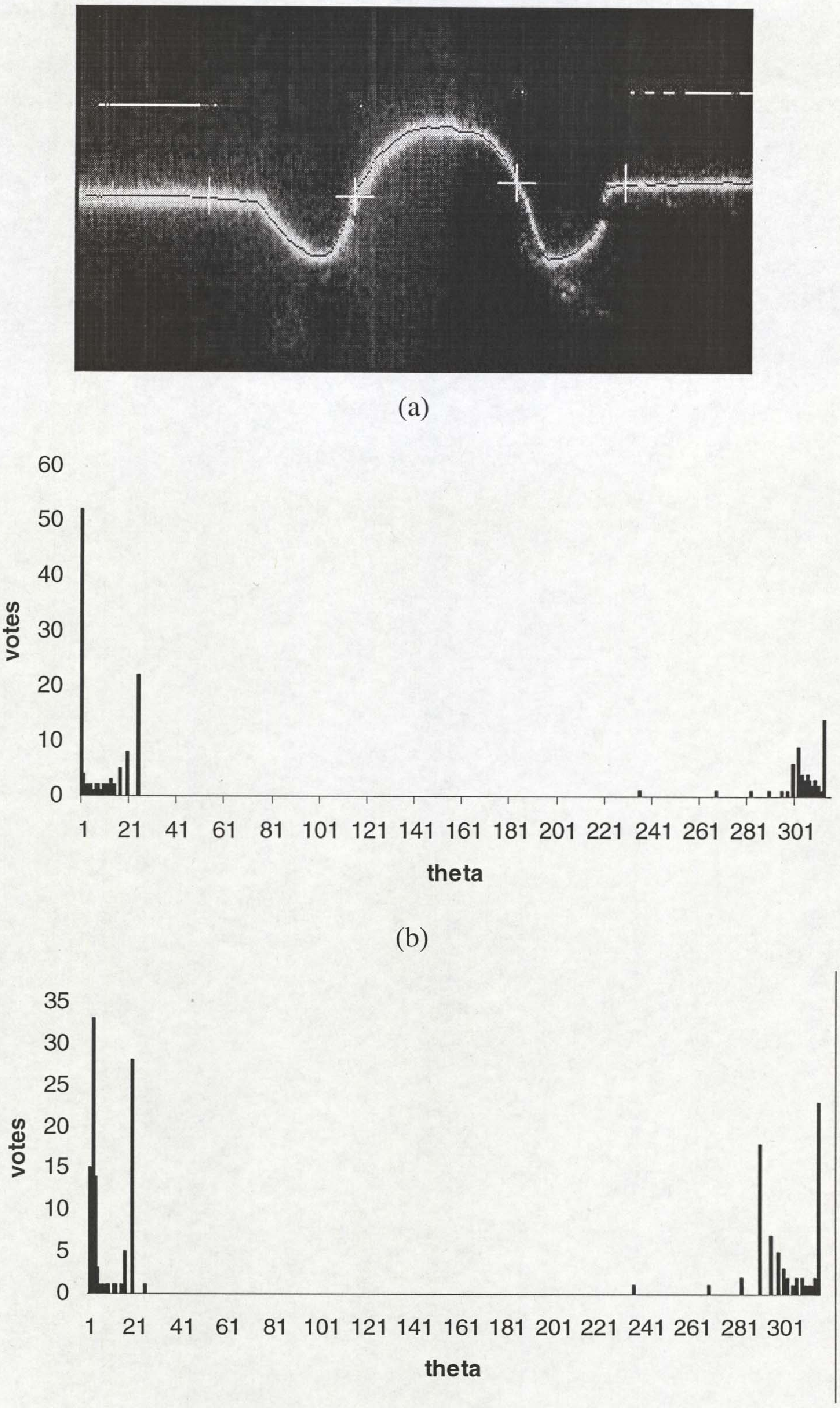

(a)

(b)

(c)

Figure 5. 9 Hough Transform with $\Delta\theta = 0.01$

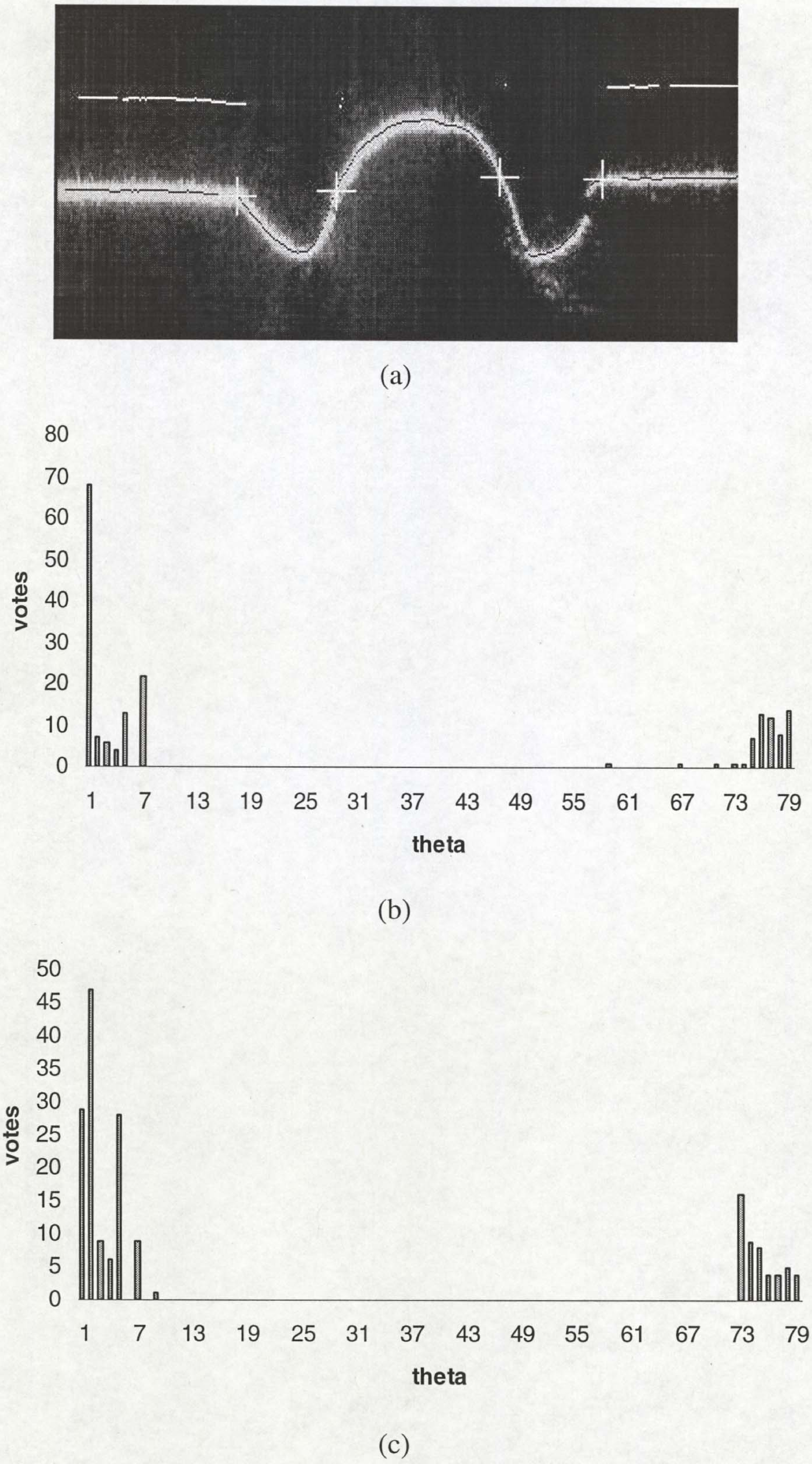

(a)

(b)

(c)

Figure 5. 10 Hough Transform with $\Delta\theta = 0.04$

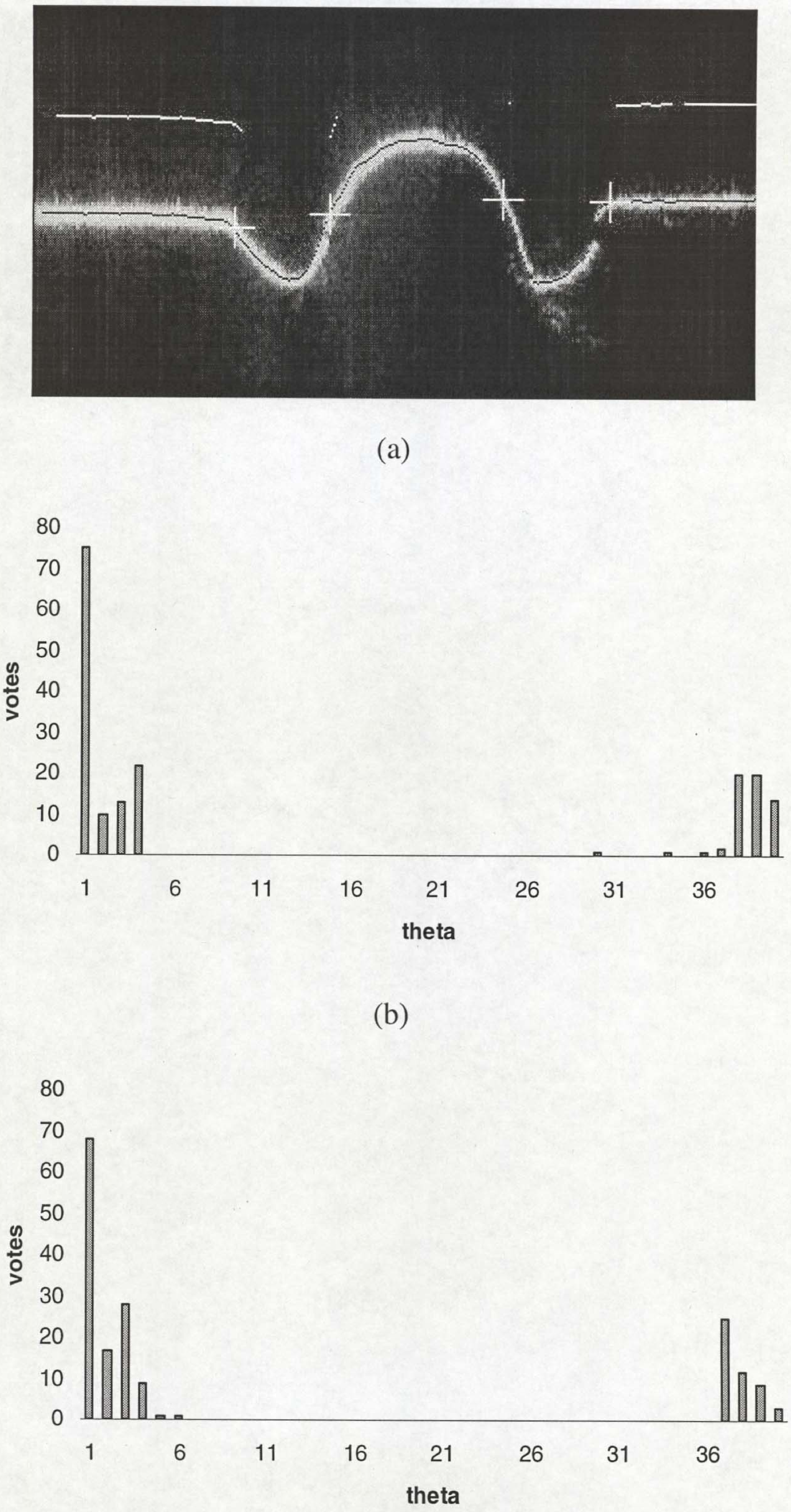

(a)

(b)

(c)

Figure 5. 11 Hough Transform with $\Delta\theta = 0.08$

Another problem encountered in the application of modified Hough transform is the constraints of the minimum occupation of either side of the parent metal in the total line length. In order to get the maximum votes, in parameter space, for the two lines on the parent metal, these two lines should occupy more than 20% each of the total line length. Otherwise the maximum votes would go for the line on the bead rather than on the parent metal, as shown in Figure 5. 12.

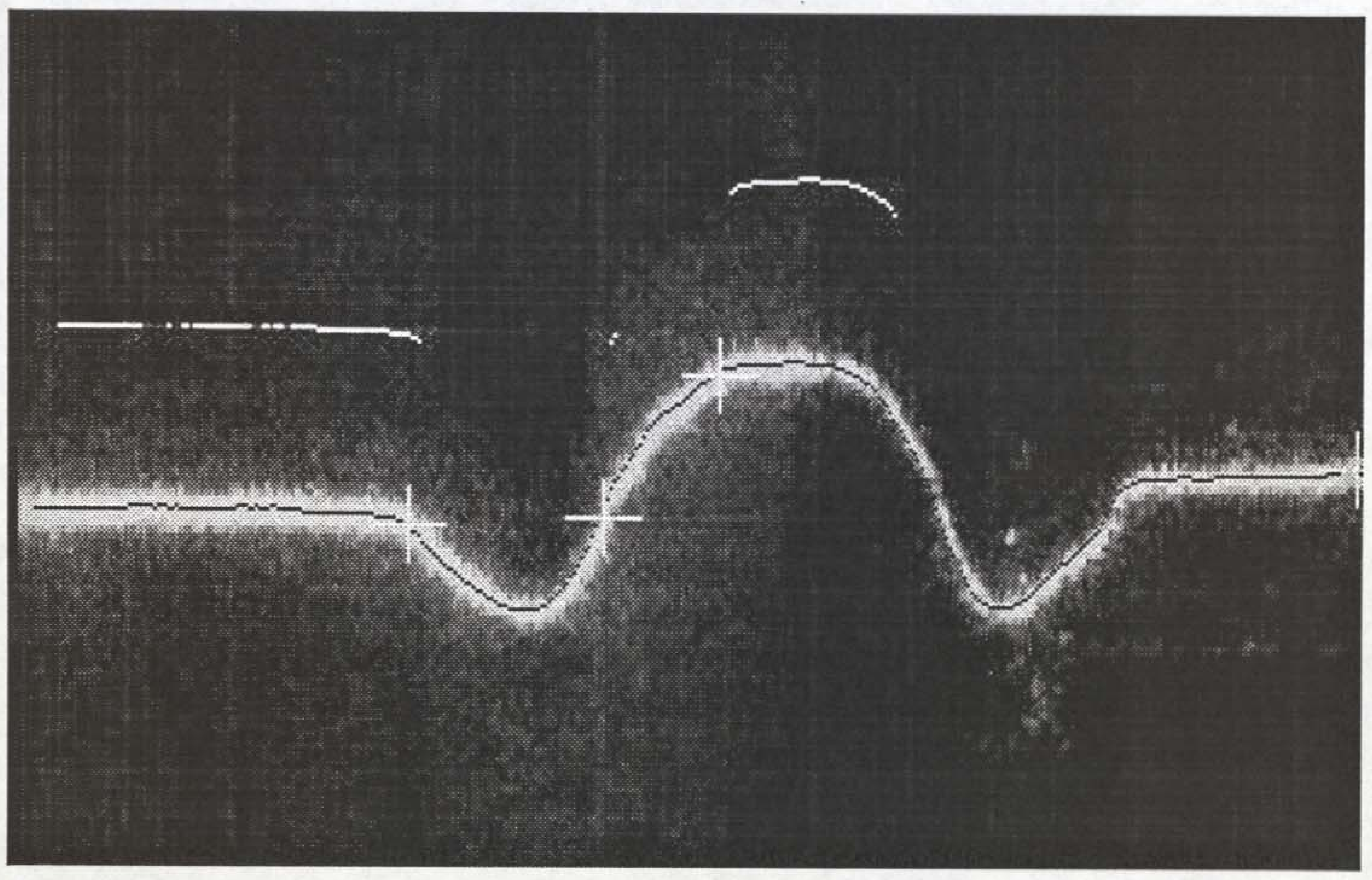

Figure 5. 12 Mis-detection

5.4.3 Feature Extraction

After using modified Hough transform, the complete description of the two straight lines can be extracted. They are the location ρ, orientation θ, line length and line ends. The former two parameters are stored in the accumulator array $A(\theta)$, while the later two can be determined from the coordinate array $X(A, \theta)$ using the search algorithm described in the following procedure. It searches for the end point of the line by defining different search ranges in the occurrence or absence of undercut based on the result of procedure ExamineUndercut().

```
Procedure SearchLineEndIntercept()
begin
    line_end = 0;
    if leftundercut is true then
        search_end = left_undercut_loc;
    else
        search_end = pos_points/2;
```

```
    for $i = 1$ to $i = \max(A[\theta])$ do
        if $X[\theta][i] \le$ search_end then
            if $X[\theta]][i] >= line\_end$ then
                $line\_end = X[\theta][i]$;
        else
            intercept = $X[\theta][i]$;
    endfor
    Repeat above procedure to search for right undercut.
end
```

The two inside ends of the straight lines are marked by white crosses and named as P_1 and P_7 in Figure 5. 13. They would be the left and right corners of the bead. Meanwhile, the intercepts of the two lines with the bead profile have been found, which fall into the same accumulator cells as the straight lines. That would be the inside limit of the undercut P_3 and P_5. At this point, the laser stripe has been segmented by the points P_1, P_3, P_5, P_7 to five parts: parent metal, left undercut, bead, right undercut and parent metal.

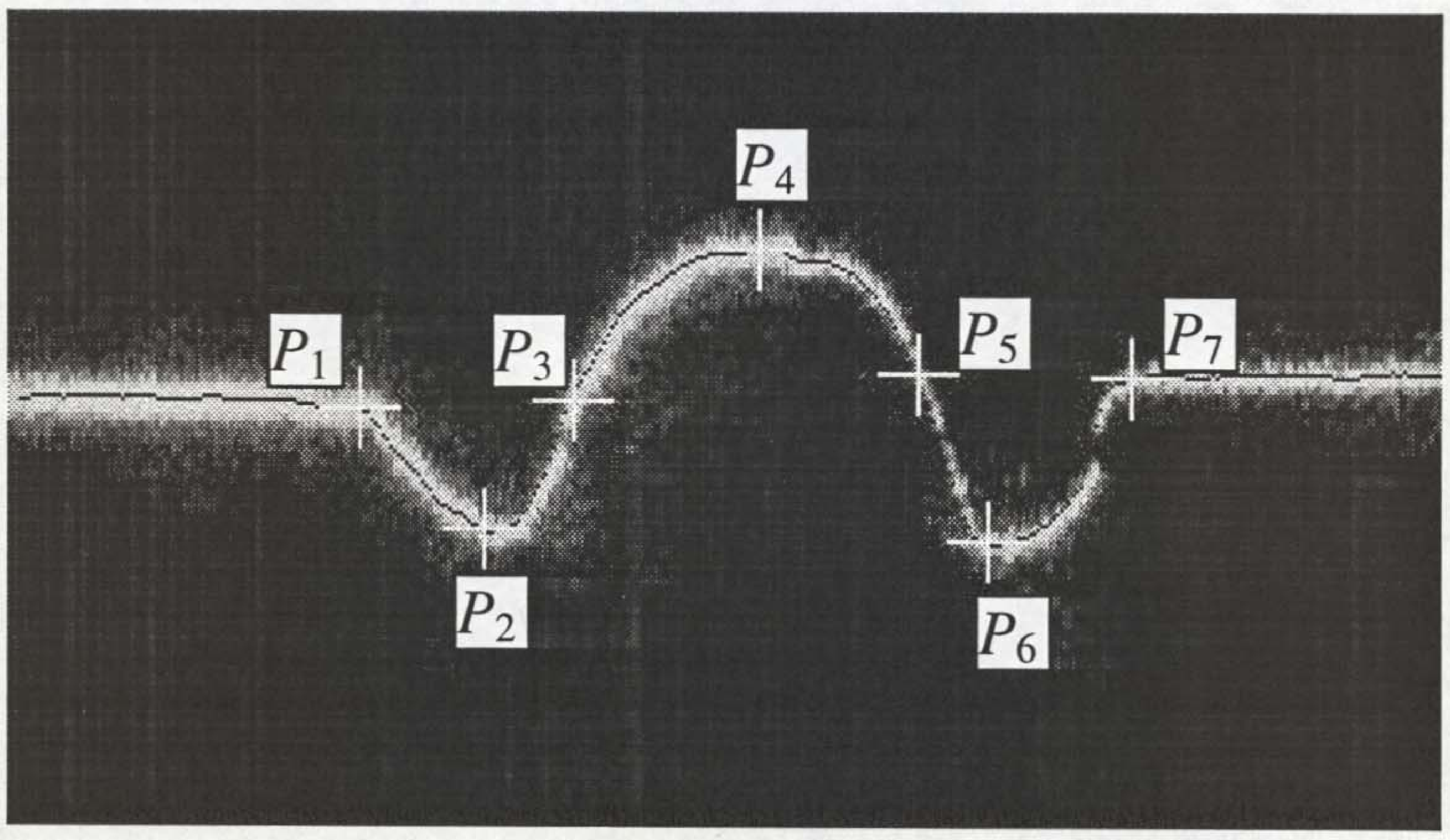

Figure 5. 13 Extracted Feature Points on Profile

The next step is to search for the peaks P_2, P_4 and P_6 of the bead and undercuts in order to decide reinforcement and the depth of undercut. They can be obtained by finding the points with the same tangent slopes as those of the two straight lines and line P_3P_5 respectively. This means that the tangent of P_2 is parallel to the left straight line, the tangent of P_6 parallel to the right straight line and that of P_4 parallel to P_3P_5.

The calculation of the tangent of a point (x_i, y_i) on the curve is carried out using the following equation:

$$\theta_{ij} = \tan^{-1}\left(\frac{y_{i+l} - y_{i-l}}{x_{i+l} - x_{i-l}}\right)$$

where the supporting length, $l \geq 1$, was decided by experimentation. Here l=3 was chosen.

Calculation of parameters relating to the classification of the weld profile can now be made. Such parameters are outlined below with a description of their respective methods of implementation.

1) Bead width

It is defined, in this situation, as the Euclidean distance between the two inner points of undercuts (P_3, P_5), and calculated as:

$$d(P_3, P_5) = \sqrt{(x_5 - x_3)^2 + (y_5 - y_3)^2}.$$

2) Reinforcement

It is given as the perpendicular distance of point P_4 to the straight line P_3P_5. If the line is specified in its normalised implicit form:

$$ax + by + c = 0$$

then r, the distance of a perpendicular from a point (x_i, y_i) to the line is:

$$r = ax_i + by_i + c$$

3) Undercuts

The width of undercuts is defined as the distance between P_1 and P_3, and P_5 and P_7 respectively for left and right undercuts. The depth of the undercuts is calculated as the perpendicular distance of the point P_2 to the line P_1P_3 for left undercut and the point P_6 to the line P_5P_7 for right undercut respectively.

5) Angle between two plates

In the profile measurement the angle between two parent weld metal plates is calculated to give a measure of angular distortion. It can be determined straightforwardly, as the tangent θ of the two straight lines on the parent metal are already known from the Hough transform.

Figure 5. 14 shows the profile of a normal bead. Three feature points are extracted here. Consequently, bead width, reinforcement and plate angle can be determined as mentioned before. In this case another parameter, toe angle, is calculated as follows.

6) Toe angle

Toe angle is defined as the difference between the average directions of the line before and after corner points $P(x_k, y_k)$ within the support region L and measured using the following equation:

$$\alpha = \frac{1}{L}\sum_{i=k+1}^{k+L}(\tan^{-1}\frac{y_i - y_k}{x_k - x_i}) - \frac{1}{L}\sum_{i=k-L}^{k-1}(\tan^{-1}\frac{y_i - y_k}{x_k - x_i})$$

where $P(x_k, y_k)$ is the corner point P_1 or P_7.

The developed algorithm for bead profile segmentation is a non-iterative computationally efficient method, which requires only one accumulation of the accumulator array. It is time saving comparing with the previous Hough transform methods. Experiments have shown that 3 seconds was required on a P5/100 computer for a frame when using the standard Hough transform. It was reduced to 200ms when the modified Hough transform was applied, which makes it attractive for use in real-time applications.

Since the feature points were found using the Hough transform algorithm, and all weld height (depth) measurements were made with respect to the surface of the parent weld metal, the laser line can have any orientation within the digitised picture frame. The laser line measurement system is said to be rotationally invariant. This rotational invariance removes the need for complex ‘set-up’ procedures.

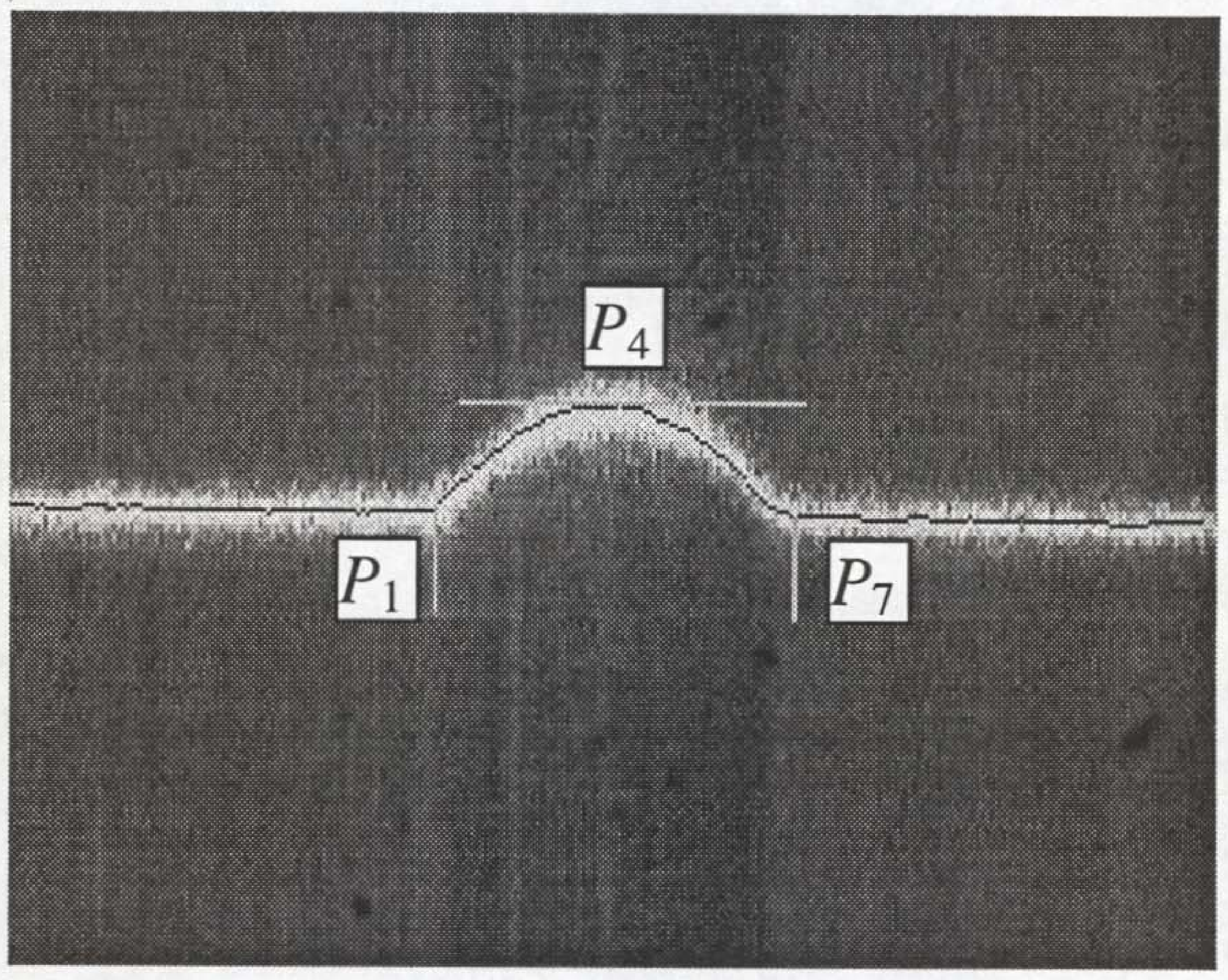

Figure 5. 14 Feature Extraction for a Normal Bead

5.4.4 Calibration

The algorithms discussed previously provide data relating to the extent of the weld profile in pixel units. To convert these units into physical dimensions the process of calibration must take place. Although theoretically possible, calculation of the number of pixels/mm from measurement of the profile monitor hardware is considered impracticable. Instead a number of ‘step’ samples are machined to a given size. Before measurement takes place, a calibration sample of known step size is placed under the sensor. The sensor digitise the profile image of this calibration piece. By entering the step size of the calibration piece, the number of pixels/mm can be accurately determined.

CHAPTER 6 SENSOR SYSTEM SOFTWARE

The image processing was undertaken on a P5/350 machine running Windows NT with the software coded in Visual C++ 6.0. This chapter gives the details of the software design. The application software is divided into two categories, based on the video capture cards used, as the support software is quite different for the WIN/TV and PICOLO cards. The WIN/TV card was used in pool monitoring with the application software named MDIPoolCap and the PICOLO was used for seam tracking and bead profile measurement with the program named PicoloSeam.

6.1 MFC, SDI and MDI

The software design in this thesis uses the Microsoft Foundation Class Library (MFC) in Visual C++. MFC is an "application framework" for programming in Microsoft Windows. Written in C++, MFC provides much of the code necessary for managing windows, menus, and dialog boxes; performing basic input/output; storing collections of data objects; and so on. All that is needed is to add the application-specific code into this framework. Given the nature of C++ class programming, it's relatively easy to extend or override the basic functionality that the MFC framework supplies.

The MFC framework is a powerful approach that lets us build upon the work of expert programmers for Windows. MFC shortens development time; makes code more portable; provides tremendous support without reducing programming freedom and flexibility; and gives easy access to "hard to program" user-interface elements and technologies, like Active technology, OLE, and Internet programming.

When an application runs under Microsoft Windows, the user interacts with documents displayed in frame windows. A document frame window has two major components: the frame and the contents that it frames. A document frame window can be a single document interface (SDI) frame window or a multiple document interface (MDI) child window. SDI applications allow only one open document frame window at a time. MDI applications allow multiple document frame windows to be opened in the same instance of an application. An MDI application has a window within which multiple MDI child windows, which are frame windows themselves, can be opened, each containing a separate document. In some applications, the child windows can be of different types, such as chart windows and spreadsheet windows. In that case, the menu bar can change as MDI child windows of different types are activated.

6.2 Pool Monitoring Program-MDIPoolCap

MDIPoolCap uses the multiple document interface in its design. Two MDI child windows are created in the main frame window, one is the video capture window for displaying the captured image and implementing image processing on it. This is the top window shown in Figure 6. 1, the other is for displaying the history of the resultant parameters extracted from the image processing. This is the bottom window in Figure 6. 1.

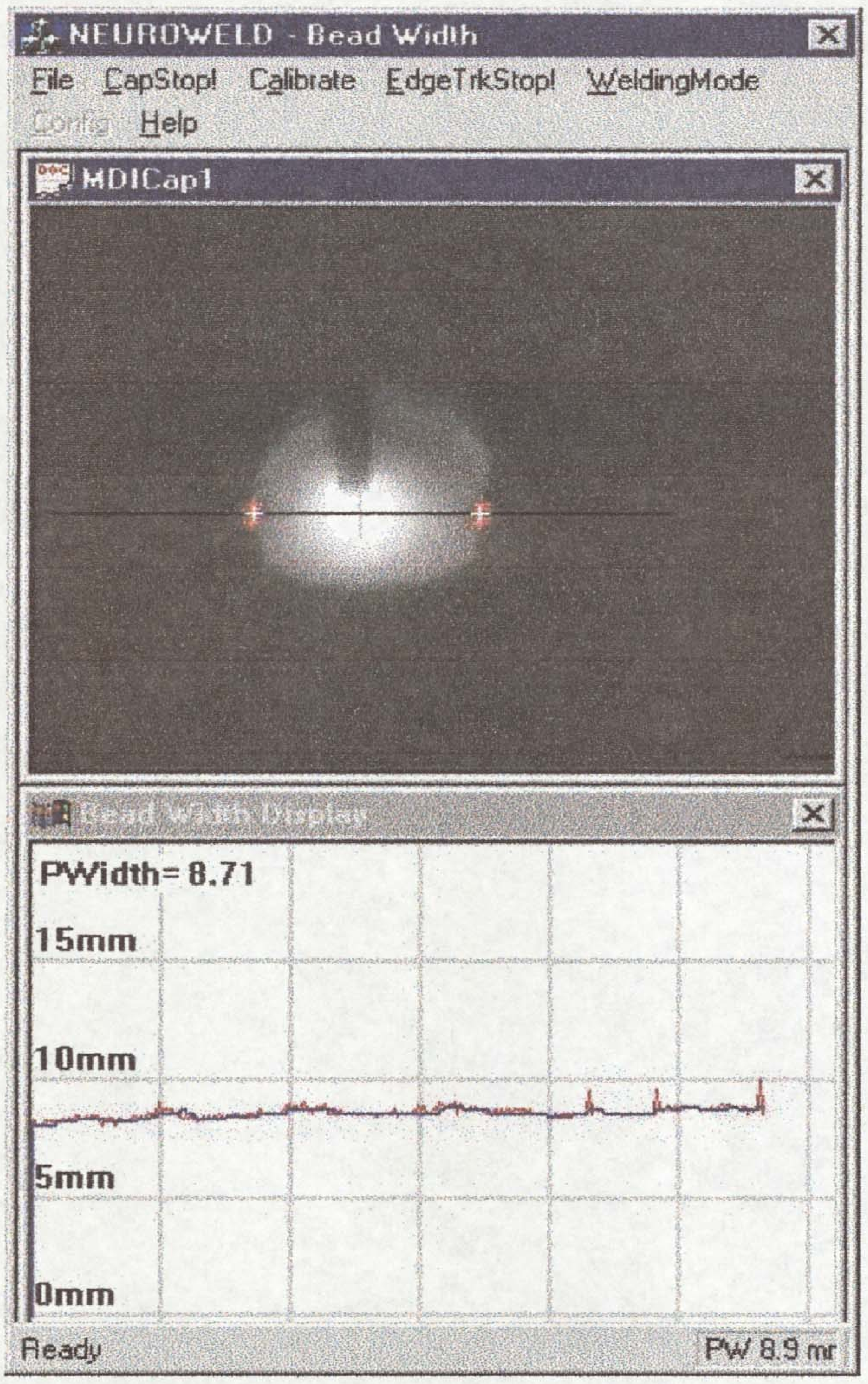

Figure 6. 1 Pool Monitoring Application Window

The window based image processing program MDIPoolCap, was first created by using the MFC AppWizard with a MDI. This MDI application makes full use of a part of the framework called document/view architecture. It contains the following objects:

- An application object CMDICaptureApp derived from class CWinApp.
- A document class object CMDICaptureDoc derived from class CDocument. It is responsible for the internal representation of the data manipulated in the view.
- A view object CMDICaptureView derived from class CView. It is a window that is attached to a document and associated with a frame window. View displays and manipulates the data contained in a document class object. All the functions associated to the menu selection are also included here.
- A frame window object CMainFrame derived from CMDIFrameWnd. In this object, the frame window's size, position and title are specified.
- A child window object CChildFrame derived from CMDIChildWnd. In this object, the child frame window's size, position and title are specified. This is the frame for the capture window.

In addition to the auto created objects by AppWizard, the following objects were created consequently by the author:

- CVidCap derived from CWnd. This object is a data-capture application that captures video sequences onto the computer system. It contains the functions and macros for video capture from Video for Windows. With CVidCap, individual images or entire video sequences from a VCR, a videodisc player, or a video camera can be captured.
- NewVidCap derived from CVidCap. In this object, image processing is implemented within the call back function.
- Another child window object CGraphWnd derived from CMDIChildWnd. This object created a window to display the resultant data of image processing in real time.
- A dialog box object CParamDlg derived from CDialog. In this object, the parameters used for image processing are specified.

- A dialog box object CCalibrateCentre derived from CDialog. This object creates a dialog box to perform the adjustment of the selected pool centre.

6.2.1 Video Capture and Image Processing Program

6.2.1.1 Video Capture

The video capture code was written in the object CMDICaptureView, along with the code to create the video capture window. These codes were executed in the function *OnCreate*, which is a handler function related to the window message WM_CREATE. The video capture program firstly connects the capture window to the capture driver via the macro *DriveConnect(0)*, then specifies the video format and the capture parameters, and finally sets a call back function for the application (the image processing algorithms is called by this function) using the macro *SetCallbackOnVideoStream(TRUE)*. The code is displayed as follows:

```
LPBITMAPINFO          bitmapInfo;
CAPTUREPARMS          parms;

VidCap.DriverConnect(0);

DWORD dwSize = VidCap.GetVideoFormatSize();
bitmapInfo = (LPBITMAPINFO) new BYTE[dwSize];

VidCap.GetVideoFormat(bitmapInfo, dwSize);
bitmapInfo->bmiHeader.biCompression = BI_RGB;
bitmapInfo->bmiHeader.biBitCount = 24;
bitmapInfo->bmiHeader.biPlanes = 1;
bitmapInfo->bmiHeader.biWidth = BMPWIDTH;
bitmapInfo->bmiHeader.biHeight = BMPHEIGHT;
bitmapInfo->bmiHeader.biSizeImage = 0;
VidCap.SetVideoFormat(bitmapInfo, dwSize);

VidCap.CaptureGetSetup(&parms);
parms.dwRequestMicroSecPerFrame = FrameInterval;
```

```
parms.wNumVideoRequested = 3;
parms.fYield = TRUE;
parms.fMakeUserHitOKToCapture = FALSE;
parms.fCaptureAudio = FALSE;
parms.vKeyAbort = 0;
parms.fAbortLeftMouse = FALSE;
parms.fAbortRightMouse = FALSE;
parms.fLimitEnabled = FALSE;
parms.fMCIControl = FALSE;
VidCap.CaptureSetSetup(parms);

VidCap.SetCallbackOnVideoStream(TRUE);
VidCap.AutoSize();
VidCap.Preview(FALSE);
VidCap.CaptureSequenceNoFile();
delete bitmapInfo;
```

There are two very important structures concerned with video capture in the above program: LPBITMAPINFO and CAPTUERPARMS. The first one is a pointer to the structure BITMAPINFO. The following section introduces these two structures in detail.

(1) LPBITMAPINFO

This structure defines the dimensions and colour information for a Windows device-independent bitmap (DIB). It has the following form:

```
typedef struct tagBITMAPINFO
{
   BITMAPINFOHEADER  bmiHeader;
   RGBQUAD           bmiColors[1];
} BITMAPINFO;
```

A device-independent bitmap consists of two distinct parts: a BITMAPINFO structure describing the dimensions and colors of the bitmap, and an array of bytes defining the pixels of the bitmap. The bits in the array are packed together, but each scan line must be padded with zeroes to end on a LONG boundary. If the height is positive, the origin of the bitmap is the lower-left corner. If the height is negative, the origin is the upper-left corner.

In the BITMAPINFO structure, the member *bmiHeader* specifies a BITMAPINFOHEADER structure that contains information about the dimensions and colour format of a device-independent bitmap. It has the following form:

```
typedef struct tagBITMAPINFOHEADER
{
   DWORD  biSize;           /*number of bytes of the structure*/
   LONG   biWidth;          /*width of bitmap, in pixels*/
   LONG   biHeight;         /*height of bitmap, in pixels*/
   WORD   biPlanes;         /*number of planes for target
                              device*/
   WORD   biBitCount        /*number of bits per pixel*/
   DWORD  biCompression;    /*type of compression*/
   DWORD  biSizeImage;      /*size of the image, in bytes*/
   LONG   biXPelsPerMeter;/*horizontal resolution*/
   LONG   biYPelsPerMeter;/*vertical resolution*/
   DWORD  biClrUsed;        /*number of color indices*/
   DWORD  biClrImportant;   /*number of color indices,
                              important*/
} BITMAPINFOHEADER;
```

Another member *bmiColors* specifies an array of RGBQUAD or DWORD data types that describes a colour consisting of the relative intensities of red, green, and blue in the bitmap:

```
typedef struct tagRGBQUAD
{
   BYTE   rgbBlue;
   BYTE   rgbGreen;
   BYTE   rgbRed;
   BYTE   rgbReserved;
} RGBQUAD;
```

(2) CAPTUREPARMS

The CAPTUREPARMS structure contains parameters that control the streaming video capture process. This structure is used to get and set parameters that affect the capture rate, the number of buffers to use while capturing, and how capture is terminated.

```
typedef struct
{
DWORD dwRequestMicroSecPerFrame;/*requested frame rate*/
BOOL  fMakeUserHitOKToCapture;  /*user-initiated capture flag*/
UINT  wPercentDropForError;
BOOL  fYield;                   /*yield flag*/
DWORD dwIndexSize;              /*max number of index entries*/
UINT  wChunkGranularity;        /*logical block size of an AVI file*/
BOOL  fUsingDOSMemory;          /*not used in Win32 applications*/
UINT  wNumVideoRequested;       /*max number of video buffers*/
BOOL  fCaptureAudio;            /*capture audio flag*/
UINT  wNumAudioRequested;       /*max number of audio buffers*/
UINT  vKeyAbort;                /*virtual keycode*/
BOOL  fAbortLeftMouse;          /*abort flag for left mouse button*/
BOOL  fAbortRightMouse;         /*abort flag for right mouse button*/
BOOL  fLimitEnabled;            /*time limit enable flag*/
UINT  wTimeLimit;               /*time limit for capture, in second*/
BOOL  fMCIControl;              /*MCI device capture flag*/
BOOL  fStepMCIDevice;           /*MCI device step capture flag*/
DWORD dwMCIStartTime;           /*start position, in milliseconds*/
DWORD dwMCIStopTime;           /*stop position, in milliseconds*/
BOOL  fStepCaptureAt2x;       /*double-resolution step capture flag*/
UINT  wStepCaptureAverageFrames;/*number of times a frame is
sampled*/
DWORD dwAudioBufferSize;        /*audio buffer size*/
BOOL  fDisableWriteCache;       /*not used in Win32 applications*/
UINT  AVStreamMaster;
} CAPTUREPARMS;
```

6.2.1.2 Visual Design of the Video Capture Window

After video capture has been specified, a variety of tasks can be performed on the captured image by selecting menu items designed on the top of the application window, as shown in Figure 6. 2. The meanings of the menu items are given as follows:

- CapStart is to start and stop the video capture.
- EdgeTrkStart can start and stop edge tracking on a weld pool image.

- WeldingMode gives four welding modes: TIG-AC is the default one for alternating current TIG welding on aluminium, TIG-DC is direct current TIG welding on stainless steel, TIG-Pulsed is pulsed current TIG welding usually on stainless steel and MIG is for MIG welding on mild steel.

- Calibrate is used to invoke a dialog boxes functioned to calibrate the pool centre.

- Config has three pop-up menu items: VideoFormat, VideoSource and ParamSetting. Every one is related to a dialog box for specifying the video format, video source and edge detection parameters respectively. These dialog boxes are introduced in the following sections.

All the functions associated with the menu selection are included in object CMDICaptureView.

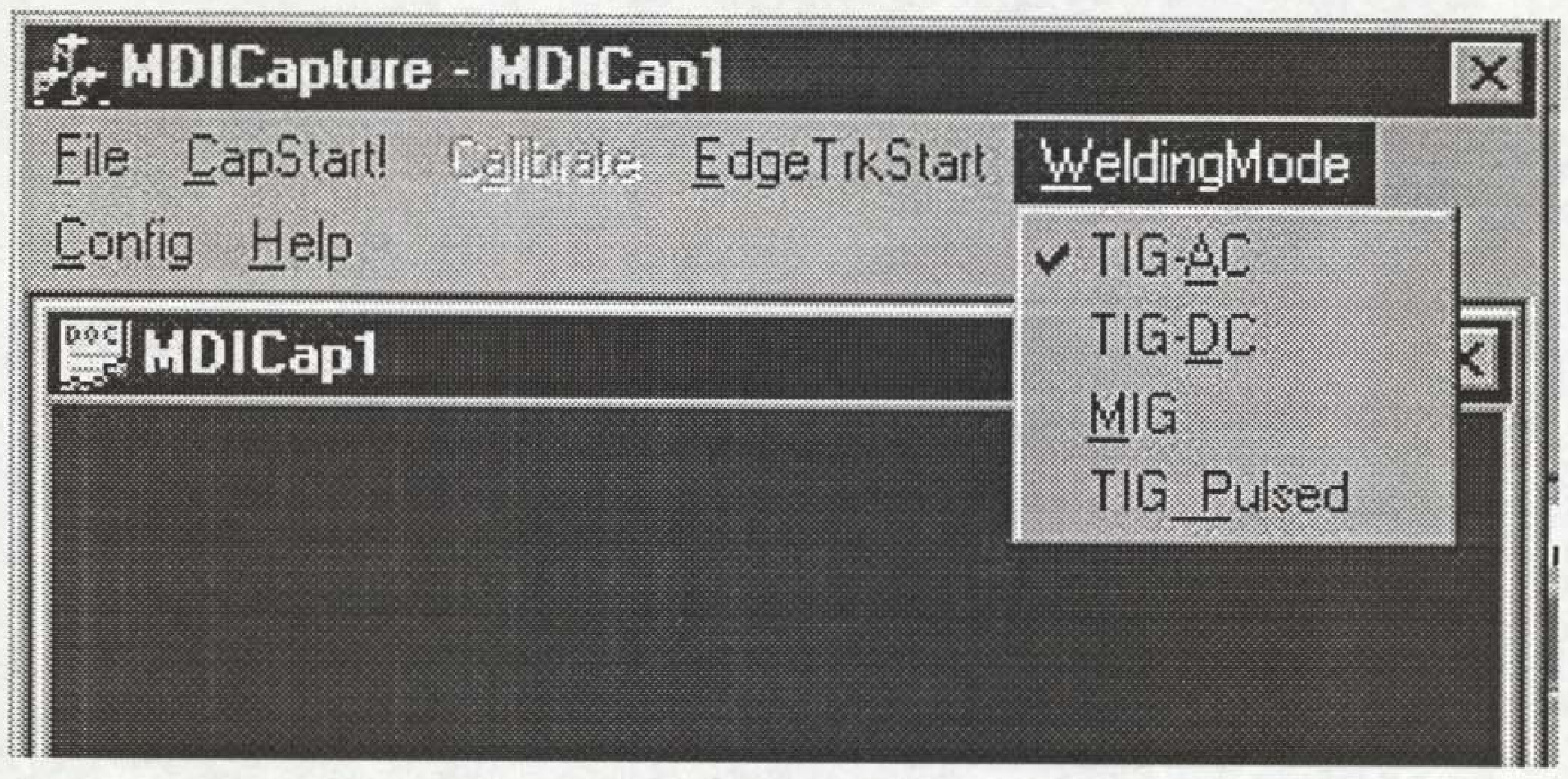

Figure 6. 2 The Window Menu

6.2.1.3 Image Processing

Video For Windows provides two callbacks, which supply a pointer to a VIDEOHDR structure. These callbacks are invoked when a new frame has been obtained from the video capture device. It must be arranged for the callbacks to be invoked. The two callbacks are created by:

- SetCallbackOnFrame() - Arranges for the callback to be invoked for each new frame supplied by the video capture device during preview mode.

- SetCallbackOnVideoStream() - Arranges for the callback to be invoked for each new frame supplied by the video capture device during video streaming.

The VIDEOHDR structure is defined in the <vfw.h> header file. Its structure has been reproduced below:

```
typedef struct videohdr_tag
{
    LPBYTE lpData;            /* pointer to locked data buffer */
    DWORD dwBufferLength;     /* Length of data buffer */
    DWORD dwBytesUsed;        /* Bytes actually used */
    DWORD dwTimeCaptured;     /* Milliseconds from start of stream
    DWORD dwUser;             /* for client's use */
    DWORD dwFlags;            /* assorted flags */
    DWORD dwReserved[4];      /* reserved for driver */
} VIDEOHDR, NEAR *PVIDEOHDR, FAR * LPVIDEOHDR;
```

The important fields of the structure are *lpData* and *dwBytesUsed*. These fields contain the pixel data and the length of the pixel data returned from the video capture device. The format of the data pointed to by *lpData* is the data portion of a Win32 Device Independent Bitmap (DIB). The DIB details can be obtained by the *GetVideoFormat()* function. This function (actually a macro) obtains a BITMAPINFO structure from the video capture driver associated with the capture window. Storage for the BITMAPINFO structure must be prealloacted and the pointer to that storage passed as a parameter. The size of the storage required to hold the BITMAPINFO structure may be obtained with the *GetVideoFormatSize()* function.

In this application, only one callback function *SetCallbackOnVideoStream()* is invoked, as video capture is set to the video streaming mode. Image processing is performed on the pixel data pointed by *lpData*. The main program has the following structure:

center = **RetrieveCentrePoint**();

PixelArray[] = **GetPixelArray**(lpData);

SmoothedArray[] = **GaussianSmoothing**(PixelArray[]);

edge_pos[] = **EdgeDetection**(SmoothedArray[]);

TemporalFiltering(edge_pos[]);

SpatialFiltering(edge_pos[]);

```
AveragingSmoothing(edge_pos[]);
CalculateParameters();
SendImageData();
```

The above procedures are introduced in detail as follows:

- RetrieveCentrePoint

The centre point could be selected by clicking on the centre position manually using the right mouse or retrieved from an initial file, which recorded the coordinate of the centre point saved when clicking the right mouse the previous time.

- GetPixelArray

After the centre point is selected, the detection line could be located. The detection lines are originated from centre points either to form a single horizontal line for only pool width extraction or spider like multiple lines for pool shape analysis. The switch between these two situations is conducted by simply changing the coefficients of the line equations.

- GaussianSmoothing

This smooths the pixel array using a Gaussian filter.

- EdgeDetection

Different algorithms are applied on the pool images for the different welding conditions. They have been described in details in chapter 3.

- TemporalFiltering

Filtering edge position using a temporal filter.

- SpatialFiltering

Filtering edge position using spatial filter. The principle of the temporal and spatial filters can be found in chapter 3.

- AveragingSmoothing

This step is to remove the impulse noises in the extracted edge data that remained after temporal and spatial filters.

- ParameterCalculation

Calculate pool width and send image data to the control procedure.

6.2.2 The Visual Display of Resultant Data

In order to provide a good observation on the history of the resultant parameters of image processing, a display window has been designed to show the fluctuations of these data in real time. As can be seen in the bottom window in Figure 6. 1, the detected pool width is displayed, where the red curve shows the original data before temporal filtering and the blue curve shows the value after filtering. The *x* direction represents the time or the frame sequence, while *y* direction gives the measured value of the pool width in millimetres. The software design of the display window is described below.

6.2.2.1 Creation of the Display Window

The application display window takes full advantage of the framework's MDI support, but does not use the framework's support for documents and views. The application object CGraphWnd is derived from CMDIChildWnd and created by overriding the *Create* function as follows:

```
BOOL CGraphWnd::Create(LPCTSTR szTitle, LONG style /* = 0 */,
        const RECT& rect /* = rectDefault */,
        CMDIFrameWnd* parent /* = NULL */)
{
    /* Setup the shared menu */
    if (menu.m_hMenu == NULL)
        menu.LoadMenu(IDR_MAINFRAME);
    m_hMenuShared = menu.m_hMenu;

    LPCTSTR lpszGraphClass =
        AfxRegisterWndClass(CS_HREDRAW | CS_VREDRAW, NULL,
            (HBRUSH)(COLOR_WINDOW+1), NULL);

    return CMDIChildWnd::Create(lpszGraphClass, szTitle, style, rect,
    parent);
```

```
}
```

The overriding of *Create* illustrates how to change the default cursor and icon of a window. Changing the default cursor or icon of a window requires registering a new WNDCLASS by calling AFXRegisterWndClass and passing the name of the WNDCLASS in the call to *Create*.

Once *Create* has been overrided, it needs to be called in the *OnCreate* in the object CMainFrame to invoke this child window when the main frame window is opened by setting a pointer to this class using the operator **new**. The code created in *OnCreate* is shown as follows:

```
CGraphWnd *pGraphWnd = new CGraphWnd;
if (!pGraphWnd->Create(_T("Bead Width Display"),
        WS_CHILD | WS_VISIBLE | WS_OVERLAPPEDWINDOW,
        rectDefault, this))
    return -1;
```

6.2.2.2 Visual Display of Pool Width

So far, a blank window has been created beneath the capture window. The next step is to draw the grid lines and display the pool width. First of all, a system timer is created in *OnCreate* in the object CGraphWnd using function:

```
SetTimer(UINT nIDEvent, UINT nElapse, NULL),
```

where *nIDEvent* specifies a nonzero timer identifier and *nElapse* specifies the time-out value, in milliseconds, NULL means that the WM_TIMER messages are placed in the applications message queue. This timer functions as the tick mark in the x direction to indicate the time elapsed. Every time a time-out occurs, the drawing pen moves one pixel right and draws a dot representing the current value of the pool width. In this way, a curve is drawn from left to right in the display window as the time elapses. The fluctuation of the pool width can be observed clearly in real time. Once the drawing reaches the right end of the window, the display is redrawn and curve is started again from the left. The drawing speed or the interval of the tick mark in the x direction can be adjusted by changing the time-out value.

6.2.3 The Parameter Dialog Box

The parameter dialog box is invoked from the menu item Config, as shown in Figure 6. 3, where three dialog boxes are involved. VideoFormat and VideoSource are ready to use from the software library, as shown in Figure 6. 4 and Figure 6. 5. The video format dialog box is used to select the video characteristics of the captured video sequence. These characteristics include the frame size and colour format. The video source dialog box specifies the signal type and format of the incoming video signal. The values shown in the figures were the default settings for this application.

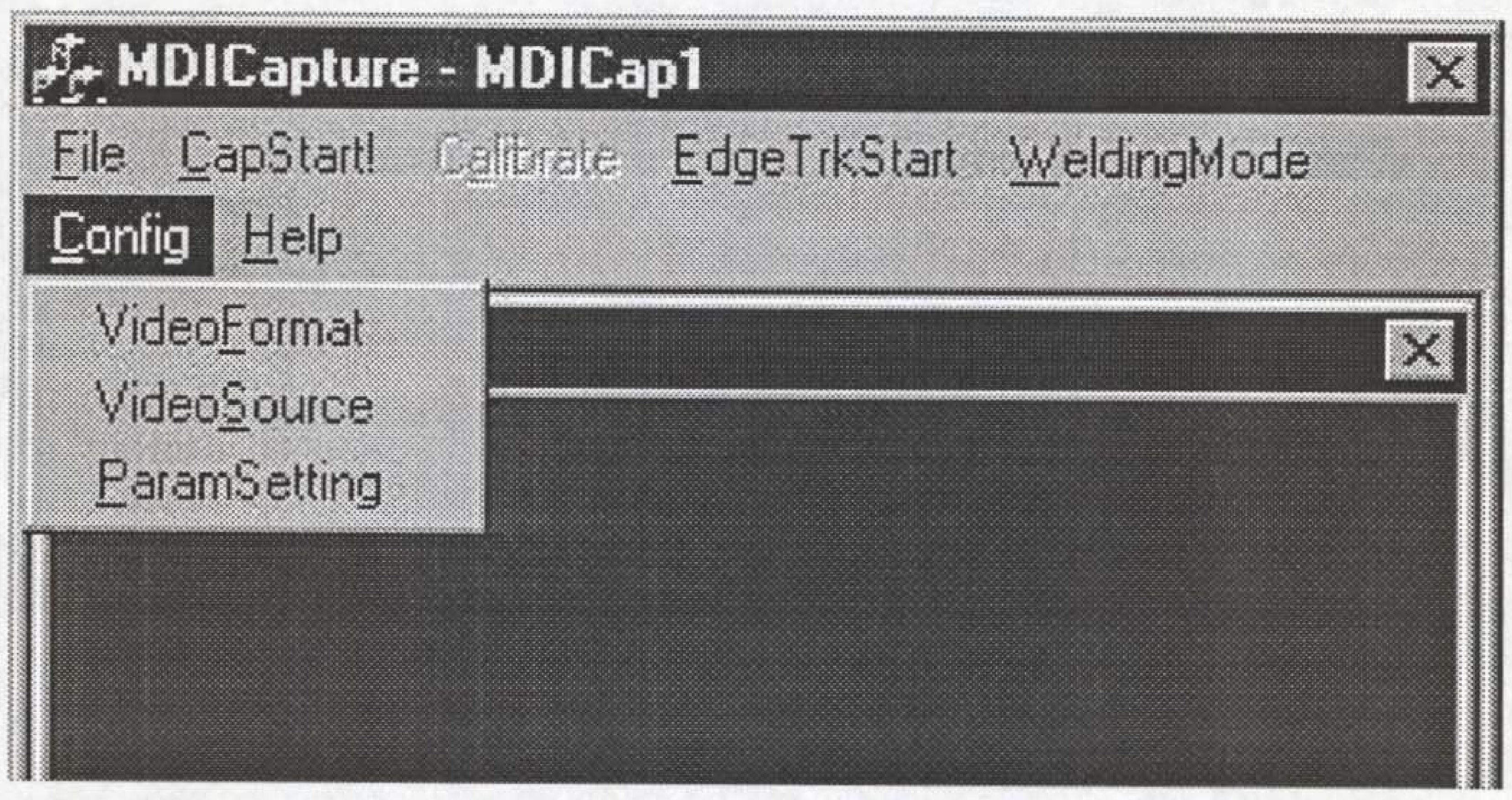

Figure 6. 3 The Menu Item Config

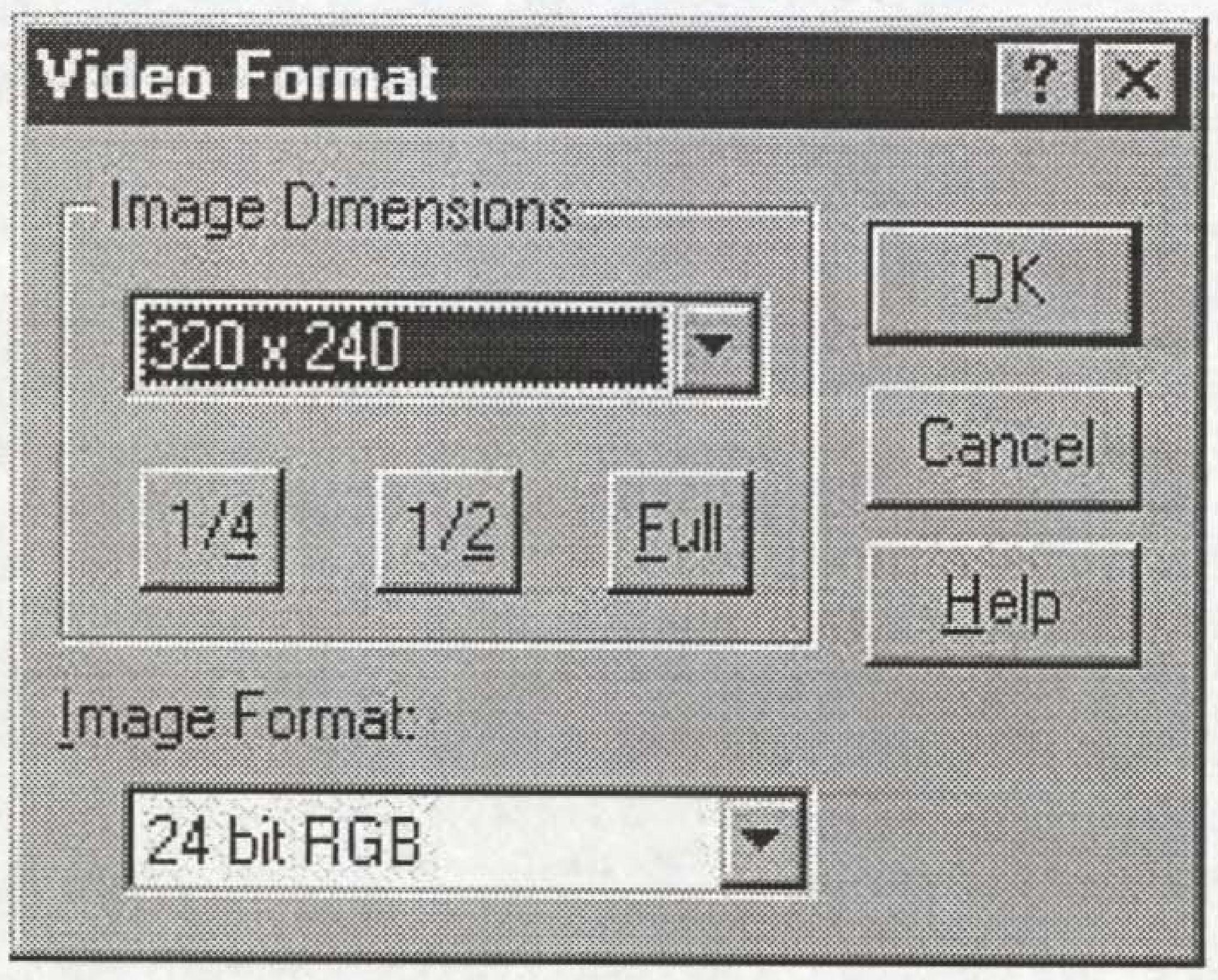

Image Dimensions: 320 x 240

Image Format: 24 bit RGB

Figure 6. 4 Video Format

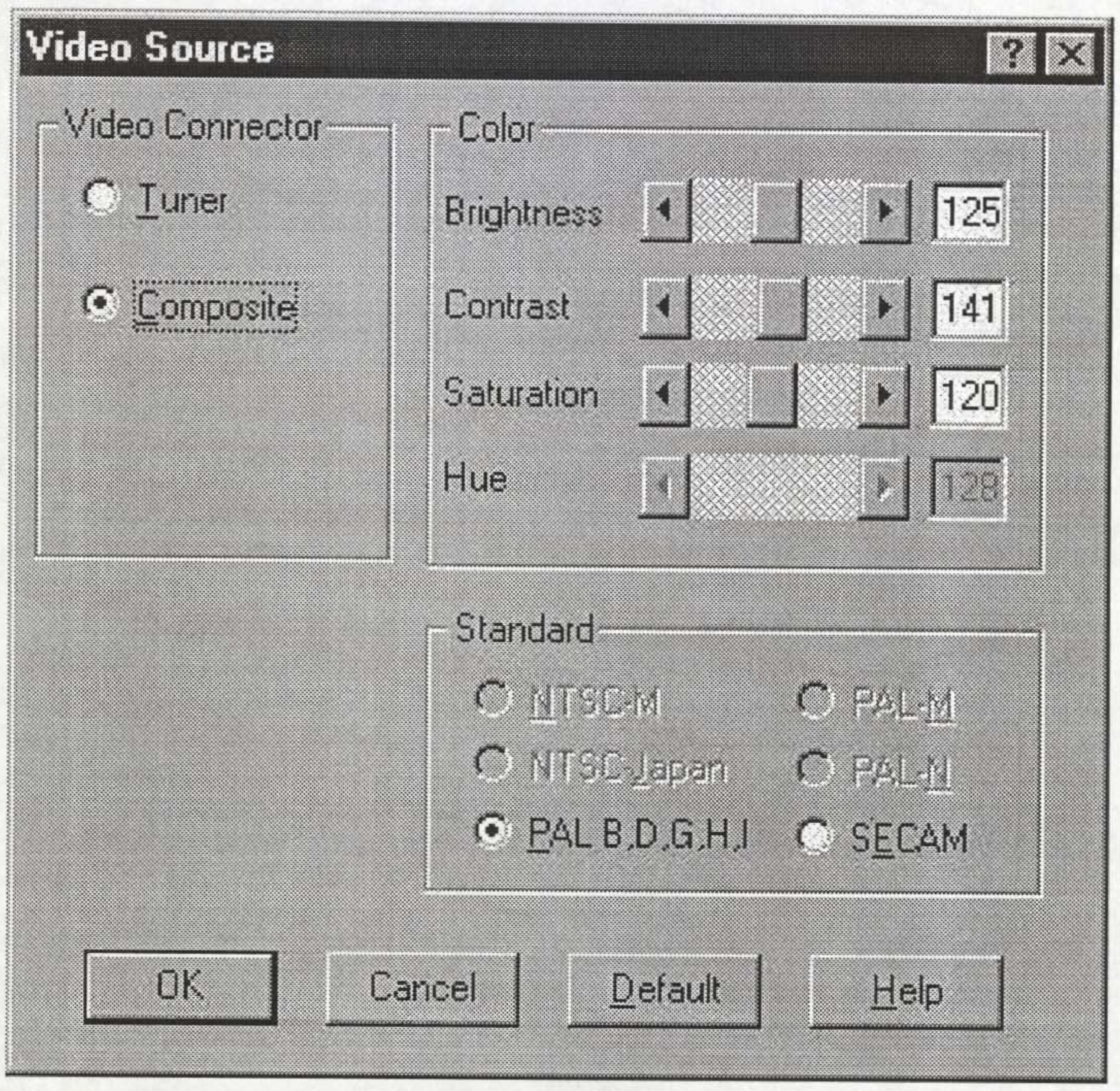

Video Connector
○ Tuner
● Composite

Color
Brightness 125
Contrast 141
Saturation 120
Hue 128

Standard
○ NTSC-M
○ PAL-M
○ NTSC-Japan
○ PAL-N
● PAL B,D,G,H,I
○ SECAM

Figure 6. 5 Video Source Dialog Box

ParamSetting is used to invoke a dialog box, as shown in Figure 6. 6, to specify the parameters used in image processing. These parameters have been divided into five categories: bead width tracking, temporal filter, spatial filter, averaging smoothing and seam tracking. The meanings of these parameters are given as follows:

1) Edge tracking parameters

- Line Length: This parameter specifies the length of the detection line with a range from 50 to 150.
- Start Point: This gives the position to start edge tracking on the detection line. The setting of this parameter is to avoid the disturbance from the arc or filler wire in the centre area.
- Tracking Range: It gives a valid range for edge tracking to avoid the centre and outside area, where usually more noises exist.
- Intensity Threshold: Once edge tracking is started, this parameter determines when to stop it by examining the average intensity on the detection line. If the average intensity is lower than this threshold, it is assumed that welding is terminated and edge tracking should stop automatically.

2) Temporal filter parameters

- No.Av.Points: This is the parameter *n* in the temporal filter described in chapter 3. It specifies the number of frames to be used to calculate the average.
- Threshold: This parameter determines the validity of the extracted edge point. If the current edge position is far from the average position taken from the previous *n* frames or if the difference between them is bigger than this threshold, the current value is assumed to be invalid and is replaced by the average.

3) Spatial filter parameters

- Averaged Lines: It specifies how many lines are detected to take the average.
- Line Step: It specifies the distance between two detection lines.

4) Averaging smoothing parameters

- Averaged Frames: It specifies the number of frames, whose edge points are averaged in the averaging smoothing process.

5) Seam tracking parameters

- Seam Distance to Bead Detection Line: This parameter is used to locate the position to start seam tracking. This position is specified by the distance to the bead detection line.

The two radio buttons at the bottom of the window are for selecting bead width detection only or both bead width and cleaning width detection in ac-TIG welding on aluminium. The values shown in the parameter dialog box are the default settings for these parameters.

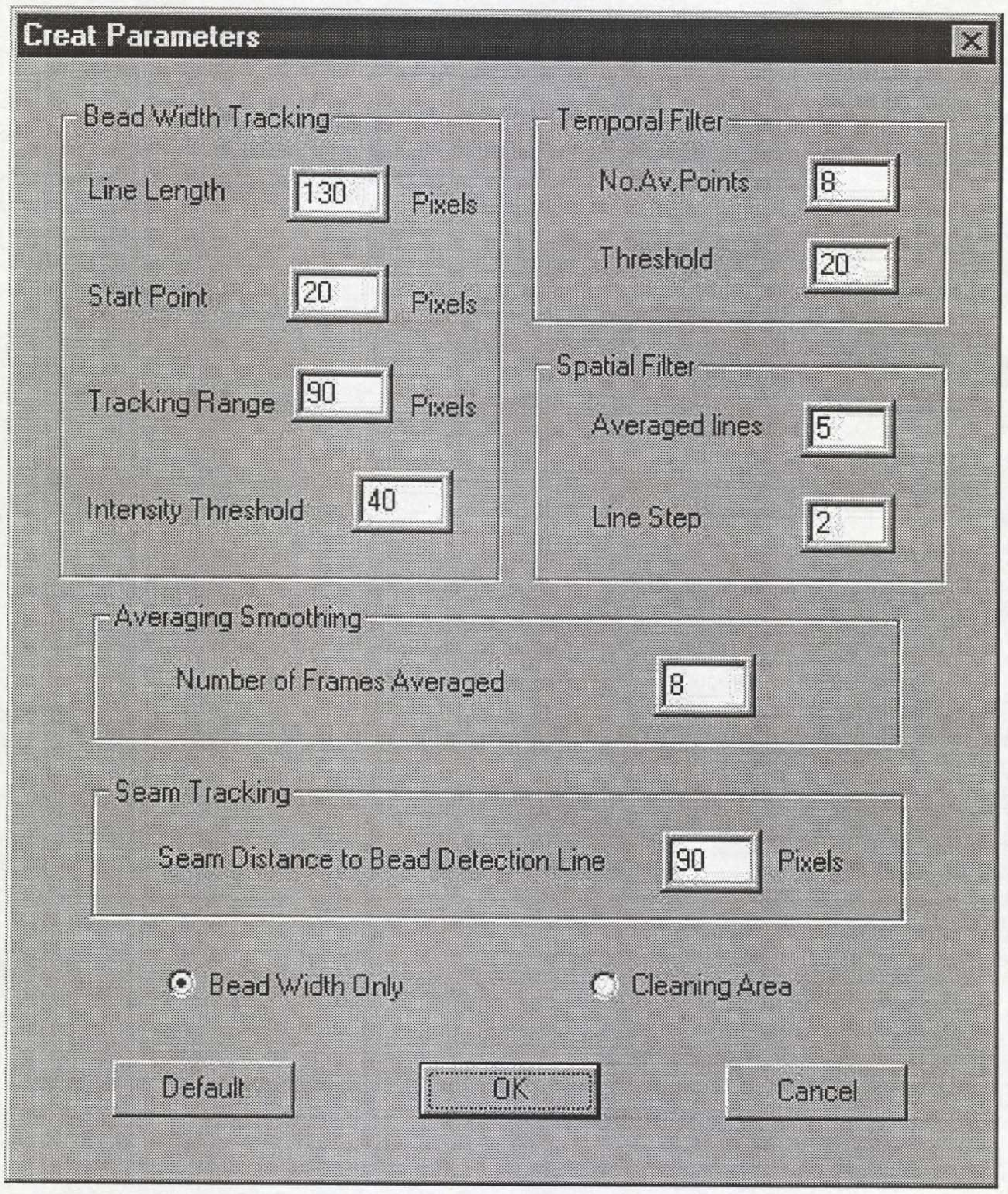

Line Length 130 Pixels

Start Point 20 Pixels

Tracking Range 90 Pixels

Intensity Threshold 40

No.Av.Points 8

Threshold 20

Averaged lines 5

Line Step 2

Number of Frames Averaged 8

Seam Distance to Bead Detection Line 90 Pixels

● Bead Width Only ○ Cleaning Area

Figure 6. 6 Parameter Setting Dialog Box

6.2.4 The Calibration Dialog Box

There are two kinds of dialog boxes derived from class CDialog:

- Modal dialog boxes, which require the user to respond before continuing the program.
- Modeless dialog boxes, which stay on the screen and are available for use at any time but permit other user activities.

The resource editing and ClassWizard procedures for creating a dialog template are the same for modal and modeless dialog boxes.

Creating a dialog box for a program requires the following steps:

- Use the dialog editor to design the dialog box and create its dialog-template resource.

- Use ClassWizard to create a dialog class.
- Use ClassWizard to connect the dialog resource's controls to message handlers in the dialog class.
- Use ClassWizard to add data members associated with the dialog box's controls and to specify dialog data exchange and dialog data validations for the controls.

To create a modal dialog box, call either of the two public constructors declared in CDialog. Next, call the dialog object's *DoModal* member function to display the dialog box and manage interaction with it until the user chooses OK or Cancel. This management by *DoModal* is what makes the dialog box modal. For modal dialog boxes, *DoModal* loads the dialog resource.

For a modeless dialog box, a public constructor must be provided in the dialog class. To create a modeless dialog box, call the public constructor and then call the dialog object's Create member function to load the dialog resource. Call Create either during or after the constructor call.

The calibration dialog box is designed as a modeless dialog box, as it needs to stay on the screen when the capture window is activated. After the dialog resource has been created using the dialog editor and ClassWizard, the following codes were added to create this dialog box on the screen:

```
CCalibrateCentre  *pCalibrateCentre = new CCalibrateCentre;
pCalibrateCentre -> Create(IDD_CALIBRATECENTRE, this);
```

Figure 6. 7 is the calibration dialog box. Using four press buttons, up, down, left and right, the centre point can be moved in these four directions with a certain step, which is specified by a variable in this object. The current coordinates of the centre are shown in the edit boxes to the right.

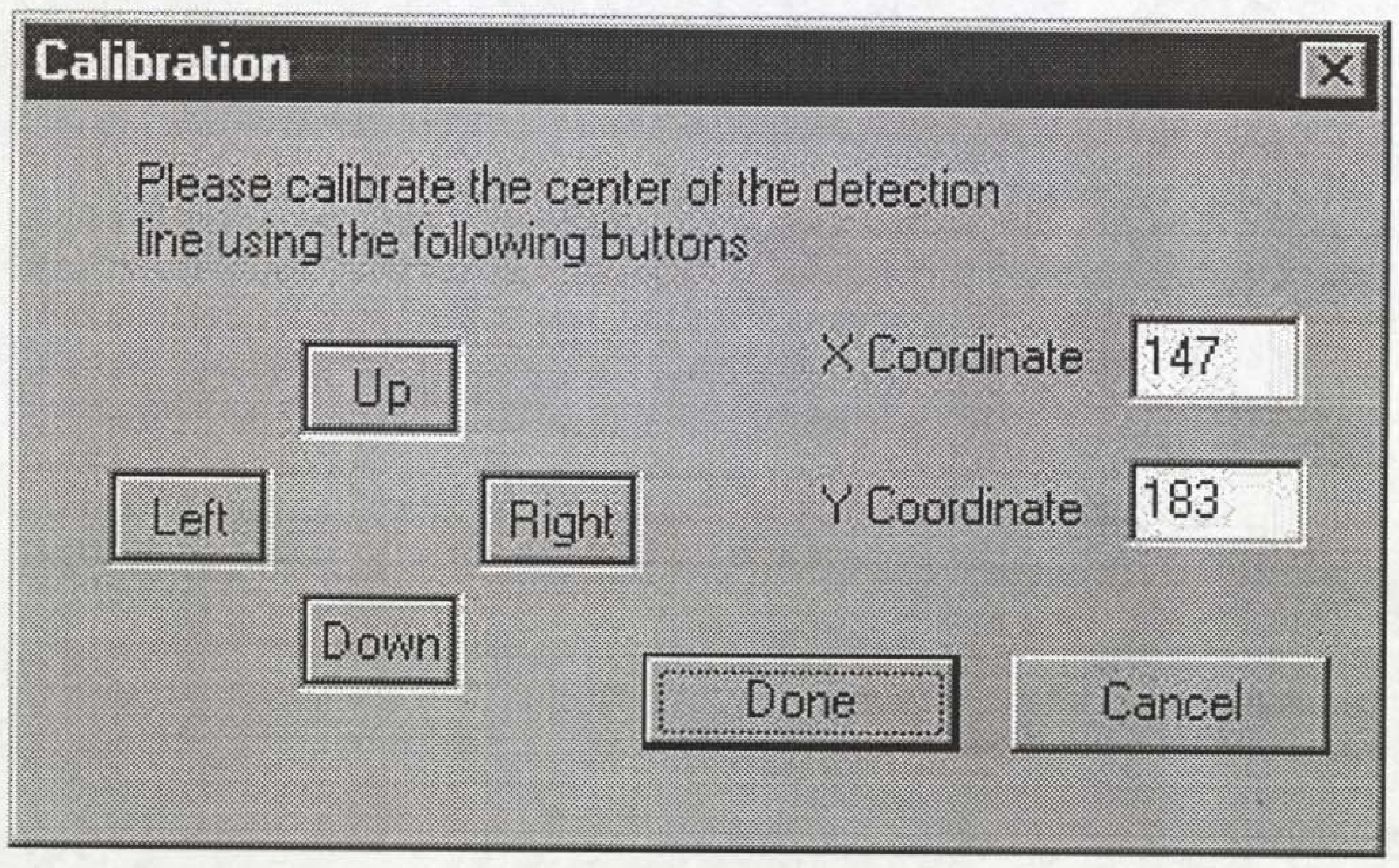

Please calibrate the center of the detection line using the following buttons

X Coordinate 147

Y Coordinate 183

Figure 6. 7 Calibration Dialog Box

6.3 Seam Tracking and Bead Profile Measurement Program-PicoloSeam

In this section, the software drivers and libraries for the Picolo card are introduced, and then the software design in this application is described.

6.3.1 The Windows NT Device Driver for Picolo

A driver is a program to interface between applications running on an operating system on a PC and the PC hardware. A driver uses the operating system specific functionalities to operate the hardware device. The driver also provides a unique (operating system independent) and well-documented interface to the applications. The Picolo provides a driver to control the hardware and acquire and save images.

In the device driver, a function library is supplied with the following function families:

- Driver Control: This includes functions for acquiring the board serial number and the driver files version. *PicoloStart()* and *PicoloStop()* are also supplied here for initializing and terminating the Picolo board. A handle to the board is returned from *PicoloStart()* for passing to other library functions .
- Acquisition Control: Acquisition can be selected by software as a single acquisition or continuous, or controlled by a trigger.
- Acquisition Settings: Those functions associated to the acquisition settings, i.e. image format, video input etc., are included here.

- Accessing the Acquired Image: These functions are used for setting and getting the image buffer and image size.
- Image Adjustments: This was for adjusting image features, i.e. gain (contrast), offset (brightness), hue etc.
- Save and Load an Image: An image at a known address can be saved in memory as a bitmap image file (.bmp), Tiff encoded image file (.tif) or JPEG compressed image file (.jpg) using the save function in this family.
- I/O Related Functions: There are four TTL compatible I/O port at the rear of the board, which can be read and written by software. One of them can be configured by software as a trigger line for image acquisition.

6.3.2 Application Program

This application program uses the single document interface (SDI) in its design, where only a capture window is presented as shown in Figure 6. 8, and was first created by the MFC AppWizard with a SDI. It makes full use of a part of the framework called document/view architecture. Similarly to the pool monitoring program, the following objects were created by the AppWizard:

- An application object CPicoloSeamApp derived from class CWinApp.
- A document class object CPicoloSeamDoc derived from class CDocument.
- A view object CPicoloSeamView derived from class CView.
- A frame window object CMainFrame derived from CMDIFrameWnd.

Besides the above auto created objects by AppWizard, a new objects was created consequently by the author:

- CImageProc derived from CWnd. This object contains all the codes concerned with the image processing algorithms on seam tracking and bead profile measurement.

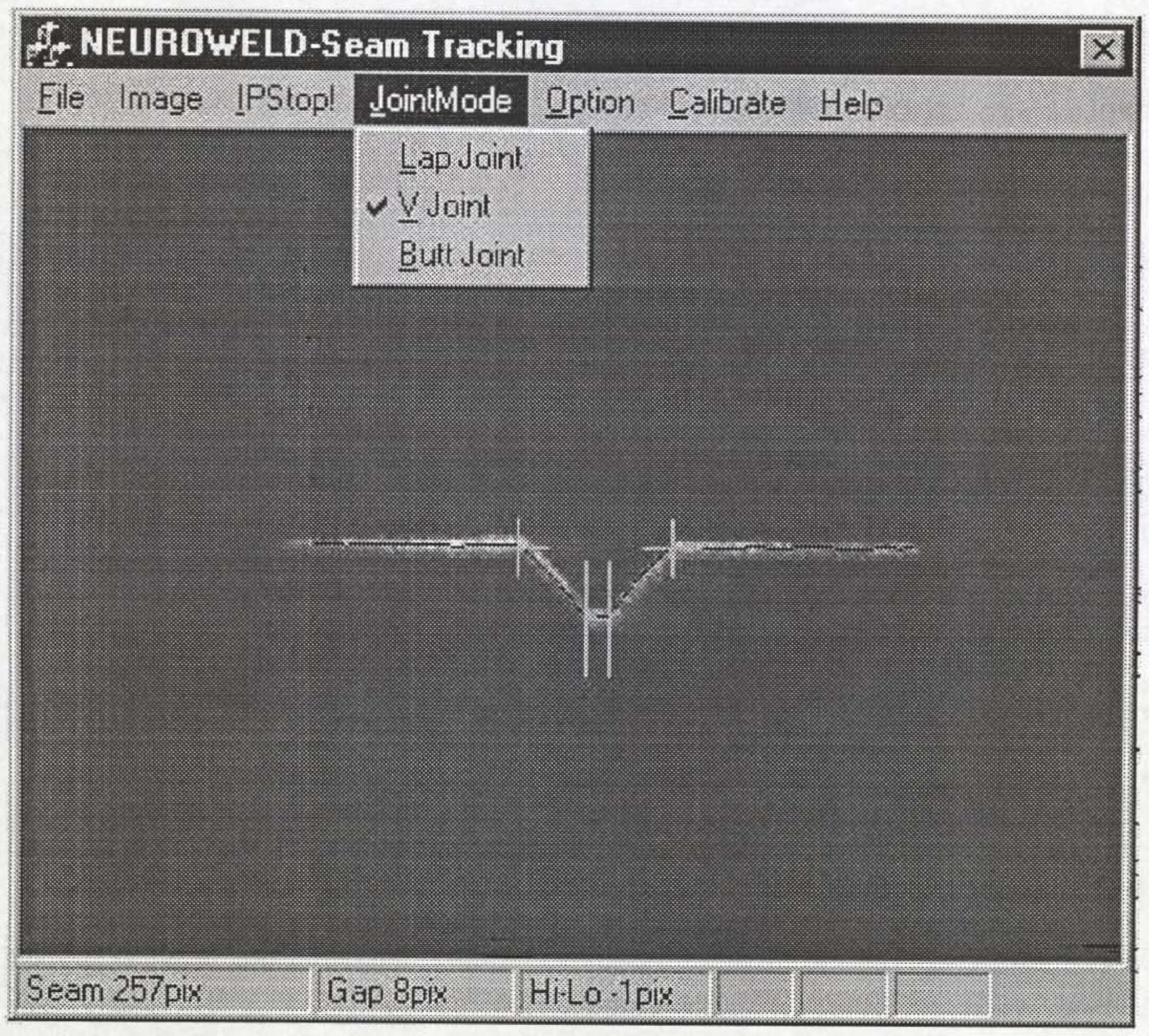

Figure 6. 8 The Application Window for Seam Tracking and Bead Measurement

6.3.2.1 Video Capture Procedure

1) The initialisation of video capture procedure

The codes concerned with the initialisation of video capture procedure and acquisition settings are created in the constructor of the document object CPicoloSeamDoc. They includes the following functions:

- PicoloStart: detects and initialises the Picolo board.
- PicoloSelectVideoInput: specifies the settings for the video input and its format.
- PicoloSelectImageFormat: selects the captured image format transferred to the PC.
- PicoloWriteGain and PicoloWriteOffset: for contrast and brightness adjustment.
- PicoloGetImageSize and PicoloGetImageBufferSize: to get the image buffer size for allocating the memory for image buffer.
- VirtualAlloc, PicoloSetImageBuffer and PicoloSetBufferList: to allocate image buffers.

- PicoloRegisterAcquisitionCallback: registers a user's callback function to be called at the end of each acquisition of an image.

After the above functions are specified, the BITMAPINFO structure is initialised for the frame image.

In the destructor of the CPicoloSeamDoc object, some functions activated in the constructor need to be released using the corresponding release functions. They are:

- PicoloReleaseImageBuffer and VirtualFree: release image buffer.
- PicoloUnregisterAcquisitionCallback: unregisters the callback function.
- PicoloStop: stops the Picolo driver.

2) The acquisition of the video

The acquisition codes are created in view object CPicoloSeamView. In the standard continuous acquisition mode the driver will acquire frames as quickly as possible. In this mode, the speed of acquisition is uncontrollable. In order to control the acquisition speed a system timer is installed in function *OnCreate* and the sequence acquisition is performed by continually acquiring a single frame in a fixed interval, which is the time-out value of the system timer. The acquisition function *PicoloAcquire* is called in *OnTimer* and specified for acquiring a single frame.

6.3.2.2 Visual Design of the Capture Window

The interface of this application is shown in Figure 6. 8. The menu items designed on the top represent the application's command. The resultant data from image processing, such as seam position, gap and high-low is displayed on the status bar at the window bottom. The meanings of the menu items are:

- <u>Image</u> is to acquire a single frame and save the image to a file.
- <u>IPStart</u> is to start and stop image processing, seam tracking or bead profile measurement.
- <u>JointMode</u> is for selecting the joint mode of the image. Three joint modes are presented: Lap joint, V joint and Butt joint.

- Option can select image processing routines for seam tracking or bead profile measurement, as shown in Figure 6. 9.

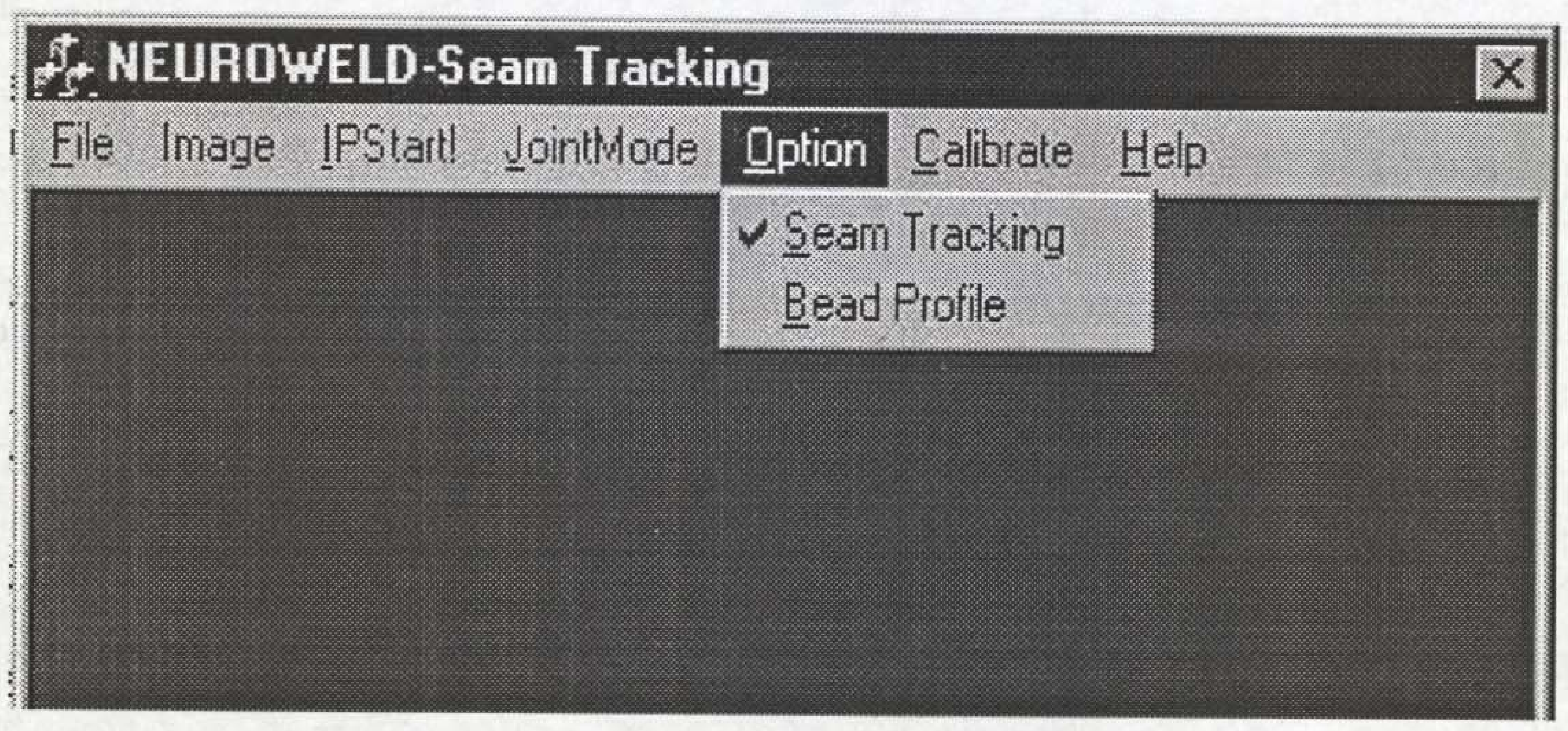

Figure 6. 9 The Menu Items

6.3.2.3 Seam Tracking and Bead Profile Measurement Program

The image processing codes are all created in the object CImageProc with several basic procedures. The main program has the following structure:

```
LaserStripeThinning();
if (m_VJoint = true || m_LapJoint = true)
    StripeHolesFillingUsingInterpolation();
    PosArraySmoothing();
    FirstDiffCalculation();
    AdaptiveSmoothing();
    if (m_seamtracking = true)
        if (m_LapJoint = true)
            LapJointProc();
        else if (m_VJoint = true)
            VJointProc();
    else if (m_beadprofile = true)
        BeadProfileProc();
else
    ButtJointProc();
SendImageData();
```

Detailed information on the procedures is as follows:

- LaserStripeThinning

This is the first and necessary step in the analysis of the laser line image. The principle of the stripe thinning was described in chapter 4. The actual laser line thinning was performed by using a localised image intensity averaging technique. This procedure is described as follows:

```
Procedure LaserStripeThinning()
begin
    for $x$ = line_start to line_end do
        for $y$ = windowing_left to windowing_right do
            /*look for the position with maximum intensity in a column*/
            average_val = average_val - averaging_array[$i$];
            pixel_intensity = *(pFrameStart + $x$ + XSize$\times y$);
            averaging_array[$i$] = pixel_intensity;
            average_val = average_val + averaging_array[$i$];
            average_intensity[$x$] = average_val / average_number;
            if (avearge_intensity[$x$] > max_val)
                max_val = average_intensity[$x$];
                max_val_pos = $y$ - average_number/2 ;
            if ($i$ >= (average_number -1))
                $i = 0$;
            else
                $i$++;
        endfor
        pos_intensity[$x$] = max_val;
        if (pos_intensity[$x$] > adaptive_threshold[$x$]))
            /*adaptive windowing*/
            windowing_left = max_val_pos - half_windowing_width;
            if (windowing_left < 0)
                windowing_left  = 0;
            windowing_right = max_val_pos + half_windowing_width;
            if (windowing_right > YSize)
                windowing_right = YSize;
            pos[$x$] = max_value_pos;
        else
```

```
                windowing_left  = 0;
                windowing_right = YSize;
                pos[x] = -1;
            endfor
        end
```

After stripe thinning, a position array of media axis pos[x], $x \in$ (line_start, line_end), is obtained with some holes marked with (-1), as the maximum intensity value in that column is lower than the intensity threshold. These holes need to be filled for the subsequent analysis of the position array except for the butt joint, where the holes will be analysed to determine whether it is either a gap between the two plates to be welded or just a hole on the central line.

- StripeHolesFillingUsingInterpolation

To keep the continuity of the laser line, the holes are filled using linear interpolation. This procedure is described as follows:

```
Procedure StripeHolesFillingUsingInterpolation()
begin
    for x = line_start to x = line_end do
        if (pos[x] = (-1))
            if (hole_counter = 0)
                hole_start = x;
            hole_counter ++;
        else
            hole_size = hole_counter;
            hole_end = x-1;
            if (hole_size >= 1)
                for i = 0 to i = hole_size do
                    gradient = (float)(pos[hole_end+1] - pos[hole_start-1])/
                               (float)((hole_end+1) - (hole_start-1));
                    pos[hole_start+i] = pos[hole_start-1] + (int)((i+1) ×
                               gradient);
                endfor
            hole_counter = 0;
```

```
    endfor
end
```

- PosArraySmoothing

To remove the impulse noises on the position array pos[*x*], smoothing is conducted by taking the average with several neighbouring position points, resulting in an averaged position array av_pos[*x*].

- FirstDiffCalculation

The first differential diff[*x*] of the position array pos[*x*] is calculated by taking the difference of the two points:

diff[*x*] = av_pos[*x* + support_length] - av_pos[*x*- support_length];

- AdaptiveSmoothing

Adaptive smoothing was performed on the first differential array diff[*x*] to sharpen the discontinuities and smooth the other regions. It was achieved by repeatedly convoluting diff[*x*] with a very small averaging mask weighted by a measure of the diff[*x*] continuity or its second differential second_diff[*x*] at each point. This procedure is given as follows:

```
Procedure AdaptiveSmoothing()
begin
    for iteration = 0 to iteration = 5 do
        for $x$ = line_start to $x$ = line_end do
            weight[$x$] = exp(- (second_diff[$x$])$^2$ ÷ (2×$k^2$));
            for $i$ = -1 to $i$ = 1 do
                diff[$x$] = $\Sigma$(diff[$x+i$] × weight[$x+i$]) ÷ $\Sigma$(weight[$x+i$]);
            endfor
        endfor
        for $x$ = line_start+1 to $x$ = line_end-1 do
            second_diff[$x$] = diff[$x$+ support_length] - diff[$x$- support_length];
        endfor
    endfor
end
```

- LapJointProc

In this case, only one local extreme exists with respect to the position of lap seam in the second differential. Therefore, the aim of this routine is to track the position of the local extreme in array second_diff[*x*] and get the high-low between the two plates to be welded.

```
Procedure LapJointProc()
begin
    for $x$ = line_start to $x$ = line_end do
        seam_pos = FindLocalMax();
    endfor
end
```

- VJointProc

Due to the shape of V preparation, there will be three local extrama while without a gap or four local extrema while with a gap corresponding to the corners on the profile line in the second differential array second_diff[*x*]. The search for these local extrema follows the procedure below:

```
Procedure VJointProc()
begin
    for $x$ = line_start to $x$ = line_end do
        bot_corner_left = FindLocalMin();
    endfor
    for $x$ = line_end to $x$ = line_start do
        bot_corner_right = FindLocalMin();
    endfor
    if (bot_corner_left = bot_corner_right)
        seam_pos = bot_corner_left.x;
        gap = 0;
    else
        seam_pos = bot_corner_left.x+(bot_corner_right.x–
                        bot_corner_left.x)÷2;
        gap = bot_corner_right.x – bot_corner_left.x;
```

```
        for x = bot_corner_left.x to x = line_start do
            top_corner_left = FindLocalMax();
        endfor
        for x = bot_corner_right.x to x = line_end do
            top_corner_right = FindLocalMax();
        endfor
        DisplaySeam();
    end
```

- ButtJointProc

There are mainly two steps in this routine. The first step is to recognise the patterns the image belongs to based on the returned value of two flags ValidLeftDrop and ValidRightDrop, which have been described in Chapter 4, and then to extract the seam features from the four different image patterns. The procedure can be described as follows;

```
    Procedure ButtJointProc()
    begin
        for x = line_start to x = line_end do
            left_drop = FindValidDrop();
            if (left_drop ≠ 0)
                ValidLeftDrop = true;
            else
                ValidLeftDrop = false;
        endfor
        for x = line_end to x = line_start do
            right_drop = FindValidDrop();
            if (right_drop ≠ 0)
                ValidRightDrop = true;
            else
                ValidRightDrop = false;
        endfor
        if (ValidLeftDrop = true & ValidRightDrop = true) /* pattern (b) */
            seam_pos = left_drop.x + (right_drop.x – left_drop.x)÷2;
```

```
        if (ValidLeftDrop = true & ValidRightDrop = false) /* pattern (c) */
            seam_pos = left_drop.x;
        if (ValidLeftDrop = false & ValidRightDrop = true) /* pattern (c) */
            seam_pos = right_drop.x;
        if (ValidLeftDrop = false & ValidRightDrop = false)/* pattern (a) or (d) */
            max_hole_size = FindBiggestHole();
            if (max_hole_size = 0) /* pattern (d) */
                dot = FindDotBeneathLaserLine();
                seam_pos = dot.x;
            else                   /* pattern (a) */
                seam_pos = hole_centre.x;
        DisplaySeam();
    end
```

- BeadProfileProc

For bead profile analysis, the first step is to examine the existence of the undercut by looking for the position drops that are bigger than a predefined threshold and representing them using two flags: leftundercut and rightundercut, then detect the feature points on the profile and finally calculate the bead parameters.

```
Procedure BeadProfileProc()
begin
    ExamineUndercut();
    ModifiedHoughTransform();
    CalculateParameters();
end
```

The routines ExamineUndercut and ModifiedHoughTransform have been illustrated in Chapter 5.

CHAPTER 7 WELDING CONTROL TRIALS

7.1 Pool Width Control

Preliminary closed-loop control trials were conducted to confirm the effectiveness and robustness of the proposed visual sensing system combined with image processing. The width of the weld pool was taken as the sensing parameter for control. Namely, consistent bead width was pursued in the experiments. A simple proportional control algorithm was applied.

Figure 7. 1 shows the bead width variation during the welding with and without closed-loop control, where the traverse speed was 3.3mm/s, the wire feed rate was 17.5mm/s, aluminium plate 150×65×1.6mm was welded with a frequency of feedback control of 10 Hz. For the results in Figure 7. 1(a), a constant alternating current was set at l00A, but a variable bead width was observed. Consistent bead width was obtained when closed-loop control is introduced. In Figure 7. 1(b), the required bead width was set to 120 pixels and the welding current was adjusted automatically to maintain the bead width. The control experiments showed that the proposed image processing algorithms can trace the weld pool edge with accuracy and speed.

Further control trails were performed on the weld samples machined to have varying thickness, as shown in Figure 7. 2. Welding was carried out on these sample plates with the thickness varied from 1.6mm to 1.3mm and 1.0mm, then back to 1.6mm.

Figure 7. 3 shows the results of welding trials on these varying thickness sample plates. The pictures in the figure are the back face appearance of the welds. The curves represent the bead width variation during welding. Figure 7. 3 (a) is the weld produced using constant current without closed loop control. It is easy to see that the bead width varied severely during welding. At the region of 1.0mm thickness, over penetration occurs and almost burn through. When simple proportional closed loop control was applied the bead width variation has been improved greatly, as shown in Figure 7. 3 (b). As can be seen from the control trial, the pool monitoring system can track the width of the pool with accuracy. However, an advanced control strategy is required for obtaining an consistent weld in this situation.

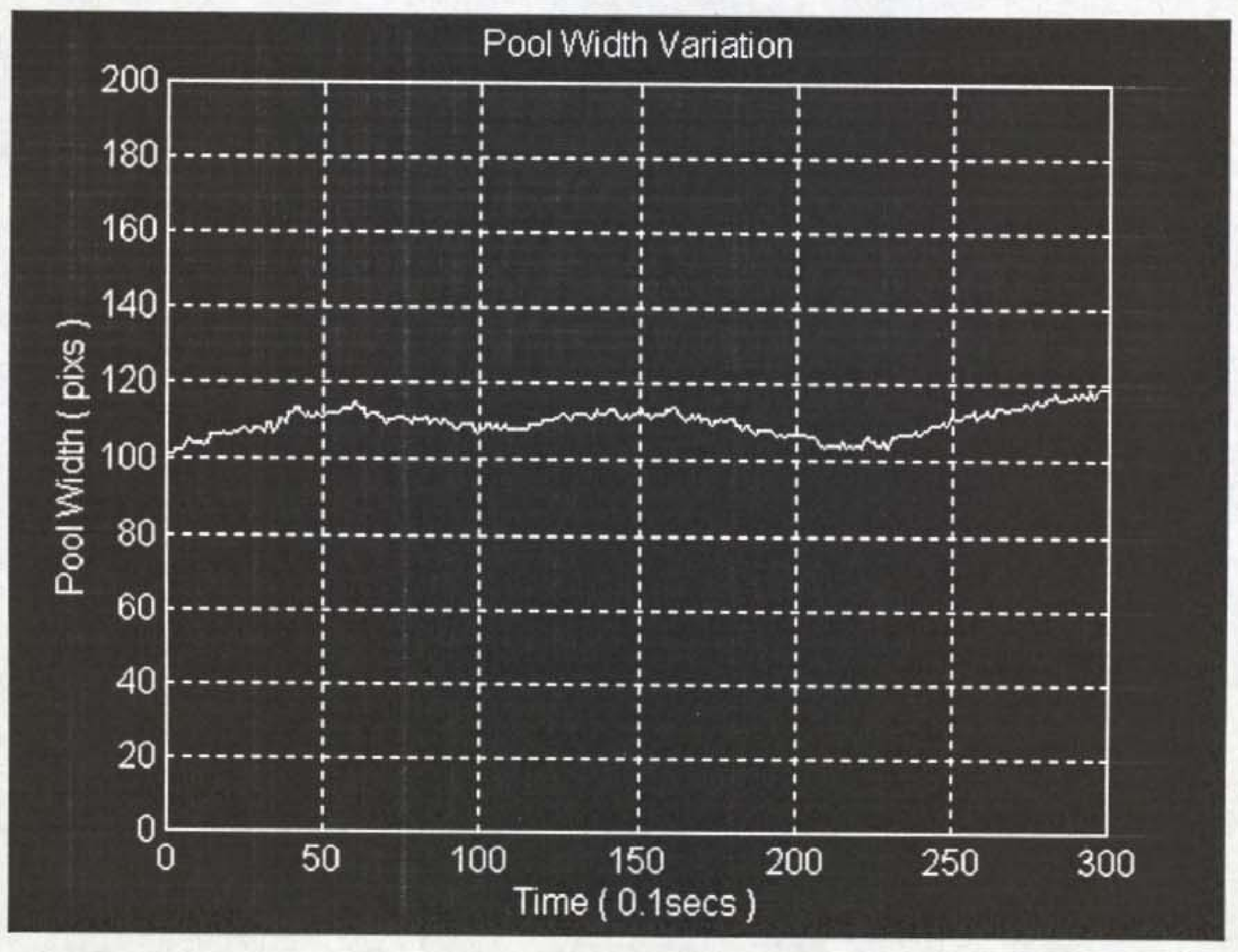

(a)

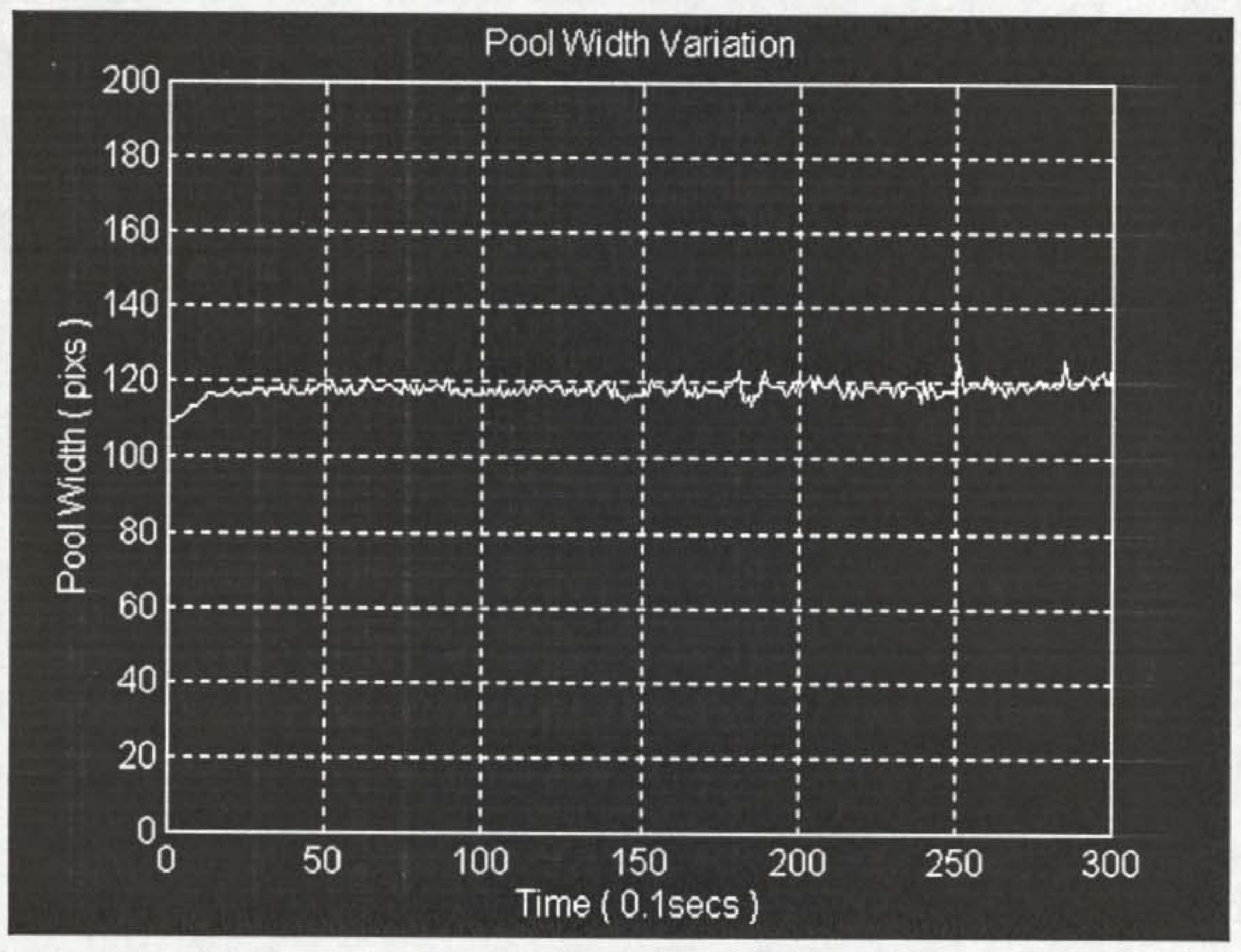

(b)

Figure 7. 1 Weld Width Variation (a) Without Control (b) With Control

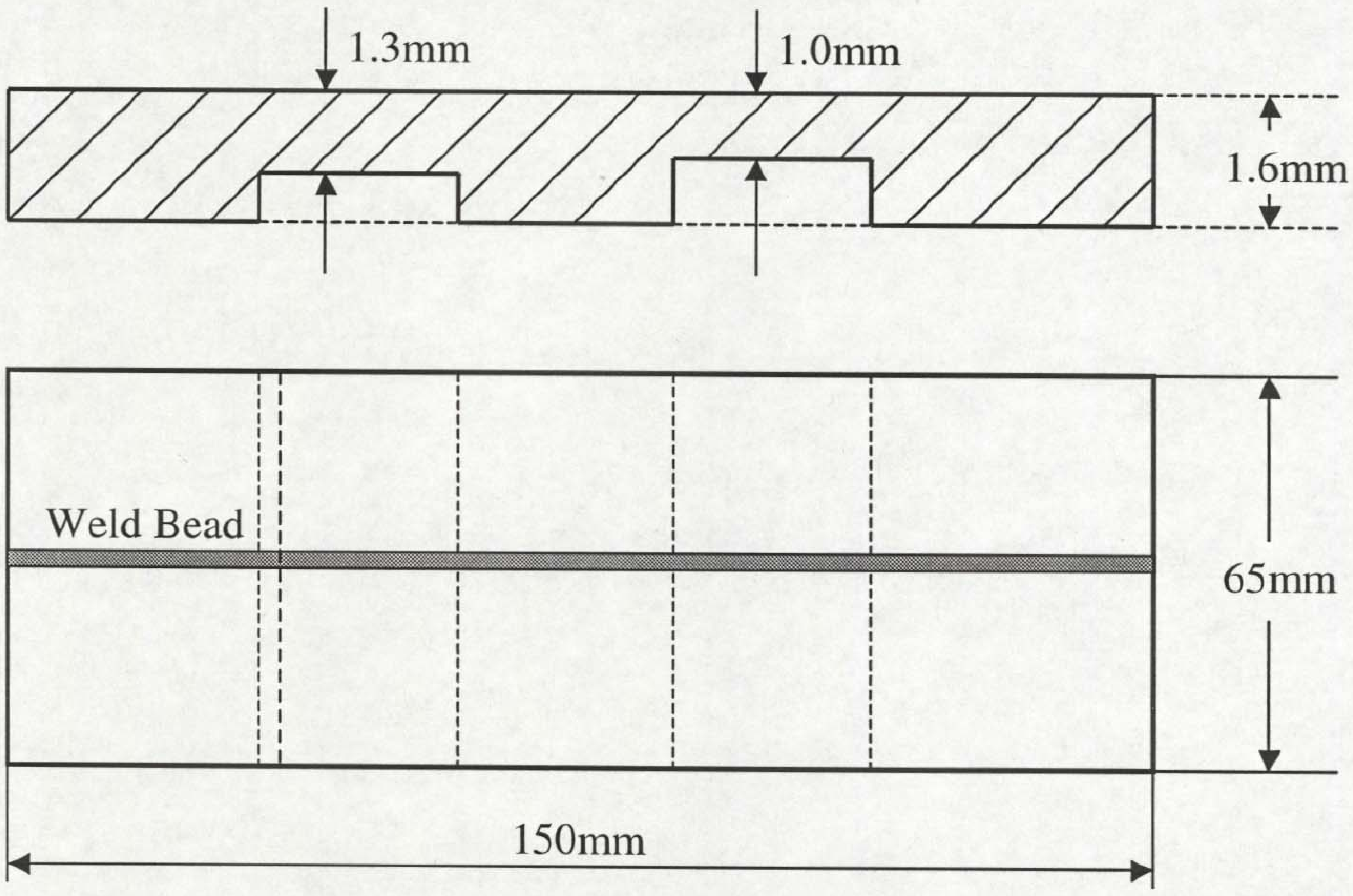

Figure 7. 2 Machined Sample

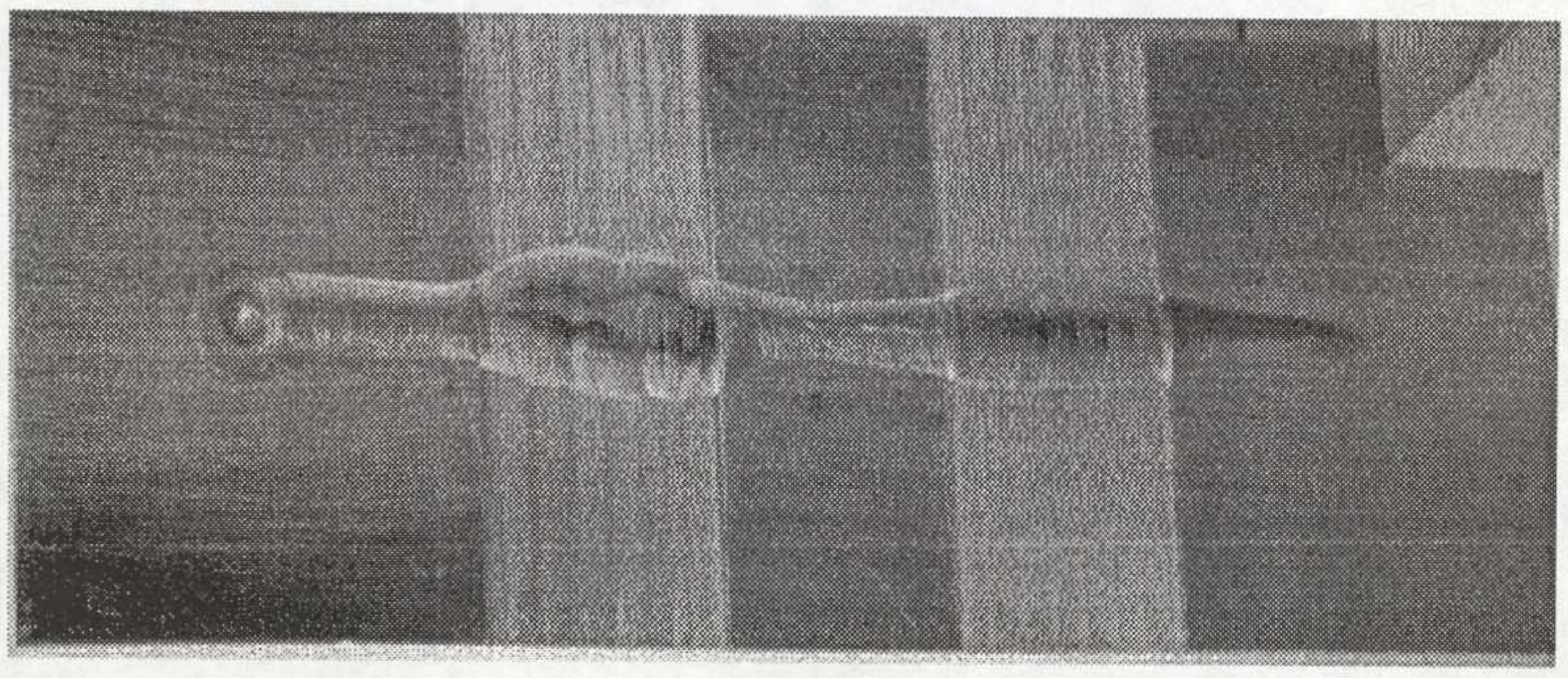

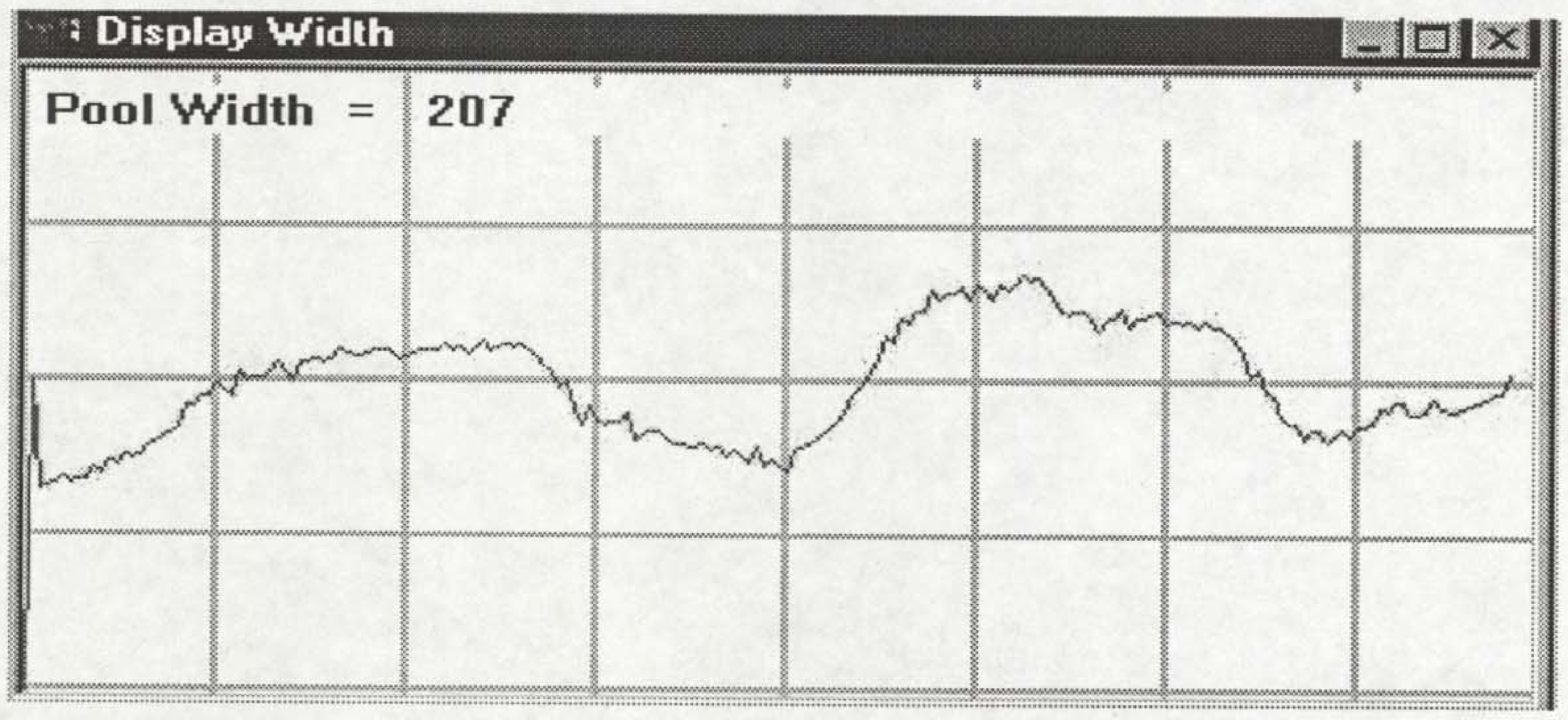

Pool Width = 207

(a)

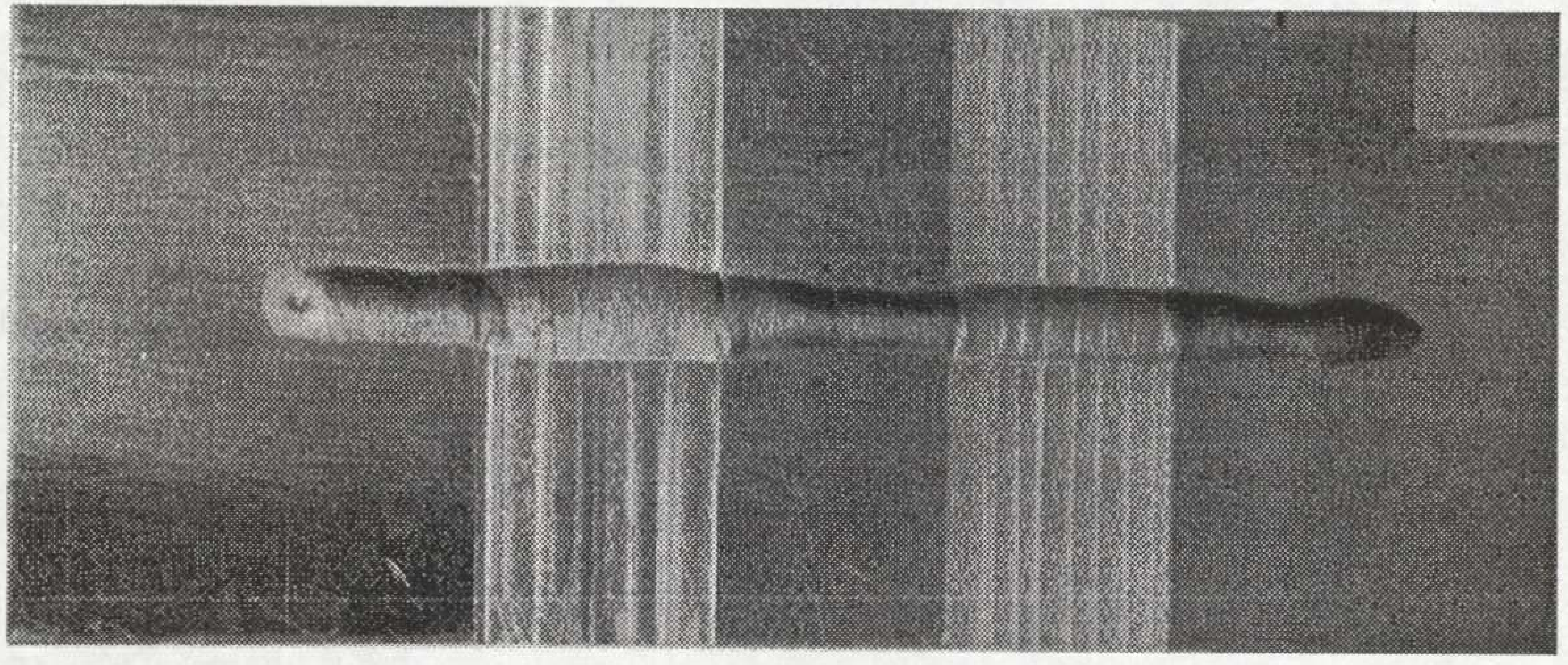

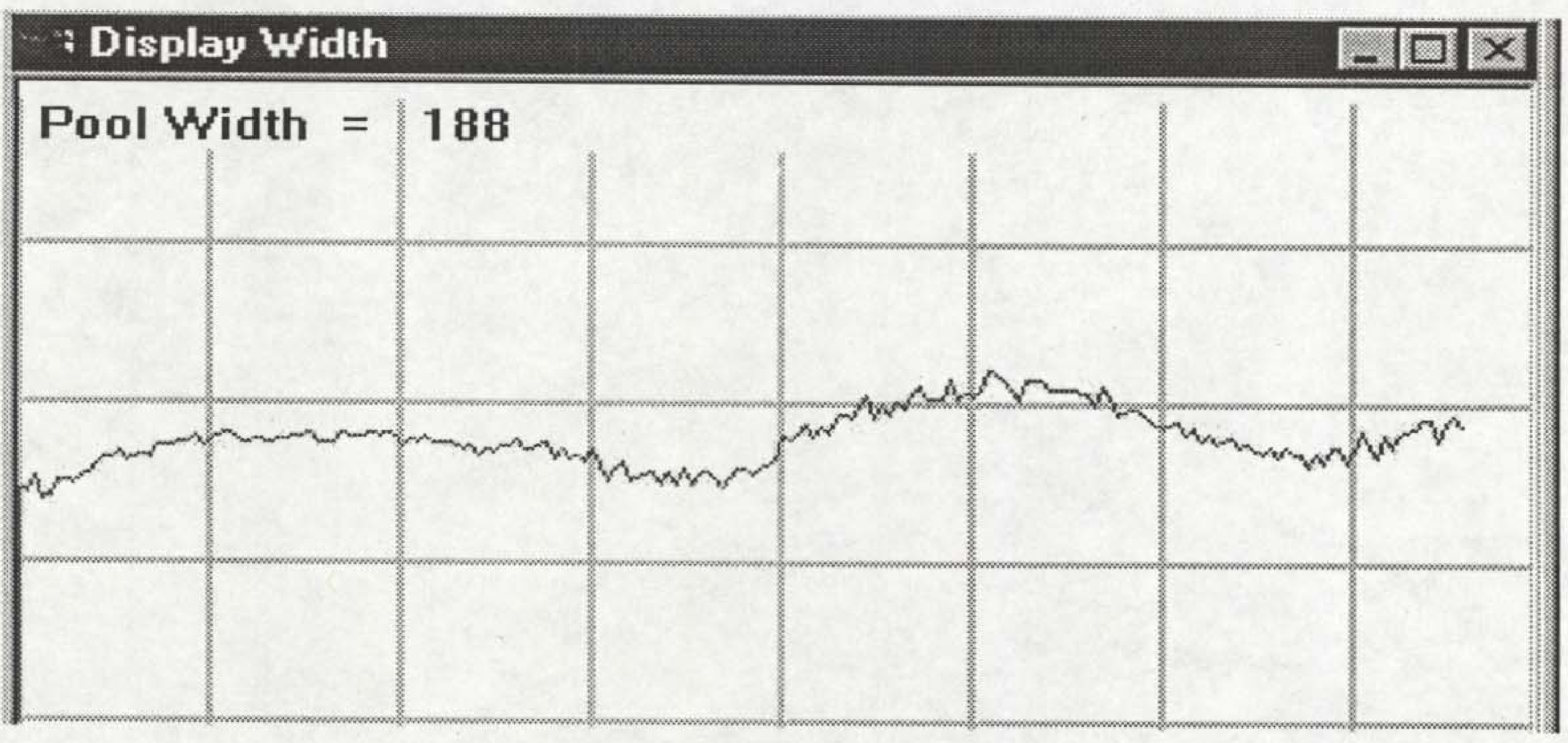

Pool Width = 188

(b)

Figure 7. 3 Welding Trials on Varying Thickness Plates

7.2 Neural Welding Parameter Predictor

During the welding process the welding parameters need to be updated to match the welding seam condition. A neural network has been created to relate the seam condition, such as gap and high-low, to the welding parameters in MIG welding. The structure of the neural network is given in Figure 7.4. The input data for each material is the thickness, joint type, high-low, gap, top and bottom bead parameters and AVC. The output data are the synergic MIG welding parameters, speed and power. For each workpiece, because of the possibility of heat build up, it is necessary to input the position of the torch along the workpiece with respect to the start position.

The neural network has been used for welding parameter adjustment during MIG welding operation in order to obtain a consistent bead width. The output of the neural gives the welding power and speed in response to inputs of the weld seam sensor. Table 7.1 gives the variation of the welding parameters in response to changes in the gap. The changes have been made over a range of ±10% and the neural indicates the respective magnitude changes required for the power and speed parameters.

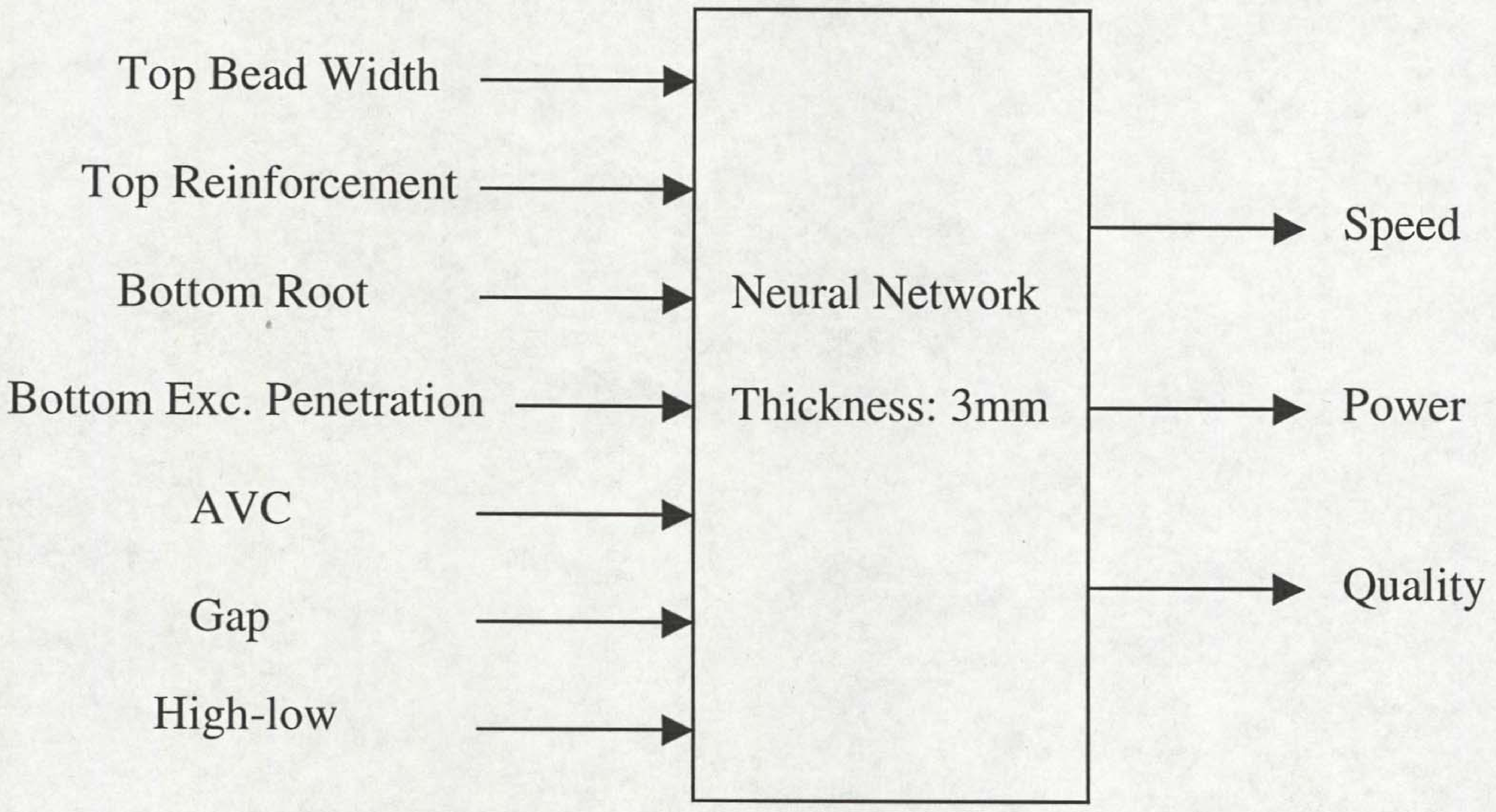

Figure 7. 4 Neural Network

Table 7. 1 Variation of the Welding Parameters

Change (%)	**Gap** (mm)	**Speed** (cm/min)	**Power** (%)
10	1.485	17.97	14.94
8	1.458	18.14	15.03
6	1.431	18.32	15.13
4	1.404	18.5	15.23
2	1.377	18.69	15.34
0	1.35	18.88	15.45
-2	1.323	19.08	15.57
-4	1.296	19.28	15.69
-6	1.269	19.48	15.8
-8	1.242	19.69	15.95
-10	1.215	19.9	16.08

CHAPTER 8 CONCLUSIONS AND FUTURE WORK

The research presented in this thesis was to produce vision-based sensors for three weld sensing tasks: penetration control, seam sensing and tracking, and bead inspection in automated welding. Conclusions on the performance of these sensors may now be drawn, with reference to the results. It is also now possible to outline some future work which may be worthy of research.

8.1 Conclusions

The conclusions to be drawn will be split into three sections, these being pool monitoring, seam sensing and tracking, and bead profile measurement.

8.1.1 Pool Monitoring

The CCD camera, combined with selected filters, provides a practical and effective approach to acquire useful images for weld pool detection. The quality of the image is dependent on the type of material and the type of welding.

Different image features are observed in TIG welding of aluminum and stainless steel and MIG welding of mild steel. The best results are obtained for welds using TIG welding on aluminum. As can be seen in chapter 3, extremely clear images of the weld pool are obtained. The images acquired in MIG welding have clear brightness contrast at the pool edge, whilst the images from TIG welding of stainless steel have unclear edges and require the use of more intelligent algorithms for edge detection.

These experiments have shown that high quality images of the top face of a weld bead can be achieved, and that any faults such as slag formations and movement in the weld pool can be clearly seen.

Image processing algorithms developed in the thesis can detect the pool edge with sufficient accuracy and speed under practical welding conditions. Their effectiveness and robustness have been demonstrated in closed-loop control experiments. The whole process of edge detection can be finished in 40 ms on a Pentium II class PC running at 350 MHz under Windows NT4. This processing rate is comparable with a standard, interlaced, CCD camera frame rate of 25Hz, allowing low cost commercially available components to be used.

8.1.2 Seam Sensing and Tracking

The development of a versatile seam measurement sensor has been presented in this thesis. The sensor head is compact, light weight, and is capable of being mounted onto the welding torch.

The seam sensing software works with different joint modes by simply selecting the appropriate algorithms for the welded joint type. Using image processing seam parameters, i.e., seam position, gap width and high-low can be obtained. The resultant seam position gives the guide for seam following by manipulating torch movement. Gap and high-low can be input to the neural welding parameter predictor for generating welding parameters.

The image processing time for the seam analysis is less than 40ms on a 350 MHz Pentium II class PC. The accuracy of the seam sensing system depends upon the camera optical arrangement used. For the sample images presented in this thesis, the typical accuracy of measurements made would be to within ±0.1mm.

8.1.3 Bead Profile Measurement

The computer vision based automated bead profile sensor is capable of measuring the contours of a weld profile and able to replace the manual measurement technique presently used daily in the welding industry.

Using the modified Hough transform instead of the time consuming standard Hough transform for contour segmentation reduced the software running time from 3 seconds per frame to about 0.2 seconds per frame on a P5/100 computer. Running the software on a faster computer could reduce the processing time further. As a result, it is possible to apply this system on-line rather than only used as a measurement gauge in off-line environments.

8.2 Future Work

The proposed future work on these systems may also be split into three sections, corresponding to the three systems.

8.2.1 Pool Monitoring

Currently, pool monitoring is undertaken by manipulating the width of the weld pool. It is well known that pool width is the most significant top face parameter with respect to penetration. The consistent penetration could be achieved, in some extent, by keeping the weld widths within required tolerances. However, the other top face parameters, such as pool length, shape and surface sag, are also closely related to the penetration. Zhang and Kovacevic [1.18] have investigated the correlation between weld pool geometry and weld penetration in TIG welding.

The new techniques are being investigated, currently, in Liverpool University, to acquire the clear complete weld pool images rather than just half pool contour either in the front or in the rear.

Future work may be able to improve the penetration control by sensing the geometry of the weld pool instead of only pool width monitoring. In order to extract the geometrical information of the pool, two dimensional edge detection is required. This in turn requires more powerful computer for its real time applications.

8.2.2 Seam Sensing and Tracking

For widespread applicability, the sensor must be capable of dealing with a wide range of joint types and joint sizes. While some plants, such as pipe mills, have a small range of joint dimensions, other processes, such as pressure vessel fabrication, have a very wide range of weld joint sizes. Since a fully capable sensor system is a significant capital investment, it should be capable of handling a wide variety of tasks to maximise customer payback. This could be achieved in the future by providing the sensor with a dynamically programmable field of view, such as one minute to measure large V joints with a wide field of view, and the next to measure narrow gap butt joints with a small field of view.

8.2.3 Bead Profile Measurement

8.2.3.1 Calibration

Off line calibration using step samples has been explained in chapter 5. This is a feasible way in laboratory condition, but it is impractical for industrial applications. An effective method of online calibration is required. This could be done in the future work by solving the basic problems in photogrammetry: absolute, relative, exterior, and interior orientation. The interior orientation problem should be solved for any camera to ensure that the camera obeys the assumptions of image formation assumed by most machine vision algorithms. The remaining calibration problems can be divided into two groups: methods used in image analysis and methods used in depth measurement. The exterior orientation problem must be solved for an image analysis application when it is necessary to relate image measurements to the geometry of the scene. The relative orientation problem is used to calibrate a pair of cameras for obtaining depth measurements with binocular stereo. The absolute orientation problem is used to calibrate the position and orientation of any system for depth measurement, including binocular stereo or active sensing, so that the depth measurement can be expressed in a common coordinate system.

8.2.3.2 Miniaturization

A number of industrial companies have expressed an interest in a portable, hand held version of the profile monitor. It is envisaged that this model would include a CCD receiver connected to a laser diode, set within a column tube. The bead profile data would then be presented on a portable computer carried by the inspector. This device would thus allow random spot checks to be made.

REFERENCES

[1.1] Xiao, Y.H., and Ouden, G. den. “Weld Pool Oscillation during GTA Welding of Mild Steel”. *Welding Journal* 72(8) 1993, 428-s to 434-s.

[1.2] Bicknell, A., Smith, J. S., and Lucas, J.. “Arc Voltage Sensor for Monitoring of Penetration in TIG Welds”. *IEE Proc. Sci. Meas. Technol.* 141(6) 1994, 513-520.

[1.3] Carlson, N.M., and Johnson, J.A.. “Ultrasonic Sensing of Weld Pool Penetration”. *Welding Journal* 67(11) 1988, 239-s to 246-s.

[1.4] Yang, J., *et al.*. “Ultrasonic Weld Penetration Depth Sensing with a Laser Phased Array”. *Proceedings of 1994 ASME International Mechanical Engineering Congress,* PED-Vol. 68-1, *Manufacturing Science and engineering,* 1994, pp. 245-254.

[1.5] Stone, D. A., Smith, J. S., and Lucas, J.. “Sensor for Automated Frontface Weldbead Area Control”. *Meas. Sci. Technol.* No.5 1994, 93-99.

[1.6] Bicknell, A., Smith, J. S., and Lucas, J.. “Infrared Sensor for Top Face Monitoring of Weld Pools”. *Meas. Sci. Technol.* No.5 1994, 371-378.

[1.7] Kovacevic, R., Zhang, Y. M., and Li, L.. “Monitoring of Weld Joint Penetration Based on Weld Pool Geometrical Appearance”. *Welding Journal,* 75(10) 1996, 317-s to 329-s.

[1.8] Bicknell, A., Smith, J. S., and Lucas, J.. “Infrared Sensor for Top Face Monitoring of Weld Pools”. *Meas. Sci. Technol.,No.5* 1994, 371-378.

[1.9] Kovacevic, R., Zhang, Y. M., and Ruan, S.. “Sensing and Control of Weld Pool Geometry for Automated GTA Welding”. *ASME Journal of Engineering for industry,* 117(5) 1995, 210-222.

[1.10] Banerjee, P., Govardhan, S., Wikle, H. C., Liu, J. Y., and Chin, B. A.. “Infrared Sensing for On-Line Weld Geometry Monitoring and Control”. *ASME Journal of Engineering for Industry,* 117(8) 1995, 323-330.

[1.11] Zhang, Y. M., Kovacevic, R., and Wu, L.. "Dynamic Analysis and Identification of Gas Tungsten Arc Welding Process for Weld Penetration Control". *ASME Journal of Engineering for Industry,* 118(2) 1996, 123-136.

[1.12] Suga, Y., Sano, Y., Naruse, M., Kojima, K., and Ogawa, K.. "Recognition of the Weld Line by a Visual Sensing System and Weld Line Tracking in Automatic Welding of Thin Aluminium Plates". *Welding International,* 7(4) 1993, 31-37.

[1.13] Zhang, Y.M., Li, L., and Kovacevic, R.. "Dynamic Estimation of Full Penetration Using Geometry of Adjacent Weld Pools". *ASME Journal of Manufacturing Science and Engineering.* Vol. 119, 1997, 631-643.

[1.14] Kovacevic, R., Cao, Z. N., and Zhang, Y. M.. "Role of Welding Parameters in Determining the Geometrical Appearance of Weld Pool". *ASME Journal of Engineering Materials and Technology,* 118(10) 1996, 589-596.

[1.15] Brzakovic, D., and Khani, D. T.. "Weld Pool Edge Detection for Automated Control of Welding". *IEEE Transactions on Robotics and Automation,* 7(3) 1991, 397-403.

[1.16] Kovacevic, R., and Zhang, Y. M.. "Sensing Free Surface of Arc Weld Pool Using Specular Reflection: Principle and Analysis". *Proc Instn Mech Engrs, part B: Journal of Engineering Manufacture,* Vol. 210, 1996, 553-564.

[1.17] Hoffman, T.. "Real-Time Imaging for Process Control". *Advanced Material & Processes* 140(3) 1991, 37-43.

[1.18] Kovacevic, R., and Zhang, Y. M.. "Real-Time Image Processing for Monitoring of Free Weld Pool Surface". *ASME Journal of Manufacturing Science and Engineering,* Vol. 119, 1997, 161-169.

[1.19] Chen, S. B., Wu, L., Wang, Q. L., and Liu, Y. C.. "Self-Learning Fuzzy Neural Networks and Computer Vision for Control of Pulsed GTAW". *Welding Journal,* 76(5) 1997, 201-s to 209-s.

[1.20] Mahajan, A., Figueroa, F.. "Intelligent Seam Tracking Using Ultrasonic Sensors for Robotic Welding". *Robotica,* 15(Pt3), 1997, 275-281.

[1.21] Zhang, S. B., Zhang, Y. M., and Kovacevic, R.. "Noncontact Ultrasonic Sensing for Seam Tracking in Arc Welding Processes". *Journal of Manufacturing Science and Engineering-Transactions of the ASME,* 120(3) 1998, 600-608.

[1.22] Estochen, E. L., and Neuman, C. P.. "Application of Acoustic Sensors to Robotic Seam Tracking". *IEEE Transaction on Industrial Electronics*, IE-31(3) 1984, 219-224.

[1.23] Umeagkwu, C., and Maqueira, B.. "Robotic Acoustic Seam Tracking: System Development and Application". *IEEE Transaction on Industrial Eletronics*, 36(3), 338-348.

[1.24] Yoo, C. D., Sunwoo, H. K., and Koh, K. I.. "Investigation on arc light intensity in gas metal arc welding .2. Application to weld seam tracking". *Proceedings of the Institution of Mechanical Engineers, Part B-Journal of Engineering Manufacture,* 211(5) 1997, 355-363.

[1.25] Nam, S. H., Oh, S. Y.. "Real-time dynamic visual tracking using PSD sensors and extended trapezoidal motion planning". *Applied Intelligence,* 10(1) 1999, 53-70.

[1.26] Kim, J. S., Son, Y. T., Cho, H. S., and Koh, K. I.. "A Robust Visual Seam Tracking System for Robotic Arc Welding". *Mechatronics,* 6(2) 1996, 141-163.

[1.27] Qu, Z. G., Salminen, A., and Moisio, T.. "Seam Tracking in Laser Welding using Vision Sensors". *International Journal of Materials & Product Technology,* 11(3-4) 1996, 276-283.

[1.28] Yu, J. Y., and Na, S. J.. "A Study on Vision Sensors for Seam Tracking of Height-varying Weldment. Part 2: Applications". *Mechatronics,* 8(1) 1998, 21-36.

[1.29] Tsuboi, R., and Asai, S. Et. al.. "Application of Laser Sensor for Automatic Welding in Japan". *Proceedings of Commission XII, IIW Lisbon.* 1999, 5-22.

[1.30] Yamane, S., and Koyame, T. Et. Al.. "Seam Tracking in First Layer of One Side Robotic Welding". *Proceedings of Commission XII, IIW Lisbon.* 1999, 54-62.

[1.31] Haug, K., and Pritschow, G.. "Robust Laser-stripe Sensor for Automated Weld-seam-tracking in the Shipbuilding Industry". *ISIE'98 Bled, Slovenia.* 1998, 1236-1241.

[1.32] Haug, K., and Pritschow, G.. "Reducing Distortion caused by the Welding Arc in a Laser Stripe Sensor System for Automated Seam Tracking". *ISIE'99 Bled, Slovenia.* 1999, 919-924.

[1.33] Smith, J. S., And Lucas, J.. "A Vision-based Seam Tracker for Butt-plate TIG Welding". *J. Phys. E: Sci. Instrum.,* 22 1989, 739-744.

[1.34] Wu, J., Smith, J. S., and Lucas, J.. "Weld Bead Placement System for Multipass Welding". *IEE Proceeding-Science Measurement and Technology,* 143(2) 1996, 85-90.

[1.35] White, R. A., Smith, J. S., and Lucas, J.. "Vision-based Gauge for online Weld Profile Metrology". *IEE Proceeding-Science Measurement and Technology,* 141(6) 1994, 521-526.

[3.1] Marr, D. and Hildreth, E.. "Theory of Edge Detection". *Proc. Royal Society of London.* Vol 207, 1980, 187-217.

[3.2] Canny, J.. "A Computational Approach to Edge Detection". *IEEE Transaction on Pattern Analysis and Machine Intelligence.* Vol. PAMI-8, 6, 1986.

[3.3] Jain, R., Kasturi, R. and Schunck, B. G.. Machine Vision. McGraw-Hill, Inc. 1995.

[4.1] Saint-Marco, P., Hen, J. S., and Median, G.. "Adaptive Smoothing: A General Tool for Early Vision". *IEEE Trans. Pattern Anal. Mach. Intell.* 13(6) 1991, 514-529.

[4.2] Wan, W., and Ventura, J. A.. "Segmentation of Planar Curves into Straight Line Segments and Elliptical Arcs". *Graphical Models and Image Processing* 59(6) 1997, 484-494.

[4.3] Teh, C. H., and Chin, R. T.. "On the Detection of Dominant Points on Digital Curves". *IEEE Trans. Patt. Anal. Machine Intell.* 11 1989, 859-872.

[4.4] Ansari, N., and Huang, K.. "Non-parametric Dominant Point Detection". *Pattern Recognition*, 24 1991, 849-862.

[4.5] Pla, F.. "Recognition of Partial Circular Shapes From Segmented Contours". *Computer Vision Image Understanding* 63 1996, 334-343.

[4.6] Inesta, J. M., and Buendia, M. etc. "Reliable Polygonal Approximations of Imaged Real Objects Through Dominant Point Detection". *Pattern Recognition*, 31(6) 1998, 685-697.

[5.1] Chutatape, O., and Guo, L.. "A Modified Hough Transform for Line Detection and Its Performance". *Pattern Recognition*, 32, 1999, 181-192.

[5.2] Kälviäinen, H., Hirvonen, P., and Xu, L.. "Probabilistic and Non-probabilistic Hough Transforms: Overview and Comparisons". *Vision Comput.* 13 1995, 239-252.

[5.3] Ben-Tzvi, D., Leavers, V. F., and Sandler, M. B.. "A Dynamic Combinatorial Hough Transform". *Proc. 5th Int. Conf. Image Analysis and Processing, Positano, Italy,* 1989, 152-159.

[5.4] Kiryati, N., Eldar, Y., and Bruckstein, A. M.. "A Probabilistic Hough Transform". *Pattern Recognition,* 24(4), 1991, 303-316.

[5.5] Leavers, V. F.. "The Dynamic Generalized Hough Transform: Its relationship to the Probabilistic Hough Transforms and an Application to the Concurrent Detection of Circles and Ellipses". *Vision Graphics Image Process: Image Understanding,* 56(3), 1992, 381-398.

[5.6] Shvaytser, H., and Bergen, J. R.. "Monte Carlo Hough Transforms". *Proc. 7th Scandinavian Conf. Image Analysis, Aalborg, Denmark,* 1991, 80-87.

[5.7] Guo, L., and Chutatape, O.. "Influence of Discretization in Image Space on Hough Transform". *Pattern Recognition*, 32, 1999, 635-644.

[5.8] Zhang, Y., and Webber, R.. "A Windowing Approach to Detecting Line Segments Using Hough Transform". *Pattern Recognition*, 29(2), 1996, 255-265.

[5.9] Leung, D. N. K., etc.. "Diagonal Quantization for the Hough Transform". *Pattern Recognition Letter*, 14, 1993, 181-189.

[5.10] Risse, T.. "Hough Transform for Line Recognition: Complexity of Evidence Accumulation and Cluster Detection". *Comput. Vision, Graphics Image Process.* 46, 1989, 327-345.

[5.11] Yuen, S. Y. K.. "An Approach to Quantization of Hough Space". *Proc. 7th Scandinavian Conf. Image Analysis*. 1991, 733-740.

PUBLICATIONS

1. Zhao, J., Smith, J. S., and Lucas, J. etc. “Computer Vision Techniques for Real Time Weld Seam Monitoring”. *Proc. 10th Int. Conf. Computer Technology in Welding and Manufacturing*. Copenhagen, Denmark, 2000.

2. Zhao, J., Houghton, M. A., and Balfour, C. etc. “Real Time Image Processing for Penetration Control in Automated Welding”. *Proc. 8th Int. Conf. Computer Technology in Welding and Manufacturing*. Liverpool, UK, 1998.

COMPUTER VISION TECHNIQUES FOR REAL TIME WELD SEAM MONITORING

Jing Zhao, Jeremy Smith, James Lucas, and Chris Balfour

ABSTRACT

The selection of suitable welding parameters depends upon many different factors. These factors may include the joint preparation, fit up of the workpiece, material type and material thickness. If suitable weld parameters are used and then maintained during the welding process, weld characteristics such as a uniform weld bead size and a constant degree of weld penetration may be achieved.

This paper presents results from the use of an automated welding control system that uses a laser range-finding sensor that has been applied to indicate the joint profile. A CCD camera is used to view a weld seam illuminated by a structured light source and the image generated is captured by computer based hardware. Novel, software based, image processing algorithms are used to extract seam geometry information. Different algorithms have been developed for butt joints, lap joints and V preparations. This allows the system to be applicable to a number of applications using differing plate thickness and welding processes. To ensure the adaptability and robustness of the software an extensive set of experimental trials have been conducted.

INTRODUCTION

For automated welding, a reliable mechanism for seam tracking is often required. The use of this type of a suitable seam position sensor ensures that the welding torch is maintained at the correct position relative to the welding seam throughout the welding process. Many different types of sensors may be used for seam tracking, such as arc, ultrasonic, mechanical and vision based [1-9]. Advancements in modern technology have allowed computer based vision systems to offer a versatile and competitive means of seam tracking. A vision based seam sensor is the possibility of making additional measurements relating to the seam geometry. This additional information may be used to tune the welding parameters in response to such factors as possible workpiece misalignment and varying seam gap sizes due to component tolerances. Computer vision sensors of this type may be easily adapted to measure characteristics of the molten weld pool [10]. Due to the inherent similarity between vision-based pool and seam sensors, multiple sensors may be integrated onto a single welding torch. This allows a compact vision based sensor system capable both seam tracking and weld pool monitoring to be implemented.

Research work relating to vision based seam tracking systems has been in progress at the University of Liverpool for some time. The early systems used specialised hardware to provide the required image analysis [3,4]. More recently, real time systems have been developed around standard, low cost PC hardware that use software based image analysis algorithms. The results obtained from the use of this type of software based seam image analysis system are presented in this paper.

---

* Department of Electrical Engineering & Electronics, The University of Liverpool, Brownlow Hill, L69 3GJ Liverpool, UK. Email j.lucas@liv.ac.uk

SEAM MONITORING SYSTEM

A typical optical seam sensor system consists of a CCD camera, a laser diode, a computer based frame processing system. The seam is illuminated by a laser line at a given angle and viewed by a CCD camera usually placed vertically. The image of the laser line images contains all the information necessary for determining the features representing a joint or seam. The CCD images are captured and analysed by a computer based image analysis system. A number of image processing activities are undertaken on these images to derive the geometrical information of the seam such as the centre position, gap and misalignment between two plates. The resultant parameters of image processing are transmitted to control system to adjust the manipulator path to ensure that the torch is at the correct position with respect to the seam and furthermore to generate the welding parameters for compensating the gap and misalignment.

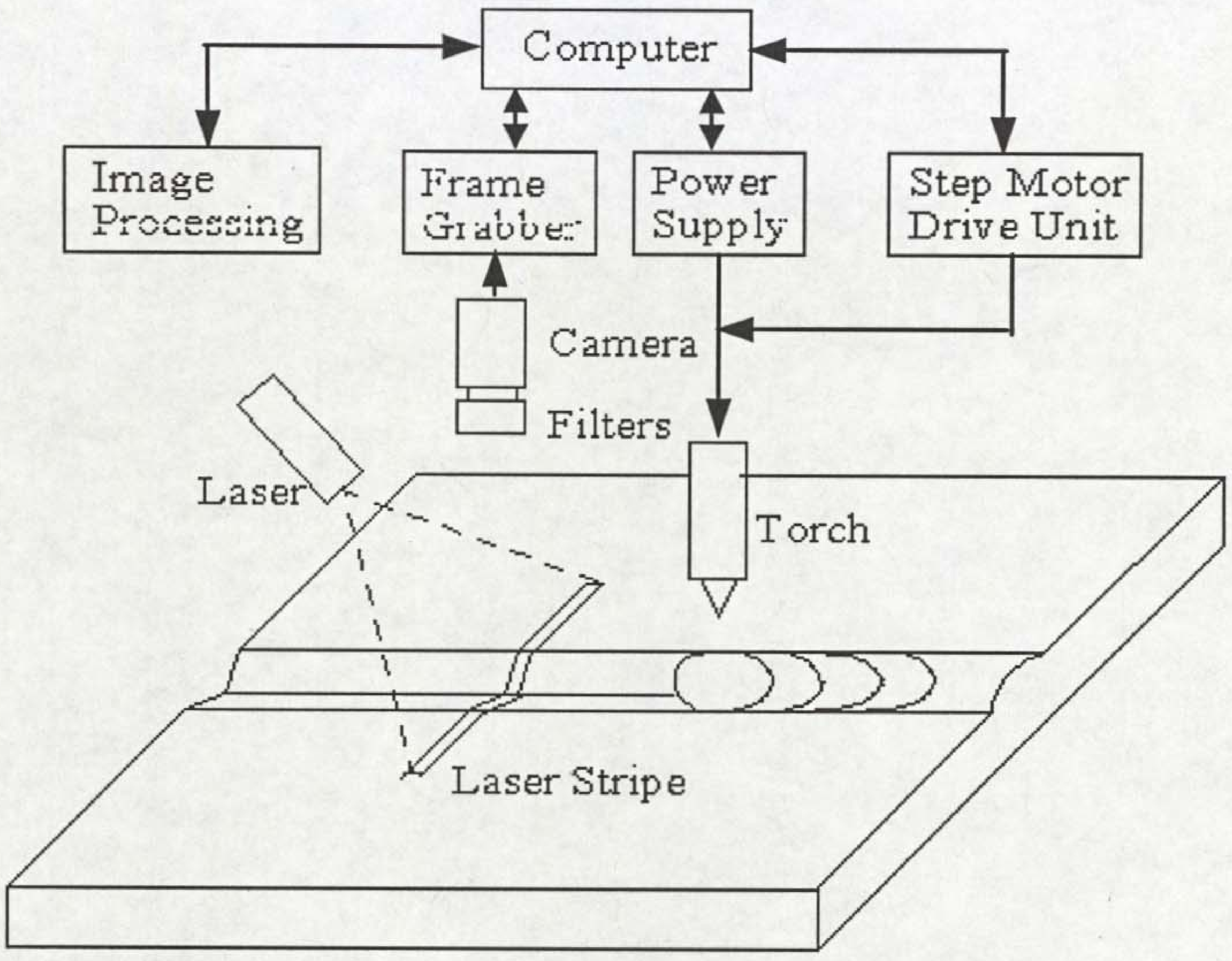

Figure 1: Seam Monitoring System

Figure 1 shows a block diagram of the seam Monitoring system. This sensor comprises of a head and the image processing system. The sensor head, including CCD camera, filters and laser (680nm) is mounted onto the welding torch and acquires visual information with regard to the seam position. In order to suppress the disturbances due to the arc light and the radiation from the hot metal, a narrow-band filter has been employed operating at the same wavelength range as the diode laser. The composite video signal output from the CCD camera is transmitted to an image capture board fitted to the computer system. The frame capture board is capable of storing images from the camera at resolutions up to 768×567 pixels at a frame rate of 25Hz.

The image processing software is written using Micorsoft Visual C++ 6.0. The window application of the image processing is shown in Fig. 2. The menus on the window top are able to start and stop image processing manually, which also can be controlled by the commands from the control system, and to select the algorithms for different joint modes. The resultant parameters of joint or seam (gap and hilo) are displayed at the window bottom in real time.

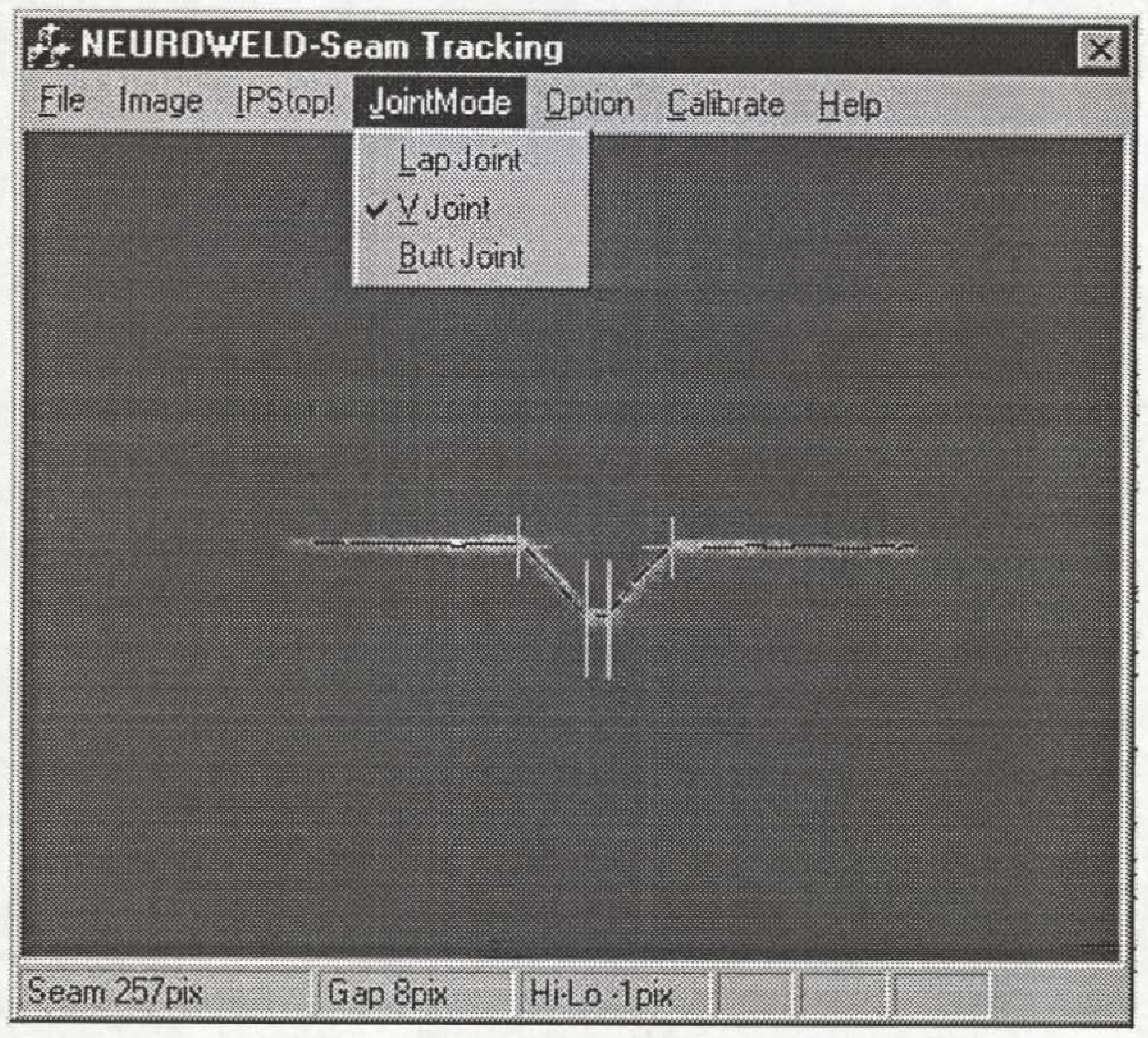

Figure 2: Image Processing Application Window

IMAGE PROCESSING ALGORITHMS

This section describes the algorithms used for processing of the image generated by the seam sensor.

Extraction of Seam Information

Depending on the thickness of plates to be welded, there are three kinds of most commonly used joint modes in welding. They are the butt joint, lap joint and V preparation. Figure 3 shows a simple diagram of the joint preparation along with the corresponding laser line images captured by a CCD camera.

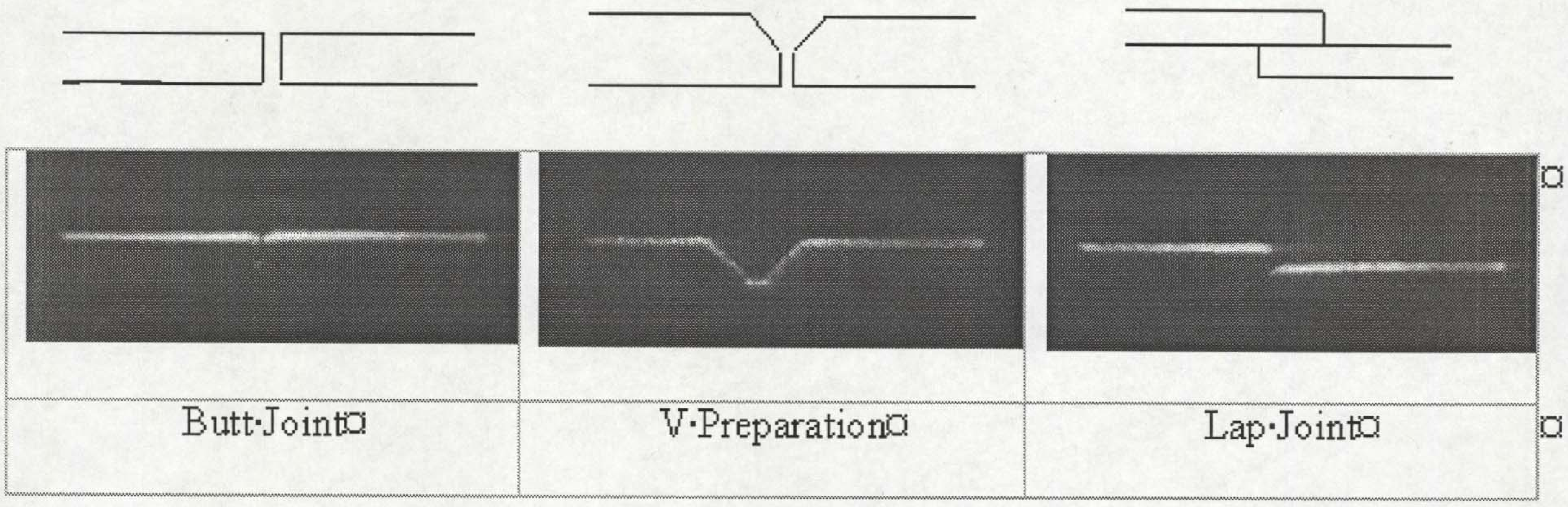

Figure 3 Weld Joint Modes

As shown on Fig. 3, the image patterns vary depending on the joint mode used. For V prep and lap joint, obvious features are presented around joints while for butt joint no significant changes occur other than a discontinuity at the seam position. A series of different image processing algorithms have been developed to accommodate each of the commonly used joint types, and the key aspects of each processing algorithm are presented in the following sections.

Laser Line Thinning

The purpose of thinning is to reduce the image components to their essential information to ease the task of image analysis and recognition. In order to reliably locate the laser line, the laser line is thinned from about five pixels to only one pixel in width to generate the central line $p_1 \dots p_k$, $k = 1, \dots, K$, denoted collectively by P. The actual laser line thinning is performed by using a localised image intensity averaging technique. For every column of the laser line image, average intensities of several neighbouring pixels are calculated. The highest average intensity value in a column is picked up and compared with a threshold T_g. If this value is greater than T_g, then the location with the highest average intensity is marked as the centre of the laser line p_k. Otherwise, the algorithm puts a value of (-1) in the media axis array P to mark it as a hole for the further processing. For lap joint and V prep, these holes will be filled with relevant values while for butt joints the holes will be analysed to determine whether it is either a gap between the two plates to be welded or just a hole on the central line.

A windowing technique is used to eliminate wasteful averaging calculations. The search range is determined dynamically according to the position of the previous extracted centre, for example, the window for p_k is given as $(p_{k-1}-1/2h,\ p_{k-1}+1/2h)$, where h is the height of the search window. For the first column or when the position of any of the holes are encountered, the full frame is processed, as no previous positions exist. This dynamic windowing technique has the potential to significantly reduce the per frame computational time. The search range should not be too restrictive, as large positional changes may sometimes occur along the laser line, especially for the lap joint. For correct operation the algorithm assumes that the laser line is always within the search window.

Algorithms for V Preparations

After the above mentioned laser line thinning, a central axis of the laser profile P is obtained. However, because the intensity of the laser line is not uniform along the x direction due to variable reflections on the surface of the workpiece, some holes exist on the media axis. Analysing the holes filled with (-1) in the central axis array P, it has been found that the size of the holes varies from one pixel to more than five pixels. For the bigger holes, bridging them by simply using the value next to the hole will cause error in the subsequent derivative analysis. Therefore, linear interpolation is used to bridge the holes. For any element i in a hole with a size of n, its value p_i can be calculated as:

$$p_i = p_{a-1} + i \times \frac{p_{b+1} - p_{a-1}}{(b+1)-(a-1)}$$

where a and b are the array indices for hole beginning and hole end, $i = 1, \dots, n$. Finally, smoothing is performed on the media axis array by taking the average of each point to its neighbours. A disadvantage of smoothing is the tendency towards a reduction in sharpness of image corner points. Therefore, excessive smoothing should be avoided by selecting appropriate numbers of neighbours from which to take the average value.

The algorithm used for extracting feature points is based on the analysis of the first and the second derivatives of the media axis array P, namely P' and P'',

$$p_k' = p_{k+l} - p_{k-l} \qquad k = l, \dots, K-l$$

$$p_k'' = p_{k+l}' - p_{k-l}' \qquad k = 2l, \dots, K-2l$$

where *l* is the supporting length.

The feature points are displayed below the laser line in the image processing window shown in Fig 4. The first and the second order derivatives have shown the significant changes at the feature points A, B, C and D. For the first derivative values, the changes at feature points just relate to the scale of the values. Usually, threshold methods are used to extract these features. For the second derivative values, the local maxima and minima are presented at these feature points. For the points A and B, the second derivatives have the negative local minima while, for the bottom points C and D, they are positive maxima. Practical trials have shown that using local minima and maxima values obtained from second order differential calculations to extract the feature points is more robust and reliable than methods based on the first order derivative calculation. For the bottom point, if there is no gap, only one local positive maximum exists, as shown in Figure 4(a). Otherwise, there will be two local positive maxima, as shown in Fig. 4(b). The search for the bottom points is started from two sides respectively until the first local maximum is found. This x and y positions of this maxima are then recorded, and the search resumes from the opposite side of the image. If the two positions from two sides are the same then this means that there is no gap between the plates. Otherwise, if these two positions are different then they are assumed to be the points C and D. Based on the bottom points, the search for two top points is started from bottom position to two sides. The positions with local negative minima are referred to be the top feature points A and B. Practical trials using this algorithm have shown that the feature points can be extracted successfully in the most situations. To improve the robustness of the algorithm, temporal filtering is used according to the continuity of the seam position.

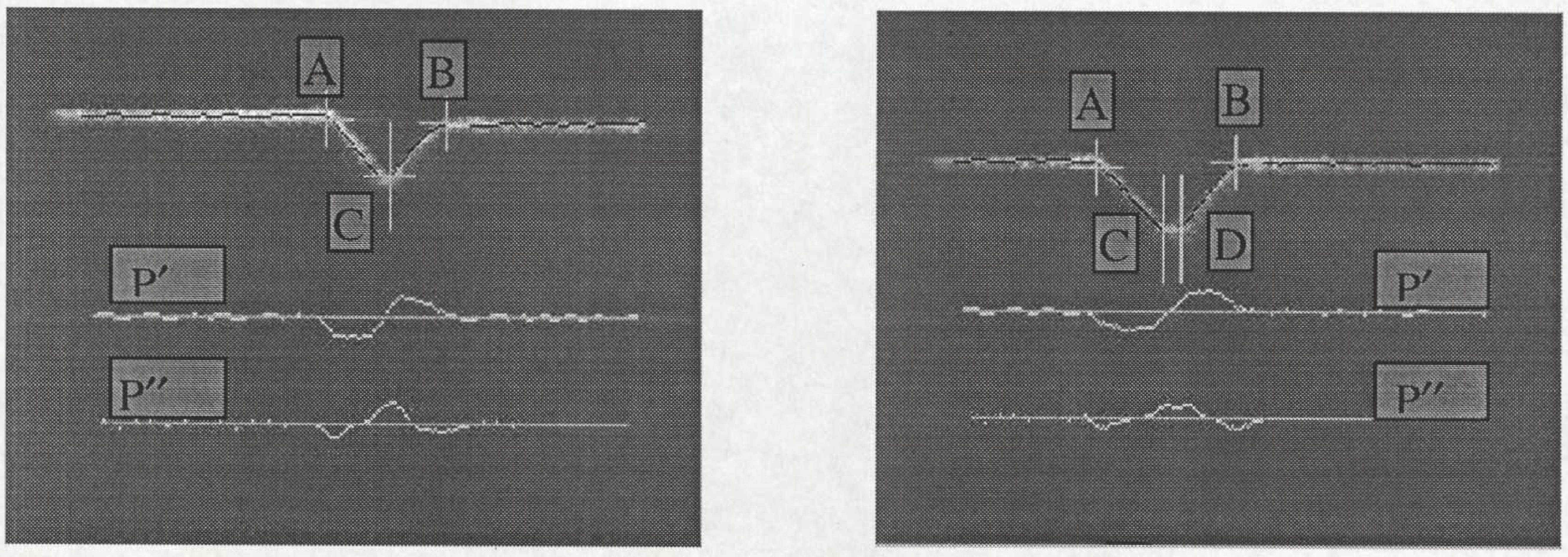

(a) Without Gap **(b) With Gap**

Figure 4 V Preparation Images

After the feature points are derived from the V prep image, three parameters are calculated and transmitted to the welding control system. They are the seam position, the horizontal centre of C and D, the gap width, the horizontal difference of C and D, and the high low, the vertical difference of A and B.

In brief, four steps are performed for the V prep seam acquisition:

- Linear interpolation to fill the holes to ensure the continuity of the media axis.
- Media axis smoothing using a 1×3 kernel (1, 1, 1).
- First and second derivative calculation.
- Feature points extraction and seam geometrical parameter calculation.

Algorithms for Butt Joints

The seam recognition for a butt joint is more difficult than that for V prep due to several different effects. Firstly, the laser line is not always continuous due to the existence of the black gap at the seam location, which is just the characteristic of the seam and must not be bridged by interpolation method mentioned in the above section. Therefore, the derivative method for the continuous line analysis cannot be used. Secondly, the patterns of the laser profile may vary during the welding, particularly if there is uneven weld plate spacing or plate distortion occurs. This can be seen in Fig. 5, where four typical image patterns are given. The most common pattern is shown in Fig. 5a. In this case, a clear gap can be seen at the seam. In the second situation, a reflection of the backing plate is displayed in the gap (Fig. 5b) while in the third case, only high low difference exists with a very small gap (Fig. 5c). In the last situation (Fig. 5d), there is no obvious gap and high low positions are presented around the seam, so other processing methods are needed to locate the seam.

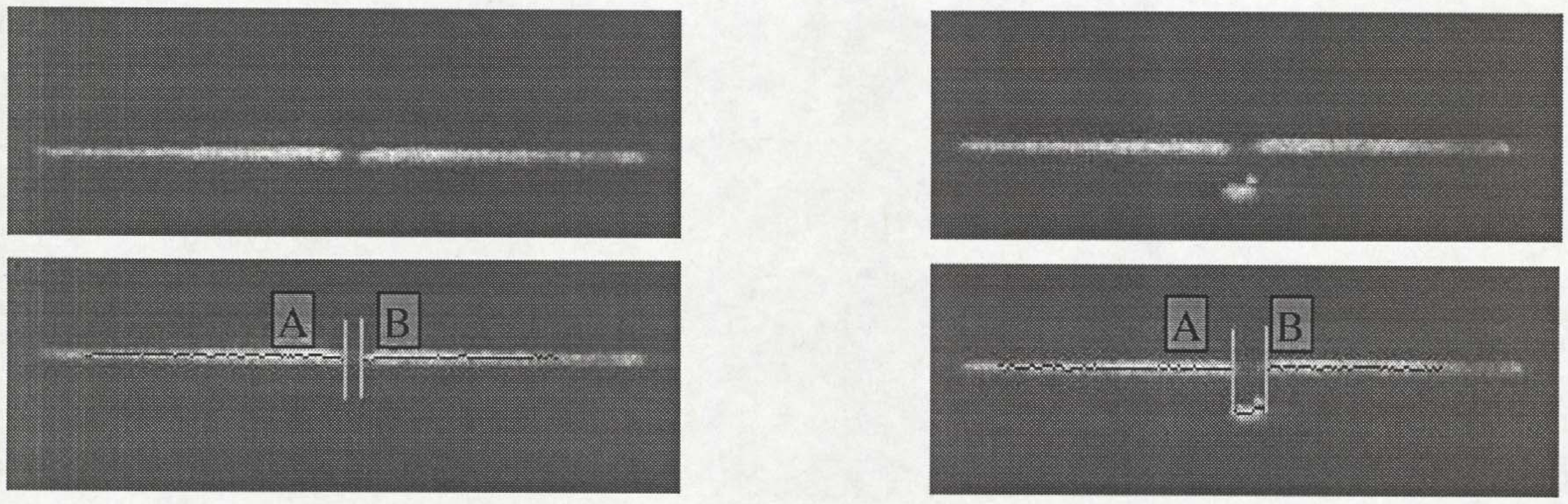

(a) Without Backing Plate **(b) With Backing Plate**

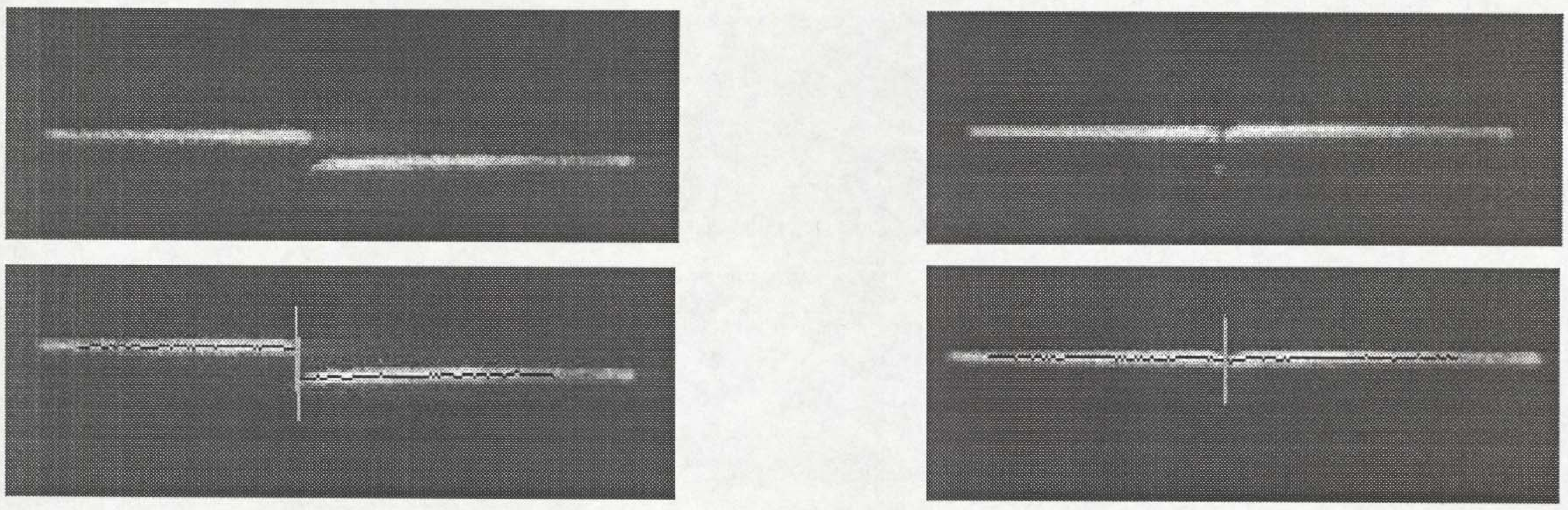

(c) Hilo Only **(d) Touching seam**

Figure 5: Butt Joint Images

The first step for seam extraction is to determine which pattern the image belongs to. Here two flags are used. They are validleftdrop and validrightdrop representing the existence of the laser line position drops at the left and the right sides of the seam. The searches for maximum position drops (max Δp_i) are taken from left to right and from right to left along the media axis respectively. If max Δp_i is greater than a threshold value, the flag is set to be true, otherwise false. Then image is categorised according to the states of these two flags. If only one flag is true the image goes to pattern (c) where only high low exists. If both flags are true it goes to pattern (b), while if both are false there will be two possible situations, pattern (a) or (d). So the further categorisation is done based on the degree of the gap between two plates. This process of judgement has been expressed in Table 1. In this way, images can be categorised into four patterns successfully.

Table 1 Pattern Judgement Table

validleftdrop	validrightdrop	Patterns
True	True	(b)
False	True	(c)
True	False	(c)
False	False	(a) or (d)

For pattern (b) and (c), the two feature points A and B are obtained during the above process of looking for the maximum position drops (max Δp_i). Then seam parameters, such as central position, gap and high low are derived. For the other two patterns, since no drops are found, further search is taken to look for the position with the maximum hole. This could be found without difficulty for pattern (a), with difficulty for pattern (d) as the gap is very small and may easily to be confused with the holes on the laser line elsewhere. Analysis of the images belonging to pattern (d) reveals that there is always be a bright dot under the seam, which is used to indicate the seam position. Accordingly, a window is set just below the laser line and, then, the position with the bright reflection is searched for within the window. The algorithm used for pattern (c) can also be used on the image of the lap joint, which exhibits the same image characteristics.

Filtering Techniques

With the above mentioned image processing, there is still a possibility of incorrect recognition due to parasitic image noise. Depending on the continuity of the seam, a temporal filter may be applied by monitoring the degree of a change in seam position between two successive frames. If the change exceeds a predefined tolerance then a judgement is made that the result is caused by noise and the measurement is discarded. Then the result from the previous frame is used to replace the current value. With this type of frame to frame temporal filter, the robustness of recognition algorithms has been further improved. A typical real time measurement of a varying gap and hilo for a butt weld incorporating the previously described filtering techniques is shown in Fig. 6.

CONCLUSIONS

The development of a versatile seam measurement sensor has been presented in this paper. The sensor head is compact, light weight, and is capable of being mounted on to the welding torch. The seam tracking software works with different joint modes by simply selecting the appropriate algorithm for the welded joint type. The image processing time for the seam analysis is less than 40ms on a Pentium II class PC running Windows NT4. This processing rate is comparable with a standard, interlaced, CCD camera frame rate of 25Hz, allowing low cost commercially available components to be used. The accuracy of the seam recognition system depends upon the camera optical arrangement used. For the sample images presented in this paper, the typical accuracy of measurements made would be to within ±0.1mm.

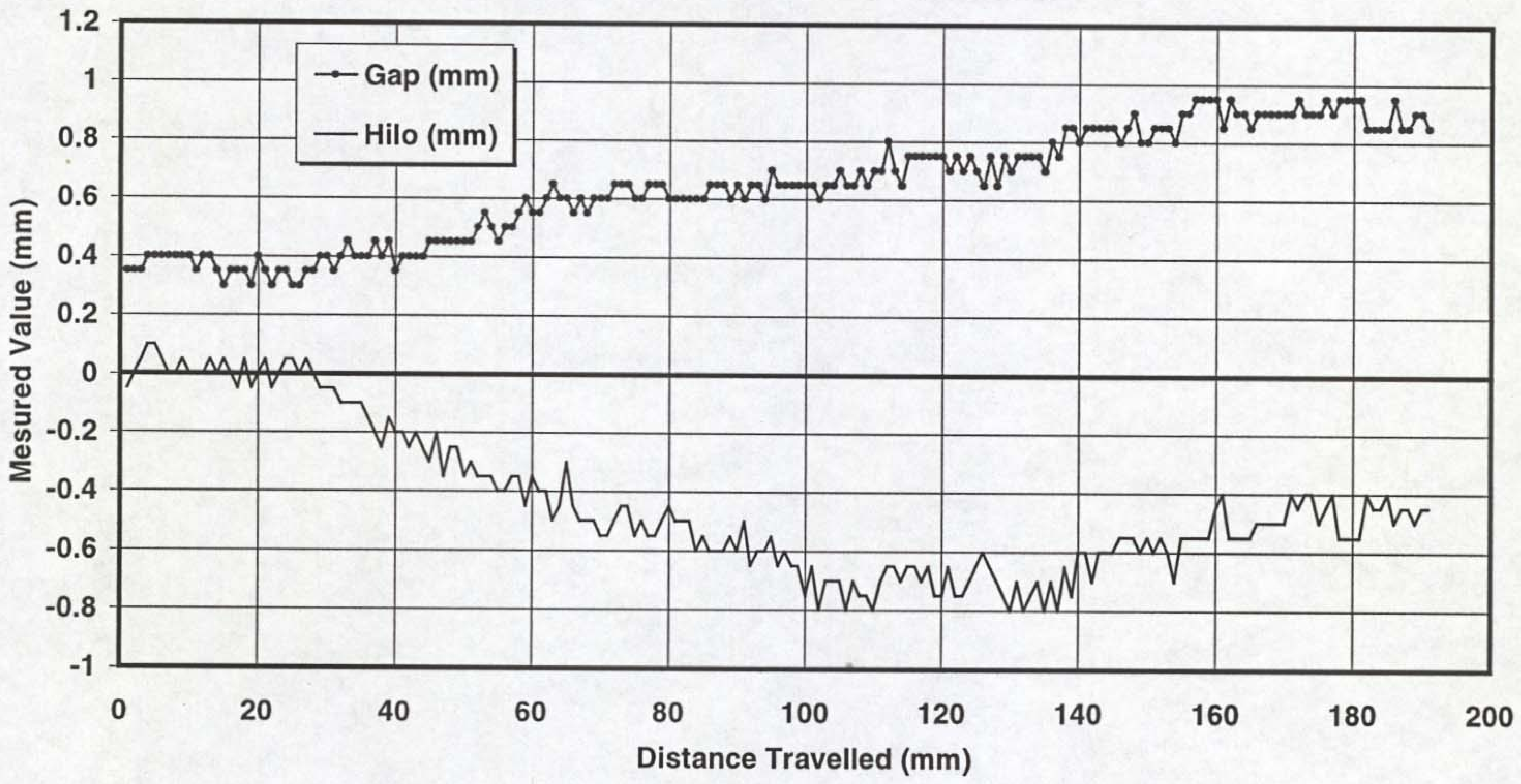

Figure 6: Real Time Gap and Hilo Measurements for a Butt Joint

ACKNOWLEDGEMENTS

The authors wish to thank the EPSRC for providing a research grant under the IMI scheme in order to research this activity.

REFERENCES

1. Zhang, S. B., Zhang, Y. M., and Kovacevic, R.. "Non-contact Ultrasonic Sensing for Seam Tracking in Arc Welding Processes". *Journal of Manufacturing Science and Engineering-Transactions of the ASME,* 120(3) 1998, 600-608.
2. Yoo, C. D., Sunwoo, H. K., and Koh, K. I.. "Investigation on arc light intensity in gas metal arc welding .2. Application to weld seam tracking". *Proceedings of the Institution of Mechanical Engineers, Part B-Journal of Engineering Manufacture,* 211(5) 1997, 355-363.
3. Smith, J. S., And Lucas J.. "A Vision-based Seam Tracker for Butt-plate TIG Welding".*J. Phys. E: Sci. Instrum.,* 22 1989, 739-744.
4. Wu, J., Smith, J. S., And Lucas J.. "Weld Bead Placement System for Multipass Welding". *IEE Proceeding-Science Measurement and Technology,* 143(2) 1996, 85-90.
5. Kim, J. S., Son, Y. T., Cho, H. S., and Koh, K. I.. "A Robust Visual Seam Tracking System for Robotic Arc Welding". *Mechatronics,* 6(2) 1996, 141-163.
6. Qu, Z. G., Salminen, A., and Moisio, T.. "Seam Tracking in Laser Welding using Vision Sensors". *International Journal of Materials & Product Technology,* 11(3-4) 1996, 276-283.
7. Yu, J. Y., and Na, S. J.. "A Study on Vision Sensors for Seam Tracking of Height-varying Weldment. Part 2: Applications". *Mechatronics,* 8(1) 1998, 21-36.
8. Tsuboi, R., and Asai, S. Et. al.. "Application of Laser Sensor for Automatic Welding in Japan". *Proceedings of Commission XII, IIW Lisbon.* 1999, 5-22.

9. Yamane, S., and Koyame, T. Et. Al.. "Seam Tracking in First Layer of One Side Robotic Welding". *Proceedings of Commission XII, IIW Lisbon.* 1999, 54-62.

10. Zhao, J., Houghton, M. A. etc.. "Real-time Image Processing for Penetration Control in Automated Welding". *8th International Conference: Computer Technology in Welding, Liverpool.* 1998, 1-7.

REAL-TIME IMAGE PROCESSING FOR PENETRATION CONTROL IN AUTOMATED WELDING

Jing Zhao, Michael A. Houghton, Christopher Balfour, Jeremy S. Smith and James Lucas*

ABSTRACT

In the automation of the welding process, in order to simplify hardware so as to enhance its feasibility and practicality, the top-face image of weld pool is obtained by using a high shutter speed CCD camera combined with selective optical filtering without the application of external illumination. However, this in turn complicates the images of the weld pool and leads to the requirements for more effective image processing algorithms. In this paper, the real time image processing algorithms applied to weld pool edge detection are reported. To ensure the robustness of edge detection, both spatial and time software filters are proposed. A wide range of weld pool images from the TIG and MIG processes have been obtained both in front of and behind the arc using aluminium and stainless steel plate. Currently, the weld pool edge can be acquired at a rate of 20 Hz. The closed-loop weld process control has been implemented using the edge model extracted by the image processing algorithms.

INTRODUCTION

For the last few years, arc welding process control has been an intensive research topic for a number of researchers world-wide. For automated arc welding, due to the variation in size and microstructure of the workpiece, even if constant welding parameters are used, inconsistent weld penetration still occurs. This, consequently, will influence the performance of weld in its working condition, especially for critical applications such as nuclear, chemical and aerospace structures. Thus, to maintain consistent penetration, during automated arc welding, has become a primary objective pursued by researchers.

For penetration control, practical and effective sensors are required. So far, a wide range of sensor systems applicable to arc welding have been developed, i.e., ultrasonic sensors (Ref.1, Ref.2), weld pool oscillation (Ref.3) and visual sensors (Ref.4-16) etc. Among the proposed sensors, the visual sensor is considered the most significant. For a skilled human welder, penetration information can be obtained by viewing the weld pool. It means that sufficient information about weld penetration exists in the geometrical appearance of the weld pool. The correlation between weld pool geometry and weld penetration in TIG welding has been intensively investigated by Y.M.Zhang and R.Kovacevic (Ref.4, Ref.10) in the University of Kentucky. In their research, a high shutter speed camera assisted with pulsed laser illumination is used to capture the clear image of the weld pool. The shutter of the camera is synchronised with the laser pulse. From developed image processing algorithms in their study, the edge of weld pool can be extracted successfully. Based up their achievements, there is still need to develop flexible, simpler and robust vision based top-face sensors suitable for a wide range of applications.

---

*Department of Electrical Engineering & Electronics, The University of Liverpool, Brownlow Hill, Liverpool, L69 3GJ Liverpool, UK. Email: jingzhao@liv.ac.uk

In this paper, a simple and practical top-face visual sensor is reported. A high shutter speed CCD camera combined with selective optical filtering without extra illumination is used to capture top-face images of the weld pool. The corresponding image processing algorithms are developed and used to analyse a wide range of images for both the TIG and MIG processes on aluminium, stainless steel and mild steel plate from many different positions and structures. Preliminary closed-loop control in TIG welding has been implemented.

EXPERIMENTAL SETUP

The principle diagram of the penetration sensing and control system is shown in Fig.1. The weld torch is held fixed while the workpiece is to move by a stepper motor. Direct and pulsed currents are used in TIG welding and in MIG welding. For aluminium, alternating current TIG welding is used. The high shutter speed CCD camera mounted on the welding torch can be positioned in front of the torch or behind the torch. A standard frame grabber, plugged into the computer, is used to capture images from the camera. Image processing, on a PC, is then performed on the image. The resultant data extracted from weld pool, which represent the penetration information, is output to the control interface board for manipulating the welding parameters, i.e. welding current, voltage (via. power supply) and welding speed (via. stepper motor drive unit) to ensure the required weld bead and penetration.

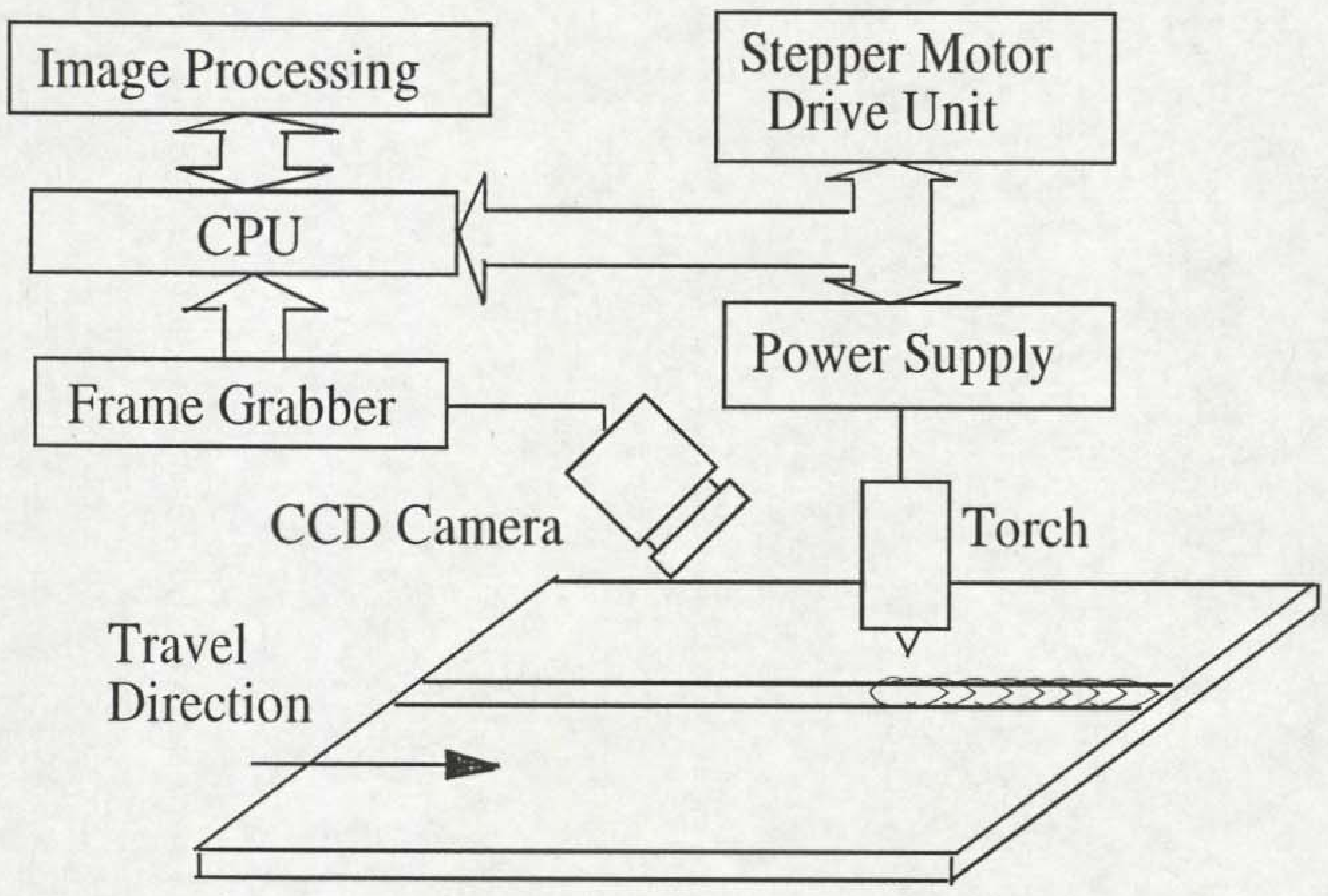

Fig. 1 Experimental Set up

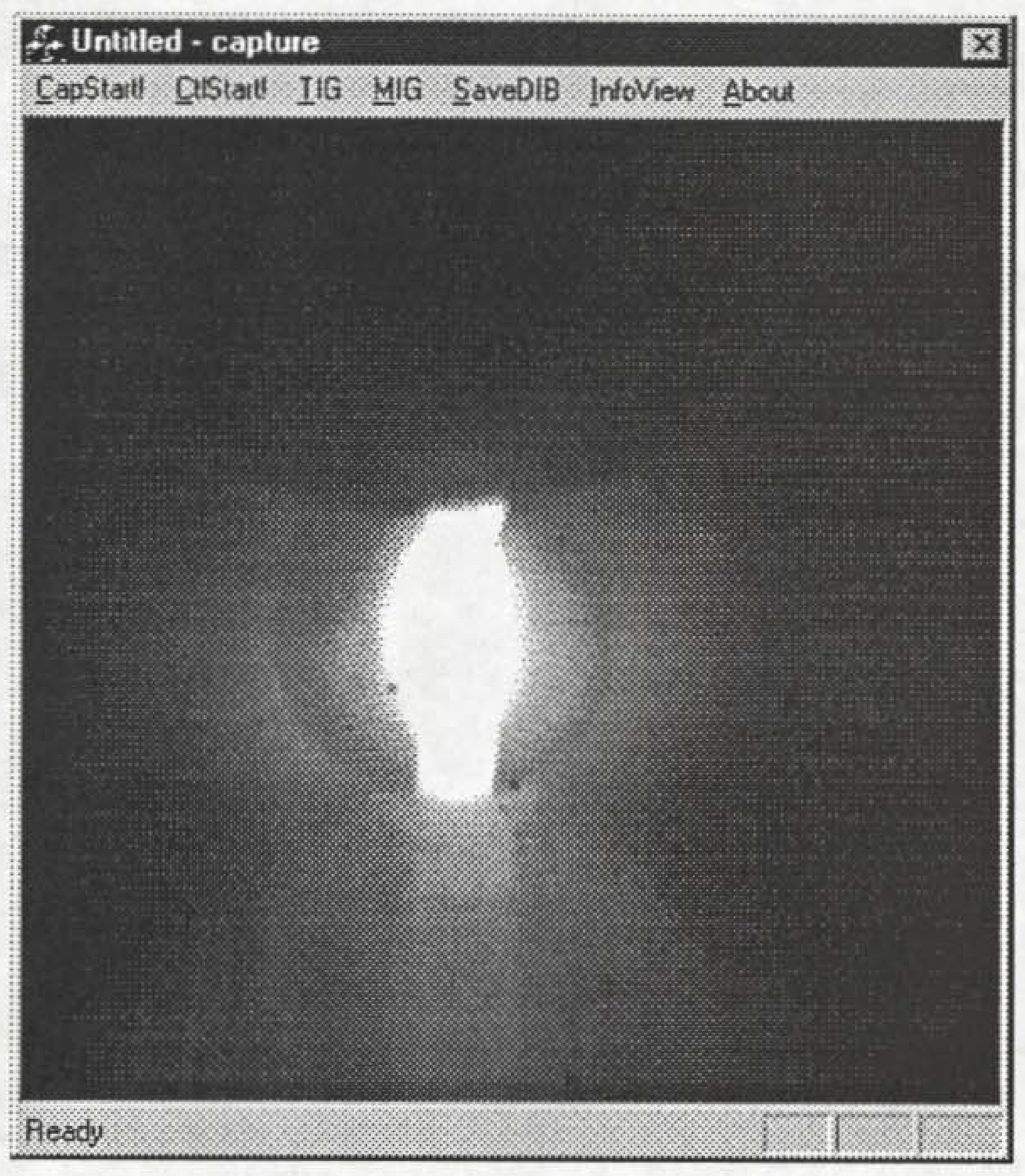

Fig. 2 Image Processing Application Window

DIGITAL IMAGE PROCESSING

The image processing is undertaken on a PC running Windows NT and the software is coded in C++. Fig.2 shows the image processing application window. By clicking the menu items on the top of application window, a variety of tasks can be performed. CapStart is to start and stop the video capture, while CtlStart is for invoking image processing and data output. Menu items TIG and MIG are used to switch image processing algorithms between TIG and MIG mode. Captured images can be saved to files by simply clicking SaveDIB. On selecting InfoView a dialog box will pop up, which is for editing the video format. The image shown in Fig.2 is a top face image of TIG welding on stainless steel.

Usually, real-time edge detection is the main objective of image processing for this kind of visual sensor. However, the computation for detecting whole edges using standard edge detection algorithms, such as Sobel, Laplacian etc. takes too long on standard image processing hardware. In addition, in some cases the contrast in weld pool images is very low. Thus, an effective algorithm must be developed based on the utilisation of the unique image features in combination with basic image processing concepts, rather than simply using existing approaches.

Three steps, in determining the edges of weld pool, have been proposed in this research:

1. Position the virtual centre $P_0(x_0, y_0)$ for locating the weld pool.
2. Get the feature points $P_k(x_k,y_k)$ $(k=1,2,\ldots,7)$ on the edge, Fig.3(a).
3. Based on the extracted feature points from step 2, modelling the weld pool edge using curve fitting.

Determination of Virtual Centre

Although it's very easy for a human to locate the centre of the weld pool, it is difficult to code as an algorithm. It is been experimentally observed that the centre of weld pool is in line with the position of highest brightness when the arc is initiated. Consequently, this is the basis of the software algorithm. Good results have been obtained especially when "Lift TIG" is used to initiate the arc. However, it does not work well in all situations. Unexpected results sometimes occur if the arc-starting process is unstable. Thus, manual selection for the centre point is made using the mouse and cursor. However, due to the camera setup, the centre position of the weld pool can be stored for use in subsequent welds.

Extraction of Edge Points

Since the welding arc is the only light source for viewing the weld pool, the variations of reflection characteristics from weld pool and adjacent area are observed for different welding processes and different kind of welded metals. Both AC TIG on aluminium and DC TIG on stainless steel have been studied whilst for MIG, observations of welding non-ferrous metals have been made. Several search algorithms have been used to extract the pool edge for the different welding processes as well as on different metals.

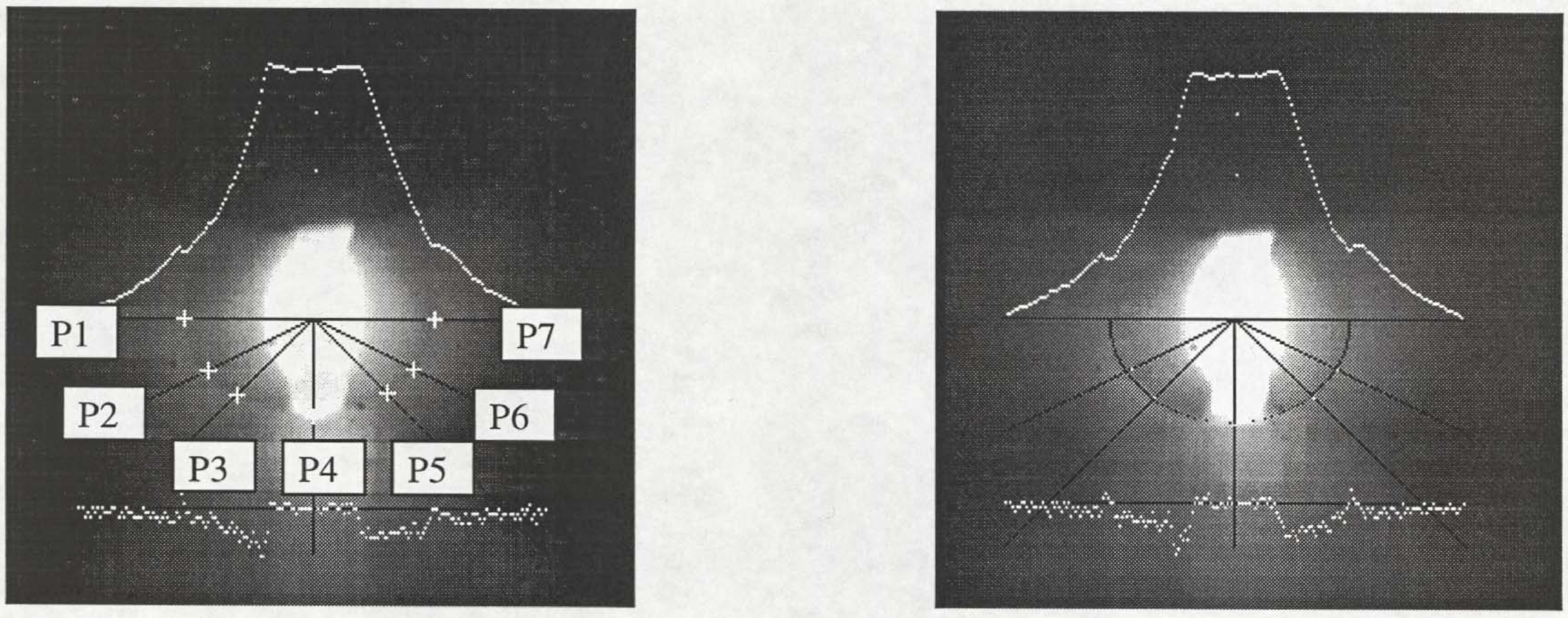

(a) (b)

Fig. 3 DC TIG Welding on Stainless Steel

In this study, instead of detecting complete edges of weld pool seven typical points are extracted, as shown in Fig.3(a). Edge points are searched along the black lines originating from the "virtual centre" which is identified when the arc is initiated or by the user with the mouse and cursor. The small white crosses intersecting the black lines represent the identified edges of the weld pool.

Fig.3 shows processed images of TIG welding on stainless steel. In this case the camera is positioned directly ahead of the weld pool with its axis at a suitable angle from the horizontal. The top white dot curve, on the Fig.3, is the grey scale distribution along the horizontal black line. The lower curve is the corresponding gradient from the centre to the sides. It can be seen that the radial grey scale distribution identifies the edge of the weld pool by a fall-rise-fall in the intensity, which is also indicated by the local large change in the gradient curve. So edge point $P_k(x_k, y_k)$ (k=1, 7) of the weld pool can be acquired theoretically by:

$$G(x_k, y_k) = \max_{a<i<b} G(x_i, y_i) \qquad 0 < (a, b) < n \qquad [1]$$

where G(x, y) denotes the gradient of the grey scale from centre to sides, and n is the pixel number of the detecting line. Due to noise and the illumination from the arc the largest gradients may not represent the edge of the weld bead. To overcome this problem the processing area is windowed to detect the local maximum, representing the bead edge, and to decrease the data requiring processing. The windowed region has been limited to an area of interest $i \in (a,b)$ whose size has been determined experimentally.

Using the above algorithm edge detection sometimes failed because the grey scale distribution varied around the bead edge. Based on the continuity of the pool edge, software for both spatial and time filters have been developed to remove the unexpected edge points. Spatially, besides detecting seven points $P_k(x_k, y_k)$, the adjacent two lines $L(y = y_k-1)$ and $L'(y = y_k+1)$ are also searched within the range $(x_k-\delta, x_k+\delta)$ depending on the current edge point $P_k(x_k,y_k)$. If the edge points exist on both lines, it can be considered that continuity is satisfied for $P_k(x_k,y_k)$, otherwise replace the current candidate edge point by the previous one on the same line. In the time domain, assume the current captured frame is t and detected edge points are $P_{k,t}(x_{k,t}, y_{k,t})$, then the average value of edge points from the last (m-1) frame is:

$$\overline{P}_k(x_k, y_k) = \frac{1}{m-1}\sum_{i=t-m}^{t-1} P_{k,i}(x_{k,i}, y_{k,i}) \qquad [2]$$

Comparing the current edge points $P_{k,t}(x_{k,t}, y_{k,t})$ with the average value, if the difference is smaller than a threshold T, then $P_{k,t}(x_{k,t}, y_{k,t})$ is selected as the candidate edge point, otherwise it is replaced with the previous one $P_{k,t-1}(x_{k,t-1}, y_{k,t-1})$. To effectively apply this filter, the selection of m and T is crucial and the values are determined by experimentation.

Using the proposed algorithm, very good results have been acquired for AC TIG welding of aluminium with wire feed, which is shown in Fig.4. Because of the obvious grey scale difference between the weld pool and surrounding solid material, large contrast occurs at the edge, which is ideal for image processing. The trailing portions of the weld pool are also investigated in this situation by positioning the camera behind the arc. This is shown in Fig.5. The brightness contrast between molten metal and solid part is not as significant as in Fig.4. It has been observed that the edge tracking in some positions fail because of the insufficient solidification of the previous weld pool producing extended images. Therefore, behind viewing is not a preferred technique for sensing the weld pool.

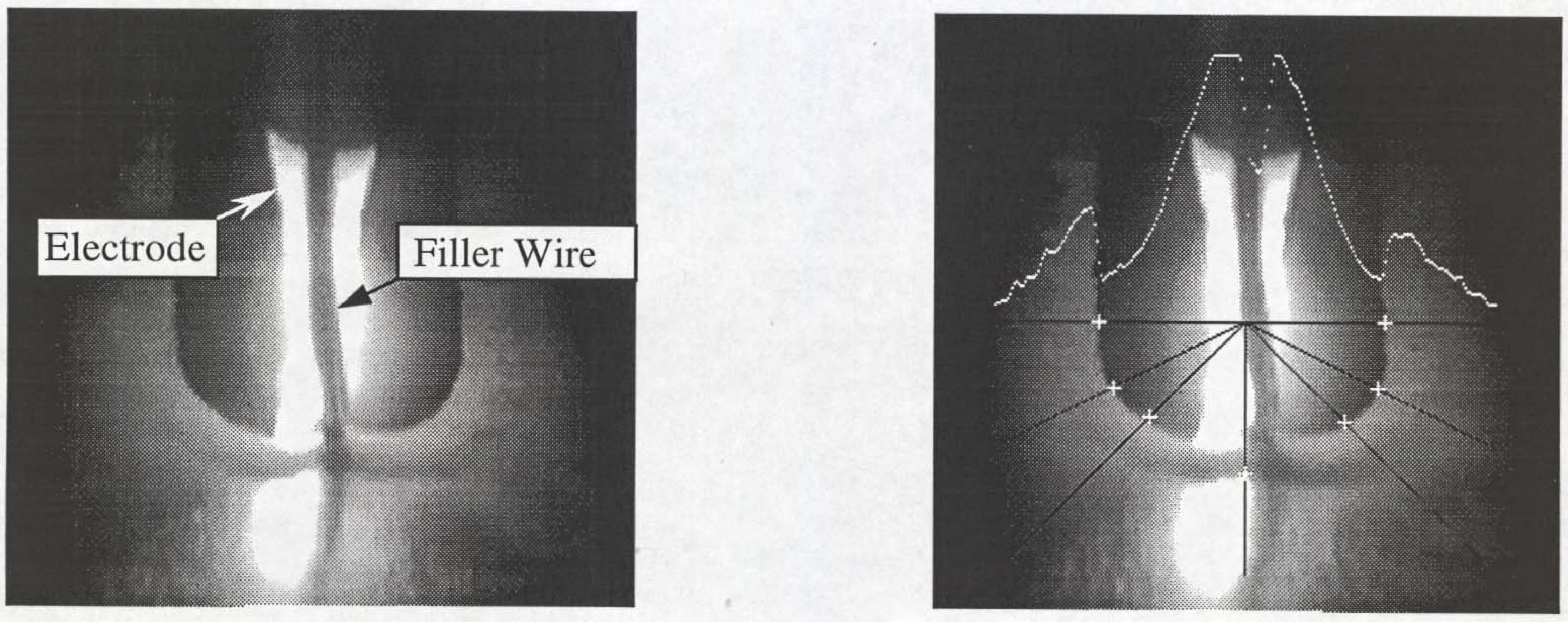

(a)

(b)

Fig. 4 AC TIG Welding on Aluminium

In MIG welding, usually higher currents are used with thicker workpieces, so that the optical radiation from the arc is greater than for TIG welding. Even though a strongly alternating optical filter is used, the brightness of the arc and the weld pool is still quite high and the adjacent solid metal surface is dark. Therefore, the intensity declines singly along the radius. The maximum negative gradients are observed at weld pool edges:

$$G(x_k, y_k) = \max_{a<i<b} |G(x_i, y_i)| \qquad 0 < (\mathrm{a}, \mathrm{b}) < \mathrm{n} \qquad [3]$$

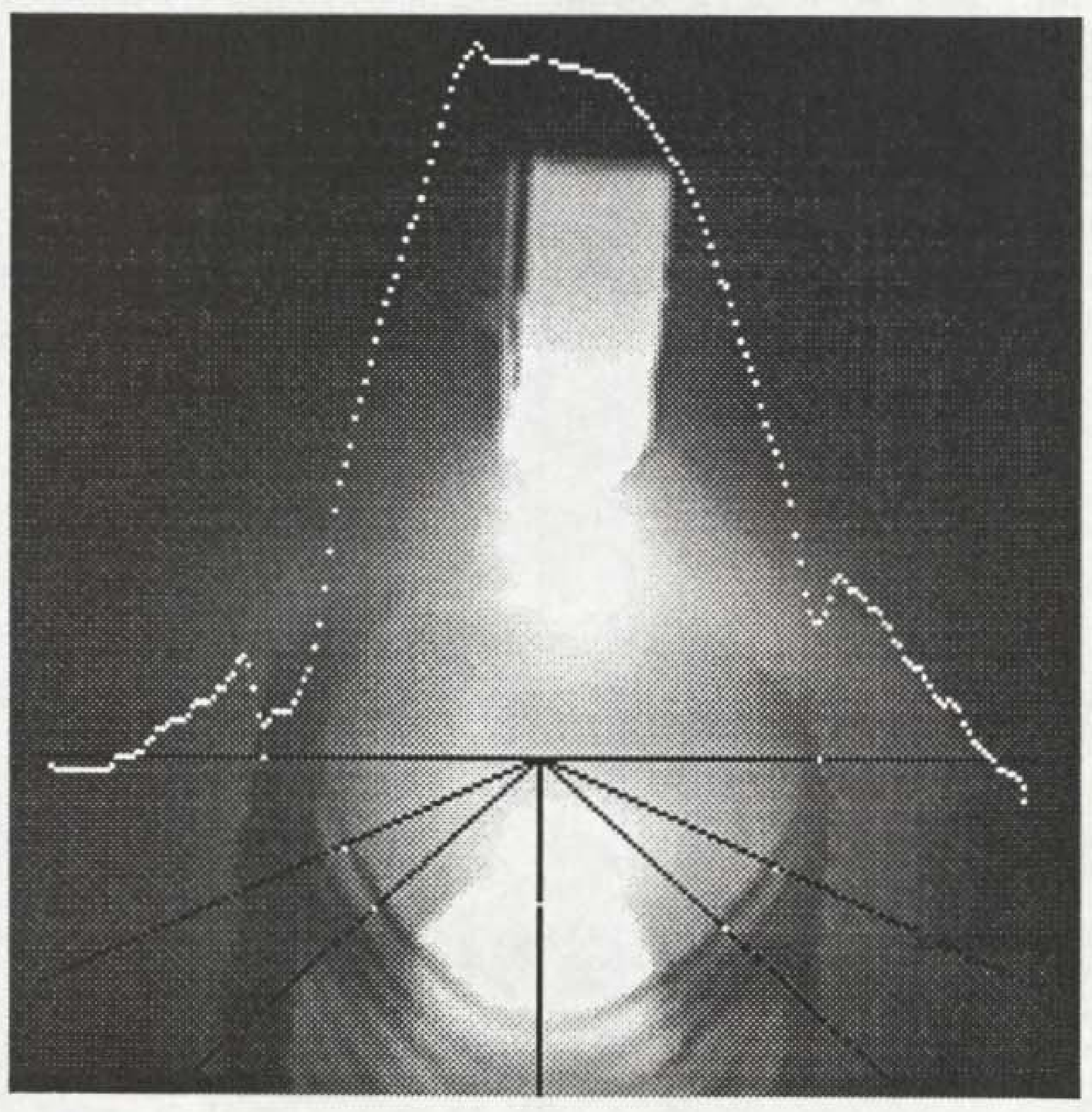

Fig. 5 Behind View of Weld Pool

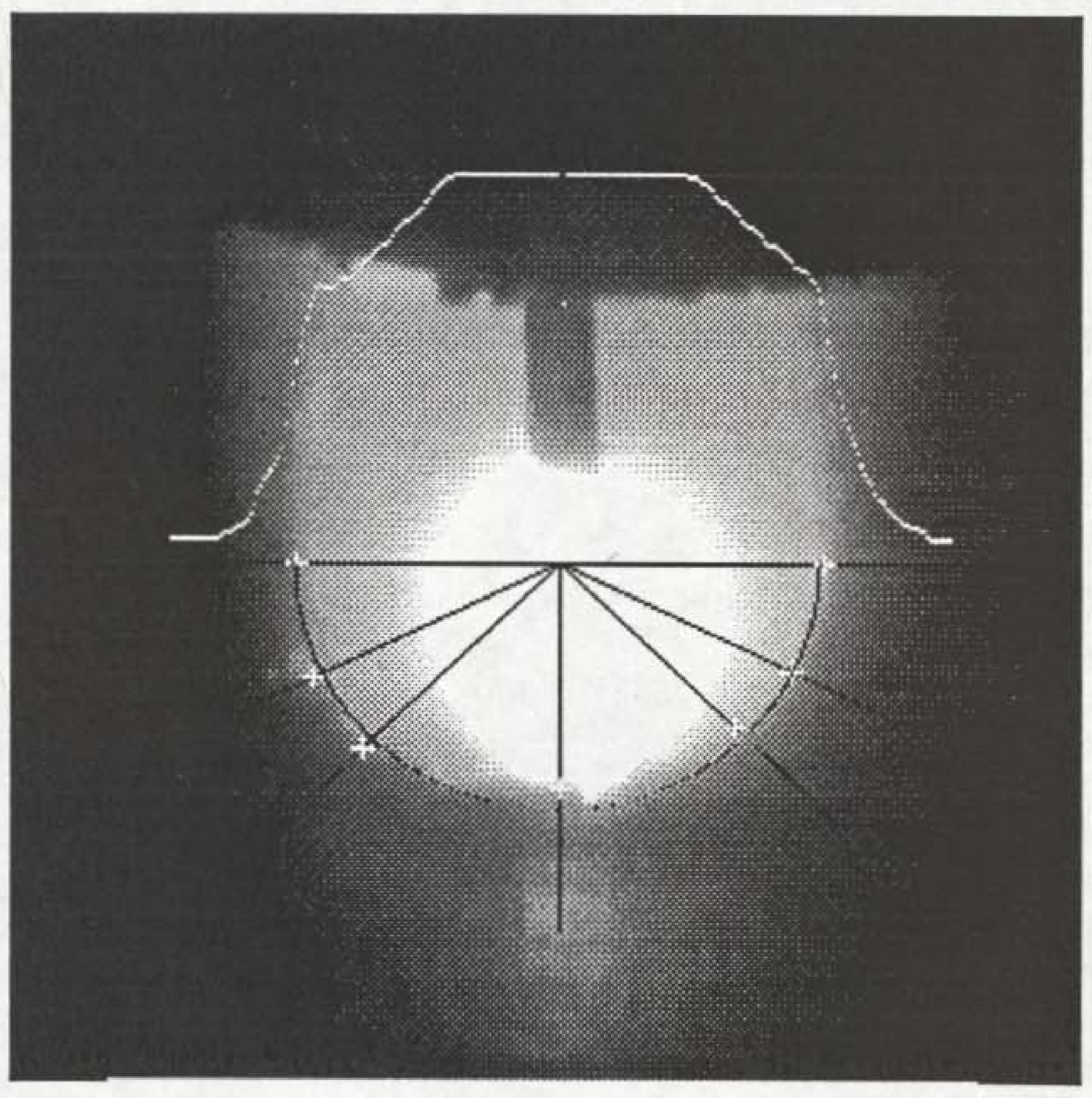

Fig. 6 MIG Weld Pool

Fig.6 shows the weld pool image for MIG welding. It demonstrates that the edge extraction algorithm performs satisfactory.

Edge Approximation

It can be clearly seen, from Fig.3(b), that the front half of weld pool is geometrically similar to a half-ellipse. Therefore an ellipse model is used to describe weld pool:

$$\frac{(x+\zeta)^2}{\alpha^2}+\frac{(y+\eta)^2}{\beta^2}=1 \qquad [4]$$

where (ζ, η) denotes the centre of the ellipse, and α and β are the half-lengths of the major and minor axes, respectively. They are calculated by $\zeta = x_1+(x_7-x_1)/2$, $\eta = y1$ and $\alpha= (x_7-x_1)/2$, while the estimation of β is a little more difficult since the edge just below the arc is not easy to obtain because of the arc light, therefore edge points P_3 and P_4 are used to calculate β. Fig.3(b) shows the ellipse model, which almost totally matches the surface shape of the weld pool. Once this model is established, the crucial features of weld pool geometry such as bead width, half-length as well as the ratio of width and length, which closely correlate to penetration, can be evaluated. Similarly, the back half of weld pool, when images are captured from behind the arc, can also be described as a half ellipse but the parameters in equation are quite different from those of front half.

CLOSED-LOOP CONTROL

Preliminary closed-loop control trials have been conducted to confirm the effectiveness and robustness of the proposed visual sensing system combined with image processing. The width of weld pool is taken as the sensing parameter for control. Namely, consistent bead width is pursued in the experiments. A simple proportional control algorithm was applied. Fig.5 shows the bead width variation during the welding with and without closed-loop control. The frequency of feedback control was 10 Hz. For the results in Fig.5(a), a constant current was set at l00A, but variable bead width was observed whilst consistent bead width is obtained when closed-loop control is introduced, Fig.5(b), where the bead width is set to 120 pixels and welding current is adjusted automatically to maintain the bead width. Control experiments show that proposed image processing algorithms can trace the weld pool edge with accuracy and speed.

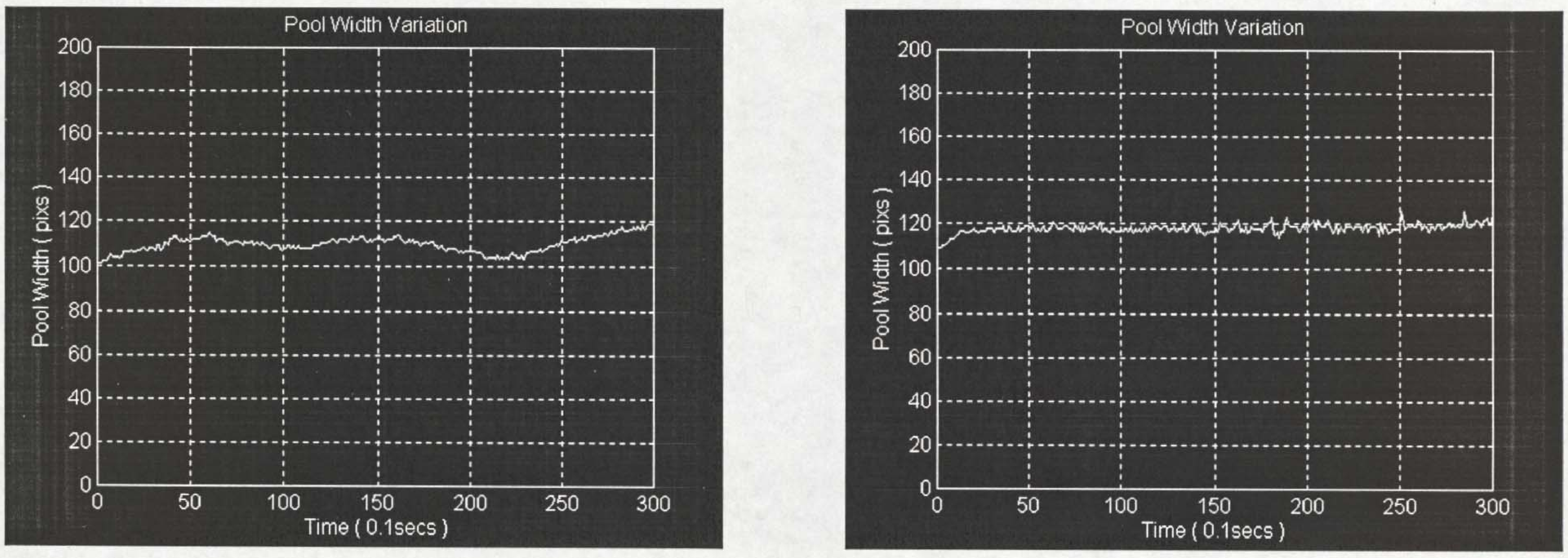

(a) **(b)**

Fig. 5 Weld Width Variation (a) Without Control (b) With Control

CONCLUSIONS

The high shutter speed CCD camera, combined with selected filters, provides a practical and effective approach to acquire useful images for weld pool detection. Image processing algorithms can detect the pool edge with sufficient accuracy and speed under practical welding conditions.

Their effectiveness and robustness have been demonstrated in closed-loop control experiments. The whole process of edge detection can be finished in 50 ms on a P5/100 computer.

Different image features are observed in TIG welding and MIG welding of aluminium and stainless steel. It has been shown that the images acquired in AC TIG welding of aluminium have a high brightness contrast at the pool edges and are suitable for detection using standard edge detection algorithms. Whilst the images from the TIG welding of stainless steel have unclear edges and require the use of more powerful algorithms for edge detection.

It has to be pointed out that further research is required to investigate more powerful control algorithms for penetration control and the correlation between weld pool geometry and penetration. This work is currently under development in the University of Liverpool using a neural network approach.

ACKNOWLEDGEMENT

The authors wish to thank the EPSRC for providing grants to support this research.

REFERENCES

1. Carlson, N.M., and Johnson, J.A.. "Ultrasonic Sensing of Weld Pool Penetration". *Welding Journal* 67(11) 1988, 239-s to 246-s.
2. Yang, J., *et al.*. "Ultrasonic Weld Penetration Depth Sensing with a Laser Phased Array". *Proceedings of 1994 ASME International Mechanical Engineering Congress,* PED-Vol. 68-1, *Manufacturing Science and engineering,* 1994, pp. 245-254.
3. Xiao, Y.H., and Ouden, G. den. "Weld Pool Oscillation during GTA Welding of Mild Steel". *Welding Journal* 72(8) 1993, 428-s to 434-s.
4. Kovacevic, R., Zhang, Y. M., and Li, L.. "Monitoring of Weld Joint Penetration Based on Weld Pool Geometrical Appearance". *Welding Journal,* 75(10) 1996, 317-s to 329-s.
5. Bicknell, A., Smith, J. S., and Lucas, J.. "Infrared Sensor for Top Face Monitoring of Weld Pools". *Meas. Sci. Technol.,No.5* 1994, 371-378.
6. Kovacevic, R., Zhang, Y. M., and Ruan, S.. "Sensing and Control of Weld Pool Geometry for Automated GTA Welding". *ASME Journal of Engineering for industry,* 117(5) 1995, 210-222.
7. Banerjee, P., Govardhan, S., Wikle, H. C., Liu, J. Y., and Chin, B. A.. "Infrared Sensing for On Line Weld Geometry Monitoring and Control". *ASME Journal of Engineering for Industry,* 117(8) 1995, 323-330.
8. Zhang, Y. M., Kovacevic, R., and Wu, L.. "Dynamic Analysis and Identification of Gas Tungsten Arc Welding Process for Weld Penetration Control". *ASME Journal of Engineering for Industry,* 118(2) 1996, 123-136.
9. Suga, Y., Sano, Y., Naruse, M., Kojima, K., and Ogawa, K.. "Recognition of the Weld Line by a Visual Sensing System and Weld Line Tracking in Automatic Welding of Thin Aluminium Plates". *Welding International,* 7(4) 1993, 31-37.
10. Zhang, Y.M., Li, L., and Kovacevic, R.. "Dynamic Estimation of Full Penetration Using Geometry of Adjacent Weld Pools". *ASME Journal of Manufacturing Science and Engineering.* Vol. 119, 1997, 631-643.
11. Kovacevic, R., Cao, Z. N., and Zhang, Y. M.. "Role of Welding Parameters in Determining the Geometrical Appearance of Weld Pool". *ASME Journal of Engineering Materials and Technology,* 118(10) 1996, 589-596.
12. Brzakovic, D., and Khani, D. T.. "Weld Pool Edge Detection for Automated Control of Welding". *IEEE Transactions on Robotics and Automation,* 7(3) 1991, 397-403.

13. Kovacevic, R., and Zhang, Y. M.. "Sensing Free Surface of Arc Weld Pool Using Specular Reflection: Principle and Analysis". *Proc Instn Mech Engrs, part B: Journal of Engineering Manufacture,* Vol. 210, 1996, 553-564.
14. Hoffman, T.. "Real-Time Imaging for Process Control". *Advanced Material & Processes* 140(3) 1991, 37-43.
15. Kovacevic, R., and Zhang, Y. M.. "Real-Time Image Processing for Monitoring of Free Weld Pool Surface". *ASME Journal of Manufacturing Science and Engineering,* Vol. 119, 1997, 161-169.
16. Chen, S. B., Wu, L., Wang, Q. L., and Liu, Y. C.. "Self-Learning Fuzzy Neural Networks and Computer Vision for Control of Pulsed GTAW". *Welding Journal,* 76(5) 1997, 201-s to 209-s.